The Pressure-Volume Relationship and Hysteresis Loss in Stirling Refrigerators

A thesis submitted to Auckland University of Technology
in fulfilment of the requirements for the degree of
Doctor of Philosophy (PhD)

Author: Danielle Francisco Yang
Supervisors: Dr Michael Gschwendtner, Dr Michael Protheroe

February 2023

School of Engineering
Faculty of Design & Creative Technologies
Auckland University of Technology
Auckland, New Zealand

For Michael – my mentor and friend.

Abstract

Stirling refrigerators consist of several spaces in which a volume of gas undergoes expansion and compression. This is also known as a 'gas spring'. In such a space, heat transfer occurs due to the cyclic temperature difference between the working gas and the adjacent walls. This causes cyclic heat dissipation, known as hysteresis loss. Hysteresis loss is one of the many losses within Stirling machines that are not completely understood.

This project investigated the underlying mechanisms of hysteresis loss, by examining the relationships between temperature, heat transfer, pressure in single and multiple space Stirling refrigeration systems. This was carried out with a thorough investigation and analysis with mathematical models, a Sage single cylinder model, and single cylinder experimental tests. An experimental validation of a Twinbird 40 W cooler, a beta-type Stirling refrigerator, was also presented. Finally, the Sage model of an alpha Stirling refrigerator and a simple cylinder with regenerator material was used to explore hysteresis loss within the multiple spaces of a Stirling refrigerator.

A simple, closed form equation was developed to show the relationship of net P-V work for given pressure and volume amplitudes with a specified pressure phase shift for sinusoidal motion, which worked for both single cylinder and Stirling refrigerator models. The sinusoidal Schmidt equations were used to show that there will always be a pressure phase shift even in ideal situations for any temperature ratio other than $\tau = 1$.

The pressure phase shift is shown to be in both sinusoidal and discrete execution of the Stirling cycle. An effective pressure phase shift in the discrete Stirling cycle is presented, and an applied cycle is discussed to show how the isochoric processes impose this effective phase shift. It was found that there will always be a pressure phase shift if there is a net heat or P-V work transfer, in both multiple and single space systems.

The Peclet number is found to be an insufficient quantity to predict hysteresis loss in Stirling refrigerators. Hysteresis loss, or the net heat transfer, is not always from the gas to the wall; in the alpha Stirling model it was found to be a net heat gain from 10 to 20 Hz. It is proposed that hysteresis is not always a loss in multiple space systems which transfer heat or do work.

The design implications from the study are to increase the hydraulic diameter where heat transfer is beneficial. Hysteresis loss was found to vary with the working gas at different frequencies. At 10 Hz, the hysteresis loss in a single space experiment with helium as a working gas was five times that of air. However, it is suggested not to base the working gas selection on hysteresis loss minimisation as the regenerator already minimises the effect of hysteresis loss, and the fact that net heat transfer is still required in the heat exchangers.

The regenerator and how it reduces heat transfer and therefore hysteresis within Stirling refrigerators was also explored. It was found that the presence of the regenerator 'isothermalises' the system by increasing the overall heat transfer amplitude and decreasing the net heat transfer, therefore reducing the pressure phase shift.

Acknowledgments

I would like to thank my two supervisors for all their support, encouragement, and patience throughout this project. To Dr Michael Gschwendtner, you went above and beyond the conventional requirements and expectations of supervision. Your hours spent working with us on our projects, your focus on wellbeing, and your steadfast insistence in doing what is right by us will never be forgotten. You taught me to trust in my own knowledge and abilities by believing in me from the very start – I can never thank you enough for that. To Dr Michael Protheroe, for your kindness, your attention to detail, and your help to pull together my rambling thesis drafts. Both of you have been not only mentors, but my first professional role models. With your encouragement for my teaching and work within in the university, you gave me a place I truly felt valued.

Thanks to my parents David Yang and Elsa Francisco Yang. Mom and Dad, you made me who I am today; all my love and all I will achieve is for you. To my siblings, Monica for being my number one fan and for believing in me since day one, and Rafael for your unlimited 3D printing services and my 'second' mechanical engineering degree from University of Auckland. To Tony for your unconditional love and support throughout the years. To Zindh, I could not have had anyone better to share an office and PhD journey with. These years would not have been the same without you.

Lastly, this project would not have been possible without financial support from the AUT Vice Chancellor's Scholarship and the Kate Edger Educational Charitable Trust.

Attestation of Authorship

I hereby declare that this submission is my own work and that, to the best of my knowledge and belief, it contains no material previously published or written by another person (except where explicitly defined in the acknowledgements), nor material which to a substantial extent has been submitted for the award of any other degree or diploma of a university or other institution of higher learning.

_____	17/02/2023
Signature	Date

Table of Contents

List of Figures

List of Tables

Nomenclature

Abbreviations

COP	Coefficient of Performance
CFD	Computational Fluid Dynamics
DV	Dead Volume
FPSE, FPSC	Free-Piston Stirling Engine, Cooler
HFC/s	Hydrofluorocarbon/s
LabVIEW	Laboratory Virtual Instrument Engineering Workbench
LossND	Non-Dimensional Loss
MATLAB	Matrix Laboratory
MIDAS	Materials in Devices as Superconductors
NASA	National Aeronautics and Space Administration
NI	National Instruments
PCB	Printed Circuit Board
P-V	Pressure-Volume
T-s	Temperature-Entropy
TDC, BDC	Top Dead Centre, Bottom Dead Centre
VDC	Volts, Direct Current

Symbols

A	Area
c_p	Specific heat capacity at constant pressure
D, D_h	Diameter, hydraulic diameter
f	Frequency
k	Thermal conductivity
L	Length
m	Mass
Nu	Nusselt number

p	Porosity of a regenerator (void volume over total volume)
P	Pressure
Pe_v	Peclet number - linear velocity based
Pe_ω	Peclet number - oscillation based
Q	Heat
r	Radius
R	Specific gas constant
Re	Reynolds number
S	Stroke (of piston)
T	Temperature
Tp	Time period, $\frac{1}{f}$
t	Time
U	Internal energy
V	Volume
W	Work
x	Displacement

Greek Symbols

α	Thermal diffusivity, or phase by which the cyclic variation of V_E leads V_C
γ	Ratio of specific heats
η	Thermal efficiency
Δ__	A change in __
δ	Schmidt analysis variable
θ	Crank angle
κ	Volume ratio, $\kappa = \frac{V_C}{V_E}$
ρ	Density
τ	Temperature ratio, $\tau = \frac{T_C}{T_E}$
ω	Rotational speed
ϕ	Pressure phase shift

Subscripts

a	Amplitude
abs	Absorber
$avg, 0$	Average, mean
c	Cold, ie. cold space
h	Hot, ie. hot space
g	Gas
hp	Heat pump
$hyst$	Hysteresis
i	Ideal
$init$	Initial
p	Piston
ref	Refrigerator
reg	Regenerator
rej	Rejector
s	Surface
t	Total
th	Thermal
w	Wall
C	Compression space
E	Expansion space
ND	Non-dimensional
Phsr	Phasor
Gt	Time-ring
Stdy	Steady

Chapter 1: Introduction

We desire control over the temperature in many areas of life, usually for our comfort or to slow the natural decay process and aid in manufacturing food and other products. Altering an object's temperature to above or below that of its surroundings requires a movement of heat in the opposite direction to which it would naturally flow according to the second law of thermodynamics. Transferring heat from one space to another (cold to hot) requires work input. The machines with which we achieve this temperature control are heat pumps or refrigerators (Garvin, 1926).

Heat pumps and refrigerators are used over a wide range of temperatures for many different situations, ranging from manufacturing, other industrial applications, to household use. Most everyday usage for heat pumps and refrigerators for the average person is to achieve comfortable ambient temperatures, such as air-conditioning and food storage. These devices therefore operate in the near-ambient temperature regime. For this study, the ambient temperature regime is defined as being between -20°C and 50°C. Appendix A details the conventional Coefficient of Performance (COP) calculations for refrigerators and heat pumps.

In May 2017, the New Zealand government announced its plan to phase down hydrofluorocarbons (HFCs) used in the air-conditioning and refrigeration industries by over 80% over the next 20 years. HFCs qualify as so-called greenhouse gases and are a primary contributor to global warming. Former Environment Minister Dr. Nick Smith stated: "The phase-down of HFCs will have implications for New Zealand industries like air conditioning and refrigeration that will need to convert to new technologies. Consumers with heat pumps will not need to upgrade them, but future replacements will need to use new technologies" (Smith, 2017).

Stirling machines have the great potential to become this 'new technology'. They use environmentally friendly working gases such as helium, hydrogen, or air, and their operation is based on the most efficient thermodynamic cycle possible. Stirling machines are very quiet in operation and are almost maintenance-free. They have been used as heat engines for power generation in co-generation plants, in waste heat recovery, and in space applications. As a refrigerator, they have been used in cryo-

cooling and lab freezer applications. However, they have not yet been able to penetrate the gigantic market of domestic and automotive refrigeration and air-conditioning in the near-ambient temperature regime (Haywood, 2004; Walker, Reader, Fauvel, & Bingham, 1994; West, 1986; Wurm, Kinast, Roose, & Staats, 1991).

The ideal Stirling cycle has the same efficiency or COP as that of the Carnot cycle. Practical Stirling machines, however, fall well short of this ideal. Well-designed Stirling machines may reach only 30% of the theoretical Carnot limit. The reason for this is only partly understood. Inevitable friction, imperfect heat transfer, and other irreversibilities certainly account for the reduction in performance; however, they do not explain where the majority of the remaining 70% is lost.

Stirling coolers consist of several spaces in which a volume of gas undergoes expansion and compression. This is also known as a 'gas spring'. In such a space, heat transfer occurs due to the cyclic temperature difference between the working gas and the adjacent walls. As the gas is compressed, the pressure and the temperature of the working gas increase, and, consequently, heat is transferred into the wall. Likewise, as the gas expands, the pressure and the temperature of the working gas drop, and heat is transferred from the wall into the gas. This causes cyclic heat dissipation, known as hysteresis loss. Hysteresis loss is one of the many losses within Stirling machines that are not completely understood, let alone quantified. This project aims to delve deeper into the underlying mechanisms of hysteresis loss to quantify how much hysteresis contributes to the missing 70%.

1.1 Novel Aspects and Contribution to Knowledge

The novel aspects of this research are as follows:

1. The effect of hysteresis loss discussed and analysed using an experimentally validated third order model of a complete Stirling refrigerator.
2. The Peclet number in each space within a Stirling refrigerator is quantified, and its suitability for predicting hysteresis loss is discussed.
3. The heat transfer effects on cyclic pressure variation are discussed.
4. The discussion on how hysteresis loss directly affects the pressure phase shift and therefore the net P-V work.
5. The pressure-volume relationship for single space vs. multiple space models is analysed.
6. The derivation of the relationship between pressure phase shift and net P-V work using sinusoidal motion is introduced.
7. The Schmidt cycle calculations are extended for the derivation of the ideal pressure phase shift.
8. The discussion of an apparent phase shift for discrete piston motion and its analogy to sinusoidal motion is presented.
9. Deeper exploration into the regenerator as an ‘isothermaliser’ with both simulation and experimental results.

Chapter 2: Literature Review

2.1 Vapour-Compression Refrigeration Cycles

The basic principles of vapour-compression were first discovered in the 1920s (Goetz, 1986). For vapour-compression refrigeration cycles, the working fluid undergoes a phase change to reject and absorb heat and is compressed and throttled between two different pressure limits. The ideal vapour-compression refrigeration cycle consists of four processes: isentropic compression in a compressor, isobaric heat rejection in a condenser, throttling in an expansion device, and isobaric heat absorption in an evaporator. The analysis of this cycle can be found in most engineering thermodynamics textbooks.

Vapour-compression-type refrigerators and heat pumps are now the most widely used refrigeration methods for standard household equipment. Vapour-compression refrigeration systems have low manufacturing costs and, therefore, low purchase costs due to the large numbers produced. They are also very reliable, and throughout their operational lifespan require little maintenance (Haywood, 2004). The combination of price, reliability and low maintenance requirements is probably one of the contributing factors of why the use of vapour-compression refrigeration cycles is so prevalent today.

Comparison of COPs for different types of vapour-compression heat pumps or refrigerators can be problematic, mostly due to how manufacturers use different test conditions in the calculation of their reported COPs. In New Zealand, for ambient temperatures between -5 °C and 20 °C, the predicted heat pump COPs can range from 2 to 4.5 (Concept Consulting Group, 2010). However, the actual COP of heat pumps and refrigerators vary depending on the ambient temperature and are also usually lower than the lab-measured COP values. For example, a heat pump with a reported COP of 3 can practically have a COP of 2.4, especially during colder months (Duncan, Hamm, & Wilkinson, 2007; French, Isaacs, & Cimilleri, 2008).

While the vapour-compression cycle seems, at first glance, to be an ideal choice for refrigerators and heat pumps, it has its limitations. One of the main drawbacks of the vapour-compression cycle is in the required properties of the working fluid or refrigerant. Vapour-compression systems would ideally have a refrigerant with high

condensation temperatures and low evaporation temperatures, which would increase the efficiency of the system. The requirement of a two-phase refrigerant with these properties usually leads to refrigerants with damaging environmental impacts. These refrigerants include ammonia or halocarbon compounds, which are usually categorised with the ANSI/ASHRAE Standard 34[1], such as the commonly used R134a and R410a (ASHRAE, 2001; Garvin, 1926; Haywood, 2004).

The global warming potential of common refrigerants used in vapour-compression systems are listed Table 2-1. This table shows the global warming potential (GWP) over 100 years, with each value based on carbon dioxide having a GWP of 1 as a reference. Table 1 also shows the type of refrigerant. Chlorofluorocarbon (CFC) and hydro-chlorofluorocarbon (HCFC) refrigerants were phased out due to their high GWPs. R12 and R22 were both common refrigerants in automobile, household and commercial refrigeration units, and have been replaced by R410a and R134a, respectively. However, even though the hydrofluorocarbon (HFC) replacements have lower GWPs than their predecessors, they still have GWPs in orders of a thousand times greater than carbon dioxide.

Table 2-1: Global warming potential of common vapour-compression refrigerants, adapted from IPCC (2007)

Product	**Type**	**Global Warming Potential (100 years)**
CO_2	Natural	1
R12	CFC	10900
R410a	HFC	2088
R22	HCFC	1810
R134a	HFC	1430

[1] The American National Standards Institute/American Society of Heating, Refrigerating and Air-Conditioning Engineers (ANSI/ASHRAE) Standard 34 is a widely used standard for designation and safety classification of refrigerants.

2.2 Gas Refrigeration Cycles

In gas refrigeration cycles, unlike the vapour-compression refrigeration cycle, the working fluid (refrigerant) exchanges heat as it passes through heat exchangers, but it does not change phase. For practical applications, the conventional cycle used is the reverse Brayton cycle. Many gas refrigeration machines need a large amount of refrigerant to produce the same amount of cooling in comparison to vapour-compression, which leads to these refrigerators being very large. Gas refrigeration cycles are therefore not usually used in household applications but are used in aircrafts. Using air as a refrigerant in these applications is convenient and provides safety benefits as it is non-flammable and non-toxic.

2.3 Regenerative Cycles

The regenerator is a type of heat exchanger which alternately absorbs and rejects heat to and from the working gas. It has an internal matrix or 'packing' that is made up of materials that should have a high heat capacity (Willmott, 2011). Cycles which utilise a regenerator to improve efficiency are known as regenerative cycles, such as the Stirling and Ericsson cycles.

The function of a regenerator is to 'recycle' heat inside the system that would otherwise be lost as the gas passes between the hot compression and cold expansion spaces (Hargreaves, 1991). This internal heat transfer can be indicated in a thermodynamic cycle as a heat flow between two processes, shown as Q_{reg} in Figure 1 (see section on the ideal Stirling cycle). Despite some physical limitations and impracticalities associated with the implementation of regenerative cycles, it is proven that regeneration can increase efficiency, as modern gas-turbine and steam power plants utilise this technology extensively.

2.4 Stirling Technology

The Stirling cycle is a regenerative gas cycle. One of the main advantages of these machines over the conventional vapour-compression heat pumps and refrigerators is that Stirling machines operate on environmentally friendly working gases such as air, helium, and hydrogen (Walker et al., 1994). The ideal Stirling cycle (explained in the upcoming section) also makes use of isothermal and isochoric processes to create a

Coefficient of Performance (COP) that is the same as the Carnot COP, the theoretical maximum COP for any refrigerator or heat pump.

Stirling machines have been recognised to hold the potential for commercial competition to the vapour-compression refrigerators and heat pumps currently in widespread use, but as of today, they have not been able to successfully break into the large markets of industrial and home refrigeration (Haywood, 2004; Walker, Reader, Fauvel, & Bingham, 1993; Walker et al., 1994; West, 1986; Wurm et al., 1991). They have, however, been effective in niche areas such as cryo-cooling for medical and laboratory applications (Stirling Ultracold, 2018; Urieli & Berchowitz, 1984).

Origins of the Stirling Cycle

The patent of the first Stirling machine was proposed by Rev Dr. Robert Stirling in 1816, but was only granted in January 1817 (Hargreaves, 1991; Stirling, 1817). The main driving force behind his invention is attributed to be his concern of the dangers inherent in the then widely-used steam engines, which were known to explode due to the high temperatures and the low quality of iron that was available at that time (The Engineer, 1917). The engine he built was a gas or 'hot air' engine, which operated on a closed cycle, and is the basis of almost all regenerative gas engines. He also developed a 'Heat Economiser' or, as it is known today, a regenerator. This invention aided in increasing the efficiency of the Stirling engine. The thermodynamic 'Stirling cycle' was still not theoretically modelled until after Sadi Carnot studied the general theory of heat engines in 1824 (Carnot, 1890; Urieli & Berchowitz, 1984).

The Ideal Stirling Refrigeration Cycle

The ideal Stirling cycle consists of two isochoric processes and two isothermal processes. The general assumptions for ideal analysis of the Stirling cycle, as defined by Walker et al. (1994, p. 51), are:

1. All processes are thermodynamically reversible, and the processes of compression and expansion are isothermal, indicating infinite heat transfer rates between the cylinder walls and working fluid.

2. All working fluid is either in the compression or expansion space during their respective processes, so that the effect of any spaces in the regenerator matrix, clearance space or dead volume is neglected.
3. The motion of the two pistons is discontinuous, which is necessary to achieve the working fluid distribution.
4. All mechanical friction, aerodynamic and leakage losses are neglected.
5. The heat transfer between the regenerator and working gas is perfect, which implies infinite rates of heat transfer, and a regenerator matrix with an infinite heat capacity.

During the isothermal processes, the working gas is either compressed or expanded, and heat flows in or out of the cycle. During the isochoric processes, heat is internally transferred by the regenerator by alternately absorbing and rejecting heat into the working gas. The processes and states for the ideal Stirling refrigeration cycle are shown in Figure 2-1, and can be described as follows:

1-2: Isothermal compression with external heat rejection.

2-3: Isochoric heat rejection to the regenerator matrix (internal heat rejection).

3-4: Isothermal expansion with external heat absorption.

4-1: Isochoric heat absorption from the regenerator matrix (internal heat absorption).

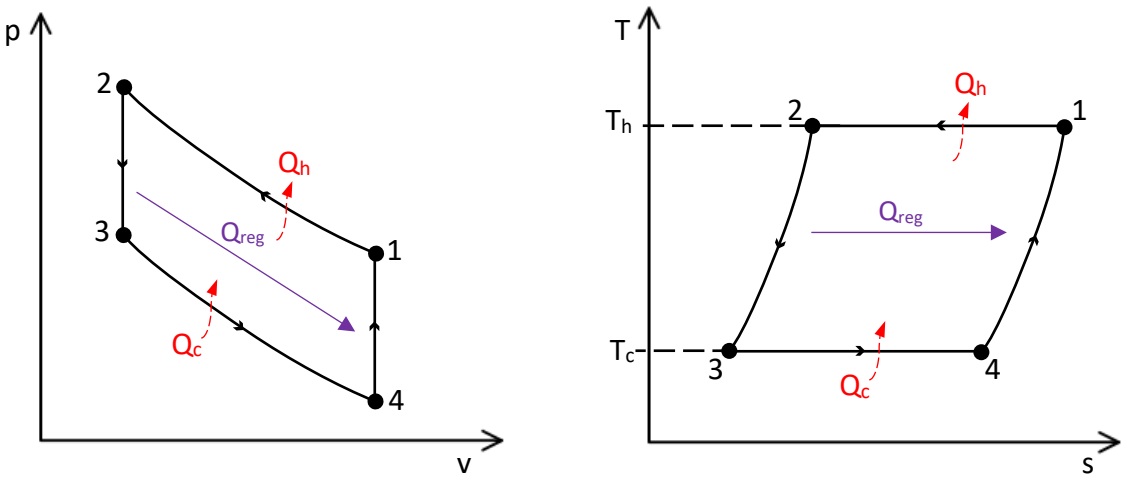

Figure 2-1: P-V and T-s diagrams of the ideal Stirling refrigeration cycle

For the ideal cycle, the heat rejected and absorbed can be calculated using an isothermal process from state 1 to 2 and from 3 to 4. The properties at each state can be defined with the ideal gas equation, knowing the variation of volumes and the temperature of the heat source and sink, tabulated in Table 2-2**.**

Table 2-2: State equations for the ideal Stirling cycle

Variable	**State 1**	**State 2**	**State 3**	**State 4**
Temperature	$T_1 = T_h$	$T_2 = T_h$	$T_3 = T_c$	$T_4 = T_c$
Volume	V_1	V_2	$V_3 = V_2$	$V_4 = V_1$
Pressure	$P_1 = \frac{mRT_1}{V_1}$	$P_2 = \frac{P_1V_1}{V_2}$	$P_3 = \frac{P_2T_3}{T_2}$	$P_4 = \frac{P_3V_3}{V_4}$
Heat Transfer	$Q_h = W_{12} = -mRT_h ln\left(\frac{V_2}{V_1}\right)$		$Q_c = W_{34} = mRT_c ln\left(\frac{V_1}{V_2}\right)$	

While the ideal Stirling cycle is straightforward, practical Stirling devices can be anything but simple. Even the definition of a 'Stirling machine' becomes convoluted. Generally, Stirling machines operate on a closed, regenerative cycle, and the cyclic variation of temperature, pressure and heat flow is driven by volume changes. Distinction between these machines and the open, valve-controlled regenerative cycle should be made. The latter devices are usually called Ericsson-cycle machines, though in practice, the two terms, Ericsson and Stirling, are sometimes (incorrectly) used interchangeably. Stirling machines are also frequently called other names, such as hot-air cycles, hot-gas cycles, or even identified by the name of the inventors of a specific configuration. To complicate matters further, practical Stirling machines actually do not work on the Stirling thermodynamic cycle (Walker, 1973). Nevertheless, the Stirling cycle's ideal analysis is an important tool to understand the difference between the ideal case and what is practically achievable.

Stirling Mechanical Configurations

The three basic mechanical configurations for Stirling devices are known as the alpha, beta, and gamma arrangements, shown in Figure 2-2. The figure illustrates the three configurations as refrigeration devices. The absorber and rejector labels illustrated are heat exchangers which respectively remove heat from the gas as it leaves the expansion space and reject heat back into the compression space. The regenerator is a component which alternately absorbs and rejects heat to and from the working gas, described previously in Section 2.3.

A piston which delivers work to the system is simply referred to as the 'piston'; while a piston which does no work, whose purpose is to simply move gas between different spaces, is called the 'displacer'. Typically, there is a large pressure and small temperature difference across a piston, and a large temperature and small pressure difference across a displacer. The alpha configuration has two pistons, while both beta and gamma configurations have a piston and a displacer each. The beta configuration differs to the gamma simply in terms of cylinder alignment – for the beta configuration, the piston and displacer share a single, in-line cylinder, while the gamma has two offset cylinders.

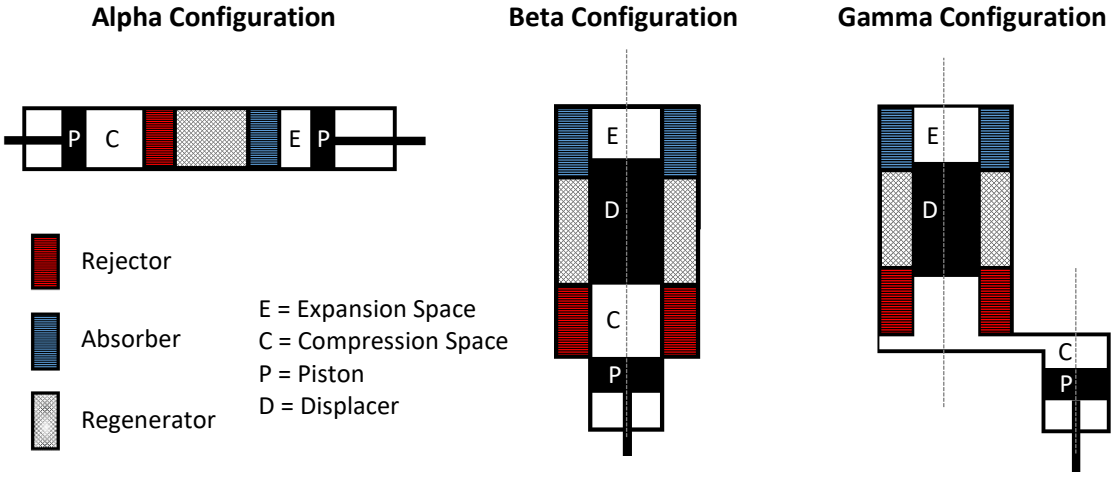

Figure 2-2: Stirling mechanical configurations, adapted from Walker (1973, p. 52)

These basic mechanical configurations are further developed into other variations and sub-divisions, which can be defined in a multitude of different ways which include characterisation by drive mechanism, number of cylinders, or even by the inventor of the arrangement, such as the Siemens-Stirling configuration (Urieli & Berchowitz, 1984; Walker et al., 1994; Wurm et al., 1991).

Practical Applications of Stirling Refrigeration

The history of using Stirling's engine concept for refrigeration has been extensively collated and documented by Walker et al. (1994). They maintain that the earliest known record of Stirling refrigeration dates back almost to the time the cycle was first used as an engine, when John Herschel proposed its use as a refrigerator in 1834. The next instance of Stirling refrigeration was in the 1860's, when Alexander Kirk described a Stirling refrigerator which had been used for over 10 years. None of these early applications were adopted by the mainstream industries at that time.

In more modern times, Stirling refrigerators have been advanced by the Philips research and development programme in the 1950's. While they considered applications of Stirling refrigeration in the near-ambient temperature regime to compete with the vapour-compression refrigerators and heat pumps, they decided that better commercial prospects lay in the cryogenic industry (Walker et al., 1994). William Beale, the inventor of the free-piston Stirling engine/cooler (FPSE, FPSC), also saw the potential of Stirling refrigeration for extremely low temperatures. He founded Sunpower, Inc. in Athens, Ohio, which develops and sells free-piston Stirling machines of many different applications and sizes today. They claim both higher performance and efficiency, while maintaining smaller sizes and more flexibility in design than traditional alternatives (Sunpower Inc., 2018).

This suitability for operation at low temperatures was also noticed by researchers in the space industry. Extensive study on Stirling refrigeration in space applications has been carried out by the National Aeronautics and Space Administration (NASA) in the United States. In 1996, their Materials in Devices as Superconductors (MIDAS) project produced a Stirling-based cooler which was eventually installed and operated for three months on *Mir*, the Russian space station (Ross & Boyle, 2006). This is only one of NASA's many Stirling cryocooler projects, many of which, as of 2016, were still ongoing (Geng, 2016). These projects are frequently collaborations with Sunpower, Inc. One of these collaborations, the Sunpower M77B Stirling cooler, was the first application of a low-cost commercial cooler to achieve multi-year operation in space (Ross & Boyle, 2006, p. 4).

The focus of this project, however, is not in the cryogenic temperature range, but for near-ambient temperature applications. The history of Stirling being used for refrigerators and heat pumps operating within this particular temperature regime is, so far, rather limited in terms of both research within that area and commercial success. This could be due to early tests comparing Stirling and vapour-compression systems in terms of operating temperatures which found that Stirling out-performed vapour-compression systems for extremely low temperatures, but showed worse performance than vapour-compression systems for operation above 230 K (-43 °C) (Finkelstein & Polanski, 1959). These preliminary results seem to have directed research toward developing Stirling technology in the cryogenic area, which is understandable from a commercially-driven standpoint, especially as another main disadvantage of Stirling machines was an increased manufacturing cost (Walker et al., 1994). However, nowadays different factors are coming into play, and issues such as sustainability and refrigerant availability are becoming more and more important. The suitability of Stirling refrigeration in terms of these factors has been recognised for a long time (Walker, 1973; Walker et al., 1994), but these have not come to the forefront as pressing issues until recently, which opens the door for more research into near-ambient Stirling refrigeration.

There have been a few ventures into designing and implementing Stirling refrigeration for the near-ambient temperature regime, but nothing as yet has enjoyed widespread commercial success. Companies such as the Stirling Technology Company and Sunpower have tested near-ambient Stirling refrigerators for the domestic market. Around 1994, there was a prototype air-charged near-ambient Stirling refrigerator designed and tested by General Pneumatics Western Research Centre in the US for NASA, though its success or even whether it was developed further or not is unclear (Walker et al., 1994). Kagawa (2000) published a paper outlining the configurations of Stirling machines and their achievable performance in the near-ambient temperature regime. In recent years, some study has been put into developing a near-ambient refrigerator which combines Stirling refrigeration with a magnetic refrigeration effect. This proved to increase the ‘cooling performance’ of the system by 24% (He, Gong, Zhang, Dai, Shen, & Wu, 2013).

Near-Ambient Stirling Refrigeration Prospects

Near-ambient Stirling refrigeration is a field full of potential for further study and development. This field is both interesting and promising as it has yet to be fully studied and successfully implemented. Interest in near-ambient Stirling refrigeration has increased over recent years (He et al., 2013; Kagawa, 2000), as more research is focussed on sustainable, non-toxic and working gases with low global warming potentials. However, the new efficient refrigerants with low GWPs been developed, and new refrigeration systems in more recent years for use in vapour-compression refrigeration technology, which poses a challenge to the wider commercial success of Stirling gas cycle coolers (Alsouda, Bennett, Saha, Salehi, & Islam, 2023; Islam, Mitra, Thu, & Saha, 2021; Makhnatch, 2019; McLinden, Seeton, & Pearson, 2020; Yataganbaba, Kilicarslan, & Kurtbaş, 2015)

The Real Stirling Refrigeration Cycle

For the opportunities of a commercially competitive near-ambient Stirling refrigerator to be realised, several challenges must first be overcome. These issues stem mostly from the discrepancies between the ideal Stirling cycle and the Stirling cycle's real-life implementation, which results in real Stirling refrigerators operating at around 30% of their Carnot COP.

Part of the difference between the practical and ideal cycles is in the assumptions made for the ideal cycle. These are unrealistic and almost impossible to achieve in real life. Once the cycle is realistically implemented, all these assumptions of reversible processes, discontinuous piston motion, and infinite rates of heat transfer no longer hold true.

To illustrate how much of an impact these assumptions have, Figure 2-3 shows how the ideal, discontinuous piston motion looks, and the ideal P-V diagram that is produced. This is compared to practical continuous piston motion, with its corresponding P-V diagram. The P-V loop of the ideal and practical cycle are very different in shape and in size. In the ideal cycle, there are four completely distinct processes, whereas processes for the real cycle cannot be clearly distinguished – the processes transition smoothly from one to another. While the volume variations seem similar, the mechanical

implementation of the real cycle results in the working gas not being completely in one space at one time. For example, parts of the gas are compressed in the hot space while some is expanded in the cold space (Hargreaves, 1991).

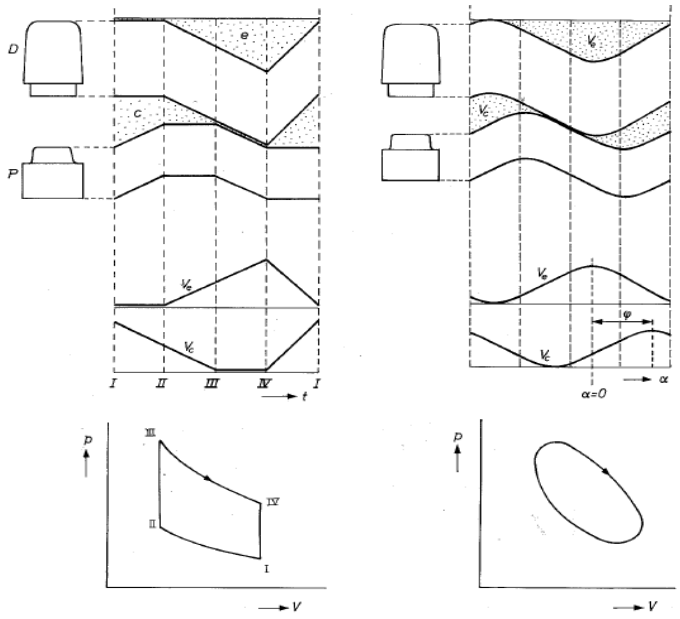

Figure 2-3: The difference between ideal discontinuous piston motion (left) and real continuous piston motion (right), adapted from Hargreaves (1991, p. 8)

None of the ideal isothermal or isochoric processes are executed for the real cycle, and there is an extreme difference in the area of the P-V diagrams, which is an indication of the extent of the simplification of the ideal cycle. Heat losses, friction and other irreversibilities will result in an even smaller P-V loop. All these losses combine for a refrigeration cycle with a much lower COP than what could ideally be obtained.

Limitations of the P-V Diagrams

The most important detail that must be recognised for both the discontinuously and continuously executed Stirling cycle P-V diagrams is the implication of uniform property values for the entire gas system at each point of the cycle. This is covered in detail by Tucker, Gschwendtner, and Haywood (2010), who point out the misleading nature of P-V and T-s diagrams. Unlike other ideal cycles, such as the Otto cycle [2] where each state point represents the actual thermodynamic state of the overall system, the points in a Stirling cycle P-V diagram only represent an average state. There is a very large variation

[2] In the practical Otto cycle, there is still some variation of properties across the cylinder at any point in time, however this variation is small relative to the variation in properties in the practical Stirling cycle.

in properties of the working gas throughout interconnected spaces at any one point in time. This means that, because of the variation in thermodynamic properties within the system, the Stirling cycle cannot be accurately represented on a property diagram (Tucker et al., 2010).

Since the Stirling cycle P-V diagram is not a property diagram, the only thermodynamically correct information that may be gained from the P-V diagram is the representation of what is experienced by the pistons which are subjected to pressure from the gas (Tucker et al., 2010). For example, the P-V diagram in Figure 2-4a, for sinusoidal piston motion provides the overall pressure and variation in total volume of the system. This means that the net P-V work into the system can be accurately predicted by the area within the cycle, as this is determined by what the pistons experience.

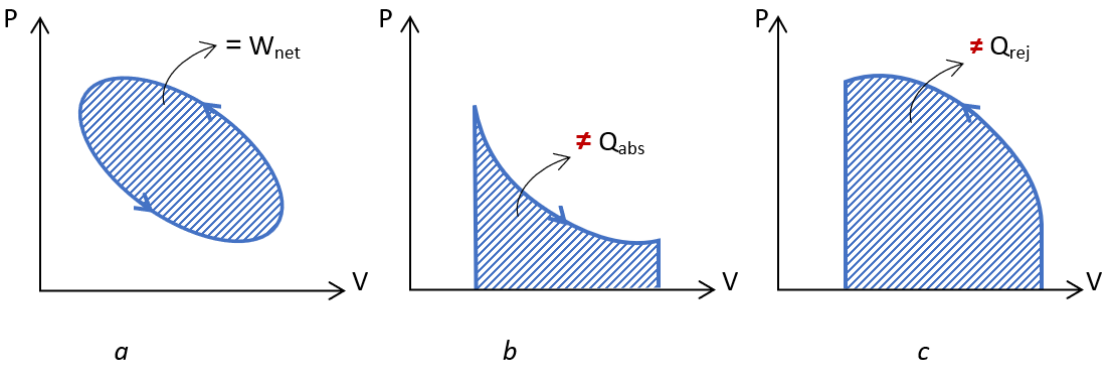

Figure 2-4: Illustration of the limitations of the overall Stirling P-V diagram

The limitation of this diagram is that it can give no information regarding the heat transfer processes, nor does it give an indication of the amount of heat absorbed and rejected by the system. When looking at the compression and expansion processes separately, as shown in Figure 2-4b-c, one cannot conclude that the heat absorbed and rejected are equal to the area under their respective processes. In fact, these do not represent the heat addition and rejection processes at all. While a T-s diagram is conventionally more appropriate for a discussion on heat flows, as a property diagram, the P-V diagram should still show equivalent processes. In this case, however, heat

absorption and rejection processes may be isothermal, adiabatic, or any other kind of process, but they are not illustrated in the overall P-V diagram. This is because of the mass distribution of the working gas across each space. For example, only a fraction of the gas is flowing through the absorber, and it is undergoing a completely different process to what the overall P-V diagram shows. Likewise, the overall P-V diagram does not give an indication of the regenerator performance, which would also influence the COP of a Stirling refrigerator.

2.5 Model Order Analysis of Stirling Machines

There has been an incredibly wide range of mathematical models developed in the attempt to predict Stirling machine performance or to specify beneficial design criteria. They vary from the simple to the complex due to a multitude of different factors, which includes the assumptions available, the solution method used, their degree of realism and so on. This section describes the mathematical models used for the thermodynamic analysis and design of Stirling machines.

Stirling machine models may be grouped into categories which are largely based on the degree of sophistication of the model (N. C. J. Chen & Griffin, 1983). As there are many criteria with which the models can be evaluated, different criteria have been produced to both categorise and assess each one. The customary model order categories are defined below. However, this is a general guideline, as the classification criteria tend to be open to interpretation (Urieli, 1983). A more detailed review and definitions of each category can be found in the reports by N. C. J. Chen and Griffin (1983), Martini (1983), and (Urieli, 1983).

First Order Models

These are approximate design calculations for preliminary predictions of Stirling engine or refrigerator performance. They are also known as ‘back-of-the-envelope’ calculations as they can literally be done on the available paper space on the back of an envelope (Martini, 1983). First order analyses provide a quick and easy relationship between factors such as size, operating frequency, power consumption or output, and efficiency or COP. They are based on ideal assumptions, and further calculations such as losses are accounted for with correction factors from experimental values. This means they can be

used to quickly determine if a Stirling engine is viable for a specified application, or to get an approximate performance for a Stirling machine, but they cannot be used to predict or troubleshoot detailed design parameters.

Possibly one of the most well-known first order models within the Stirling community is the analysis by Gustav Schmidt published in 1871, which produced a series of closed-form solutions for the performance of the Lehmann engine (Schmidt, 1871). This model takes into consideration sinusoidally varying working spaces and assumes isothermal heat transfer. The Schmidt equations are presented, and their solutions are discussed in Section 2.6.

Second Order Models

Second order analyses take the detail a step further than those of the first order by identifying and quantifying individual loss mechanisms rather than just consolidating them into generalised correction factors (N. C. J. Chen & Griffin, 1983). These include, but are not limited to, the equations for gas leakage, fluid and mechanical friction, hysteresis, shuttle heat transfer, and other heat transfer losses. While they are still relatively simple, the fact that the losses are modelled make second order calculations useful for optimising the design of a Stirling machine. The limitation of this type of analysis is that while the losses are modelled, the energy losses due to each loss mechanism are considered independently from one another, which does neither model nor lead to an understanding as to how loss mechanisms interact or affect one another. Due to this disconnected nature, second order models are also known as decoupled design methods (N. C. J. Chen & Griffin, 1983).

Second order models can be categorised into subsections which relate to the way the gas volumes are handled: isothermal, adiabatic, and semi-adiabatic (or polytropic). Isothermal models assume an infinite heat transfer rate, and many of these models are based on the first order Schmidt cycle analysis (N. C. J. Chen & Griffin, 1983; Schmidt, 1871). Adiabatic analyses assume that the heat transfer rate between the gas and walls is zero, while semi-adiabatic analyses include a nonzero heat transfer coefficient.

Adiabatic assumptions are generally more realistic than the isothermal assumption, even though the ideal Stirling cycle has isothermal processes. Isothermal, adiabatic, and

semi-adiabatic models all assume perfect regeneration (N. C. J. Chen & Griffin, 1983). Isothermal models based on the Schmidt analysis generally have closed form solutions, which make them easier to work with, while adiabatic and semi-adiabatic analyses need numerical integration for their solutions because the resulting differential and partial differential equations are too difficult to solve analytically.

Third Order Models

Third order models take into account the interaction between different spaces by dividing the engine or refrigerator into a network of nodes or control volumes, leading to the term also used to describe it: 'nodal analysis' (N. C. J. Chen & Griffin, 1983). The equations of state for each node and the equations of momentum, mass and energy are simultaneously solved for each node, using a chosen numerical method. Third order models can be further subdivided into two branches: rigorous and less rigorous methods (N. C. J. Chen & Griffin, 1983). Rigorous methods solve all the governing equations, while less rigorous methods simplify the calculations by disregarding parts of the governing equations such as inertia within the momentum equation.

While third order models are the most sophisticated in terms of their assumptions and computation requirements, they should be experimentally validated before making any conclusions about the inner workings of the simulated Stirling machine (Martini, 1983). However, a significant benefit of using third order models is that once experimentally validated, one can calculate parameters such as heat flow, temperatures, and pressures within the machine which might be difficult or impossible to practically measure.

The following sections outline the Schmidt theory, one of the first order reference cycles, and Sage, a third-order computer program used for the analysis of Stirling machines, which are used as tools to analyse and understand hysteresis loss in this project.

2.6 Schmidt Theory

The Schmidt cycle provides the foundational loss-free analysis of many first order models upon which the first order correction factors are applied for more realistic performance parameters. While this model is highly idealised, due to the Schmidt analysis assumption for sinusoidal volume variations, it is closer than the ideal Stirling cycle to the actual mechanical operation of Stirling machines. Considering its suitability and establishment within literature, the Schmidt cycle analysis with the isothermal assumptions for Stirling machines as per Walker (1983) is also used as the theoretical ideal limit in this project.

Schmidt Cycle Assumptions

Schmidt assumptions modified for Stirling analysis according to Walker (1983, pp. 134-135):

1. The regenerative process is perfect.
2. The instantaneous pressure is the same throughout the system.
3. The working fluid obeys the characteristic gas equation $PV = mRT$
4. There is no leakage, and the mass of the working fluid remains constant.
5. The volume variations in the working space occur sinusoidally[3].
6. There are no temperature gradients in the heat exchangers.
7. The cylinder wall and piston temperatures are constant[4].
8. There is perfect mixing of the cylinder contents.
9. The temperature of the working fluid in the ancillary spaces is constant.
10. The speed of the machine is constant.
11. Steady state conditions are established.

[3] The volume variations occur sinusoidally with respect to time and are due to the movement of the pistons and displacers.
[4] The temperatures of the walls are constant with respect to time but vary with location.

Schmidt Cycle Equations

The Schmidt cycle model assumes that the expansion and compression spaces vary sinusoidally with the swept volumes being $V_{E,swept}$ and $V_{C,swept}$. The ratio of these swept volumes is $\kappa = \frac{V_C}{V_E}$, while the volume variation of the expansion space leads that of the compression space by the phase angle, α, and the crank angle is θ, which varies from 0 to 360°, or from 0 to 2π. The dead volume of the system is defined as V_D. The volume variation in the expansion and compression space are defined in Equations 1 and 2.

Cyclic volume variation of the expansion space:

$$V_E = \frac{1}{2} V_{E,swept}(1 + \cos(\theta)) \qquad \text{Equation 1}$$

Cyclic volume variation of the compression space:

$$V_C = \frac{1}{2} V_{C,swept}\big(1 + \cos\big(\theta - \alpha_p\big)\big) = \frac{1}{2}\kappa V_{E,swept}(1 + \cos(\theta - \alpha)) \qquad \text{Equation 2}$$

The derivation of the following parameters can be found in Walker's (1983) comprehensive text on cryocoolers. The temperature ratio is the ratio of the compression space temperature to the expansion space temperature, $\tau = \frac{T_C}{T_E}$. The instantaneous pressure over one cycle is defined as:

$$P = \frac{P_{max}(1 - \delta)}{1 + \delta\cos\,(\theta - \phi)} = \frac{P_{min}(1 + \delta)}{1 + \delta\cos\,(\theta - \phi)} \qquad \text{Equation 3}$$

where $\phi = \tan^{-1}\left[\frac{\kappa \sin(\alpha)}{\tau + \kappa\cos\,(\alpha)}\right]$ and $\delta = \frac{(\tau^2 + \kappa^2 + 2\tau\kappa\cos\,(\alpha))^{\frac{1}{2}}}{\tau + \kappa + \frac{V_D}{V_{E,swept}}\left(\frac{4\tau}{\tau + 1}\right)}$

The minimum and maximum pressures in the cycle are at:

$$\theta_{P_{min}} = \phi = \tan^{-1}\left[\frac{\kappa \sin(\alpha)}{\tau + \kappa \cos(\alpha)}\right] \quad \text{Equation 4}$$

and

$$\theta_{P_{max}} = \theta_{P_{min}} + \pi \quad \text{Equation 5}$$

The work done is equal to heat transferred over one cycle:

$$W = \int_0^{2\pi} PdV = -\frac{1}{2}\pi P_0 V_{E,swept}\left(\frac{2\delta}{1 + (1-\delta^2)^{\frac{1}{2}}}\right)\sin(\theta) \quad \text{Equation 6}$$

Thermal efficiency as an engine:

$$\eta_{th} = \frac{Q_E - \tau Q_E}{Q_E} = 1 - \tau = \frac{T_E - T_C}{T_E} \quad \text{Equation 7}$$

COP as a refrigerator:

$$COP_{ref} = \frac{Q_E}{Q_E - Q_C} = \frac{1}{1-\tau} = \frac{T_E}{T_E - T_C} \quad \text{Equation 8}$$

COP as a heat pump:

$$COP_{hp} = \frac{Q_C}{Q_E - Q_C} = \frac{\tau}{1-\tau} = \frac{T_C}{T_E - T_C} \quad \text{Equation 9}$$

Note that these derived equations are the same as the Carnot cycle performance.

2.7 Sage

While heat transfer scenarios with various initial and boundary conditions have been extensively and rigorously modelled by experts in mathematics and physics, the phenomenon of hysteresis loss has, so far, been analysed with comparatively imprecise approaches. Many thermal models for hysteresis rely on steady state modelling which results in a simple amplitude and phase shift response to an input, assuming the mean values of the input and output sinusoids are constant. An explanation for this is the inherent incompatibility of hysteresis loss with steady state methods due to the underlying mechanism of hysteresis loss which causes a change in the overall mean value of the heat transfer, not simply an amplitude and phase shift.

The effect of hysteresis loss on the net value of heat transfer as well as changes in the amplitude and phase lends itself to a more iterative approach. This is due to the interdependence of pressure and temperature, which both influence and are in turn influenced by the gas-wall heat transfer. Another justification for the use of numerical models is the effect of hysteresis loss within multiple spaces of Stirling refrigerators, which has yet to be investigated.

Sage is a numerical software package for Stirling machines, developed by David Gedeon (Gedeon, n.d.). It contains a library of different components whose properties, inputs, and dimensions can be defined by the user. These components are all joined by connections that model flows such as heat flow, mass flow, force, and pressure (Gedeon, 2016). Sage has the ability to model heat transfer processes and fluid friction of oscillating flow – even through porous media such as the regenerator matrix. Each component of the system is analysed in a one-dimensional form subdivided into a user-defined number of spatial increments. In this respect, Sage can be regarded as a very powerful 3rd order model.

While Sage primarily models the thermodynamic behaviour of the working gas, it also accounts for the interaction of the gas with the adjacent walls, as well as heat transfer by conduction in the canister walls in both axial and radial directions. In this sense, Sage is somewhere between a one- and two-dimensional modelling tool. Sage also has the capability to output variables as Fourier series, therefore allowing analysis of the cyclic magnitude and phase for all parameters of interest.

The following sections give a brief overview of how models are set up within Sage, and the underlying equations which govern Sage, and its solution method. For more background to Sage and detailed instructions on how to model specific components, the reader is pointed towards the Sage user manual (Gedeon, 2016) and the paper on Sage and its uses by the creator of Sage himself, David Gedeon (1995).

Sage Model Structure

Sage models consist of a range of components which can be connected in different ways. An example of a Sage model from its topmost level can be seen in Figure 2-5, which shows a two-piston Stirling cooler. The generic cylinder component in Figure 2-6 is commonly used as the compression space and expansion space, as used in Figure 2-5. Different types of channels are used as the heat exchangers (rejector and absorber), and the more complex canister components can be used to model the regenerator.

The compression and expansion spaces, the heat exchangers, and regenerator are all gas-filled components. What makes these components individual are the boundary conditions – each of these components have custom sets of input dimensions which can represent more accurately the specific type of component to be modelled. In these cases, a volume-varying canister of a specific mean volume and diameter, a space with a user-specified number of channels of a specified length and width, or a canister filled with different types of regenerator matrix.

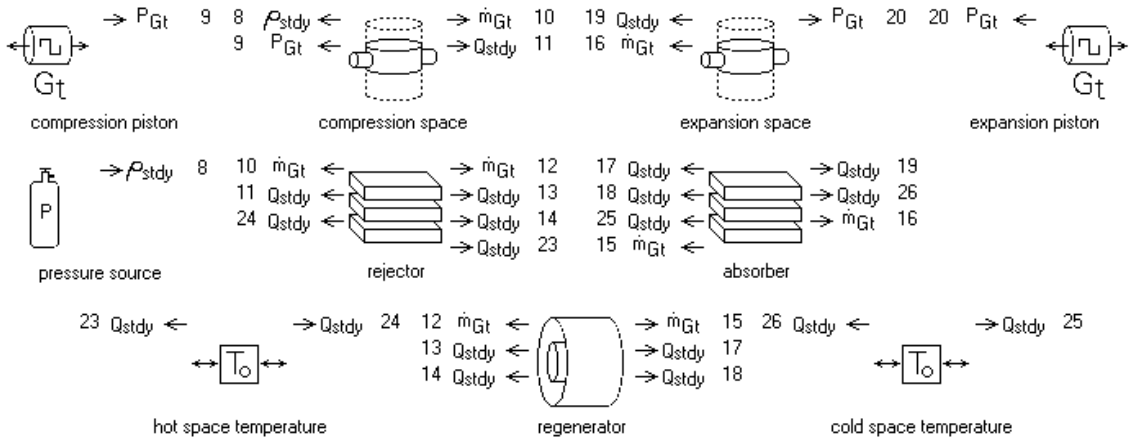

Figure 2-5: A Stirling refrigerator Sage model as seen from the top-level edit window

The moving components (expansion and compression pistons) in Figure 2-5 are simple constrained pistons, but Sage also has many other moving model components such as springs, dampers, flywheels, and even a linear motor model component. These components can be connected to gas-filled spaces by pressure (by using an input area) or force attachments. The attachments used in Figure 2-5 are pressure attachments, as shown by the connection arrow label 'P_{Gt}'. The subscript 'Phsr' (not shown) or 'Gt' stands for phasor or time-ring, respectively, which represents the type of connection. Phasor connections use complex sinusoidal inputs and output variables of the same type, while time-ring component variables also assume periodic motion, but higher harmonics can be specified and are solved on a periodic time grid.

Set temperatures such as wall conditions which represent the hot and cold sinks, or ambient temperature, are set by the temperature source components. As in this model, several temperatures can be specified in different parts of a Sage model. There are two temperature sources in Figure 2-5, which are labelled as the hot space temperature and the cold space temperature. These temperature sources are connected to and set the temperature for component walls by the heat flow attachments.

Gas spaces are joined by heat flow, mass flow, or pressure charge line attachments, shown by the connector arrow labels Q_{stdy}, $\dot{m}_{Gt/Phsr}$, and ρ_{stdy}. The mean pressure of the system is set with the pressure source, which needs to be anchored to only one of the spaces by a gas charge line which sets it for all the other spaces connected by mass flow. In the case of Figure 2-5, the gas charge line is in the compression space.

Attachments, surfaces, and gas domains are specified on different levels within each component, which have their own edit window. These levels are also known as 'child' components. The level hierarchy of a generic cylinder, one of the most basic gas-filled components, is shown in Figure 2-6, with the arrows pointing in the direction of decreasing levels. A more complex component, the regenerator, is shown in the same way in Figure 2-7**.**

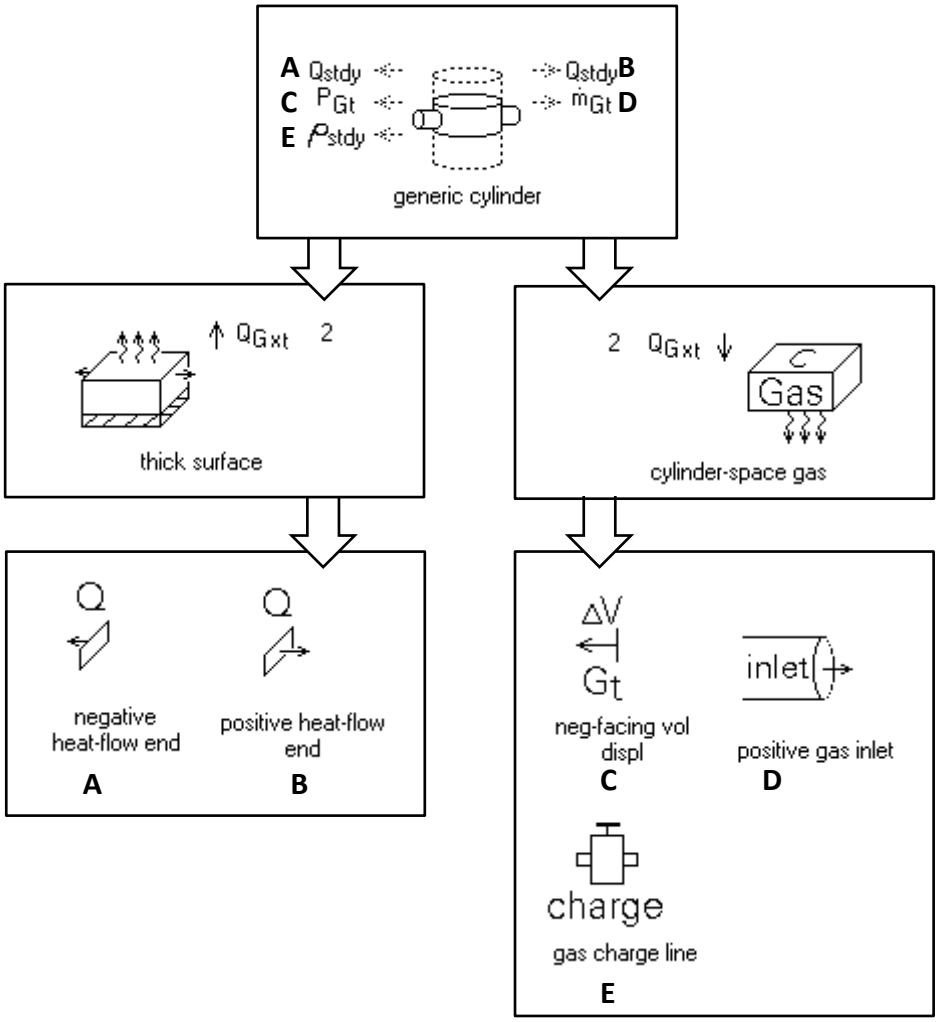

Figure 2-6: Generic cylinder with all 'child' levels

Each gas-filled component has in its first child level a surface component, which represents the walls of the modelled space, and a matrix gas component, which represents the gas within that space. These each have their own child components within which the attachments are placed. In the case of Figure 2-7, since the component shown is a regenerator, it also has the regenerator matrix to consider, so the gas domain is modelled within the matrix structure. There are now two surfaces – the surface that represents the regenerator matrix, which the gas is in direct contact with, and the regenerator wall, which houses the regenerator matrix.

Figure 2-6 also shows how the attachments are defined in the model's lowest levels, and how their corresponding connector arrows can be 'pushed' up to the top level of that component, labelled A through to E. Figure 2-7 shows how child components are connected to each other: the regenerator wall surface contains a positive heat-flow

face, and the regenerator matrix contains a negative heat-flow face. These faces are connected to model the heat transfer between the regenerator wall and matrix.

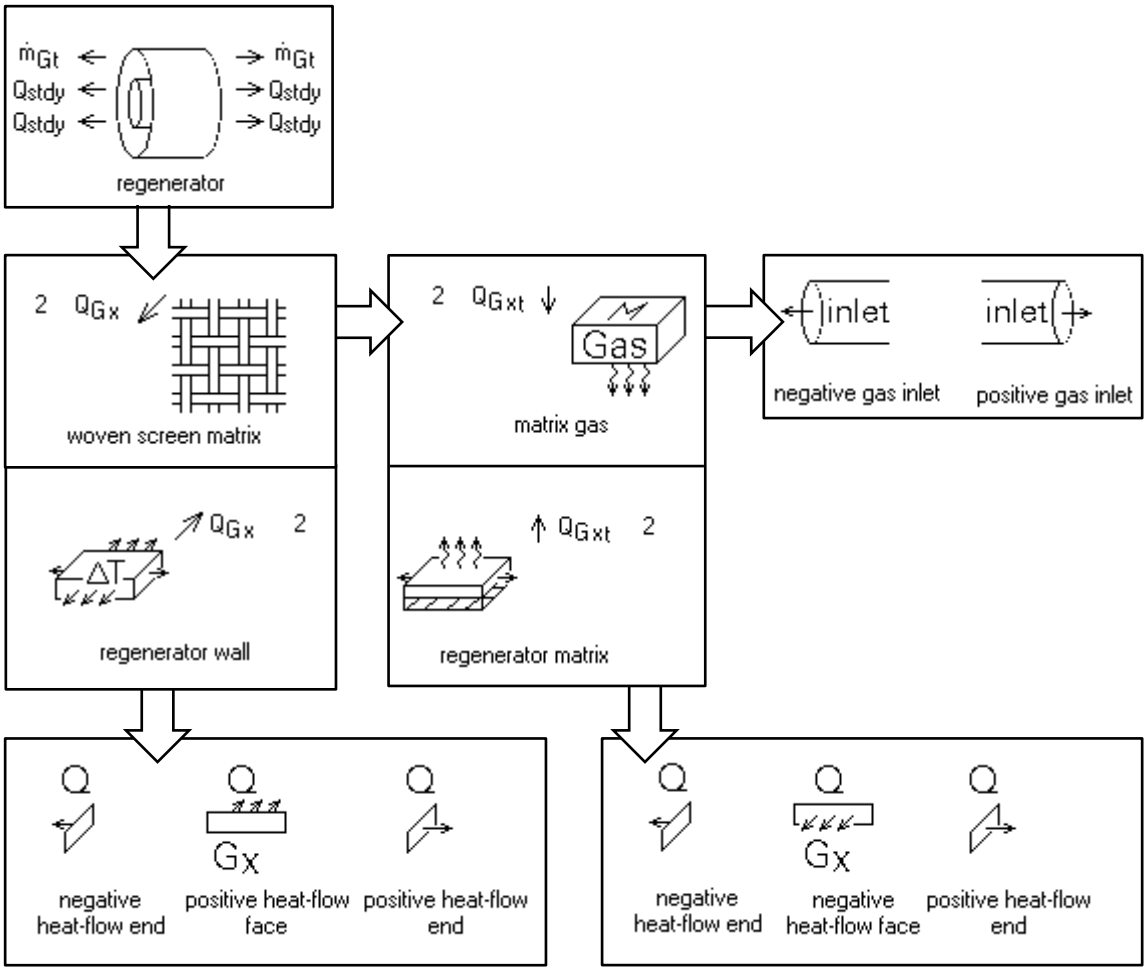

Figure 2-7: Regenerator canister in Sage with all 'child' levels

These components and attachments all represent real physical properties of a system. For example, the cylinder space gas in Figure 2-6 has mass flow only in the positive (right-facing) direction, as there is only a positive gas inlet attachment defined ($\dot{m}_{Gt}$), while the regenerator in Figure 2-7 can have mass flow through the component as it has attachments on both sides. The negative (left-facing) volume displacement in Figure 2-6 (label C) means that the volume is displaced from the left side of the cylinder, so a piston which defines the volume variations of that cylinder can be added on that side.

The ability of Sage to build up models component by component, and the relative ease with which to change these component dimensions makes it an extremely useful modelling tool. Sage also includes a mapping feature, which allows different parameters to be 'mapped', which means that they are varied over a user-defined number of

increments, and the model is solved for each increment. This tool is useful for parameter studies and is used extensively in this project. Another useful feature is the optimisation feature, which allows the user to specify a parameter to be maximised or minimised for a range of user-defined constraints.

Sage uses the model components to create a large system of non-linear equations, which is solved in the frequency domain. The theory behind these equations and Sage's solution method will be briefly covered in the following section. These are summarised from the Sage user manual, which should be consulted for a more in-depth explanation of anything pertaining to Sage.

Gas Domain Theory

Sage applies a variation of the three basic momentum, continuity, and energy equations to each control volume. They are not in the standard form as they are designed specifically for one-dimensional internal flows with space- and time- variable flow area (Gedeon, 2016). The starting integral form equations are listed below in Equations 10-12. In these equations, the control volume, v, is fixed only at the inlet and exit boundaries, but considers moving side boundaries which consist of time-variable flow areas. However, these side boundaries are impermeable so that flow only enters and leaves through the inlet and exit boundaries.

Continuity: $$\frac{d}{dt}\int_v \rho dv + \int_s \rho n \boldsymbol{V_r} ds = 0 \qquad \text{Equation 10}$$

Momentum: $$\frac{d}{dt}\int_v \rho \boldsymbol{V} dv + \int_s [(n\boldsymbol{V_r})\rho \boldsymbol{V} - n\boldsymbol{\sigma}] ds = 0 \qquad \text{Equation 11}$$

Energy: $$\frac{d}{dt}\int_v \rho e dv + \int_s n(\rho e \boldsymbol{V_r} - \boldsymbol{\sigma V} - \boldsymbol{q}) ds = 0 \qquad \text{Equation 12}$$

where $e = \varepsilon + u^2/2$ (the mass-specific total gas energy), $\boldsymbol{n}$ = unit outward normal of s, $\boldsymbol{q}$ = heat flux vector, t = time, v = control volume, $\boldsymbol{V}$ = Newtonian-frame flow velocity vector, $\boldsymbol{V_r}$ = boundary-relative flow velocity vector, ε = mass-specific internal gas energy, ρ = gas density, and $\boldsymbol{\sigma}$ = stress tensor.

The continuity equation states that the time rate of change of mass into the control volume is equal to that leaving the control volume through the inlet and exit boundaries.

The momentum equation is the equation form of Newton's second law of motion: the difference between the control volume time rate of change of momentum and the momentum leaving through its surface boundaries is equal to the net force acting on all surfaces.

Finally, the energy equation is a statement of the first law of thermodynamics: the time rate of change of the control volume's internal energy plus kinetic energy minus the energy leaving through its surface boundaries is equal to the net heat flux and the mechanical work through its boundaries.

For these equations to be applied within Sage, they must be converted to one-dimensional differential equations in conservative form. For all equations, dv in the time integrals is replaced with Adx, where A is the flow area and x is the principal flow direction. The limit $\Delta x \rightarrow dx$ is applied, and the equation is divided through by dx. The considerations for the surface integrals are also applied, accounting for the unique inlet, outlet, and side boundary conditions. The derivation of each one-dimensional differential equation is covered in the Sage user manual. The resulting one-dimensional differential equations are as follows:

Continuity: $$\frac{\partial \rho A}{\partial t} + \frac{\partial \rho u A}{\partial x} = 0$$ Equation 13

Momentum: $$\frac{\partial \rho u A}{\partial t} + \frac{\partial u \rho u A}{\partial x} + A\frac{\partial P}{\partial x} - FA = 0$$ Equation 14

Energy: $$\frac{\partial \rho e A}{\partial t} + P\frac{\partial A}{\partial t} + \frac{\partial}{\partial x}(u\rho eA + uPA + q) - Q_w = 0$$ Equation 15

where u = the mean-flow velocity in the x direction, P = pressure, and F = a viscous flow resistance, which is equal to the force per unit length per unit flow area due to shear stress. The empirical terms F, Q_w, and q are explained in the Sage User's Guide (Gedeon, 2016).

Solution Method

Sage uses the three gas dynamic equations to determine the three independent solution variables: ρ, ρuA, and ρe. These variables are used to determine the dependent variables pressure, $P(\rho, T)$, and temperature, $T(\rho, \rho e, \rho uA)$ using the inbuilt gas property functions within Sage.

Each of the control volumes are discretised over their spatial domain and the cycle period. The solution variables are solved or interpolated explicitly with 'staggered grid' logic: ρuA is solved at alternate nodes in the spatial direction from ρ and ρe. This staggered grid scheme prevents solution instability. It also creates global conservation of mass, momentum, and energy when a first-order central differencing method is applied to the continuity and energy equations.

Sage uses a non-linear solver to iteratively solve the large system of those gas dynamic non-linear equations, whose boundary conditions, degree of discretisation, and control volume dimensions are set by user input to their respective model components. The solver solves a sequence of linear approximations to the non-linear equations and uses the results to set a direction along which to search for the non-linear solution, repeating the process until the non-linear model equations are all satisfied within a certain error range. Readers familiar with numerical techniques would recognise this as Newton's method, which is a relatively fast solution method but encounters some problems when the initial approximation is far from the actual solution, resulting in the solver cycling around local maxima or minima, or diverging towards infinity. More on the underlying mathematics and tolerances of the solver can be found in the Sage user manual.

Prediction Accuracy

While Sage is a conventional modelling software used for simulation of Stirling machines, the errors and validity of this software are important to understand. The use of Sage as a modelling tool is also shown here through a survey of experimentally validated studies.

In as early as 2003, Qiu and Peterson from the Stirling Technology Company (now INFINIA Corp.) found that their un-calibrated models had an expected accuracy of 10 - 20% while the models calibrated over a range of test data were expected to have

accuracy within 5% (Qiu & Peterson, 2003). It should be noted that these data were produced using an earlier version of Sage, which has been refined further in the last 20 years.

Metscher (2014) carried out a model development, validation, and analysis of a free-piston Stirling convertor for space power systems in Sage. The model was tuned with test data from Sunpower Inc., which was then validated against experimental data. They compared efficiency and power output for varying rejector temperatures. It was found that the Sage models agreed with experimental data with a maximum error of 7% (Metscher, 2014).

Zhao, Li, Li, Zhang, and Qiu (2021) developed 3D models of both fluid dynamics and heat transfer within a free-piston Stirling engine. The Stirling engine were modelled in ANSYS Fluent, and a steady simulation without oscillating flow was used to initialise the computation, and then a transient simulation was employed in both fluid and solid domains, with oscillating pressure-inlet boundary conditions. They found that the CFD results for pressure drop in the regenerator are “nearly the same” (Zhao et al., 2021, p. 1) as Sage results, but the pressure drop inside the cold heat exchanger had a 10.43% difference.

In 2022, Chen, Zhong, Niu and Liu compared a thermodynamic-dynamic tuned Sage model of an advanced Stirling radioisotope generator to experimental data from Oriti and Blaze (2007). It was found that the maximum deviations for the output power and efficiency between the Sage model and experiment were approximately 6.1% and 6.4%, respectively (P. Chen, Zhong, Niu, & Liu, 2022).

2.8 Hysteresis Loss Related Studies

The following studies provide a more detailed background to the study of heat transfer within cylinders undergoing compression and expansion. While some are not completely applicable to the study of hysteresis loss, they provide a foundation upon which hysteresis loss came to be understood and modelled throughout time.

Annand (1963) and Woschni (1967)

Annand and Woschni studied the heat transfer within the cylinders of spark-ignition engines. Annand carried out a review of then-existing formulae for instantaneous heat transfer and found that many of the models failed in certain aspects ((Nusselt, 1923), Eichelberg (1922), Elser (1954), Briling and Chirkov and Stefanovski as per Chirkov and Stefanovski (1958), Oguri (1960), Overbye, Bennethum, Uyehara, and Myers (1961), and (Pflaum, 1961)).

They proposed that a power relationship akin to Chirkov and Stefanovski's equation between the Nusselt and Reynolds numbers was more suitable for modelling instead of the previous linear relationships of Nusselt and Briling, but modified it to be simpler and dimensionally consistent (Annand, 1963):

$$Nu = aRe^{b} \qquad \text{Equation 16}$$

where a and b are experimentally obtained coefficients.

The total heat flux was then taken as the sum of the convection and radiation heat fluxes, where the radiation is multiplied by a coefficient, 'c', which ≡ 0 during compression, and c = a constant during combustion and expansion which varies with surface type and combustion mode. Woschni also derived an equation to predict the instantaneous heat transfer coefficient which was more complex than that of Annand and can be found in his 1967 paper (Woschni, 1967).

While the conclusions from this study are not so relevant to the study of hysteresis loss as they involve combustion in the cylinders of spark-ignition engines, the degree of success when predicting heat transfer within internal combustion engines must be recognised. While they are less applicable to the steady state analysis of gas springs due

to the omission of the phase lag between temperature difference and heat transfer, they can still give insight into trends which can be expected. With Elser's experimental data, Annand showed that the heat flux increased during the compression stroke, which shows the heat transfer is driven by the temperature increase due to the work input of the piston alone, as can be seen in Figure 2-8. Of course, due to the combustion within the cylinder, the heat flux peaks after TDC, presumably around the point of combustion.

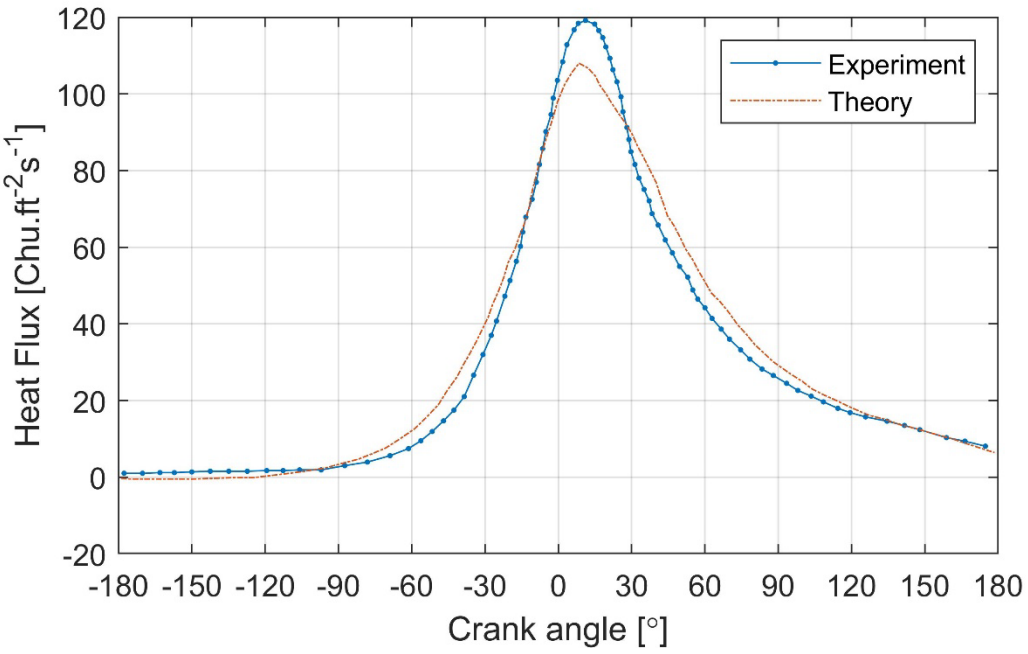

Figure 2-8: Annand's heat flux equation compared with Elser's experimental data for a four-stroke engine at full load, adapted from (Annand, 1963, p. 981)

Nikanjam and Greif (1978)

Nikanjam and Greif (1978) carried out an experimental and theoretical investigation into unsteady heat transfer during the compression of a single cylinder device. Their analytical model was based on the solution of laminar boundary equations within a gas, and these results agreed well with their experimental results for air and argon. They also proposed the heat transfer coefficient as a function of time. They found that the heat flux also increased substantially as the piston approaches the end of the compression stroke, shown in Figure 2-9.

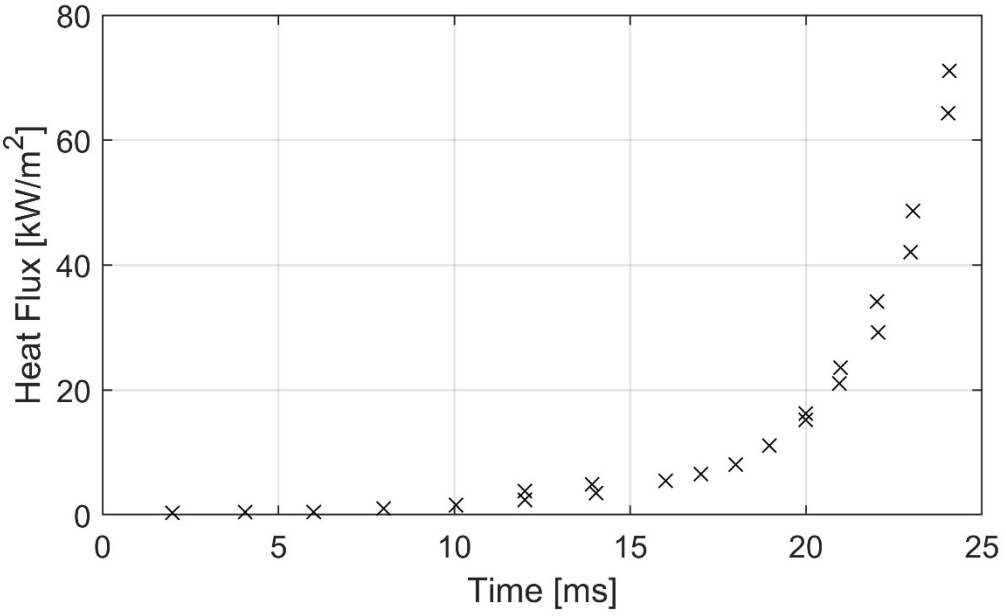

Figure 2-9: Heat flux vs time results adapted from Nikanjam and Greif (1978, p. 529)

Lee, Smith, and Faulkner (1980)

Lee, Smith, and Faulkner (1980) presented a closed form expression for cyclic heat transfer power loss in a Stirling engine based on first harmonics of pressure, volume, and temperature. This heat transfer power loss is defined as the difference in adiabatic net P-V work and the real P-V work:

Cyclic Heat Transfer Power Loss =

$$f\left[\oint_E (P - P_{adiabatic})\, dV_E \; + \oint_C (P - P_{adiabatic})\, dV_C \right] \qquad \text{Equation 17}$$

This was based on the assumptions of isothermal heat transfer in the heat exchangers and the pressure wave being constant in all spaces. They used multiple enhancement factors which were calculated from empirical correlations. They also referenced another second order, adiabatic analysis (Foster-Miller Associates, 1980) which showed that this loss could be as high as 10% of the power output of a Stirling engine, but do not mention Stirling refrigerators.

Lee (1983)

Lee (1983) developed a simple analytic heat transfer model which produced correlations for a non-dimensional cyclic loss against a non-dimensional hydraulic radius. His model comprised of a layer of ideal gas between two parallel walls, at mean temperature T_0, whose pressure variation was driven by the periodic volume changes. The wall-to-gas heat transfer was modelled with a simplified energy equation for which the derived equations can be found in Appendix B. The non-dimensional power loss was given by the integral $\int PdV$, and normalised against the adiabatic compression work:

$$Loss_{ND} = \frac{\oint PdV}{P_0 V_0 \left(\frac{P_a}{P_0}\right)^2 \frac{\gamma - 1}{\gamma}} \qquad \text{Equation 18}$$

where P_0 = mean pressure, P_a = pressure amplitude, V_0 = mean volume, and γ = the specific heat ratio.

In this study, it was suggested that power loss is strongly dependent on heat transfer and its phase difference with the bulk gas temperature. Most importantly, this model predicted a peak in the loss when plotted against the non-dimensional hydraulic radius, as shown in Figure 2-10, which Lee suggests that a transition from low to high non-dimensional hydraulic radius represents a transition from isothermal (r = 0) to adiabatic (r = ∞) cases.

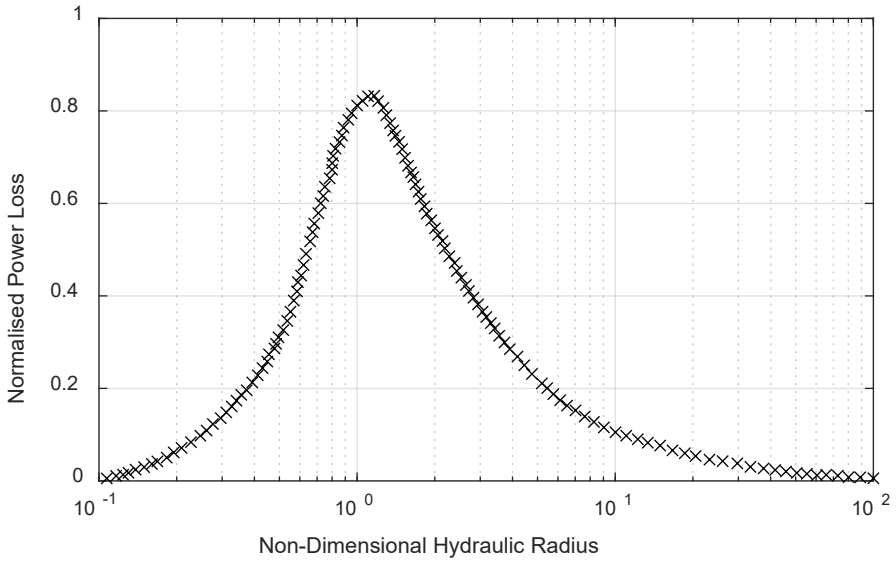

Figure 2-10: Normalised power loss vs non-dimensional hydraulic radius, adapted from Lee (1983, p. 723)

Urieli and Berchowitz (1984)

Urieli and Berchowitz based their equation to predict hysteresis loss on Lee et al. (1980). They assumed a 2-dimensional problem with negligible leakage and viscous dissipation. They used constant specific heats and assumed that the heat capacity of the wall was much larger than that of the gas, which meant that the wall temperature was taken as a constant. They came up with the following equation for hysteresis loss:

$$\dot{W}_{hyst} \cong \sqrt{\frac{1}{32}\omega\gamma^3(\gamma-1)T_w p_{mean} k}\left(\frac{\Delta V}{V_B}\right)^2 A_w \qquad \text{Equation 19}$$

where V_B = the mean gas spring volume, ΔV = the volume amplitude, and A_w = the wetted area.

They suggest that this equation can be used for sizing gas spring geometries and that the volume ratio and the wetted area be kept small to reduce hysteresis loss. They also stress the importance of the location of the gas spring; to position it in a location where the wall temperatures are lowest. They state that hysteresis loss is small enough that it can be considered negligible in machines 1 kW and larger.

Pourmovahed and Otis (1984, 1990)

Pourmovahed and Otis studied this thermal loss for a hydraulic motor-accumulator system. They extended the work of Svoboda et al (Svoboda, Bouchard, & Katz, 1978), and Graze (Graze & Forrest, 1974), who established methods of computing thermal time constants for similar applications such as air chambers and fluid systems. They derived a linearised mathematical solution for a non-dimensional pressure amplitude and phase lag, and derived a theoretical thermal time constant for pressure relaxation at constant volume after rapid compression (Pourmovahed & Otis, 1984; Pourmovahed & Otis, 1990).

Their results were based on a dynamic analysis which is represented by a double spring and dashpot system presented by Zener (1948), shown in Figure 2-11. Their models show a peak in pressure amplitude rather than the non-dimensional power loss depicted

in Lee's case, in between the isothermal and adiabatic limits in Figure 2-12, and that the phase shift of pressure changes between 0 and 180° at resonance. They did not state an equation for the hysteresis loss, but since a function for pressure is given, it could be found by integrating their pressure equation over one cycle.

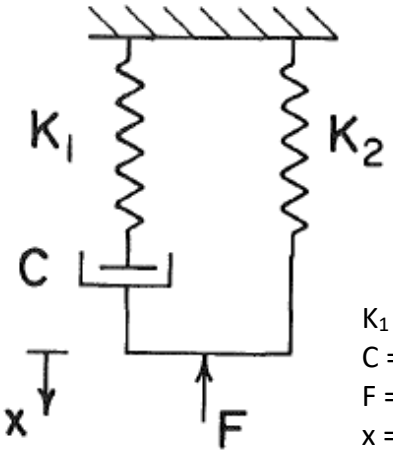

K_1 and K_2 = spring constants [N/m]
C = damping coefficient [Ns/m]
F = driving force [N]
x = displacement [m]

Figure 2-11: Linearised model for the hydraulic motor-accumulator system from (Pourmovahed & Otis, 1984, p. 22)

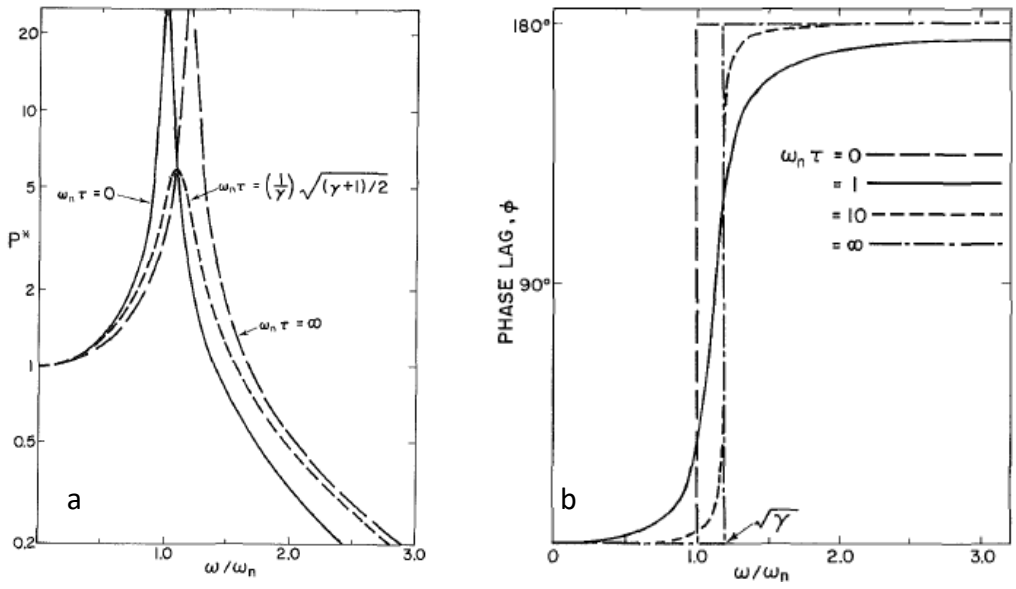

Figure 2-12: a) Dimensionless pressure amplitude, P, and b) phase lag, ϕ, versus the frequency ratio, from (Pourmovahed & Otis, 1984, p. 25)*

Cooke-Yarborough and Ryden (1985)

Cooke-Yarborough and Ryden developed analytical calculations for the mechanical power losses caused by imperfect heat transfer in a nearly-isothermal Stirling engine (Cooke-Yarborough & Ryden, 1985). This engine was a thermo-mechanical generator which used a spring-mounted displacer and a metal diaphragm for the power input. This meant that the effective stroke was extremely short and shallow, and the working volumes extremely small. Their analysis resulted in a peak pressure and phase shift equation, and an equation for the mean rate of energy dissipation (power) needed to compress and expand a unit volume of gas, but in relation to a 'cavity gap', or the length of their working space, from 0 to 4 mm. The resulting pressure amplitude, phase shift, and power loss equations are given in Appendix C. They concluded that the power loss due to temperature fluctuations of the gas could be important, however, their analysis was only accurate if the working gas volume is small, the gas flow is laminar, and the gas temperature distribution is consistent between spaces.

Orlowska and Davey (1987)

Orlowska and Davey experimentally measured the losses in a miniature split Stirling cycle refrigerator in 1987 (Orlowska & Davey, 1987). Their focus was on measuring all power losses, rather than heat transfer hysteresis loss in particular. They defined hysteresis loss as the "effect of irreversible compression" and measured it as the net P-V work input while the displacer was held stationary to ensure that the refrigeration effect was neglected. Unsurprisingly, they found this was equivalent to the net electrical work input minus electrical power losses (Joule heating losses), which is the actual power transferred to the gas. The most significant finding was that for specified piston amplitudes, hysteresis loss was independent of frequency and concluded that it is a fixed loss per cycle. However, as this conclusion was drawn from the P-V work measured from the displacer being held stationary, it cannot be concluded that the loss would be the same under normal operating conditions.

Kornhauser, Chafe, Scheck, and Wang (1987 – 1993)

In the late 1980's to 1990's, Scheck, Chafe, Kornhauser, and Wang carried out several studies investigating gas spring heat transfer at MIT (Chafe, 1988; Kornhauser, 1989; Kornhauser & Smith, 1987; Scheck, 1988; A. C.-M. Wang, 1988).

Scheck developed empirical equations based on the test results for different working gases, and the experiments were based on a transient, free vibration setup. These empirical results were compared against the theoretical hysteresis power loss equations presented in Table 2-3. Their success was limited in terms of predicting the thermal hysteresis loss – both experimental and analytical results differed greatly. The empirical results were only marginally closer than the analytical predictions, and the empirical relations still needed to be multiplied by a factor that ranged between 0.03 and 5.9 to match with experimental data (Scheck, 1988).

Table 2-3: Gas spring models, from Scheck (1988, p. 29)

Author	Hysteresis power loss equation [W]
Breckenridge, Heuchling, and Moore (1971)	$\dot{W} = \frac{1}{2}\gamma^{\frac{1}{2}}(\gamma-1)^{\frac{3}{2}}\sqrt{\pi k f P_0 T_0}(r_{\Delta V})^2 A$
Gedeon (1976)	$\dot{W} = \frac{1}{2}\gamma^{\frac{1}{2}}(\gamma-1)^{\frac{3}{2}}\sqrt{\pi k f P_0 T_0}(r_{\Delta V})^2 A$
Berchowitz (1979)	$\dot{W} = \frac{1}{4}\gamma^{\frac{3}{2}}(\gamma-1)^{\frac{1}{2}}\sqrt{\pi k f P_0 T_0}(r_{\Delta V})^2 A$
Polman (1981)	$\dot{W} = \frac{1}{\sqrt{2}}\gamma^{\frac{1}{2}}(\gamma-1)^{\frac{3}{2}}\sqrt{\pi k f P_0 T_0}(r_{\Delta V})^2\ G(\lambda)H(\Delta A)$

where γ is the specific heat capacity ratio, k is the thermal conductivity, f is the oscillation frequency, P_0 and T_0 are the mean pressure and temperature respectively, $r_{\Delta V}$ is the gas spring volume ratio, A is the wetted heat transfer area, and $G(\lambda)$ and $H(\Delta A)$ are coefficients to account for the thermal boundary thickness, λ, and the variable heat transfer area, ΔA.

Scheck concluded that a Stirling engine typically loses 5% of its output power to thermal hysteresis but can lose up to 25% if the engine is small and operates at high frequencies. Scheck also suggested that *"an isothermaliser, in the form of a high surface area, high*

heat capacity matrix, could be installed in the spring cavity in pursuit of the ideal loss-less gas spring" (Scheck, 1988, p. 76), as was investigated by Breckenridge et al. (1971).

Both Chafe and Kornhauser used the Peclet number as a non-dimensional quantity to normalise the results for different working gases, operating frequencies, and cylinder dimensions. There were two Peclet numbers used – the linear velocity Peclet number, Pe_v, using the mean piston speed, V_p, or the oscillation Peclet number, Pe_ω, using the rotational frequency of the piston:

$$Pe_v = \frac{V_p D}{\alpha_0} \qquad \text{Equation 20}$$

where D = the cylinder diameter, $V_p = \frac{2S}{Tp}$ the average piston speed, and $\alpha_0 = \frac{k_0}{\rho_0 C_{p,0}}$, the mean thermal diffusivity of the working gas.

$$Pe_\omega = \frac{\omega {D_h}^2}{4\alpha_0} \qquad \text{Equation 21}$$

where $D_h = \frac{4V_0}{A_{s,0}}$, the mean hydraulic diameter of the cylinder.

The work of Kornhauser and Smith (1987) and Chafe (1988) used the piston linear velocity in the calculation of the Peclet number. Studies by Kornhauser from 1989 onwards, and by A. C.-M. Wang (1988) used the oscillation Peclet number.

Chafe carried out experiments at three different temperatures: room temperature, 77 K, and near liquid helium temperature. It was found that regardless of operating temperature, the hysteresis loss had a strong correlation to the "$SPEED$" dimension, a 'non-dimensional speed' which varied from a Peclet number relationship to a variable, 'τ', as defined in Appendix D (Chafe, 1988). Chafe also stated that the most important factors influencing gas spring heat transfer were the gas properties, and not the cylinder

wall properties. He also found that the hysteresis losses were the highest when recorded around near-ambient operating temperatures.

Kornhauser and Smith (1987) extended Lee's model to calculate pressure magnitude and phase, and defined the non-dimensional hysteresis loss as the practically measured cyclic lost work in a piston cylinder device divided by the adiabatic compression work, as given in Equation 18 by Lee (1983).

For all Kornhauser's studies, the experimental setup was a single-space piston-cylinder device, shown in Figure 2-13. This apparatus was modular, so the bore-stroke ratio could be varied, and the area for heat transfer could be changed by addition of different numbers of brass fins. The piston was driven by a DC motor, and cylinder pressure was measured using strain-gauge pressure transducers. The volume was calculated via the crank-connecting rod relationship and angle measured using an optical encoder.

The working gas, amount of heat exchanger fins, bore-stroke ratio and volume ratios were all varied in Kornhauser's experiments. The 'baseline' case had no fins, used helium as the working gas, and the bore-stroke and volume ratios were 0.67 and 2.0, respectively (Kornhauser, 1989). The cyclic lost work was found by integration of the pressure and volume data and normalised using Equation 18.

The pressure wave magnitude and phase shift were calculated through a Fourier analysis of the pressure and volume data, with only the first harmonics considered. The non-dimensional loss and pressure magnitude and phase shift were all recorded for a range of operating frequencies, from 0.034 Hz to 16.8 Hz. This range was chosen as it was the widest range that the apparatus and instrumentation allowed (Kornhauser, 1989).

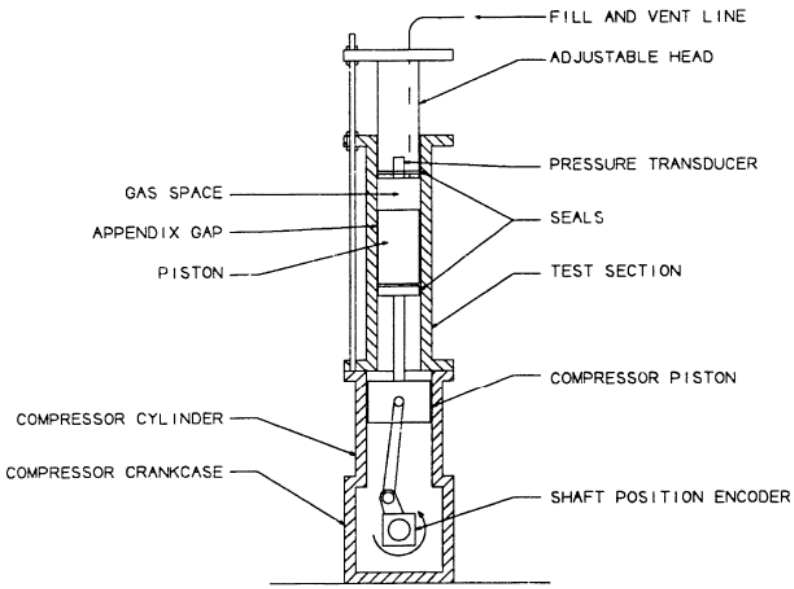

Figure 2-13: Kornhauser's single-space experimental setup from Kornhauser (1989, p. 21)

Kornhauser compared the measured, non-dimensional hysteresis loss to the theoretical expressions of Annand (1963), Woschni (1967), Breckenridge et al. (1971), Otis (1974), Svoboda et al. (1978), Lee (1983), and Cooke-Yarborough and Ryden (1985). It was found that of all models, the Cooke-Yarborough and Ryden prediction best matched the experimental data of Kornhauser and Smith (1987).

Kornhauser then predicted the non-dimensional loss, pressure magnitude and phase based on Lee's model, and compared them with experimental results. Kornhauser's experimental data fit the theoretical prediction very well, as shown in Figure 2-14 to 16. This reinforced the findings of Lee: the non-dimensional loss peaks in an area between isothermal and adiabatic conditions. However, it should still be noted that their experimental non-dimensional results exceed unity by far – reaching over 1.5 in its peak area.

The non-dimensional pressure magnitude and phase were calculated based on the adiabatic pressure wave. Interestingly, the pressure phase lead follows the same trend as the non-dimensional loss, with a maximum at approximately Pe_ω = 10. The non-dimensional pressure magnitude, however, follows a curve which rapidly increases to be equal to the adiabatic pressure magnitude.

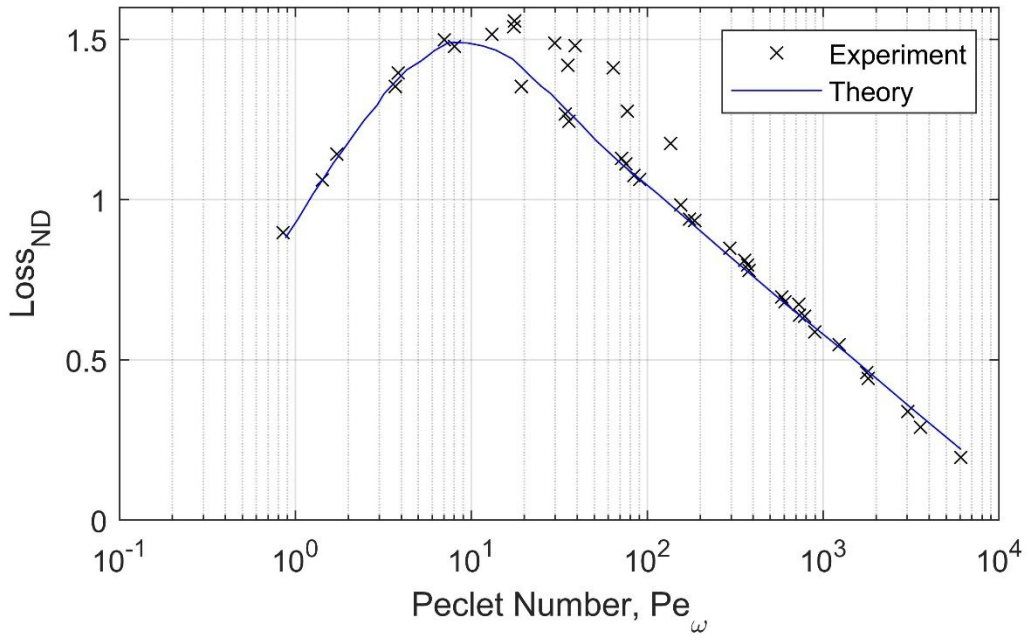

Figure 2-14: Experimental and theoretical non-dimensional loss vs Peclet number for Helium, adapted from Kornhauser (1989, p. 48)

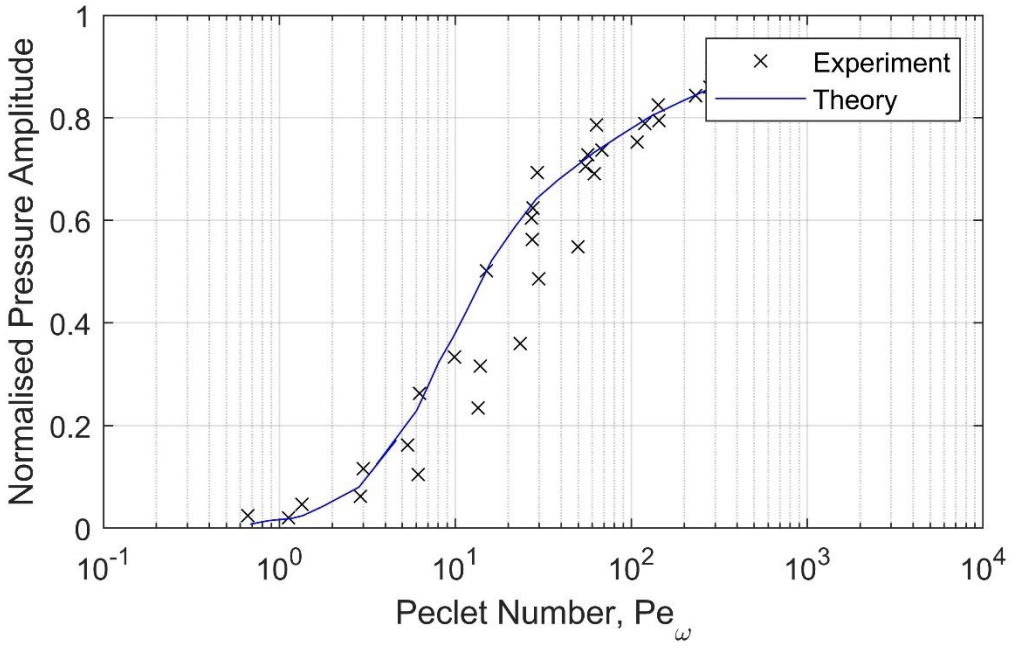

Figure 2-15: Experimental and theoretical normalised pressure amplitude vs Peclet number for Helium, adapted from Kornhauser (1989, p. 60)

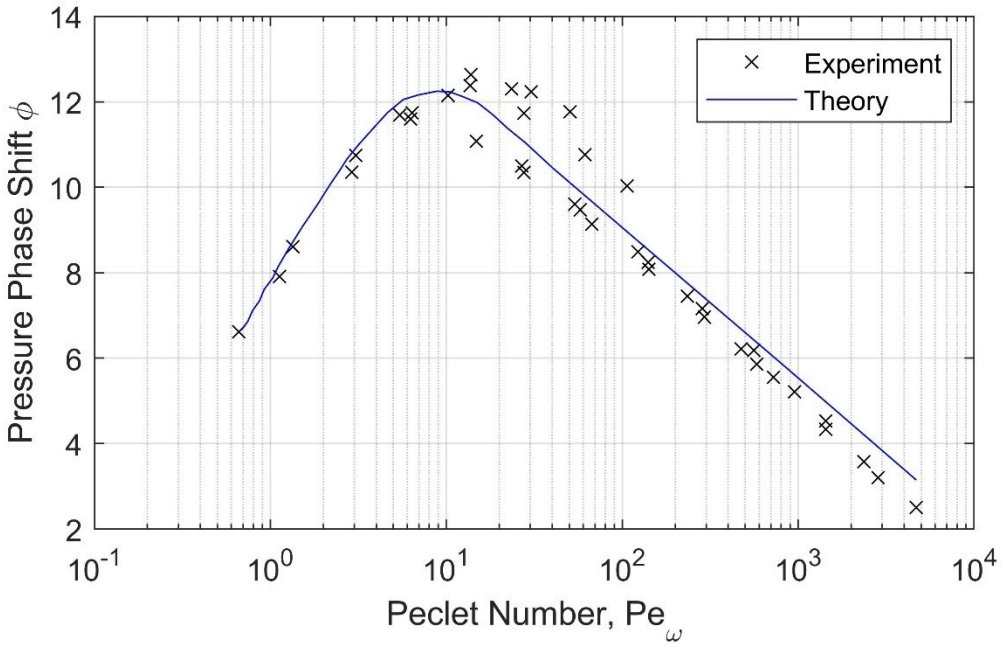

Figure 2-16: Experimental and theoretical pressure phase shift vs Peclet number for Helium, adapted from Kornhauser (1989, p. 60)

Kornhauser and Smith (Kornhauser & Smith, 1994) also proposed a relationship for the complex Nusselt number to account for the phase shift between heat transfer and the bulk gas temperature difference. They converted an equation by Annand and Pinfold (1980) for a real Nusselt number expression into a complex one, resulting in Equation 22, and they found that for high Peclet numbers, the real and imaginary parts are approximately equal, shown in Equation 23**.**

$$Nu_{complex} = 0.3Re^{0.7} + \left(0.25\frac{D}{S}Re^{0.7}\right)i \qquad \text{Equation 22}$$

$$Nu_{real} = Nu_{imaginary} = 0.56(Pe_\omega)^{0.69} \quad for\ Pe_\omega \geq 100 \qquad \text{Equation 23}$$

Wang investigated the origin of hysteresis loss assuming three different causes: gas mixing during inflow to the cylinder, mixing during outflow from the cylinder, or gas-to-wall heat transfer in the cylinder (A. C.-M. Wang, 1988, p. 32). He used a numerical computer model to solve his governing equations as a steady state boundary value problem. State variables initialised at the beginning of the cycle at 0°, and then

compared when it reaches 360°. If the initial and end values do not fall within an acceptable difference, the state variables are initialised again with the previous end values, and the calculation is carried out again until the solution converges. Wang evaluated the previous heat transfer models of Lee and Kornhauser and Smith using this model and concluded that the equations were not adequate for making accurate heat transfer predictions.

Park and Chang (1997)

Park and Chang applied the heat transfer predictions of Lee & Smith (Lee et al., 1980), Kornhauser & Smith (1994), and Jeong and Smith Jr (1992) to a modified ideal adiabatic analysis of the Stirling cycle by adding the heat transfer term in the energy balance equation, as seen in Equation 24, which was numerically solved with the 4th-order Runge-Kutta method (Park & Chang, 1997).

$$\frac{dm}{dt} = \frac{1}{RT^*}\left\{p\frac{dV}{dt} + \frac{V}{\gamma}\frac{dp}{dt} - \frac{\gamma - 1}{\gamma}\dot{Q}\left(T, \frac{dp}{dt}, \frac{dT}{dt}\right)\right\} \qquad \text{Equation 24}$$

The results for the cyclic pressure variation with the Jeong-Smith model are shown in Figure 2-17. They did not show the cyclic pressure variation for the Kornhauser-Smith relations, nor did they quantify the pressure phase shift for each. However, from Figure 2-17, the predicted pressure phase shift does not have a peak. Instead, it has a steady increase in phase shift from isothermal to adiabatic operating frequencies. Since the Kornhauser-Smith results are not shown, it is not clear whether this is due to the use of the Jeong-Smith relationships or the derived mass and energy balance equation.

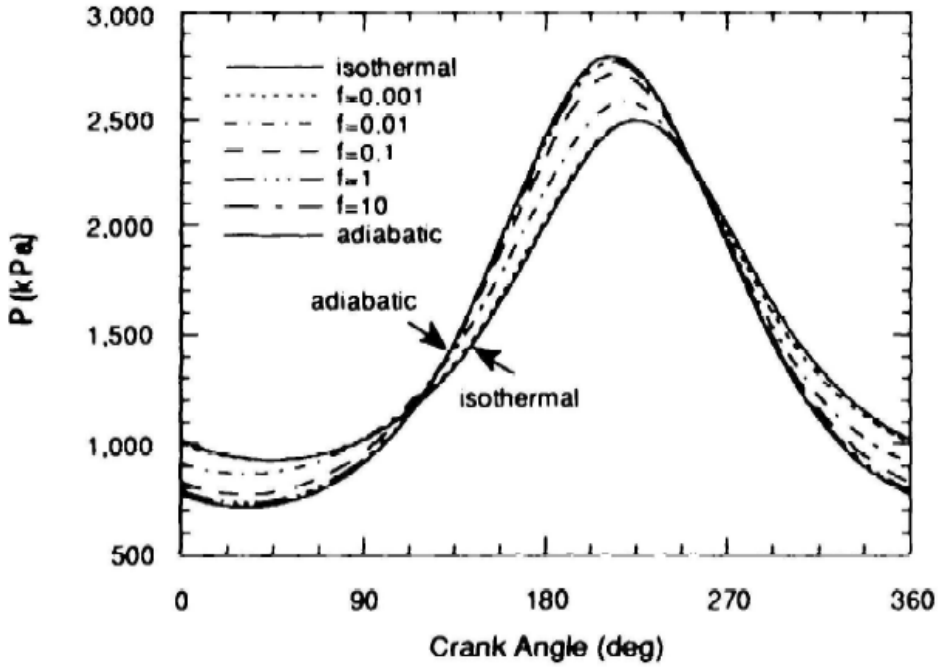

Figure 2-17: Pressure variation over a cycle for various frequencies for Jeong-Smith model from Park and Chang (Park & Chang, 1997)

In contrast to previous studies, they concluded that the effect of hysteresis would be negligible except in the case of low-speed miniature coolers. While this may be the case, their reasoning is based on the COP calculations. There is no discussion on pressure phase shift, and minimal evidence or analysis is provided in terms of their conclusions and validation of results, so a more detailed exploration of how and why this loss may be negligible in Stirling coolers is needed.

Bailey, Dadd, Stone, Reed, and Davis (2007)

Bailey et al. (2007) studied a clearance seal linear compressor attached to a simple gas spring volume. They wanted to understand how relevant Lee, Kornhauser and Smith's correlations were when clearance seals were used instead of normal sliding seals. They measured static flow through the clearance and measured this flow for a variety of piston positions and used these measurements to estimate seal losses. They calculated the gas spring loss by measuring the P-V work done by the piston and subtracting the estimated seal losses. They presented the results for helium, krypton, neon, and nitrogen over a range of frequencies and strokes. They found that Kornhauser's modified version of Lee's equation gave good results and were still valid for clearance

seal machines, once the seal loss had been accounted for. However, they also noted that their data in the Peclet number range from 1 to 10 had significant scatter, and indicated that more work is required to determine compression losses within this region for real cryocoolers.

Willich, Markides and White (2017)

Willich, Markides, and White (2017) presented a computational fluid dynamic (CFD) study of heat transfer losses in gas springs, which was part of their work in high-efficiency compression and expansion devices in energy conversion applications. They ran two simulations of single-cylinder compression and expansion: one simulation of Kornhauser's experiment (Kornhauser & Smith, 1994) and one resembling an experiment by Mathie, White, and Markides (2014), which has a higher compression ratio. They also used the Peclet number to determine a range of near-isothermal and near-adiabatic working conditions. As the CFD simulation models the internal fluid dynamics and heat transfer within the cylinder, they were able to determine that the wall heat fluxes can have a large variance across the internal surfaces due to flows within the cylinder. Their focus was more on understanding how valve flows affected this heat transfer loss, so they also ran their model with a flat perforated plate (an 'internal grid') within the cylinder to simulate the flow of gas through valves. They found that hysteresis losses are small, but with the internal grid this loss can increase significantly at adiabatic speeds. While they clarify that the internal grid is not an exact representation of real valve flows, they note that the resulting irreversibilities could be an important limiting factor in reciprocating machines.

Li and Grosu (2017)

Li and Grosu carried out a parameter effect analysis for a Stirling cryocooler. They used an isothermal model and included a number of different losses such as regenerator imperfection thermal loss, piston finite speed loss, gas spring hysteresis loss, displacer shuttle heat loss, clearance heat pump loss, heat conduction loss, and flow viscosity loss (Li & Grosu, 2017). In their estimation of hysteresis loss, they simply used Kornhauser and Smith's 1993 equation. They found that mechanical friction loss was the largest mechanical loss, while conduction loss was the largest heat loss. Kornhauser and Smith's

equation predicted that that hysteresis loss was a considerable loss, at 8.4% when looking at an exergy distribution of the input power.

Sapin, Taleb, Barfuß, White, Fabris, and Markides (2016)

Sapin et al. (2016) studied reciprocating-piston devices' usefulness as high-efficiency compressors or expanders. They compared experimental results from piston-cylinder crankshaft driven device to CFD predicted results. They used Lee's equation (Equation 18) to calculate the non-dimensional cyclic lost work. They found that for calculations at 109.34 rpm, the hysteresis loss was 78% of the total experimental loss, and 56% of the total CFD predicted loss.

Recent Studies

More recent studies have been carried out to investigate thermodynamic losses. Taleb, Barfuß, Sapin, White, Fabris, and Markides (2022) used CFD models to simulate thermodynamic losses in reciprocating compressors and expanders, taking into consideration the behaviour of real gasses and other effects. They developed their model in OpenFOAM (Open-source Field Operation And Manipulation) where they used four different fluid models: a perfect-gas constant property model, a temperature-dependent ideal-gas model, a real-gas model using the Peng-Robinson equation of state, and a real-gas model using property tables. They found that for simple gases, mono-and diatomic gases, there was no significant difference in the pressure and temperature results over a cycle between ideal and real-gas models. However, they found for heavier (organic) molecules such as propane, ideal-gas models overestimate the real-gas models by as much as 20%.

Interestingly, much recent literature still use Urieli and Berchowitz (1984) equation to predict hysteresis loss. S. Wang, Liu, Xiao, and Ni (2021) used it in their simple Stirling engine and refrigerator model. Getie, Lanzetta, Bégot, and Admasu (2021b) use it directly in their investigation of thermal and fluidic losses in a Stirling refrigerator and using this equation they found it to be 1% of the average power loss. It was also used in a near-ambient beta-type refrigerator study by Getie, Lanzetta, Bégot, Admassu, and Djetel-Gothe (2021a).

Hysteresis Literature Summary

The existing literature provided some insights into the characteristics of heat transfer within a cyclically compressed volume of gas, but also showed the large discrepancies in the understanding of what hysteresis loss is, and how large it is in terms of Stirling refrigerators.

Most studies conclude that this heat transfer loss is the difference between compression and expansion work when looking at a simple single space system, but do not go further into its definition (Chafe, 1988; Kornhauser, 1989; Kornhauser & Smith, 1993; Lee et al., 1980; Scheck, 1988). Others have slightly different definitions or methods of measurement, such as the net P-V work when no refrigeration work is being performed (Orlowska & Davey, 1987).

Hysteresis loss seems to have a peak in between two distinct operating conditions, the most common being isothermal and adiabatic (Chafe, 1988; Kornhauser & Smith, 1993; Lee et al., 1980; Scheck, 1988; A. C.-M. Wang, 1988), but parameters such as cavity gap length (Cooke-Yarborough & Ryden, 1985) and non-dimensional hydraulic radius (Lee, 1983) are also presented. Instead of the loss peaking between two operating conditions, Pourmovahed and Otis (1984) found that the pressure amplitude has a peak. However, this is most likely due to the system being analysed as a resonant system with the pressure amplitude modelled as the output over a range of operating frequencies.

Other insights such as the fact that hysteresis loss is dependent in some way on heat transfer and its phase difference with the bulk gas temperature (Lee, 1983), that the heat transfer is more affected by the gas properties and not the cylinder properties (Chafe, 1988), and that the heat flux increases substantially at the end of the compression stroke (Nikanjam & Greif, 1978) are important to consider.

Most significantly, there seems to be no consensus on the magnitude of hysteresis loss and its overall effect on the efficiency or Coefficient of Performance of Stirling engines and refrigerators. The literature concludes hysteresis loss in a Stirling engine ranges from a loss of a maximum of 10% (Foster-Miller Associates, 1980) or is typically 5%, but can get up to 25% of the power output (Scheck, 1988). Some do not quantify it, but rather state that it is a large or important thermal loss (Lee et al., 1980), and do not offer

a conclusion on its effect, but conclude that existing methods are either sufficient (Bailey et al., 2007; Kornhauser, 1989; Kornhauser & Smith, 1987; Kornhauser & Smith, 1993; Pourmovahed & Otis, 1984) or insufficient (A. C.-M. Wang, 1988; Willich et al., 2017) at determining its magnitude. Furthermore, yet another study concludes that hysteresis loss is negligible (Park & Chang, 1997). In addition, most of the conclusions are made specifically for the configuration, dimensions, and temperature regime of interest of each study, and the effect of hysteresis loss in a Stirling refrigerator and its similarities or differences between a Stirling engine are not discussed.

2.9 Motivation for this Study

The literature shows that hysteresis is a poorly understood heat transfer phenomenon in Stirling machines. Many have attempted to explain and quantify hysteresis loss, but modelling has only been done for simple single or double space models, with no analysis of hysteresis loss as it appears in an actual Stirling refrigerator. When refrigerator models are considered, they are usually very simplified models with no regenerator included. Furthermore, the conclusions from these studies also vary, leading to inconclusive interpretations on the magnitude and effects of hysteresis loss in Stirling applications.

In this section it has been clearly shown that more work must be done on understanding the underlying mechanism of hysteresis loss to truly quantify it and make a statement on the magnitude of its effect on the performance of Stirling machines. While A. C.-M. Wang (1988), Park and Chang (1997) do apply heat transfer models to ideal adiabatic analyses of Stirling refrigerators, these models are highly idealised second order models at best, so do not account for the interaction between different losses, nor are they experimentally validated. The only third order model attempt at modelling hysteresis loss (Willich et al., 2017) was basic in the fact it only modelled a single cylinder with an internal grid, not a complete Stirling refrigerator. In addition, some recent studies simply use Urieli and Berchowitz' 1980 equation to predict hysteresis loss (Getie et al., 2021a; Getie et al., 2021b; S. Wang et al., 2021)

Most previous analyses point to a peak in hysteresis loss when considering a range of different factors, such as dimensions or operating frequency. The idea of a peak between isothermal (at low frequency) and adiabatic (at high frequency) conditions

arises regularly, however, there is no mention about what determines the peak magnitude or position, nor is the underlying mechanism fully explained. Also, there was no explanation given as to why the pressure phase follows the trend of the loss so clearly. Questions about hysteresis loss in Stirling refrigerators remain to be answered, and the following research questions were formulated to direct the study:

1. How are the pressure-volume relationship and hysteresis loss linked?
2. What is the importance of the pressure phase shift?
3. Is the Peclet number a sufficient parameter for hysteresis loss prediction in Stirling refrigerators?
4. Is hysteresis loss a significant loss within Stirling refrigerators?
5. How does hysteresis loss manifest within a Stirling refrigerator system?
6. What parameters can be changed to minimise hysteresis loss?

To fully answer these questions, the relationship between temperature, heat transfer, pressure and hysteresis loss must be examined in greater detail. This was carried out with a thorough investigation and analysis with a range of theoretical models, Sage computer models, and experimental tests. The objective of this study and methodology undertaken to explore these relationships are covered in the following section.

2.10 Objectives and Methodology

The objective of this study was to carry out a thorough investigation into understanding hysteresis loss and how it may manifest in Stirling refrigerators. This involved thorough modelling and simulation of the thermodynamic processes taking place within the refrigerator system. This modelling was primarily carried out using Sage, a Stirling simulation software, and MATLAB.

This project consisted of several components. These could not be done simply in sequential order, as they required feedback from each other and were interconnected. This meant that all the following elements were mostly carried out in parallel or had an iterative approach, such as the thermodynamic modelling and the test rig results analysis. The theoretical analysis was constantly revised to better explain simulation and experimental results. The four components of this study are defined as follows:

Literature Review: This provided an insight into Stirling technology and the underlying theory. The literature review helped in understanding the current knowledge regarding how losses in Stirling refrigeration are categorised and quantified, and where the gaps in the knowledge are. From the preliminary research, one of these gaps was identified to be the quantification of hysteresis loss for Stirling refrigeration in the near-ambient temperature regime.

Modelling: Using the commercial Stirling simulation software Sage, various Stirling configurations along with simpler piston-cylinder devices were examined with the intent to understand hysteresis loss and its effect on performance. A systematic parameter study was carried out in terms of heat flows, pressure, temperature, and other variables of interest.

Single cylinder experiments with and without regenerator material were also analysed and modelled using MATLAB. Existing heat transfer correlations were examined for their adequacy in calculating hysteresis loss, and a transient step model was developed.

Test Rig Experiments: Various experimental rigs were used to validate the Sage models. The test rigs consisted of a beta configuration Stirling refrigerator, and a piston-cylinder experimental setup with regenerator material.

Synthesis: The findings from modelling and experiments brought up many questions. These questions arose as the project progressed and were re-synthesised into discussions, such as further analysis of the pressure-volume relationship and the understanding of the pressure phase shift for both sinusoidal and discrete piston motion, all of which are interwoven into a deeper understanding of hysteresis loss.

The structure of the report reflects the organic nature of this project. Analysis, simulation, and experimental results were all carried out concurrently and were fed back to one another and are therefore organised together into relevant chapters.

Chapter 3: Foundations

This chapter establishes the foundations of heat and work transfer and introduces the pressure-volume relationship with the pressure phase shift conventions which will be discussed in more detail in later chapters. This chapter provides answers to Research Questions 1 and 2. The following sections detail the preliminary single-space Sage model and test rig produced to identify the quantities of interest. The Sage model is validated against the test rig experimental results and results from Kornhauser (1989). Parameter studies using Sage were carried out, and the effect of working gas, cyclic and net energy transfers, temperature variations, and the P-V relationship are presented. This chapter also analyses the relationship between heat transfer and the pressure phase shift with a simple step model developed in MATLAB and looks into the consequences of different idealising assumptions.

3.1 Single Cylinder Sage Model

A Sage model of a simple piston-cylinder device, with its physical representation shown in Figure 3-1 and Sage interface in Figure 3-2 was created to investigate how pressure, temperature, heat transfer, and P-V work are correlated. This model is validated against Kornhauser's results and experimental results obtained in the lab, in Section 3.3.

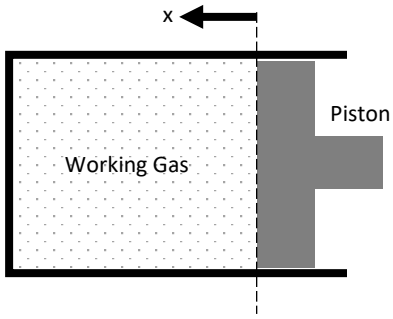

Figure 3-1: Piston-cylinder schematic

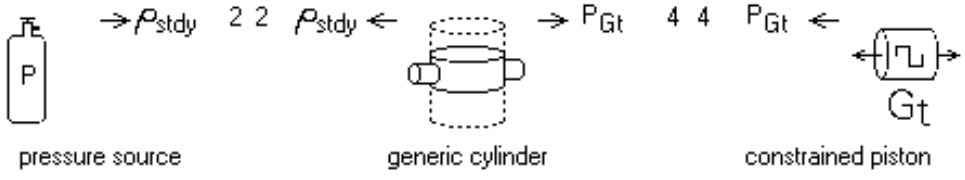

Figure 3-2: Sage model of piston-cylinder experiment

The cylinder wall was modelled as a 'thick surface', which has two layers: a thermally large cylinder wall layer, held constant at a temperature T_w = 300 K to simulate room temperature surroundings, and a thin layer on its surface with a time-varying heat flux, adjacent to the working gas. The magnitude and phase data for properties of interest were recorded for different operating frequencies, mean pressures, and three different working gases (helium, hydrogen, and air). The following chapters detail the verification of this Sage model using both lab-obtained data and Kornhauser's results.

3.2 Single Cylinder Test Rig

An existing single cylinder piston seal test rig was used to obtain experimental results to validate the Sage model in Section 3.1. The entire setup can be seen in Figure 3-3. This includes, from left to right, a) the laboratory computer running LabVIEW, b) the National Instruments myRIO, the c) H-Bridge, the d) piston-cylinder test rig, and e) the power supply. The NI myRIO is a reconfigurable input/output device which was used for data acquisition, and the H-Bridge controlled the voltage polarity to the linear motor driving the piston.

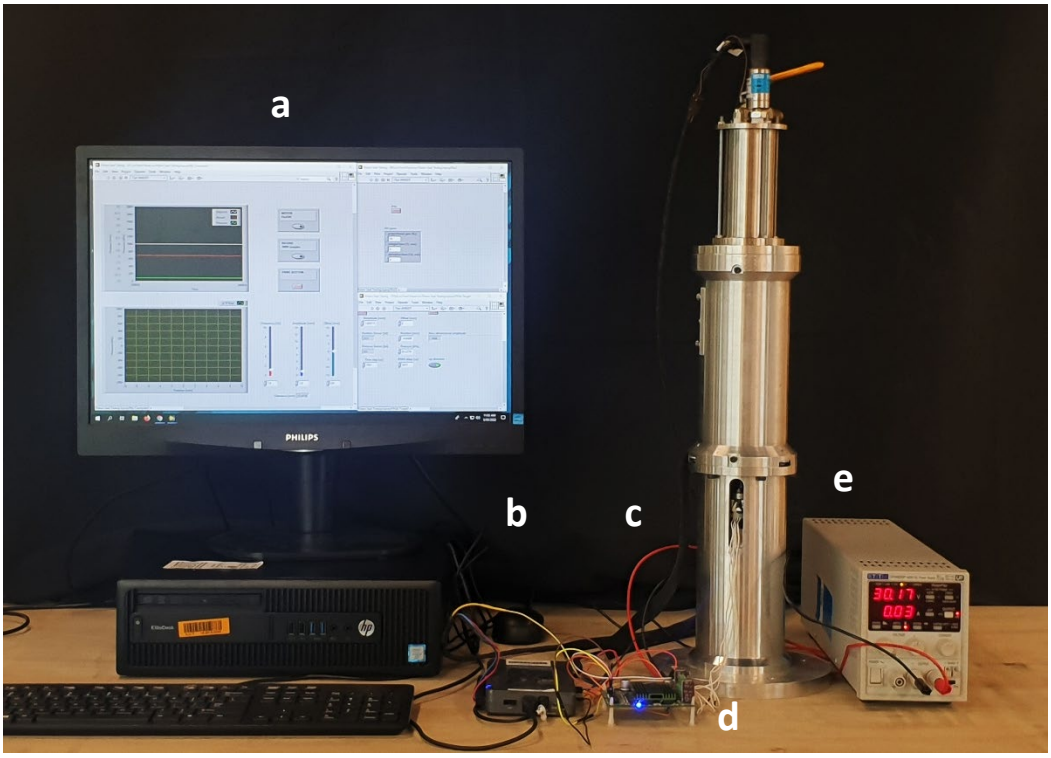

Figure 3-3: Single cylinder test rig set up

The test rig consisted of a modular stainless-steel cylinder with a removeable head, and a piston driven by a moving coil linear motor, supported by flexure bearings. The test rig stood vertically, with the linear motor housing at the base, with the piston shaft going through a middle section with the flexure bearings, and with the piston-cylinder housing at the very top, as shown in Figure 3-4. The test rig had a ball valve which could be opened and closed to allow pressure equalisation with the surroundings, also shown in Figure 3-4. As the test rig was vented to the surroundings, the working gas was air. The piston was sealed with a viton O-ring which was lubricated with a very thin oil film. Close-up views of the myRIO and H-Bridge can be seen in Figure 3-5a and Figure 3-5b.

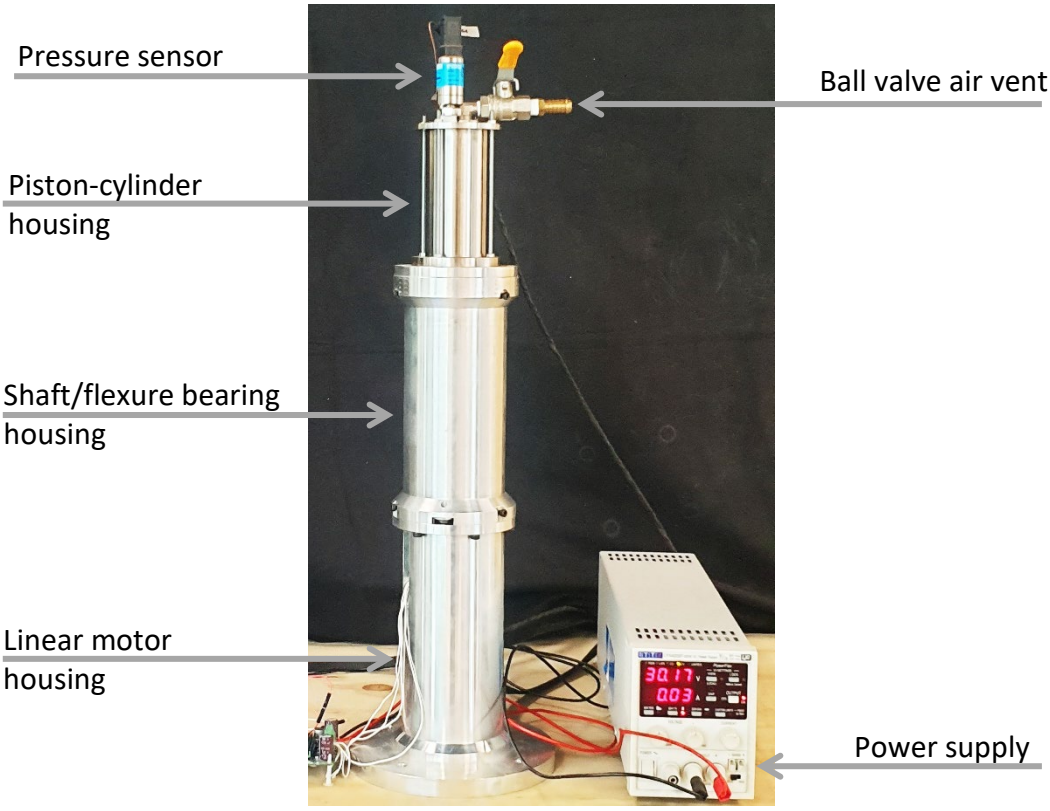

Figure 3-4: Single cylinder test rig labelled components

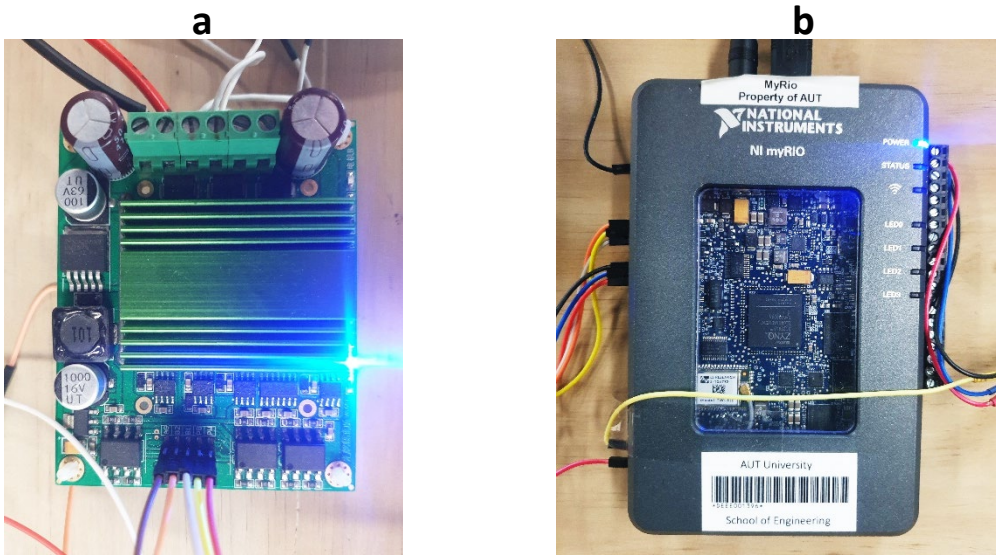

Figure 3-5: Close-up views of a) H-Bridge circuit and b) the MyRio

The labelled cross-sectional view of the piston-cylinder test rig is shown in Figure 3-6. The actual working gas space is a small part of the setup, located at the very top. The flexure bearings ensure that the movement is confined to the axial direction, as they have low axial stiffness and high radial stiffness. Relevant dimensions of the test rig are detailed in Table 3-1.

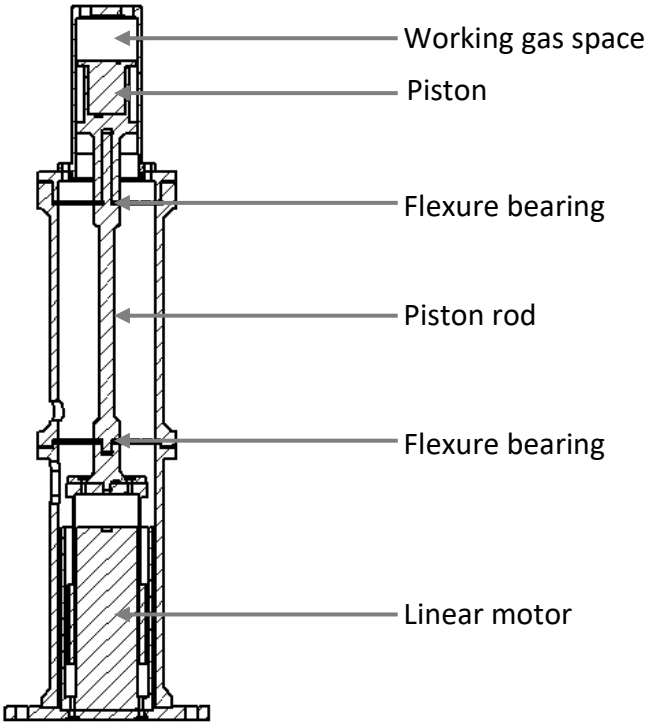

Figure 3-6: Single cylinder test rig labelled cross sectional view

Table 3-1: Piston-cylinder test rig model dimensions

Parameter	Value	Unit
Diameter	0.05	m
Stroke	0.01	m
Stroke Volume	1.9634×10^{-5}	m^3
Volume Ratio (Compression Ratio)	1.5178	
Average Volume	4.775×10^{-5}	m^3
Piston Face Area	7.854×10^{-3}	m^2
Average Wetted Surface Area	7.747×10^{-3}	m^2
Hydraulic Diameter	2.465×10^{-2}	m

Data Acquisition

Gas pressure and piston position were recorded to compare with Sage model results of the single cylinder experiment. These results were recorded using their respective sensors, shown in Figure 3-7. These results were then processed into their respective physical pressure and position units and written to files through LabVIEW.

The pressure data was recorded using an IPS Series Industrial Pressure Sensor number 7974970, a piezo-resistive thick film ceramic sensor with a stainless-steel body. The pressure sensor full scale range is -1 bar to 9 bar, corresponding to 0 to 5 VDC. The accuracy of the pressure sensor is stated to be less than ± 0.25 % of the full-scale output range.

The position data was recorded using a Honeywell SMART 35 mm Position Sensor, which consisted of an array of magnetoresistive sensors combined with an application-specific integrated circuit to determine the piston position within a magnetic field. This position data was also used as the feedback in the control of the piston. The full-scale range is 0 mm to 35 mm, corresponding to 0.55 and 4.14 VDC. The linearity of this sensor is ± 1.0 % of the full-scale output range.

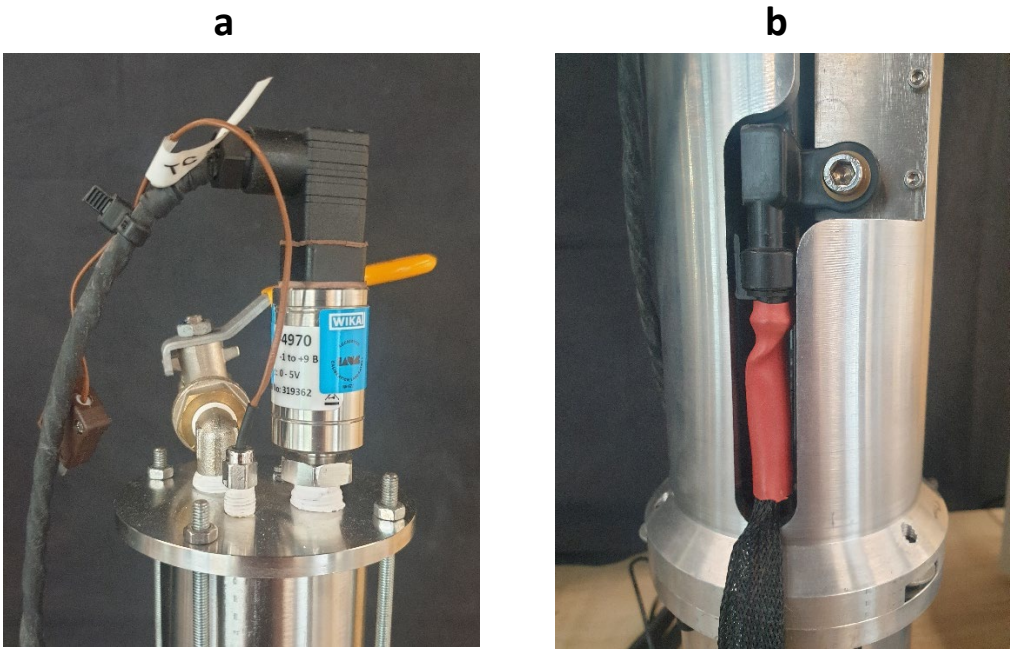

Figure 3-7: a) Pressure sensor and b) Position sensor mounted on test rig

Experimental Method

The piston motion was controlled via LabVIEW using closed-loop proportional control. The amplitude of the piston was not able to be accurately set as the piston was not able to reach the full amplitude of the control signal, as seen in Figure 3-8. To compensate for this, the amplitude control was set higher than the required amplitude in order for the piston to reach the required amplitude. It was found that the discrepancy between the control amplitude and actual piston amplitude was around 2-3 mm, and it depended on the amplitude and frequency of oscillation, so some trial and error was needed to obtain consistent readings.

The displacement sensor reading can be seen in Figure 3-8 in red, while the pressure sensor reading can be seen in green. The displacement signal is very clean, while the pressure signal is extremely noisy. The data processing carried out to get a clear pressure signal can be found in the following section.

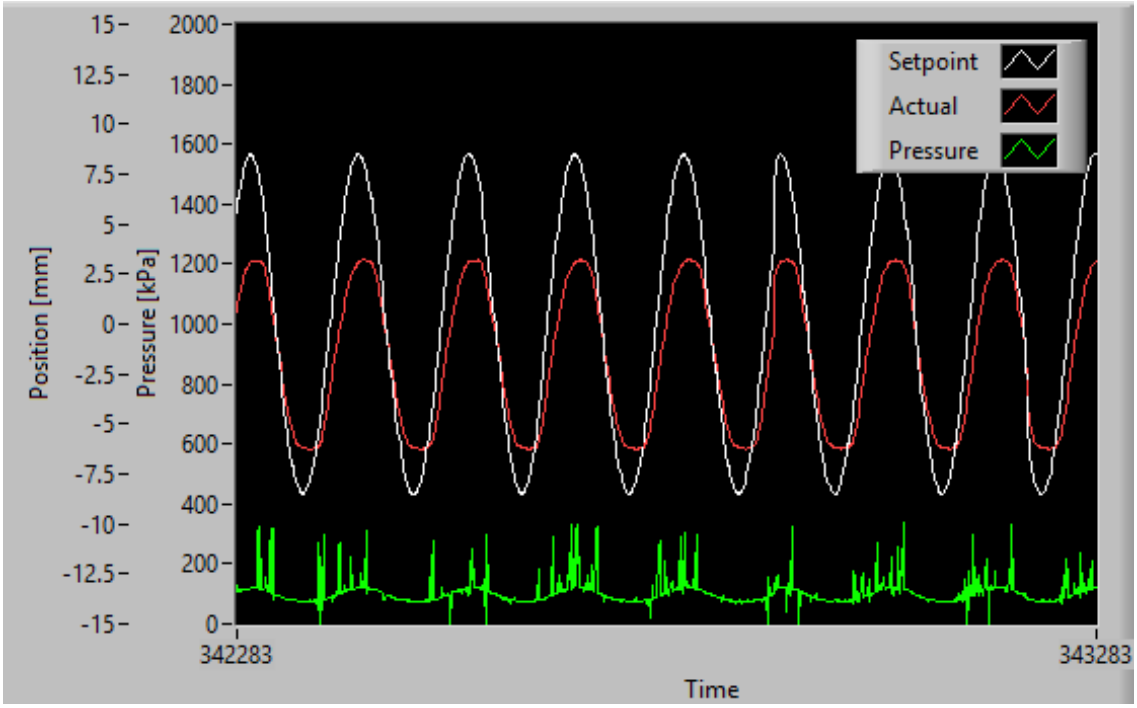

Figure 3-8: Displacement control signal, actual displacement reading, and pressure reading displayed in LabVIEW

Each experimental sample of pressure and position was taken in real time over one second in millisecond increments, after waiting for just enough time for the position signal to stabilise. The experiment was run in steps of 1 Hz from 1 to 10 Hz. For each frequency, 5 - 10 experimental data sets were taken, and the data set closest to 5 mm amplitude was used while the rest were discarded. This was to ensure that the swept volume was kept as consistent as possible.

Experimental Data Processing

While the raw displacement data from the displacement sensors did not require processing to get a clean displacement plot, the results from the pressure sensor were extremely noisy. It was found that the PWM signal driving the motor was interfering with the pressure readings, which lead to the noise spikes in the data. To find the experimental pressure wave magnitude, the results were smoothed using MATLAB's inbuilt smoothing function, a robust local regression which uses a linear least squares method fit within a 6 % window of the data range to a 2nd degree polynomial model. Figure 3-9 shows the measured piston displacement, unprocessed pressure, and the resulting smoothed pressure curve for the experiment with the cylinder only, run at 5 Hz.

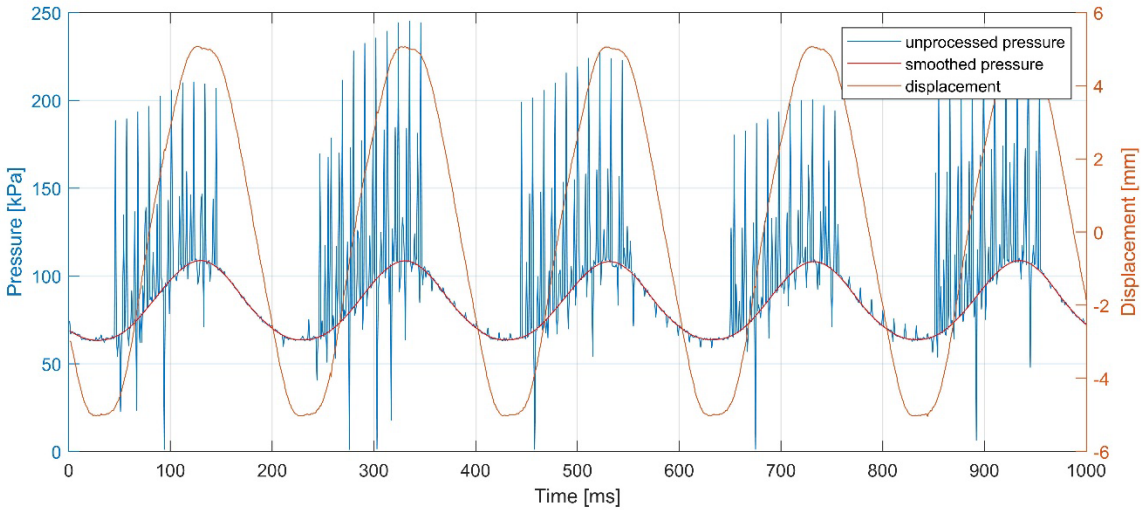

Figure 3-9: Pressure and displacement results for the single cylinder experiment at 5 Hz

To compare the experimental results with the Sage model results, some further processing needed to be done. This was mostly due to the inability to precisely control the piston offset and amplitude, which resulted in slightly different mean volumes and therefore different mean pressures. To compensate for this, the pressure amplitude data was normalised against the respective mean pressures, and the Sage mean volume for each frequency was changed to match the experimental mean volume. The results of the pressure normalisation of both experimental and Sage results can be seen in the following Section 3.3, in Figure 3-10.

3.3 Sage Model Validation

Experimental and Sage Results

The single cylinder Sage model was set up to replicate the experimental test rig, using air as the working gas and dimensions as outlined in Table 3-2. It was run in steps of 1 Hz, from 1 to 10 Hz, with the mean pressure and volume as an input from the experimental readings for each frequency step. The normalised pressure results for both the single cylinder test rig and its Sage model are displayed in Figure 3-10. The error of the pressure reading is ± 0.25 % of the full-scale range, and this error was also normalised against the mean pressure to show the experimental error range and where the Sage values fall in respect to these error ranges. The full table of errors for each frequency are shown in Table A-1, Appendix E.

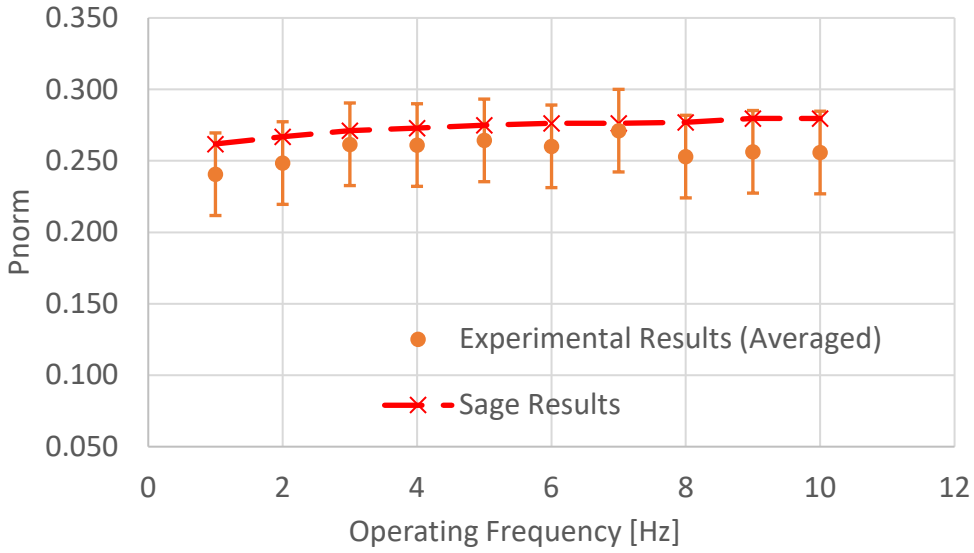

Figure 3-10: Experimental and Sage normalised pressure vs operating frequency for single space piston-cylinder experiment

The Sage-calculated results follow the experimental data very well, although the Sage data is systematically higher than the experimental values. This can be due to seal leakage losses within the experiment, and heat flow from the gas into the piston head or other parts of the experiment that are not modelled in Sage, which would lead to a lower than theoretical pressure amplitude.

This agreement validates the Sage model, but to further validate Sage, it was compared against externally collected data. Kornhauser's (1989) experimental data was also used, as detailed in the following section.

Kornhauser and Sage Results

The single cylinder Sage model was also set up to replicate the baseline conditions of Kornhauser's experiments in Section 2.8 with helium as the working gas, and dimensions as outlined in Table 3-2. The results for Kornhauser's experiments needed to be compared differently to the test rig results as the data from Kornhauser was in the form of the non-dimensional loss, $Loss_{ND.}$

The operating frequency in Sage was mapped from 0.1 to 17 Hz, and the mean pressure was varied from 100 kPa to 1700 kPa. Gas properties are built into Sage, so for every frequency step, the oscillation Peclet number, Pe_{ω}, was calculated based on the temperature-dependent thermal diffusivity of the working gas.

Table 3-2: Piston-cylinder model dimensions as per Kornhauser (1989)

Parameter	Value	Unit
Diameter	0.0508	m
Stroke	0.0762	m
Stroke Volume	1.544×10^{-4}	m^3
Volume Ratio	2	
Average Volume	2.317×10^{-4}	m^3
Piston Face Area	2.027×10^{-3}	m^2
Average Wetted Surface Area	0.0223	m^2
Hydraulic Diameter	0.04156	m

The mean heat flow out of the gas in the Sage model is net P-V work, or the cyclic integral of P-dV (the numerator of Equation 18), representing the absolute value of the hysteresis loss within a single-cylinder system. The hysteresis loss was then normalised using Equation 18 to compare with Kornhauser's data, as shown in Figure 3-11.

The Sage-calculated results follow the trend of Kornhauser's experimental data reasonably well. The peak in non-dimensional loss occurs at approximately the same Peclet number for both sets of data. The largest difference in results is also at that peak loss area, where the experimental data exceeds unity, which is impossible and, thus, is an indication of the magnitude of the experimental error in Kornhauser's experiment.

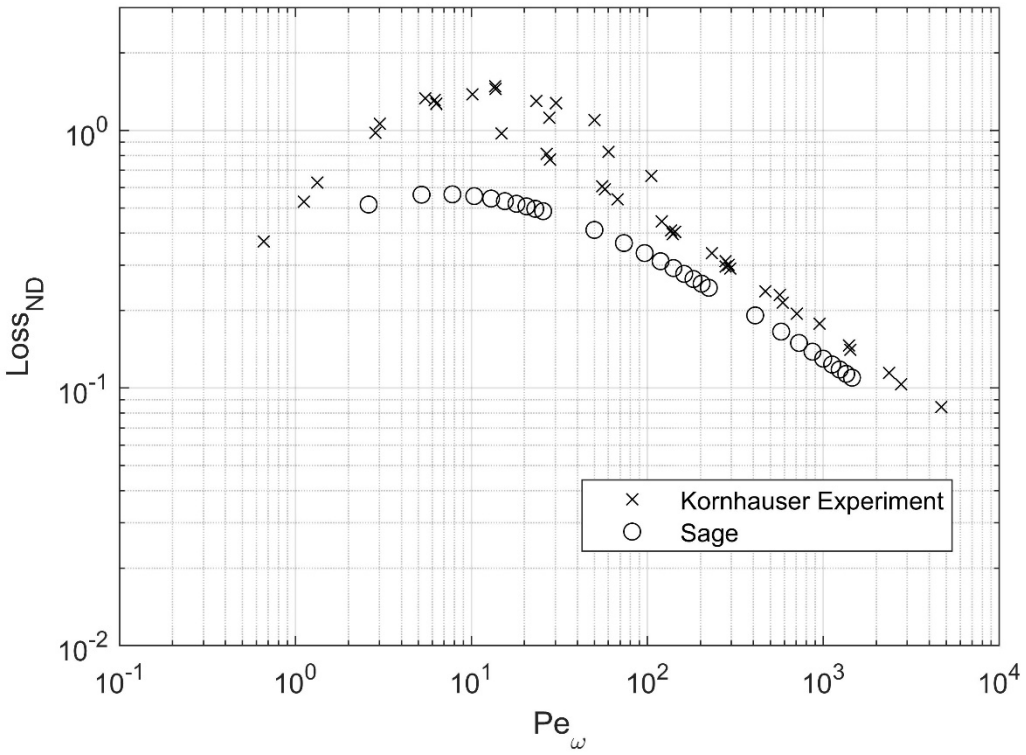

Figure 3-11: Sage-calculated loss vs Kornhauser's experimental data

This agreement also validates the Sage model. Two separate experimental results both agreeing with Sage provides reasonable confidence to use Sage for further investigation into outputs for pressure, gas temperature, and heat flow for different working gases, wall materials, and other operating conditions.

3.4 Single Cylinder Sage Parameter Studies

Parameter studies using Sage were carried out for three different gases – helium, hydrogen, and air. For each gas, the operating frequency was varied from 0.01 to 10 Hz, and the cylinder material was kept as stainless steel (SS304). The Sage model for these parameter studies had the same dimensions as Kornhauser's model for comparison. The net P-V work, pressure, gas temperature, and heat flow Fourier series variables were logged. The relevant results are presented and discussed in this section.

The Effect of Working Gas

Plotting the non-dimensional loss over the oscillation Peclet number as in Figure 3-12 obscures the fact that the maximum loss occurs at different frequencies for different working gases since the Peclet number is dependent on the fluid property thermal diffusivity. Therefore, it was found more appropriate to show changes in non-dimensional loss and other important parameters against the operating frequency.

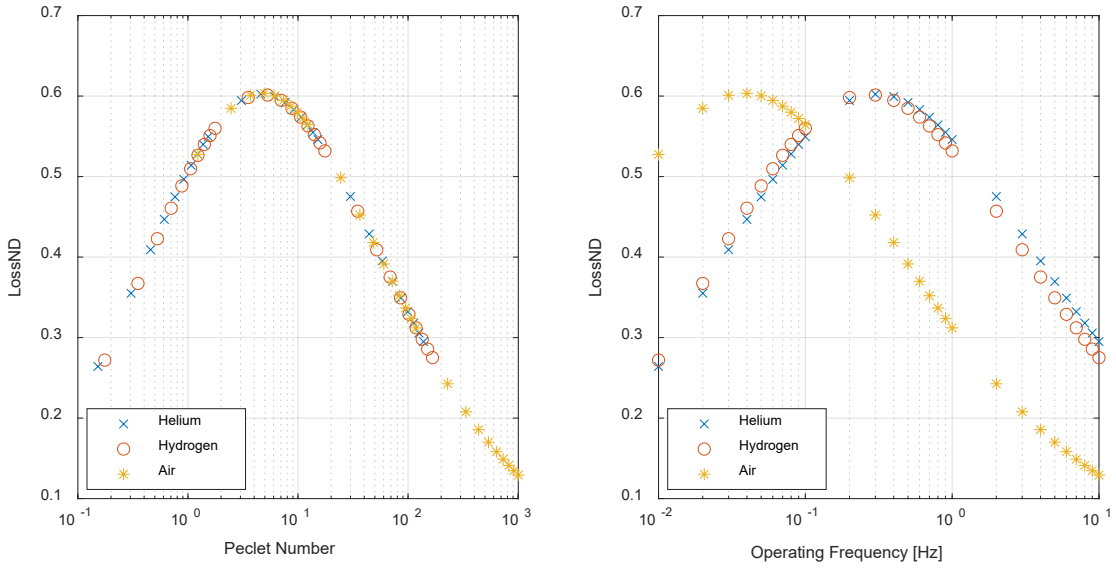

Figure 3-12: Non-dimensional loss vs a) Peclet number and b) operating frequency for different working gases

Thermal diffusivity, 'α', is the thermal conductivity of the working gas divided by its density and specific heat capacity:

$$\alpha = \frac{k}{\rho c_p} \quad \left[\frac{m^2}{s}\right] \qquad \text{Equation 25}$$

When the thermal diffusivities of helium, hydrogen, and air in Table 3-3 are compared with the peak positions of their respective losses in Figure 3-12, it can be established that, while the magnitude of the non-dimensional loss remains unchanged, the peak shifts to higher frequencies as the thermal diffusivity of the working gas increases. The non-dimensional loss magnitudes are the same for all working gases because the denominator of the non-dimensional loss (as seen in Equation 18) is also dependent on the gas properties. This means that, as the magnitude of the hysteresis loss , i.e., the net heat transfer, increases, so does the work of adiabatic compression in equal proportion. Figure 3-13 shows how the magnitude of the hysteresis loss alone is affected by the working gas, without normalisation.

Table 3-3: Thermal diffusivities of helium, hydrogen, and air at 20 °C

Substance	**Thermal diffusivity [m^2/s]**
Air	2.11×10^{-6}
Hydrogen	1.47×10^{-5}
Helium	1.74×10^{-5}

The thermal diffusivity seems to not only influence the position of the maximum loss, but also on the actual magnitude of the hysteresis loss. Figure 3-13 shows the absolute values of the hysteresis loss for the three different working gases against operating frequency. Gases with higher thermal diffusivities have higher hysteresis losses. For a given operating frequency higher than where the maximum loss occurs, the hysteresis loss can be, for example, as much as five times higher for helium than for air (see Figure 3-13, 10 Hz).

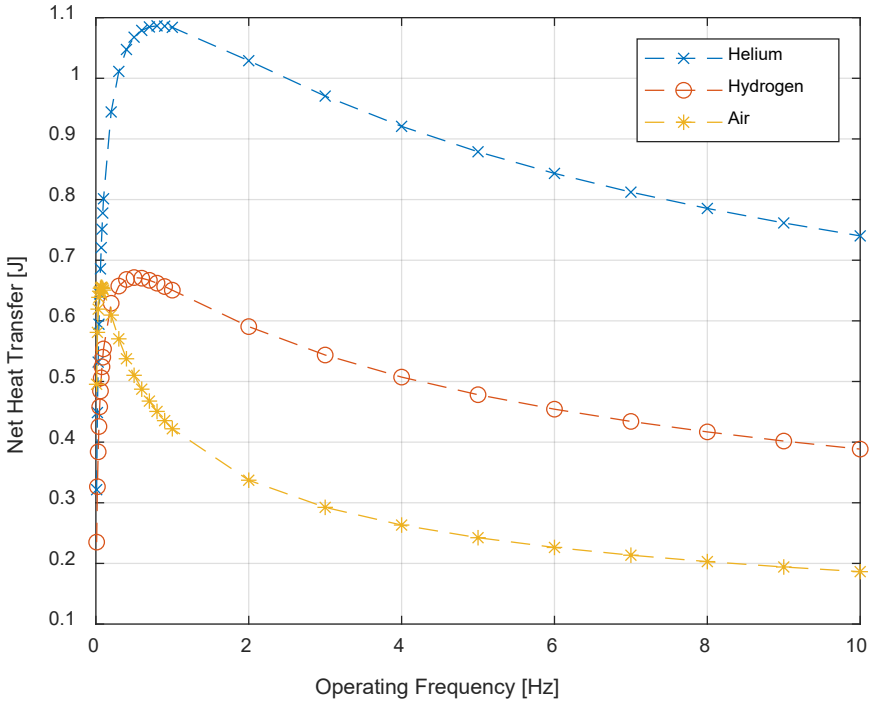

Figure 3-13: Net heat transfer vs operating frequency for different working gases

As thermal diffusivity is a ratio of thermal conductivity to specific heat capacity, a higher thermal diffusivity implies that heat propagates through the gas faster compared to how much heat it stores. It is evident from Figure 3-13 that the gases with a higher thermal diffusivity transfer more heat to the walls per cycle than the gases with a lower thermal diffusivity, so proper working gas choice could reduce unwanted heat transfer. However, in components such as heat exchangers, high heat transfer is required, so choosing a gas with low thermal diffusivity to reduce hysteresis loss could have an overall detrimental effect to the operation of a refrigerator or heat pump.

The Pressure-Volume Relationship

Literature has shown that the net P-V work input and pressure phase are intrinsically linked (Chafe, 1988; Kornhauser, 1989; Kornhauser & Smith, 1987; Kornhauser & Smith, 1993; Scheck, 1988). To clarify conventions before going into the results from the Sage model, Figure 3-14 shows pressure and volume as sinusoidally varying functions.

As discussed by Chafe (1988), Kornhauser and Smith (1987), in ideal situations, the pressure and volume waves are exactly 180° out of phase. The pressure phase shift is

defined by how much the actual pressure leads the ideal pressure wave. In Kornhauser's experiments, this phase shift ranged from approximately 0.5 to 12 degrees.

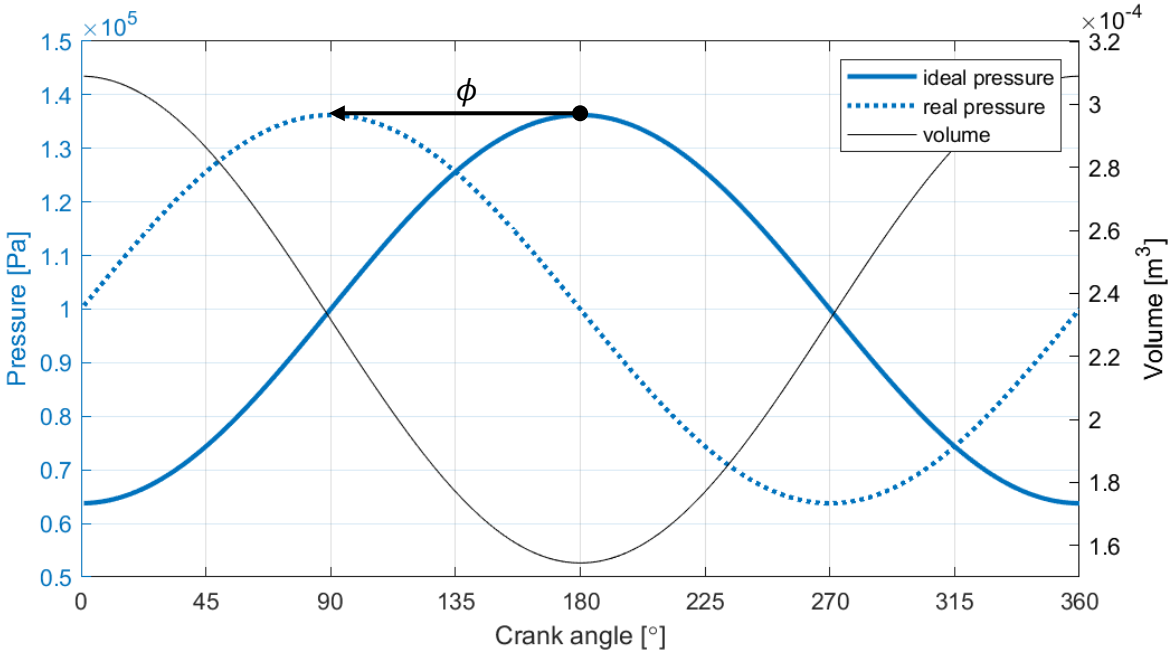

Figure 3-14: Volume, ideal and real pressure as sinusoidally varying functions

The Sage single cylinder model was also used to investigate this phenomenon. The results of the pressure phase shift and the net P-V work for the Sage single cylinder model are shown in Figure 3-15. The pressure phase shift and the net P-V work input are closely related. They both are low at both extremes of low and high operating frequencies or Peclet numbers and have a peak between the two at very similar places. This indicates a connection between the pressure phase shift and the net P-V work. While this relationship between the net P-V work and the pressure phase shift is still not clearly defined, the modes of operation over the range of frequencies can still be interpreted.

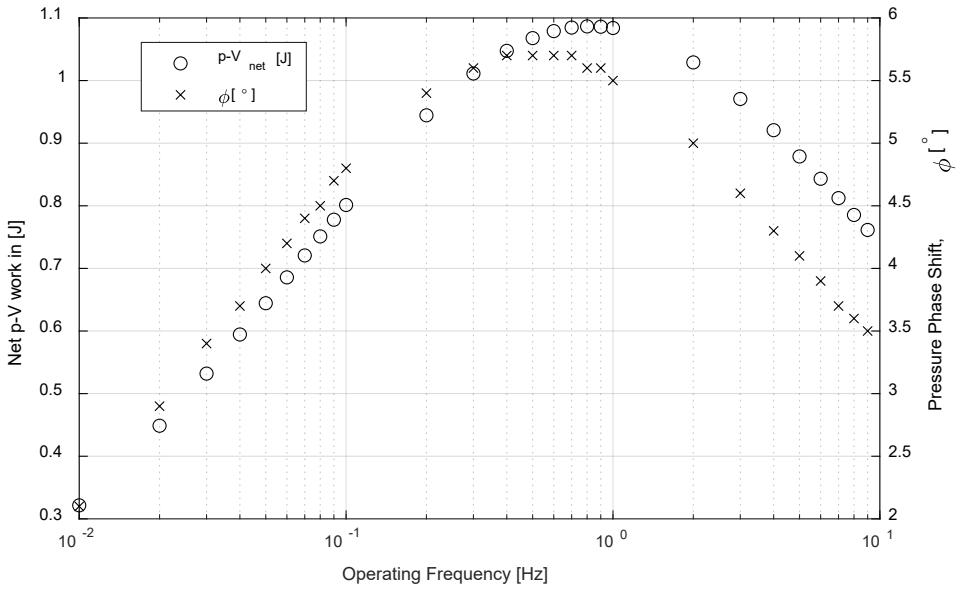

Figure 3-15: Net P-V work and pressure phase lead vs operating frequency for piston-cylinder Sage model

Temperature and Heat Transfer

The cyclic variation of heat transfer and gas temperature can be seen in Figure 3-16 and 3-17. The heat transfer amplitude decreases with frequency, while the temperature amplitude increases. This suggests a transition from close to isothermal operation to near adiabatic operation. The heat transfer phase and temperature phase both increasingly move further toward the right (lag increases), but the heat transfer phase shift makes more sense when viewed with respect to the cyclic P-V work (Section 3.5), and temperature in reference to its decreasing lead on the cyclic volume. The complete variation of amplitudes and phase shifts of both heat transfer and temperature are plotted over the operating frequency in Appendix F.

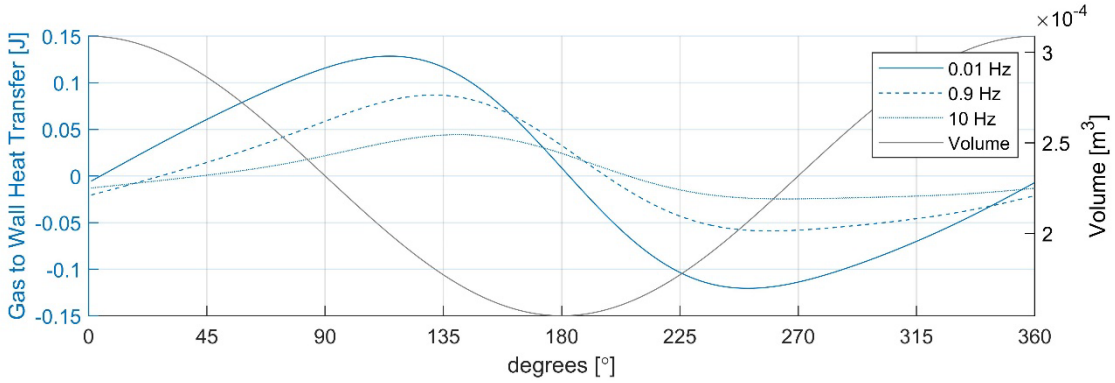

Figure 3-16: Cyclic heat transfer vs gas volume

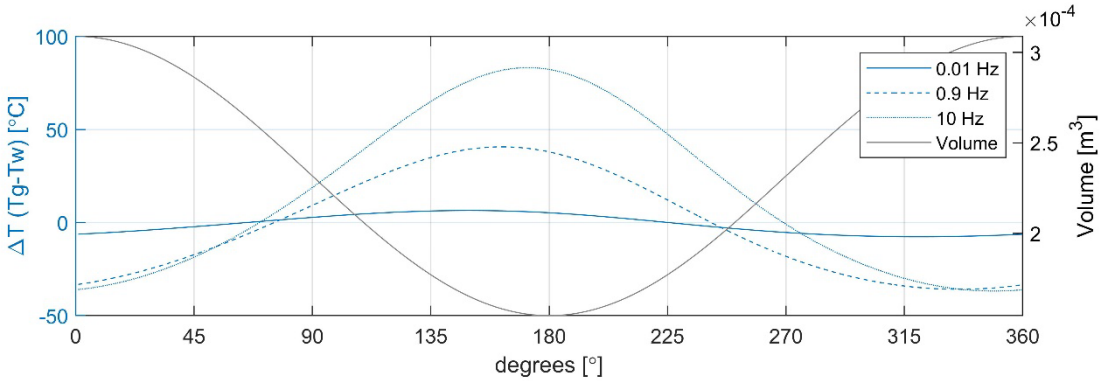

Figure 3-17: Cyclic temperature difference vs gas volume

3.5 Heat and Work Transfer

Net Energy Transfers

In a piston-cylinder device, the walls are maintained at an approximately constant temperature. As the piston compresses the gas, the compression work into the system raises the temperature of the gas, T_g, to be higher than that of the wall, T_w, which causes heat to flow into the cylinder wall. As the gas is expanded and if T_g becomes less than T_w, then conversely, heat flows back from the walls into the working gas. Due to the variation of gas temperature, there is a net heat flow out of the gas into the wall. This mean heat flow out of the gas results in the net P-V work to be non-zero; which is essentially the cyclic integral of P-dV. This means that for a single space piston-cylinder device with no other losses, the hysteresis loss is simply the net heat transfer output by the system (and therefore the net P-V work input to the system). This can be seen in Figure 3-18, which shows the net heat and P-V work against the operating frequency.

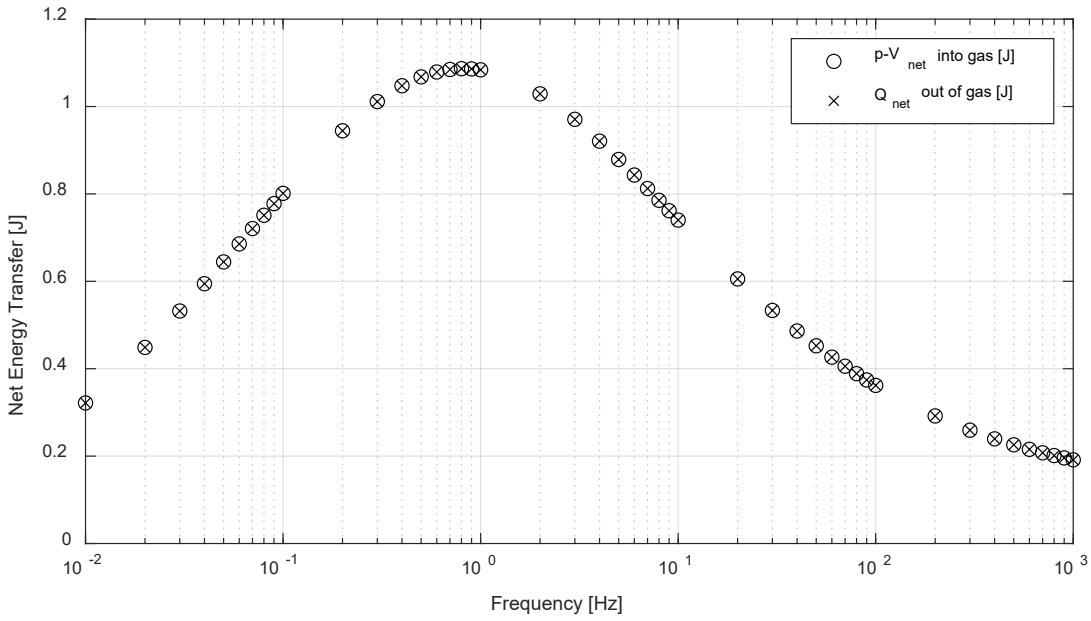

Figure 3-18: Net heat transfer and P-V work against the operating frequency

For the remainder of this study, the net P-V work will be discussed, and the reader should remember that for a single cylinder, the net heat out (the heat lost in one cycle) is the same as the net P-V work input (work input in one cycle).

Cyclic Energy Transfers – Amplitude and Phase

The instantaneous heat output over one cycle from the gas, and P-V work input for low, medium, and high frequencies (0.01, 0.9, and 10 Hz) are shown in Figure 3-19 to 3-21. The Sage results of the single space model which are closest to isothermal heat transfer can be seen in Figure 3-19. This shows that for low frequencies, the instantaneous heat output is almost identical to the P-V work input. It is not quite perfectly isothermal as the heat output wave is slightly lower in magnitude and has a small lag on the P-V work.

As the operating frequency increases, the instantaneous heat transfer starts to lag the p-V work input due to the decreasing time available for heat transfer, while the heat transfer amplitude decreases. This can be seen in Figure 3-20. An example of near-adiabatic heat transfer can be seen in the Sage results in Figure 3-21. The heat transfer amplitude is small (truly adiabatic heat transfer, the heat transfer amplitude would be zero) and the phase lag is large.

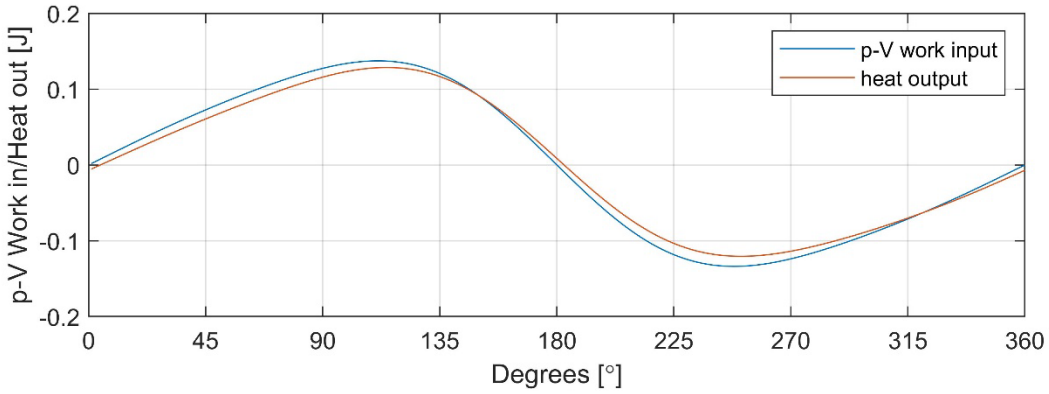

Figure 3-19: Cyclic heat transfer and P-V work for 0.01 Hz

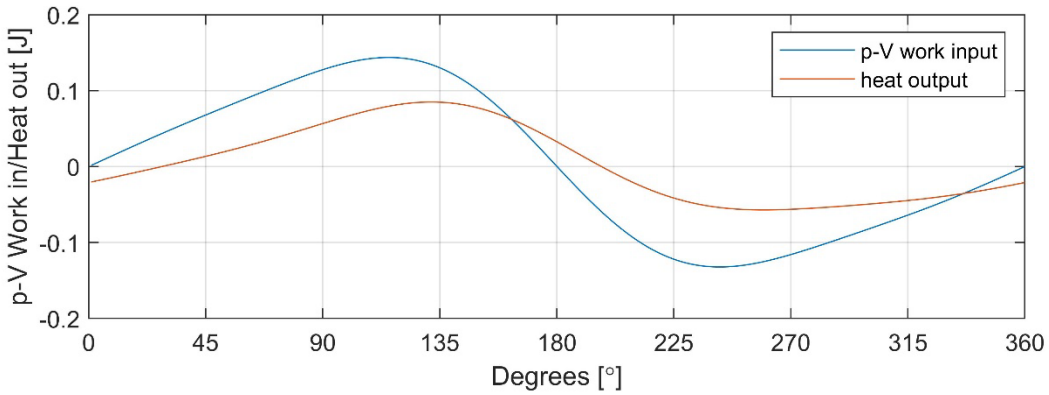

Figure 3-20: Cyclic heat transfer and P-V work for 0.9 Hz

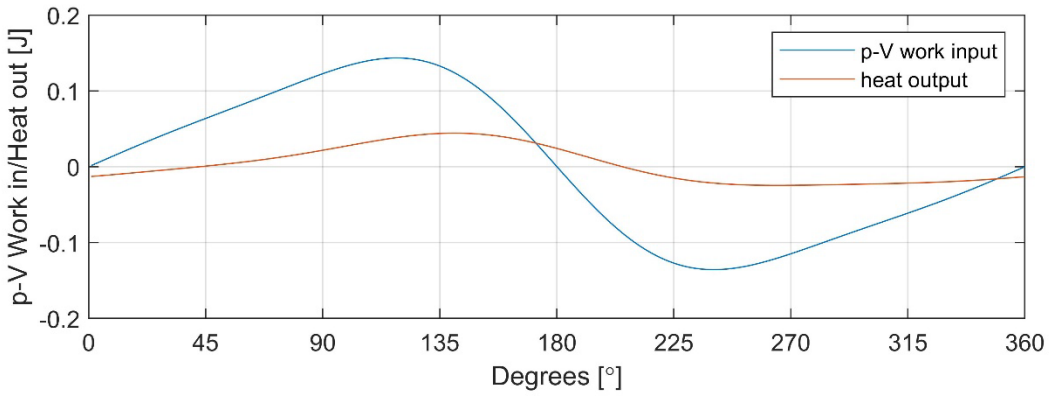

Figure 3-21: Cyclic heat transfer and P-V work for 10 Hz

With the instantaneous heat and P-V work transfer information, an understanding of the energy transfers can be formed. These amplitude and phase characteristics of the energy transfers can be looked at with respect to the cyclic gas temperature data. This will form a more complete understanding on how both heat transfer and temperature affect the pressure phase shift and its relationship with the P-V work.

3.6 The Time-Dependence of Heat Transfer

An iterative model for single space heat transfer was developed to demonstrate the interdependency of heat transfer and the pressure phase shift. Heat transfer from the gas to the cylinder walls was modelled as if the walls were a semi-infinite body: a single plane surface which extends to infinity, with constant thermophysical properties, of which heat transfer only affects the temperature variation near the surface. The equation for the heat transfer was based on a constant surface temperature, T_s, at the surface for $x = 0$, where x is the perpendicular distance into the wall. The formulation for heat transfer as per Çengel (2006, pp. 241-243) is described as follows:

Differential equation:
$$\frac{\partial^2 T}{\partial x^2} = \frac{1}{\alpha}\ \frac{\partial T}{\partial t} \qquad \text{Equation 26}$$

Boundary conditions:
$$T(0,t) = T_s \quad \text{and} \quad T(x \to \infty) = T_i \qquad \text{Equation 27}$$

Initial condition:
$$T(x,0) = T_i \qquad \text{Equation 28}$$

The resulting heat flux equation is shown in Equation 29, determined from Fourier's law.

$$\dot{q}(t) = \frac{k(T_s - T_i)}{\sqrt{\pi \alpha t}} \qquad \text{Equation 29}$$

Where k = thermal conductivity of the wall $\left(\frac{W}{mK}\right)$, T_s= surface temperature (K), T_i = initial gas and wall temperature (K), α = wall thermal diffusivity $\left(\frac{m^2}{s}\right)$, and t = time taken for heat transfer (s).

The heat flux equation (Equation 29) was applied in a simple model programmed in MATLAB. The model was based on a specified sinusoidal variation in a volume of working gas, as shown in Figure 3-22, discretised into steps. Properties such as temperature,

pressure, and the change in internal energy were initialised for the first step and then were subsequently calculated for each volumetric change.

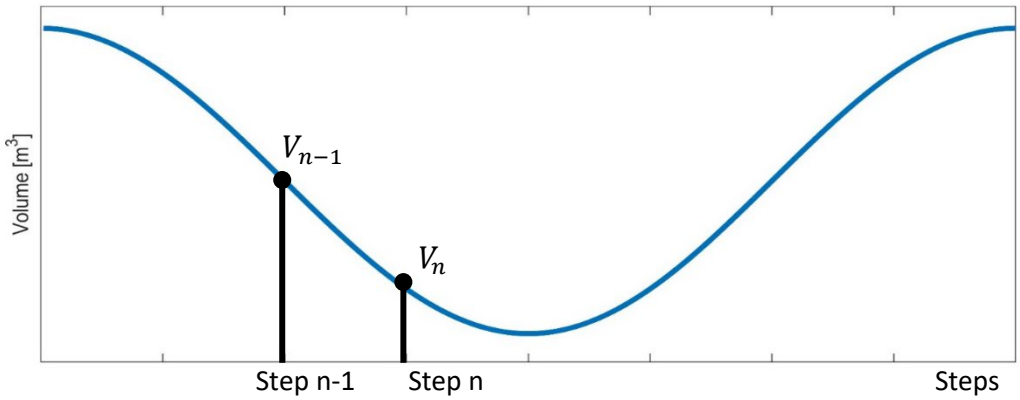

Figure 3-22: Notation used for sinusoidal volumetric change for model

In order to apply Equation 29 in this model, it was multiplied by the instantaneous surface area, A_s, and the change in time for one time step, dt, to obtain Equation 30, the amount of heat transfer in Joules for one incremental change in volume, dV. The variable dt replaces t in the denominator as the time taken for heat transfer is the same given for one time step:

$$q(t) = \frac{kA_s(T_s - T_i)}{\sqrt{\pi\alpha dt}}dt \qquad \text{Equation 30}$$

In the step model, T_s is the gas temperature, which changes with each volumetric change of the control volume, dV, as a sinusoidal function. The steps can be visualised as a transient situation for each step with a constant boundary condition of T_s to calculate heat transfer, but for each step, T_s changes by a small amount, and the model is solved again. The working gas used was helium, and the wall material used was SS304.

The solution process is shown in Figure 3-23. This shows the equations used to calculate all the properties for one volumetric step. For each step, an isentropic temperature change is assumed from T_{n-1} to T_{is_n} as the volume changes from V_{n-1} to V_n. The

isentropic assumption is used only as an initial estimate for the temperature change, for which heat transfer can be estimated using Equation 30 and using $T_{is_n} = T_n$. The work input is calculated using the assumption that $W_n = P_{n-1}dV$, and the change in internal energy, dU_n, is calculated using the first law.

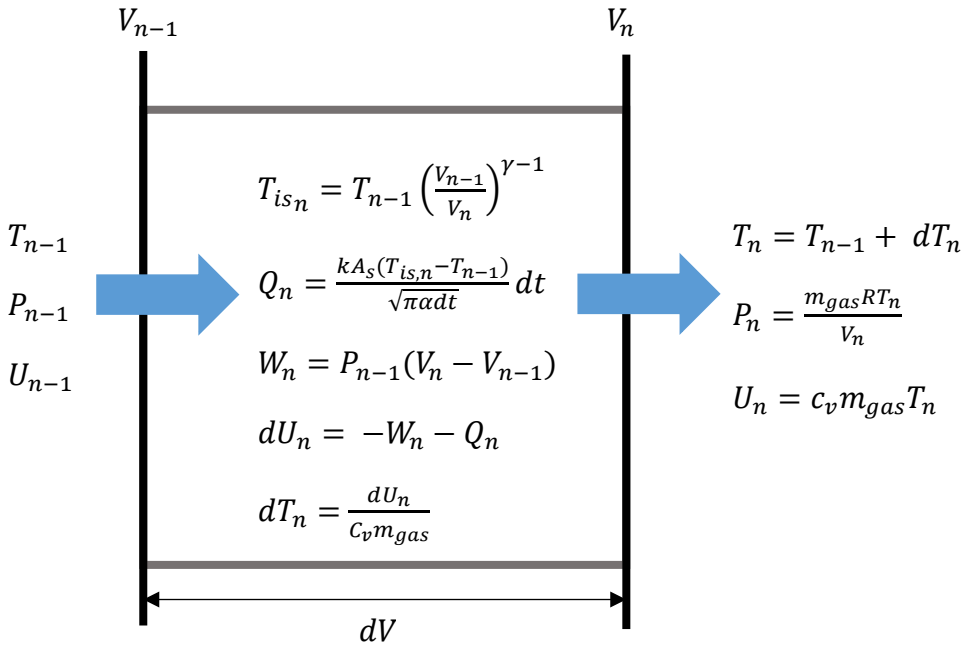

Figure 3-23: Solution process for one volumetric step in the transient heat flow step model

The model was checked from 1 to 10 Hz to make sure the net PV work and net heat transfer should be the same, and it was found the difference ranged from 0.08% to 3.1%, with the lowest and highest error corresponding to the 1 and 10 Hz, respectively.

Adiabatic, polytropic, and isothermal results for temperature and pressure were also calculated with the step model. For the adiabatic step model results, the heat transfer was set to zero. This results in all the P-V work being transferred to the internal energy of the gas. In the isothermal model, the change in internal energy was set to zero.

The polytropic results were calculated slightly differently as both pressure and temperature of the next step could be defined with the polytropic relationship, so the isentropic assumption for the temperature was not needed. The polytropic index for helium was kept constant at $n = 1.668$.

The following results are all from the step model with transient heat transfer, polytropic, adiabatic, and isothermal assumptions, at an operating frequency of 1 Hz. The P-V diagram for the step model for all assumptions is shown in Figure 3-24. The P-V diagram of the transient heat transfer model shows that all models start with the same initial conditions at the maximum volume, and then converges to a higher pressure and temperature.

The only P-V diagram with a difference between the compression and expansion processes, and therefore an enclosed area, is the model with transient heat transfer. A phase shift is therefore only present in the transient heat transfer model, as shown in Figure 3-25.

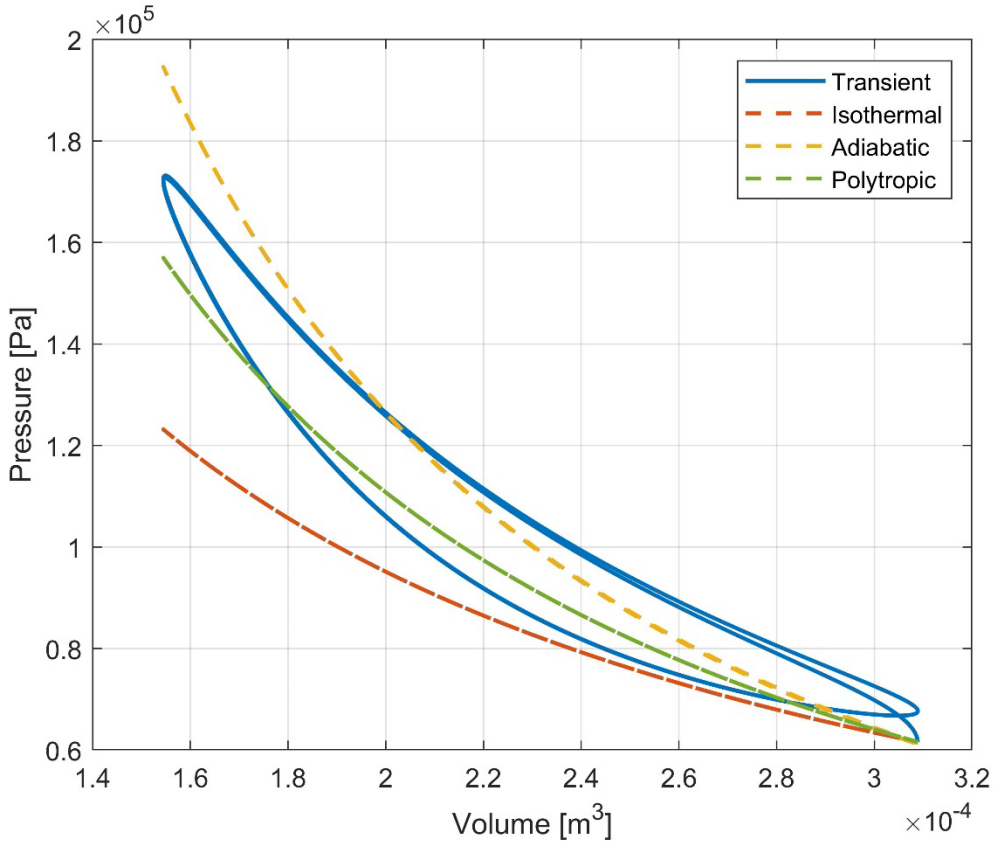

Figure 3-24: P-V diagrams for step model with transient heat transfer, polytropic, adiabatic, and isothermal assumptions

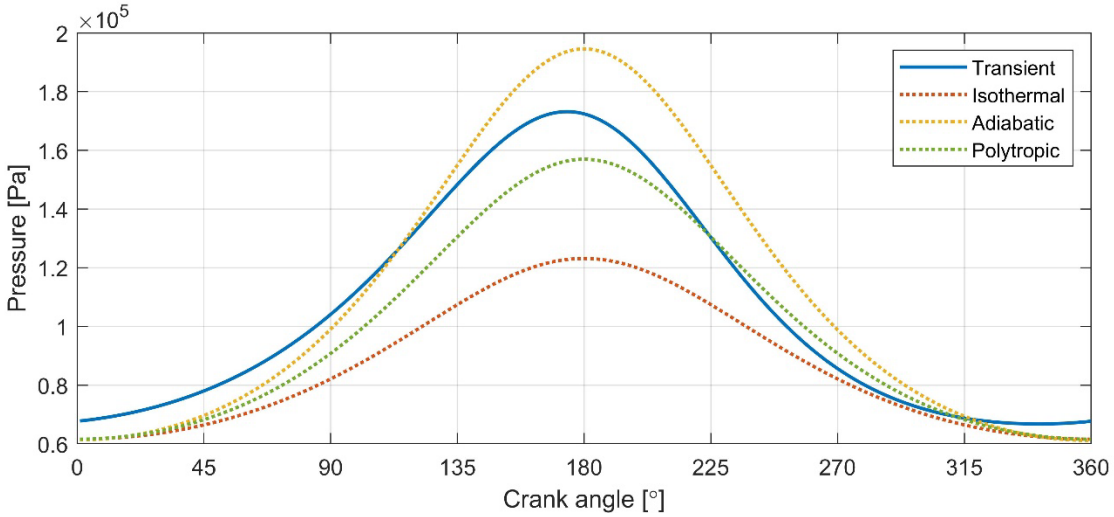

Figure 3-25: Pressure vs crank angle for transient heat transfer, polytropic, adiabatic, and isothermal assumptions

The difference between the polytropic assumption and the transient heat transfer assumption is how the latter takes into consideration the time required for heat transfer to take place, which leads to a phase shift in heat transfer that increases with frequency. While the polytropic assumption still assumes there is heat transfer, this heat transfer is perfectly in phase with the P-V work input. This can be seen in Figure 3-26. This lag in heat transfer is what causes the pressure and temperature to peak before the piston reaches the top dead centre, therefore leading to the pressure phase shift.

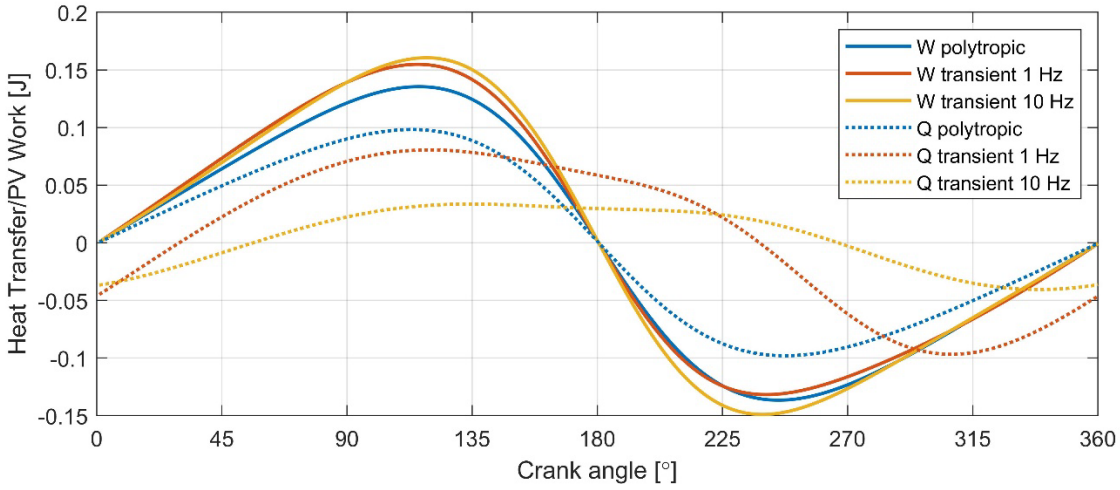

Figure 3-26: Polytropic and transient cyclic P-V work and heat transfer in the step model for 1 Hz and 10 Hz

This simplistic model predicts net heat transfer, which in a single space is hysteresis loss. The only assumption which predicts net heat transfer is one where the heat transfer lags the P-V work, which indicates that the time-dependence of heat transfer is what causes the difference between the compression and expansion work. Since this model is simplistic in that it only contains the fundamental thermodynamic relationships, it can be concluded that the resulting pressure phase shift is purely a result of the relationships between gas properties and the conversions between work, heat, and internal energy.

3.7 Mechanisms of the Pressure Phase Shift

How is the pressure phase shift connected to both heat transfer and net P-V work? All the information from Sections 3.4 through 3.5 regarding net values, amplitude, and phase shift should now be considered for the full picture of the energy transfers occurring in a compression and expansion process and how this affects the pressure phase shift. Looking at this information and understanding them with respect to the fundamental equations of the first law and the ideal gas law leads to a simple explanation.

Firstly, consider the two ideal cases at infinitely low and infinitely high operating frequencies. Isothermal heat transfer occurs at slow operating frequencies, so that there is enough time that the temperature, and therefore the internal energy of the gas, to remain constant as the gas is compressed and expanded. This can be seen in Figure 3-27. There is no temperature difference developed between the gas and the wall, so there will also be negligible net gas-wall heat transfer, which can be seen in the low frequency range of Figure 3-18.

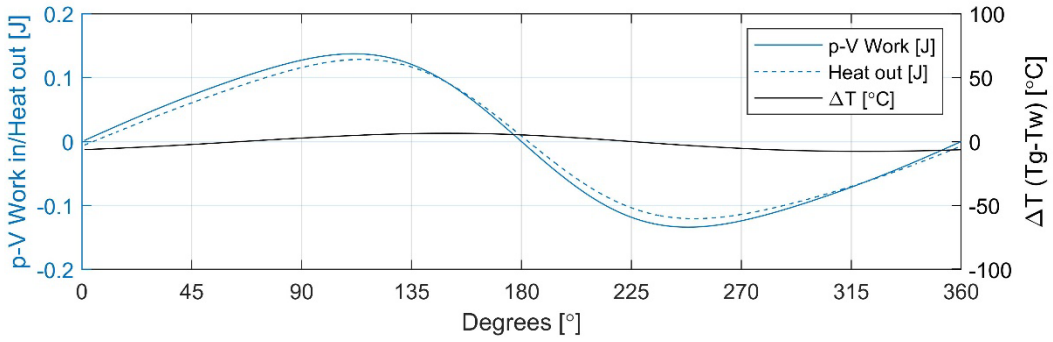

Figure 3-27: Cyclic P-V work, heat transfer and temperature difference at 0.01 Hz

Adiabatic operation would occur at high frequencies, so there would not be enough time for heat to transfer between the gas and the cylinder walls. All the P-V work into the system is converted into a change in internal energy, and therefore there is a large temperature increase in the gas, as seen in Figure 3-28. However, due to the time required for heat transfer, even though there is a temperature difference developed

between the gas and the wall, there is no net heat out of the gas, which can be seen in the high frequency range of Figure 3-18.

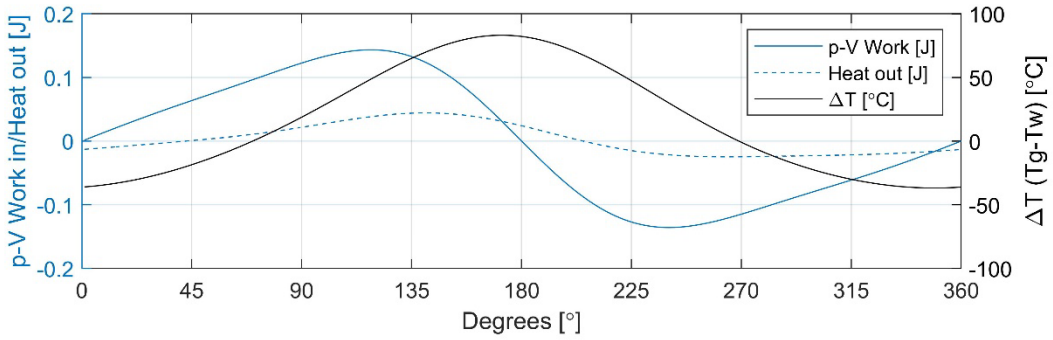

Figure 3-28: Cyclic P-V work, heat transfer and temperature difference at 10 Hz

For both extreme processes, the pressure phase shift is zero, and so is the net P-V work. A zero value for net P-V work makes sense for both these scenarios. This follows from the first law: for both isothermal and adiabatic processes, the net heat transfer over each cycle is zero. For isothermal processes, this is due to complete conversion between heat and work, and for adiabatic processes this is due to insufficient time for heat transfer, resulting in the work being completely converted to internal energy. Following the first law, as there is no net heat transfer out of the system, the net P-V work transfer into the system is also zero. This was shown in Figure 3-18 where, taking the working gas as the control volume, the net heat out and net P-V work input are equal and opposite.

When the heat transfer characteristics fall in between the two extreme processes, the input P-V work is "distributed" between the change in internal energy and the heat transfer out of the gas, so the full first law applies:

$$\oint Q + \oint W = \oint dU \qquad \text{Equation 31}$$

The quantities affecting the pressure of a closed system are the volume and temperature of the gas, as outlined in the ideal gas equation of state:

$$P = \frac{mRT}{V} \qquad \text{Equation 32}$$

The ideal gas equation was used instead of a real gas equation such as the Redlich–Kwong equation of state because the compressibility effects would obscure the pressure phase shift due to heat transfer.

Since the volumetric change is specified by the piston motion, it must be the temperature that affects the pressure variation. During the compression process, the temperature of the gas increases to be higher than that of the adjacent walls, which causes gas-to-wall heat transfer, decreasing the internal energy (and therefore temperature) of the gas before the piston reaches the top dead centre. This decrease in temperature also causes the pressure to drop before the top dead centre – this lead is the pressure phase shift (Figure 3-24).

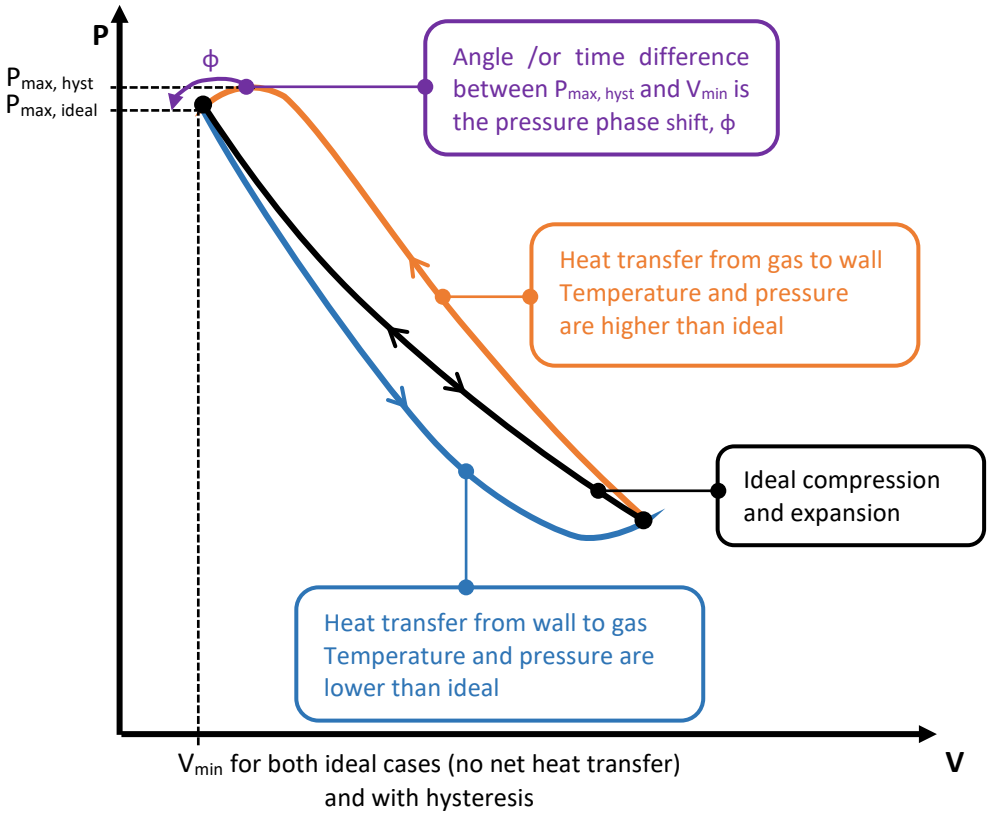

Figure 3-29: P-V diagram showing pressure phase shift

As the bulk of the heat transfer out of the gas occurs at the end of the compression process, pressure and temperature of the gas are high during compression. Subsequently, the pressure is lower during the expansion process than it would have been, had there not been heat transfer out of the gas during the compression process.

Because of the aforementioned process, not all the compression work is recovered during expansion, and there is a net P-V work input required which is equal to the net heat lost. It is therefore no surprise that the maximum phase shift of the pressure wave coincides with the P-V work in terms of the frequency, as seen in Figure 3-15.

3.8 Summary

In this chapter, a single cylinder Sage model was created and validated against Kornhauser and our own experimental values. Using this validated Sage model, the effect of working gas and gas pressure on the non-dimensional loss was studied, and the non-dimensional loss was considered. The underlying mechanisms which contribute to the pressure phase shift were investigated, such as the cyclic temperature variation of the working gas, as well as the cyclic heat transfer variation.

While the amplitude of the cyclic heat transfer simply increases with operating frequency (from isothermal to adiabatic operation), the net heat transfer peaks in the middle, and is equal and opposite to the net p-V work, in accordance with the first law. The pressure phase shift and its relationship with the net p-V work is also observed, as predicted by experiments and theory by Kornhauser (1989).

It was found, as expected from the findings of Annand (1963), Nikanjam and Greif (1978), that the bulk of the heat transfer occurs at the end of the compression process. We suggest that this heat transfer causes the temperature and therefore pressure of the working gas to decrease before reaching TDC, which is the pressure phase shift.

The idea was developed on how fundamental the pressure phase shift is in the relationship between heat transfer and work input. The transient step model demonstrated how the pressure phase shift manifests in a model as simple as a single space with only the first law and ideal gas law applied, with heat transfer modelled

between isothermal and adiabatic limits. The important finding of this model was that the phase lag of heat transfer in reference to the input P-V work is the key to the difference between compression and expansion work, leading to net heat transfer and P-V work by means of the resulting pressure phase shift.

Chapter 4 goes into greater detail into discussing whether the pressure phase shift is a cause or effect of the net P-V work, and how the pressure phase shift manifests in different refrigeration models such as models with discrete and sinusoidal piston motion.

Chapter 4: Understanding the Pressure Phase Shift

Chapter 3 and previous literature (Cooke-Yarborough & Ryden, 1985; Kornhauser, 1989; Pourmovahed & Otis, 1984); Pourmovahed and Otis (1990) have established that there is a relationship between cyclic net heat transfer, the pressure phase shift, and work input for a single space system. In a single space system, any net heat transferred out of the system could be classified as a loss. As gas hysteresis has been analysed from the point of view of a single space system, it has often been identified as a possible loss mechanism in more complicated systems such as refrigerators, heat pumps, and engines. However, very little work has gone into quantifying the relationship between the pressure phase shift and heat transfer, P-V work, and other quantities such as pressure and temperature within one of these devices. The focus of Chapter 4 is to answer these questions:

There are different ways to model refrigeration cycles and their various spaces. How does the pressure phase shift manifest in a refrigeration cycle? Does it change with different models (ideal, Schmidt, with losses) and piston motion (sinusoidal, discrete)?

The interactions between heat transfer characteristics such as the net heat transfer, the heat transfer amplitude and phase, and the pressure wave are also important. For example, this chapter explains that with any net heat transfer (and therefore net P-V work) there must be a pressure phase shift – it cannot be eliminated entirely.

This section builds on the idea that the pressure phase shift is a fundamental phenomenon which is directly linked to the first law of thermodynamics, specifically linking net heat transfer and net P-V work together, regardless of the piston motion or the model's degree of idealisation.

While others have attempted to derive correlations to predict this pressure phase shift for single space cylinders, the purpose of these sections was to understand why and how they are connected. Two scenarios are analysed: sinusoidal and discrete piston motion. For sinusoidal piston motion, an equation is derived correlating the pressure phase shift with the net P-V work based on simple harmonic motion. For discrete piston motion, the pressure phase shift is instead qualitatively identified, as previous literature misses the existence of a pressure phase shift, especially for the Ideal Stirling cycle.

4.1 Sinusoidal Piston Motion

The most common physical manifestation of the Stirling cycle utilises sinusoidal or approximately sinusoidal piston motion. The effect of the pressure phase shift on the net P-V work on a single space is examined in the following calculations. The pressure phase shift for an ideal Stirling refrigerator using sinusoidal piston motion is then derived by extending the Schmidt cycle calculations.

The two varying quantities in this problem are the pressure and volume within a single cylinder. For sinusoidal piston motion, the net P-V work would be the integral of pressure and the change in volume as two sinusoidally varying functions. Figure 4-1 shows normalised pressure and volume waves and how an increasing phase shift, ϕ, affects the pressure wave. Figure 4-2 shows the resulting pressure – volume diagrams produced for increasing pressure phase shifts. It should be noted that this analysis is for one harmonic only, at any frequency.

The functions for pressure and volume are defined below, where P and V are pressure and volume, θ is the crank angle in radians, and ϕ is the phase shift of pressure with respect to the ideal pressure wave (exactly 180° out of phase with volume), which is also equal to the phase lead of the pressure to the volume wave. Subscripts '*0*' and '*a*' represent mean values and amplitudes, respectively:

$$P = P_0 + P_a \cos(\theta + \pi + \phi) \qquad \text{Equation 33}$$

$$V = V_0 + V_a \cos(\theta) \qquad \text{Equation 34}$$

$$dV = -V_a \sin(\theta)\, d\theta \qquad \text{Equation 35}$$

As the net P-V work input is the integral of P-dV between $0 \leq \theta \leq 2\pi$, the net P-V work can be calculated by substituting the functions for pressure and volume and integrating:

$$\int_0^{2\pi} PdV = \int_0^{2\pi} (P_0 + P_a \cos(\theta + \pi + \phi))(-V_a \sin(\theta))\, d\theta \qquad \text{Equation 36}$$

After integration and substitution of limits:

$$\int_0^{2\pi} PdV = -\pi P_a V_a \sin(\phi) \qquad \text{Equation 37}$$

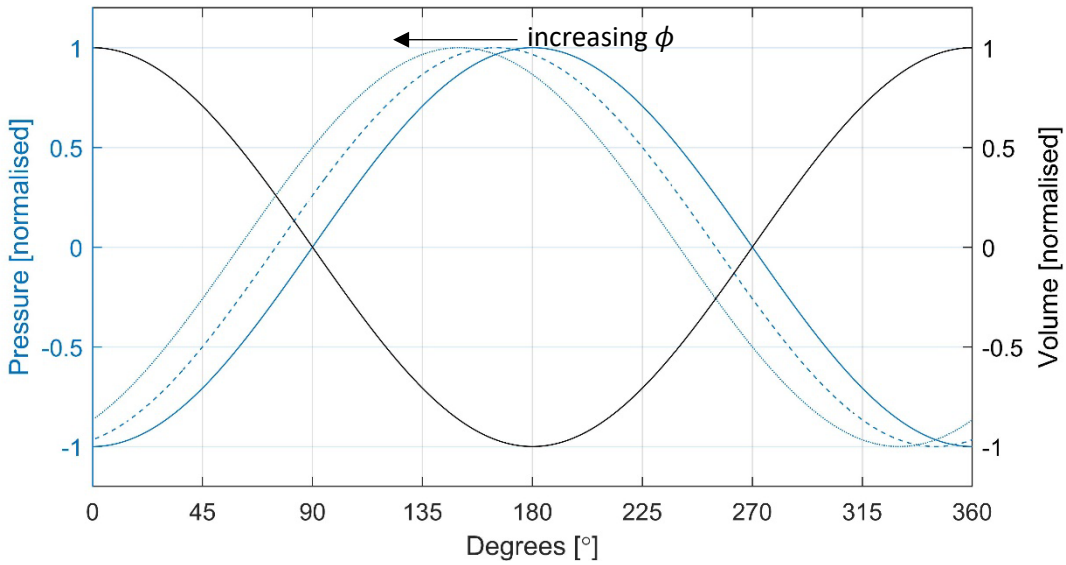

Figure 4-1: Volume and pressure as sinusoidally varying functions with an increasing pressure phase shift, ϕ

The derived expression for net P-V work (Equation 37), is simply the area enclosed by the P-V loop. The area of an ellipse would have the equation $A = \pi r_1 r_2$, where r_1 and r_2 are the radii on the x and y axes. In this case, the x and y axes are volume and pressure, as shown in the P-V diagram in Figure 4-2. The radii used for the calculation of the P-V diagram area are simply the corresponding amplitudes of the volume and pressure waves. Therefore, the maximum area is given as $A = \pi P_a V_a$. The $\sin(\phi)$ component of the P-V equation gives a proportion of maximum area, as $\sin(0) \rightarrow \sin(90\,°)$ ranges from 0 to 1.

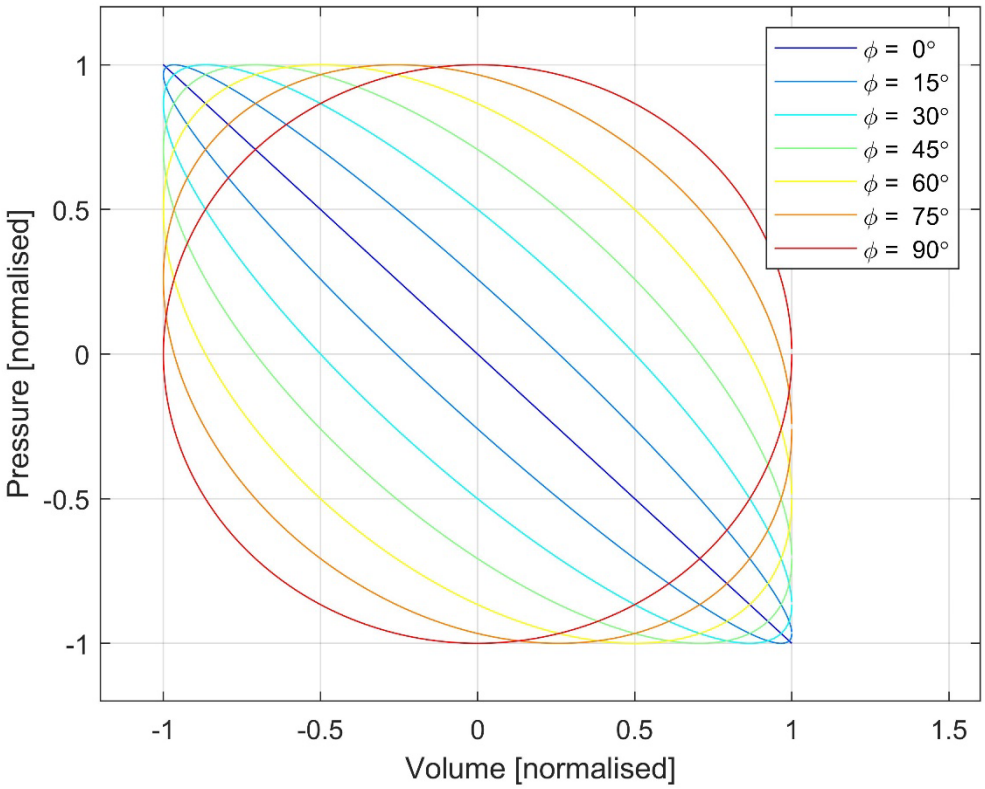

Figure 4-2: The P-V diagrams produced assuming single harmonic sinusoidal piston motion for increasing pressure phase shift, ϕ

It should be noted that Equation 37 and the P-V diagram in Figure 4-2 can approximate only the net P-V work for given pressure and volume amplitudes. It cannot predict the heat absorbed and rejected (and therefore the COP) of a Stirling refrigerator, as the pressure and volume variations used are the overall values, and the heat transfer processes (including the internal regeneration effect) are occurring in separate spaces in the refrigerator. Likewise, it cannot predict the heat absorbed and rejected in a single space, but it does predict the net P-V work, and therefore the cyclic net heat transfer.

The Schmidt equations give the ideal isothermal performance of a Stirling refrigerator executed with sinusoidal piston motion. It takes into consideration the expansion and compression space volume separately and assumes that the heat exchangers and regenerator are ideal and contribute to the total dead volume of the system. The total volume mean value, amplitude and phase shift need to be derived.

The Schmidt theory does not explicitly give an equation for the pressure phase shift (the angle the maximum pressure leads the minimum volume). However, ϕ can be derived

by finding the total volume phase shift and the relationships given for the Schmidt theory defined angles at which the pressure is minimum and maximum. For this analysis, α = the angle by which volume variations in the expansion space leads those in the compression space, $\kappa = \frac{V_C}{V_E}$, the swept volume ratio, and θ = the crank angle in either degrees or radians. The derived total volume, V_t, can be found by using the Sage equations, Equations 1 and 2. It results in an addition of two cosine waves, shown in Equation 38:

$$V_t = V_e + V_c = \frac{1}{2}V_E(1+\kappa) + \frac{1}{2}V_E(\cos(\theta) + \cos(\theta - \alpha)) \qquad \text{Equation 38}$$

Adding these two cosine waves and finding the resulting mean, amplitude, and phase shift of the total volume gives:

$$V_t = V_{t,mean} + V_{t,amplitude}\, cos(\theta + \phi_{V_t}) \qquad \text{Equation 39}$$

where:

$$V_{t,mean} = \frac{1}{2}V_E(1+\kappa) \qquad \text{Equation 40}$$

$$V_{t,amplitude} = \frac{1}{2}V_E\sqrt{\kappa^2 + 1 + 2\kappa cos(\alpha)} \qquad \text{Equation 41}$$

$$\phi_{V_t} = tan^{-1}\left(\frac{-\kappa\, sin(\alpha)}{1 + \kappa\, cos(\alpha)}\right) \qquad \text{Equation 42}$$

The angle where volume is maximum, $\theta_{V_{max}}$, is located at $\theta = -\phi_{V_t}$.

The Schmidt theory defines that the pressure is minimum where $\theta = \theta_{p_{min}}$ (Walker, 1983):

$$\theta_{p_{min}} = \tan^{-1}\left(\frac{\kappa \sin(\alpha)}{\tau + \kappa \cos(\alpha)}\right) \qquad \text{Equation 43}$$

The difference between $\theta_{V_{max}}$ and $\theta_{p_{min}}$ is the phase shift of the pressure in relation to total volume, ϕ

$$\phi = \theta_{V_{max}} - \theta_{p_{min}} = -\phi_{V_t} - \tan^{-1}\left(\frac{\kappa \sin(\alpha)}{\tau + \kappa \cos(\alpha)}\right)$$

$$\phi = \tan^{-1}\left(\frac{\kappa \sin(\alpha)}{\tau + \kappa \cos(\alpha)}\right) - tan^{-1}\left(\frac{-\kappa\, sin(\alpha)}{1 + \kappa\, cos(\alpha)}\right) \qquad \text{Equation 44}$$

It can be seen here that the pressure phase shift, according to the Schmidt theory, is purely based on α, the angle that the expansion space volume variation leads the compression space, κ, the swept volume ratio, and τ, the temperature ratio. This does not take into consideration any losses or heat transfer which could also affect the pressure phase shift.

Setting Equation 44 to equal zero leads to κ and α becoming redundant, leaving $\tau = 1$. The working for this is shown in Appendix G. This means for an ideal Stirling cycle with sinusoidal motion, the pressure phase shift is only ever zero when there is no temperature difference created, meaning there is no net P-V work required. It is becoming increasingly clear that there is a pressure phase shift for any net P-V work requirement, and that for any refrigeration effect there is an ideal minimum P-V work, and therefore a minimum pressure phase shift associated with it.

It can be concluded from these calculations that for a single space, the pressure phase shift directly relates to the magnitude of the net P-V work. Likewise, and more interestingly, the modified Schmidt equations show that a Stirling refrigerator executed with sinusoidal piston motion must have a pressure phase shift even in the ideal operation. Without this pressure phase shift, there would be no net P-V work and therefore no refrigeration effect. The following section discusses the pressure phase shift in relation to discrete piston motion, and its similarities to the phase shift in sinusoidal motion.

4.2 Discrete Piston Motion

The ideal Stirling cycle is traditionally modelled using discrete piston motion to describe the cycle's isochoric and isothermal processes. The phase shift and net P-V work relationships for the ideal discrete cycle have not been previously discussed in literature, due to the assumption that the pressure phase shift is inherently a loss mechanism. This assumption exempts the lossless ideal cycle from consideration. However, it is becoming increasingly apparent that the pressure phase shift is related to the net P-V work and is not a loss-specific phenomenon. Furthermore, the question of whether the pressure phase shift is piston motion related and only manifests within sinusoidally executed machines must also be answered. The appearance of the pressure phase shift and its relationship to the net P-V work with discrete piston motion is discussed in this chapter. It is found that the pressure phase shift also exists and directly relates to the net P-V work for refrigerators with discrete piston motion.

A Single-Space Ideal Discrete Stirling Cycle

A piston-cylinder device can be theoretically transferred between a cold bucket (heat source) and a hot bucket (heat sink) of water. The following processes are illustrated in Figure 4-3, with its familiar P-V diagram in Figure 4-4. The piston-cylinder device is placed inside the cold bucket and, after reaching temperature equilibrium, expanded, so heat is absorbed by the gas inside the piston from the water at low temperature. It is then moved and placed into the hot bucket, where it is held at constant volume until it reaches temperature equilibrium. The piston is then compressed so heat is rejected into the hot bucket at the higher temperature. After this heat rejection into the hot bucket takes place, it is moved back into the cold bucket and held at constant volume to reach the low temperature equilibrium, and the cycle begins again.

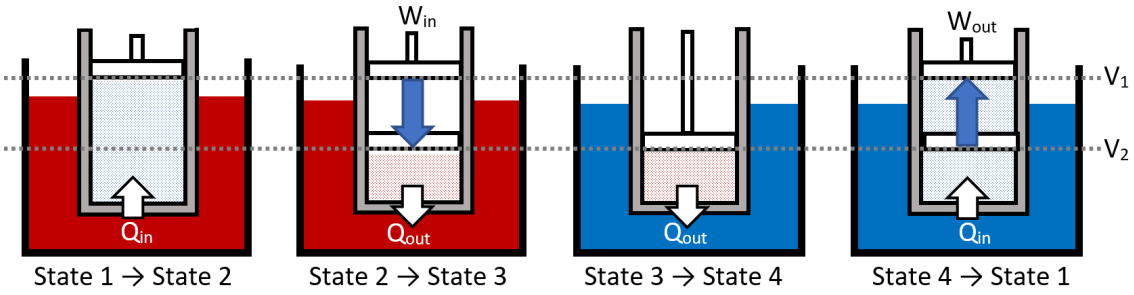

Figure 4-3: Single space discrete cycle processes

While this is only a hypothetical experiment, it does illustrate that in reality, the Stirling cycle can be executed with discrete piston motion, albeit not in a very practical way. The absence of a regenerator in this scenario reduces the COP quite significantly since the cooling and heating of the cylinder wall and the gas at constant volume means a direct and unrecoverable heat loss. Nevertheless, this theoretical cycle operates as a Stirling refrigerator with discrete piston motion. The following processes correspond to Figure 4-3, with the corresponding ideal cycle process in italics:

1-2: Isochoric heat absorption from the hot bucket

Isochoric heat absorption from the regenerator matrix - internal heat absorption

2-3: Isothermal compression with heat rejection into the hot bucket

Isothermal compression with external heat rejection

3-4: Isochoric heat rejection to the cold bucket

Isochoric heat rejection to the regenerator matrix - internal heat rejection

4-1: Isothermal expansion with heat absorption from the cold bucket

Isothermal expansion with external heat absorption

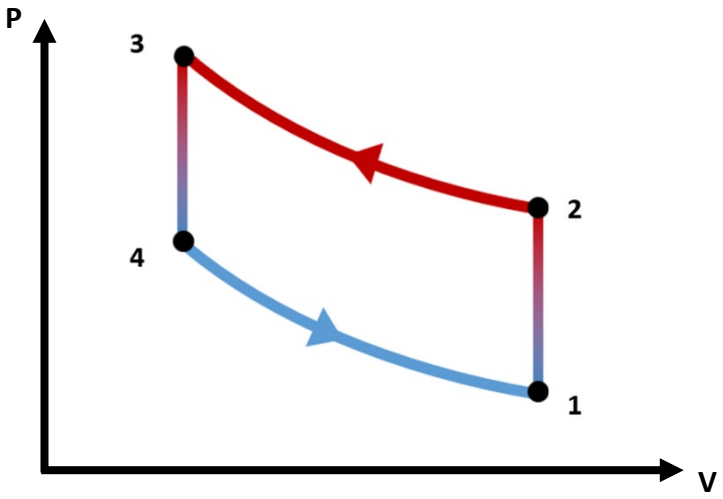

Figure 4-4: The single space ideal discrete Stirling cycle

Discrete Pressure Phase Shift

While the pressure phase shift and its necessity for any net P-V work is easy to describe and rationalise for sinusoidal piston motion, the pressure phase shift is not immediately apparent when considering discrete piston motion. This can be seen in the ideal Stirling cycle P-V diagram in Figure 4-4, as the pressure and volume reach minimum and maximum respectively at the same point in the cycle. This can lead to the incorrect reasoning that for discrete piston motion there is no phase shift, and that the pressure phase shift manifests only in machines implemented with sinusoidal piston motion.

The problem lies in the way a phase shift is quantified. The definition of a phase shift for sinusoidal motion does not translate well to discrete piston motion. In the ideal Stirling cycle, the pressure reaches maximum at the same time the piston arrives at the top dead centre, so there is no obvious pressure phase shift in the P-V diagram. However, once the pressure and volume (or displacement) profiles are plotted over time, the phase shift becomes more obvious.

The discrete pressure phase shift is illustrated in the pressure and volume plot over crank angle in Figure 4-5. While the crank angle is technically not applicable for discrete piston motion, it can still be used as a quantity for visualising the cycle processes and locating maximum and minimum in pressure and volume. The discrete pressure phase shift can be clearly seen at the point where the pressure reaches its peak at 180° and starts falling; as the pressure decreases, the volume lags the pressure in the isochoric process. The only difference between discrete and sinusoidal motion is that the pressure phase shift can be directly measured at all points in the cycle for sinusoidal motion, but for discrete piston motion the phase shift is in the inherent 'lead' the pressure has on the volume.

This phase shift is not directly quantifiable at every point in the cycle, but this lag caused by the isochoric processes undeniably results in a P-V loop with a finite area and the same effect as a phase shift in sinusoidal motion, which leads to the inevitable net P-V work that is required for a refrigeration effect. This phase shift caused by the isochoric process will be referred to as the ideal discrete phase shift, ϕ_d, shown in Figure 4-5.

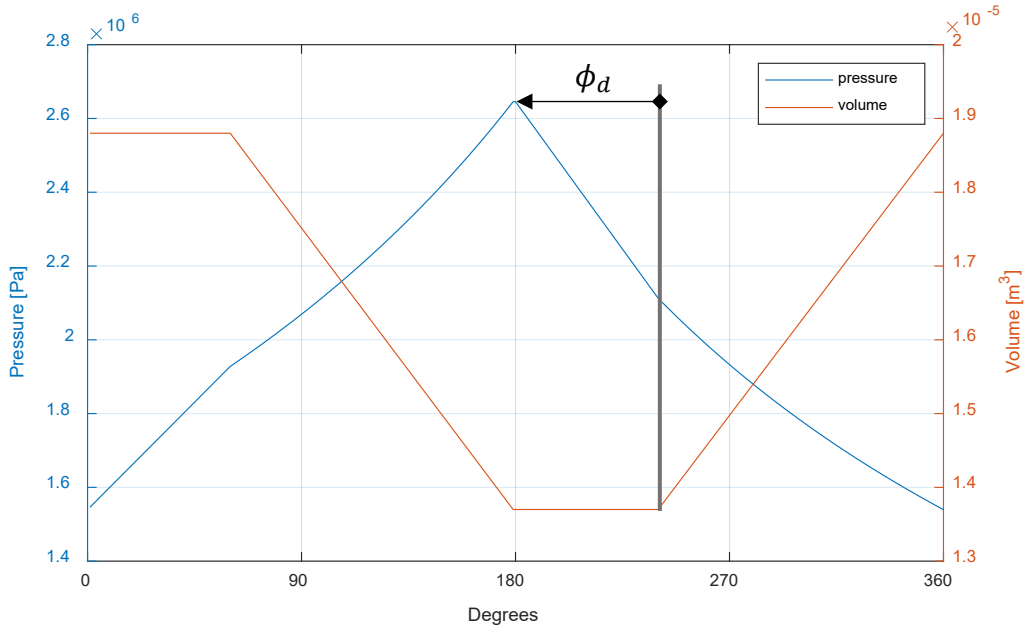

Figure 4-5: Ideal pressure and volume vs crank angle with discrete piston motion

The discrete pressure phase shift only exists when there is a net P-V work input due to the expansion and compression at two different temperature levels. A simple piston cylinder device operated with discrete motion around one temperature can be considered, shown in the isothermal process of Figure 4-6. In fact, as long as the heat transfer follows the same path during compression and expansion, there will be no refrigeration effect, no net P-V work, and no pressure phase shift, similar to sinusoidal motion. This can be seen in the adiabatic and polytropic processes without hysteresis loss in Figure 4-6.

A single space piston cylinder example (like Kornhauser's experiment) is where the pressure phase shift due to hysteresis loss can be seen by itself, isolated from the ideal discrete pressure phase shift due to producing a heat lift. The pressure phase shift due to hysteresis, ϕ_h is shown in Figure 4-7.

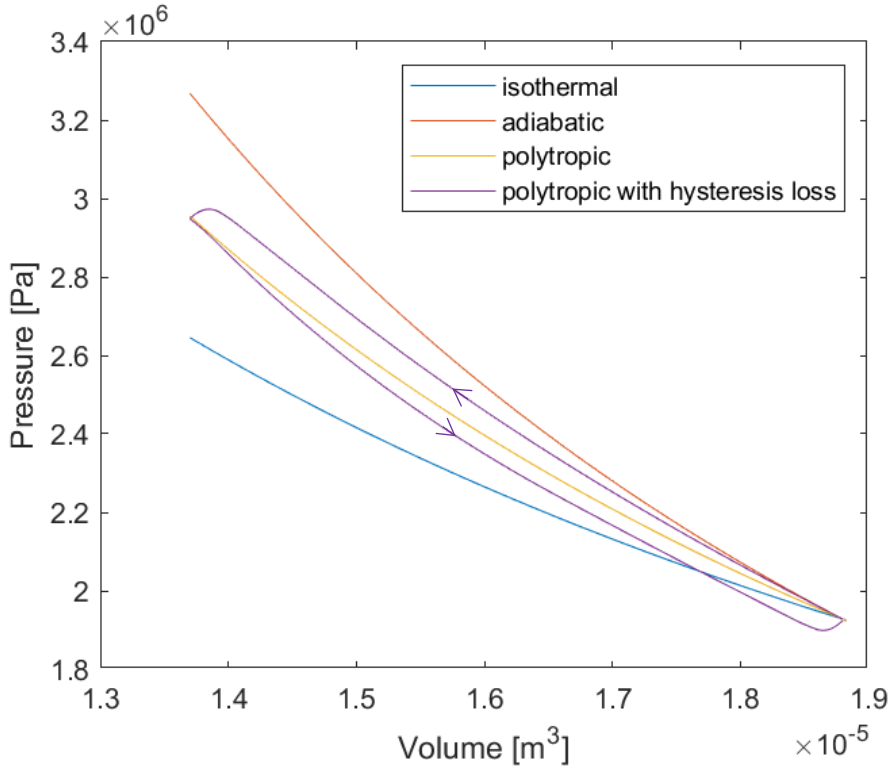

Figure 4-6: P-V diagram for a single piston cylinder device with discrete piston motion

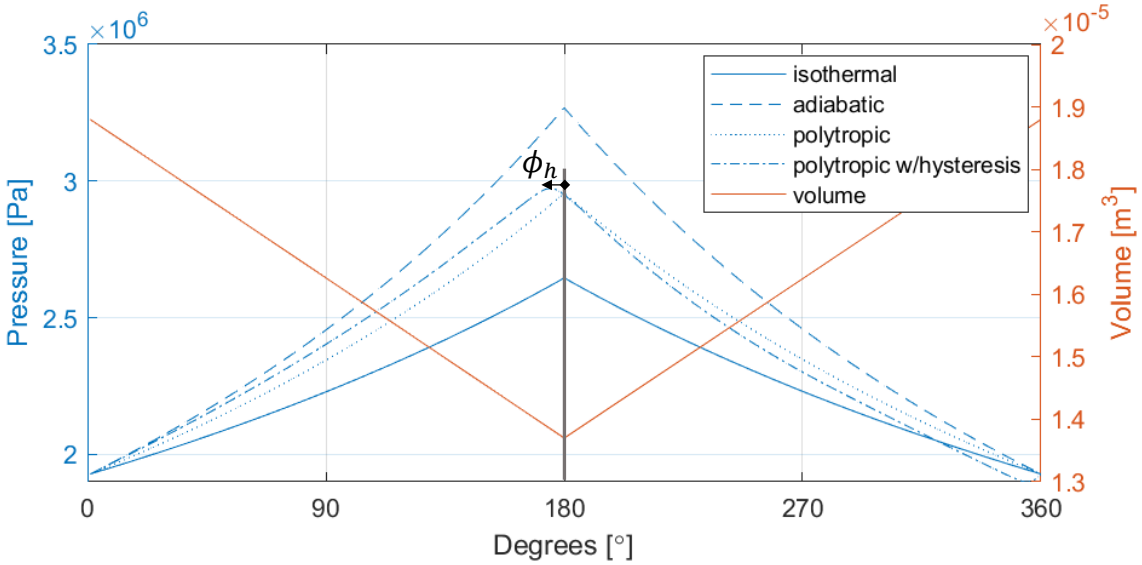

Figure 4-7: Pressure and volume against crank angle for a single piston cylinder device with discrete piston motion

The combined ideal discrete phase shift and hysteresis phase shift can be seen in the ideal Stirling cycle with discrete piston motion. The P-V diagram shown in Figure 4-8 shows an ideal cycle and a cycle with heat transfer losses. The non-dimensional pressure and volume plotted against crank angle in Figure 4-9 shows how the ideal pressure phase shift and the hysteresis phase shift combine for the total pressure phase shift, ϕ.

If there were other losses, ϕ_h would increase, increasing the required net P-V work input, while ϕ_d would stay the same. The only time ϕ_d changes is when the temperature ratio changes.

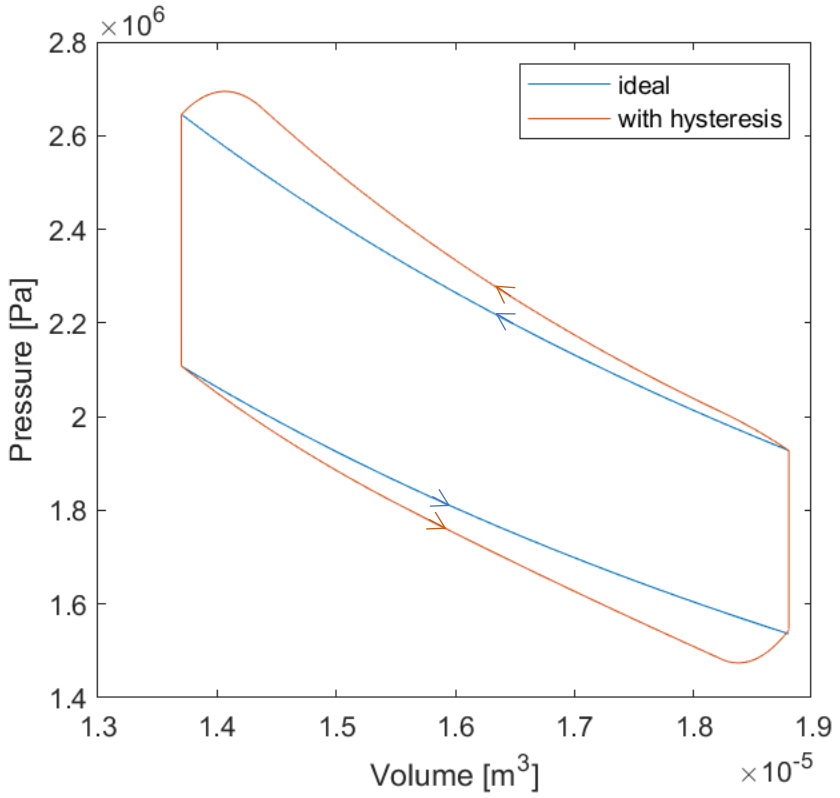

Figure 4-8: P-V diagram of Stirling cycle with discrete piston motion – ideal and with hysteresis loss

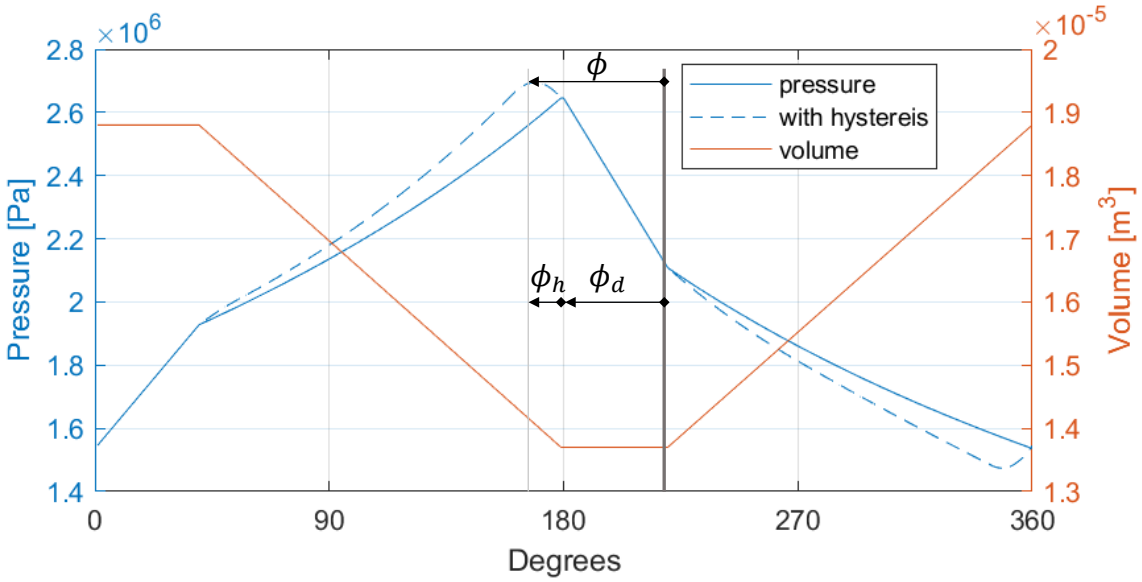

Figure 4-9: Pressure and volume against crank angle of Stirling cycle with discrete piston motion – ideal and with hysteresis loss

The Pressure Phase Shift in a Stirling Engine

While the subject of this study are Stirling refrigerators, it is worthwhile to discuss how hysteresis loss would affect a Stirling engine. The difference is that pressure lags volume in the case of a Stirling engine. An increased shift between pressure and volume would increase the net work output, a desired effect. Temperature oscillations of the working gas around the wall temperature would still cause there to be a net heat output and therefore hysteresis loss. The hysteresis loss in an engine would, in the same way as in a Stirling refrigerator, cause there to be a pressure phase lead. In a Stirling engine, this would have the effect of reducing the lag that the pressure wave has on the volume wave. This therefore decreases the work output of a Stirling engine. While out of scope of the current study, more research will be carried out in this area to better understand hysteresis loss.

4.3 Summary

Chapter 4 built a more conclusive picture on how the pressure phase shift manifests with different piston motion and idealising assumptions. Sinusoidal piston motion was considered, looking at a single space and by extending the Schmidt equations to find the conditions that the pressure phase shift would be zero. Even with ideal analysis, the only time the pressure phase shift is ever zero is when the temperature ratio, the ratio of the heat source to heat sink temperature, is 1. For discrete piston motion, the pressure phase shift manifests in the isochoric processes, which create the asymmetry between the compression and expansion. All of them show that the pressure phase shift is the key component required for a heat lift (eg, opening up the area on the P-V diagram), so there is no net heat transfer and therefore no net P-V work without a pressure phase shift, regardless of piston motion. It simply manifests in different ways.

Chapter 5: Hysteresis Loss in Stirling Refrigerators

The relationship between the net P-V work and the pressure phase shift, and how it manifests regardless of piston motion was established in Chapter 4. With this understanding, methods of identifying and reducing hysteresis loss within Stirling refrigerators are explored in this chapter. Sage is used to create a complete Stirling refrigerator model, and the inter-component net heat transfer is discussed, as well as the relationship between net P-V work and the pressure phase shift in a refrigeration model. The suitability of the Peclet number in predicting hysteresis loss is discussed, as well as the effect of a regenerator on the magnitude of hysteresis loss.

5.1 Stirling Refrigerator Test Rig

An existing test rig using a commercial Stirling cooler was used to validate Sage as a suitable modelling tool for Stirling coolers. The primary reason for using this test rig was that it has existing commercial validation data, and the results from testing could be compared with Sage model data and with the existing data to ensure that the measured operating parameters were within realistic ranges. The test rig setup used a Twinbird 40 W (SC-TA04) cooler, with its main specifications outlined in Table 5-1**.**

Table 5-1: SC-TA04 cooler specifications from Twinbird Corporation (n.d., p. 2)

Item	Specification
Size	W 130 x D 115 x H 240 mm
Weight	Approximately 1.9 kg
Refrigerant	Helium
Refrigerant amount	2.5 g
Internal pressure	2.6 MPa
Power source	12 VDC for control PCB
Cooling capacity at specified temperature conditions	35 W or more under the following conditions: T_{cold} = -23.3 °C $T_{ambient}$ = 25 °C Input voltage to set output voltage: 5 V
Power consumption	60 W or less
Ambient temperature limits	0 to 40 °C
Cold side temperature limits	-50 to 10 °C

The Twinbird schematic diagram and labelled components within the test rig are shown in Figure 5-1 and 5-2, respectively. It is a beta-configuration Stirling refrigerator and consists of a moving magnet linear motor-driven piston, with a free displacer in the sense that it is not driven by a motor but by the oscillating gas pressure. The piston and the displacer are both supported by flexure bearings to fix their motion to the axial direction and to provide a resonant system.

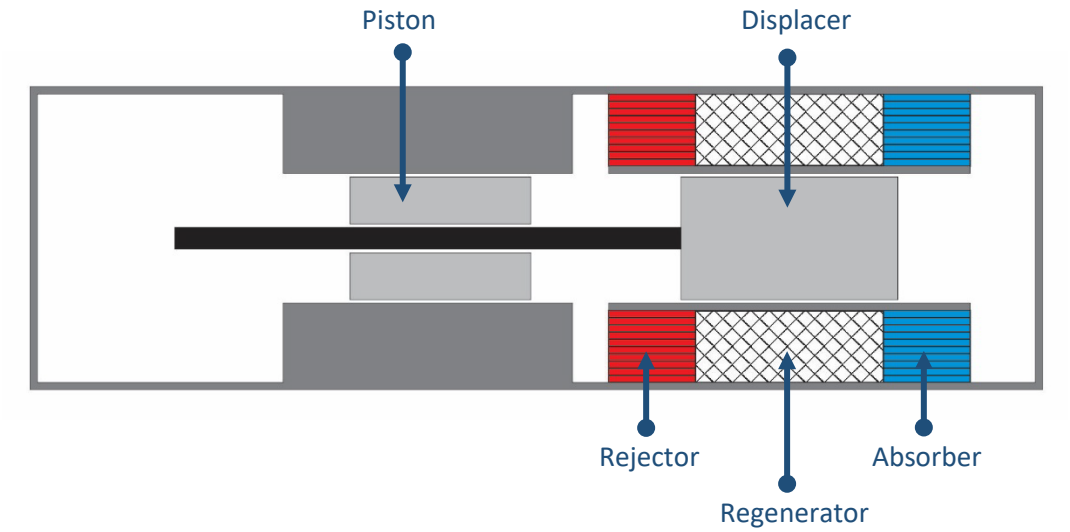

Figure 5-1: Schematic diagram of the Twinbird beta Stirling refrigerator

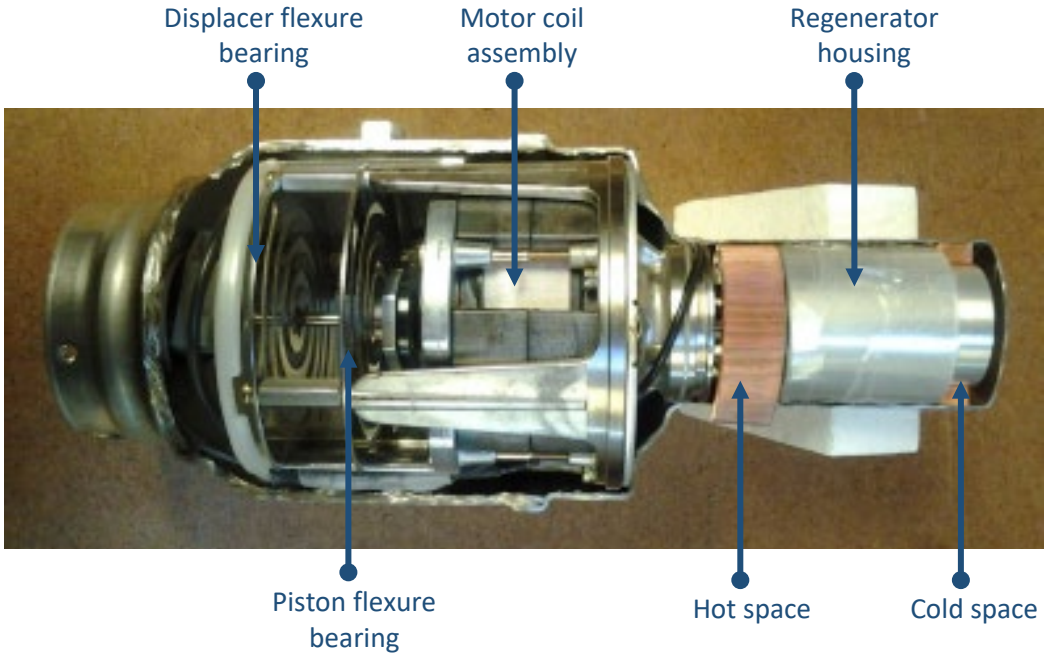

Figure 5-2: Labelled cross-section of Twinbird test rig

Data Acquisition

The schematic diagram of the refrigerator along with a list of the recorded inputs and outputs of the experiment is shown in Figure 5-3. The hot and cold end temperatures were measured with fine wire K-type thermocouples, while the pressure was measured with an Omegadyne pressure transducer. The cooling load was measured using a heater band around the cold end; at steady operation the power input to the heater band is equal to the cooling load. The test rig with labelled data acquisition set up is shown in Figure 5-4.

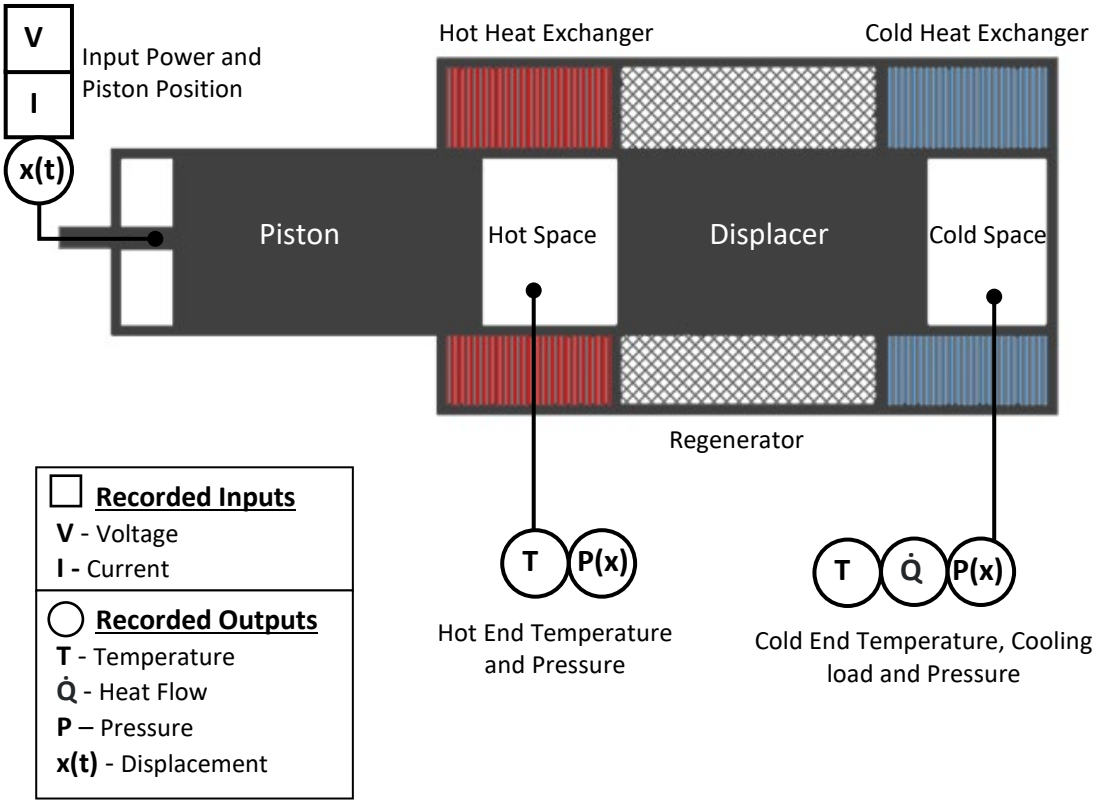

Figure 5-3: Twinbird refrigerator test rig inputs and outputs

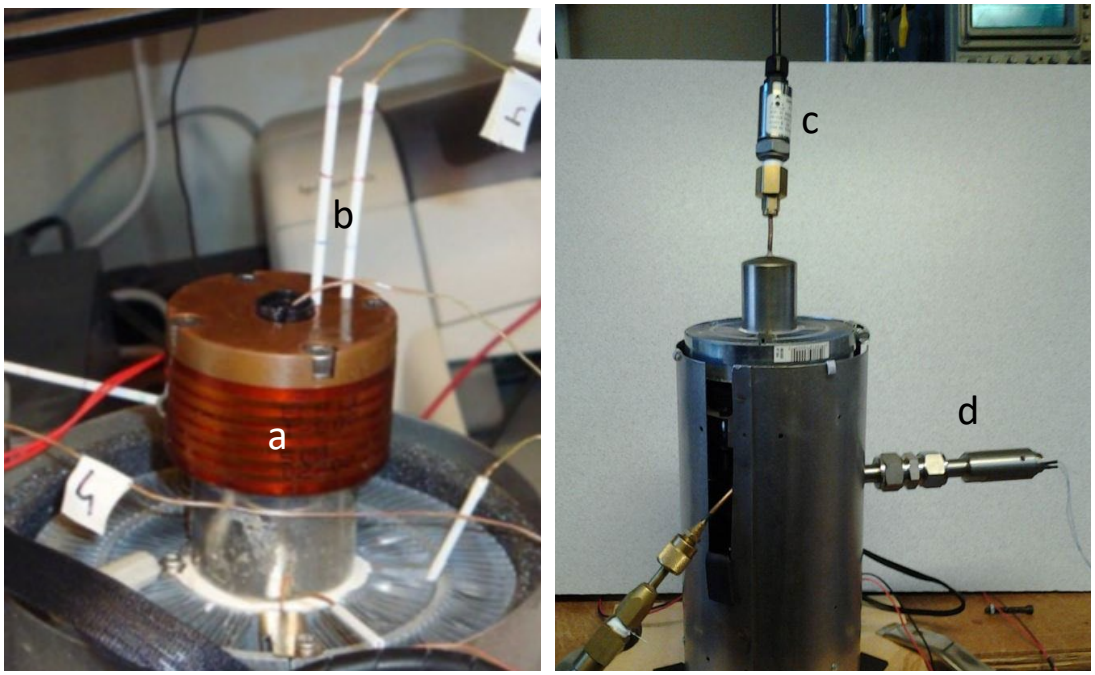

a) heater band to measure cooling load
b) temperature thermocouples
c) pressure transducer
d) strain gauge for displacement feedback

Figure 5-4: Labelled Twinbird test rig data acquisition setup

Experimental Method

The cooling capacity was measured for a cold end temperature range of around -70 °C to 0 °C. To measure this, the power input to the heater band around the cold heat exchanger was varied, and the refrigerator was run. The temperature of the cold end was recorded, and when the temperature reached a steady state value, this meant that the power input to the heater band was equal to the cooling capacity at that cold end temperature. Two sets of data were taken – one for a hot end temperature of 50 °C, and another for 60 °C.

5.2 Stirling Refrigerator Sage Model

A Sage model of the Twinbird refrigerator was created to validate Sage's agreement with multiple-space refrigeration devices, shown in Figure 5-5. The hot end temperature was set at 50 °C and 60 °C, while the cold end temperature was varied from -70 °C to 20 °C, and the cooling capacity was mapped. A comparison of the experimental refrigerator results and the Sage results are presented in the following section.

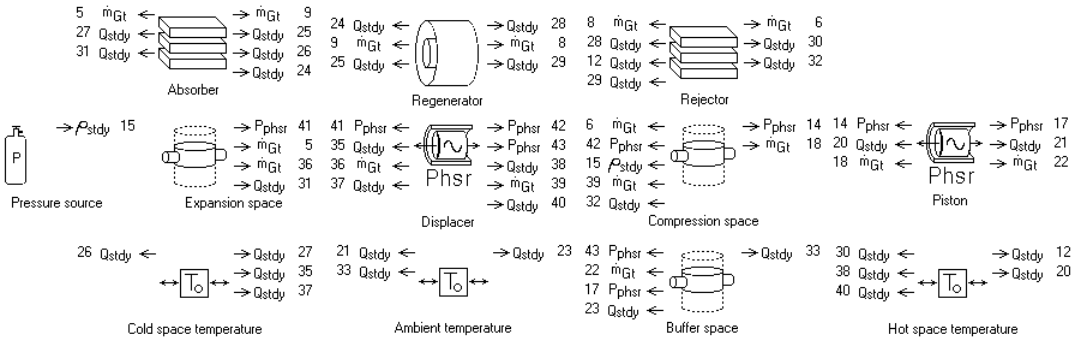

Figure 5-5: Twinbird Sage model

5.3 Stirling Refrigerator Sage Model Validation

The experimental and Sage model results are shown in Figure 5-6. The error in the experimental temperature readings were ± 2 °C, while the error in the cooling capacity was calculated using uncertainty propagation, with the errors in voltage and current readings being ± 2% of each respective reading. The experimental data and resulting errors are tabulated in Table A-2, Appendix E. The experimental and Sage results agree very well, with only a slight variation in experimental results. This agreement validates Sage for the modelling of Stirling refrigerators.

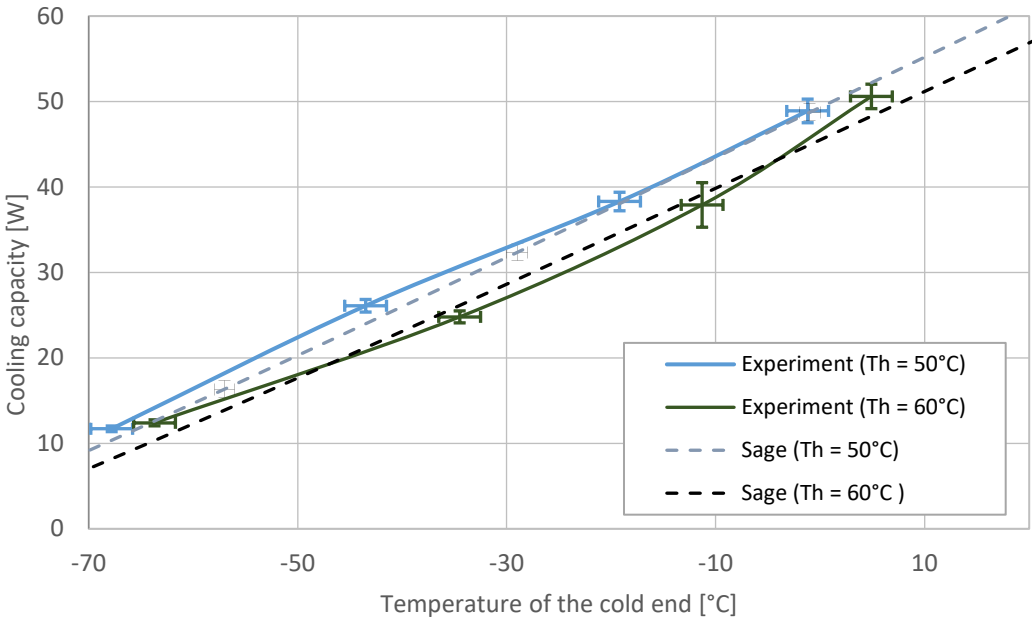

Figure 5-6: Experimental and Sage results for cooling capacity vs cold end temperature

5.4 Alpha Stirling Sage Model

After experimentally validating Sage's abilities to model Stirling refrigerators with the Twinbird test rig, it could be used further to carry out parameter studies to understand the underlying mechanisms of hysteresis loss within Stirling refrigerators. An alpha Stirling configuration was chosen to be the configuration analysed, as shown in Figure 5-7.

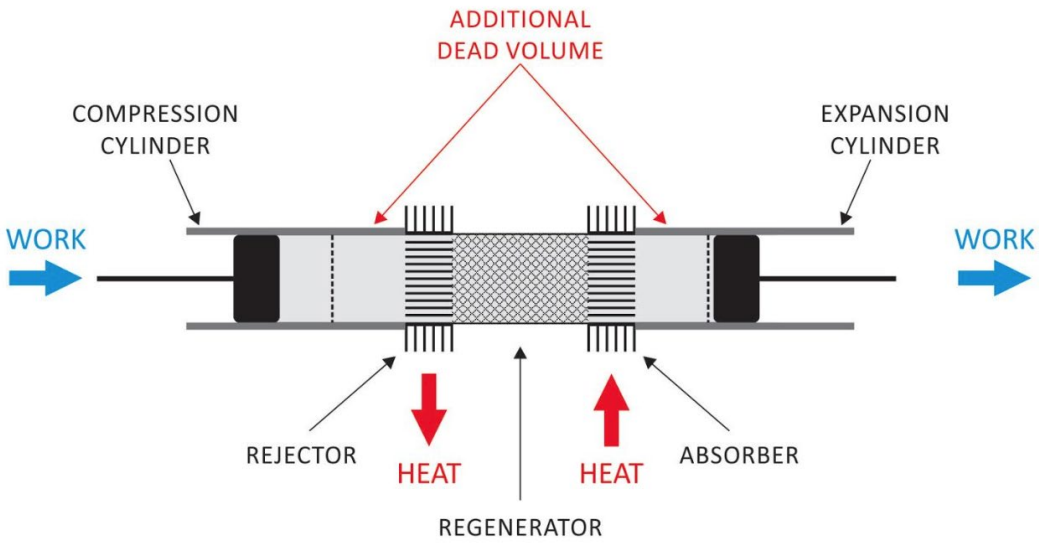

Figure 5-7: Schematic diagram of an alpha type Stirling refrigerator

The reason for choosing an alpha configuration as opposed to the free displacer beta configuration was the simplicity of design, and the control of both piston and displacer. The motion of the free displacer of the Twinbird refrigerator was dependent on gas forces and gas-spring resonance, which changed the operating parameters of the system, and the frequency ranges in which the refrigerator could physically operate. As both piston and displacer motion are controlled in the alpha configuration, the effects of hysteresis loss can be more easily identified as this control removes the resonant system considerations of the free displacer when analysing the system. The Sage model of the alpha Stirling refrigerator can be seen in Figure 5-8, and a comparison of Sage results of cooling capacity against cold end temperature can be found in Figure 5-9, where similar trends are predicted for both models.

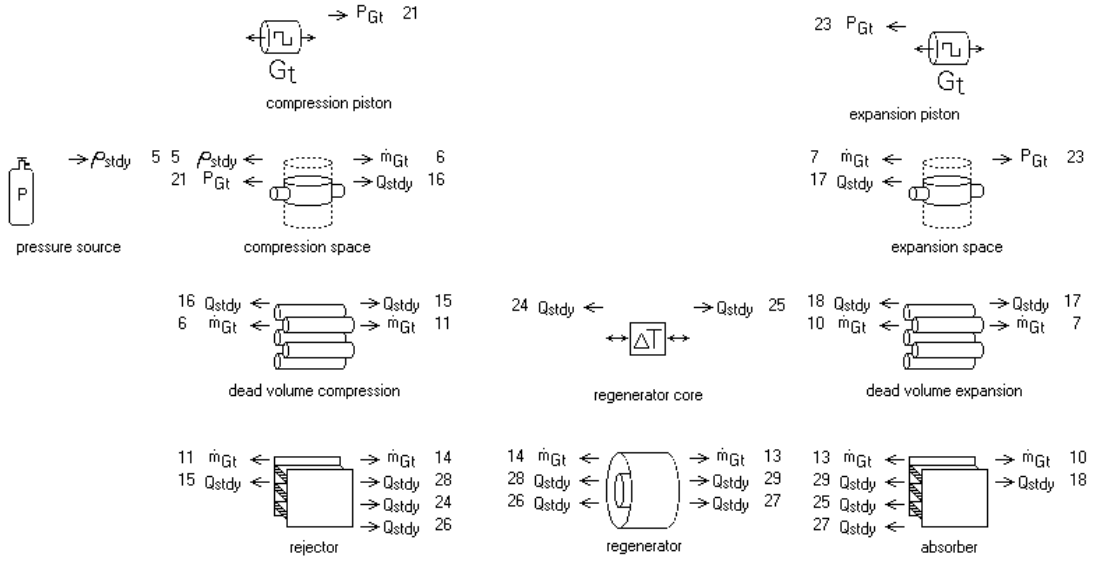

Figure 5-8: Alpha Stirling Sage model

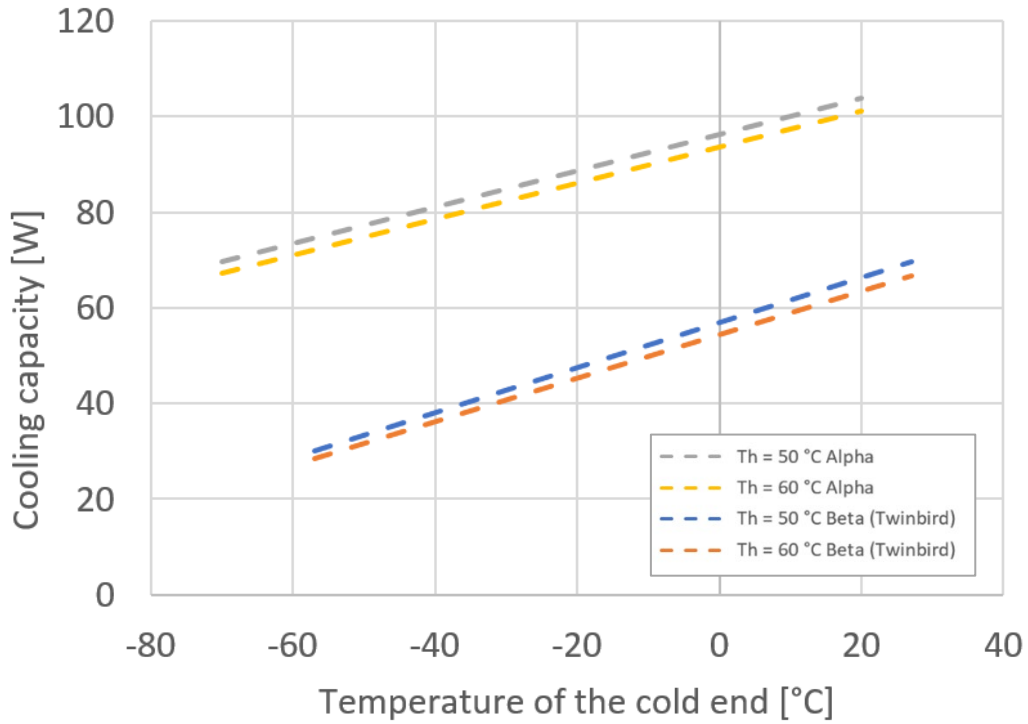

Figure 5-9: Sage results for cooling capacity vs cold end temperature for alpha and beta Sage models

5.5 Alpha Stirling Results and Discussion

The operating parameters of the alpha Sage model are shown in Table 5-2. The working gas input was helium, to match the Twinbird beta refrigerator, and the mean pressure input to Sage was 2 MPa. The regenerator was set to replicate the wire mesh available in the lab, which was a woven screen matrix of with a wire diameter of 0.1 mm and a porosity of 0.7.

The model was mapped from 0.1 to 160 Hz. The temperature range of interest was the near-ambient range, with an absorber temperature of 20 °C and a rejector temperature of 50 °C, but further studies should be done over a wider range of operating temperatures.

Table 5-2: Operating parameters of alpha Stirling Sage model

Item	Specification
Working gas	Helium
Mean pressure	2 MPa
Total mean volume	0.016294 L
Absorber temperature	293 K, 20 °C
Rejector temperature	323 K, 50 °C
Piston diameter	19.5 mm
Piston stroke	6 mm
Mean volumes of the compression and the expansion spaces	3.196×10^{-6} m^3
Dead volumes of the compression and the expansion spaces	1.404×10^{-6} m^3
Rejector volume	1.55×10^{-6} m^3
Absorber volume	1.388×10^{-6} m^3
Regenerator void volume	4.156×10^{-6} m^3
Regenerator porosity	0.7
Regenerator material	SS304
Phase shift between expansion and compression piston	90 °
Mapped frequency range	0.1 – 160 Hz
Operating frequency range (approx.)	1 – 160 Hz

Refrigerator Performance

The pressure, temperature, heat, and work parameters were recorded for each space. The COP, net P-V work, and the absorbed and rejected heat against the operating frequency of the refrigerator are shown in Figure 5-10 on a logarithmic scale. The logarithmic scale is used to show the changes which occur at low frequencies. For perspective, the same quantities can be found but plotted against a linear scale in Appendix H.

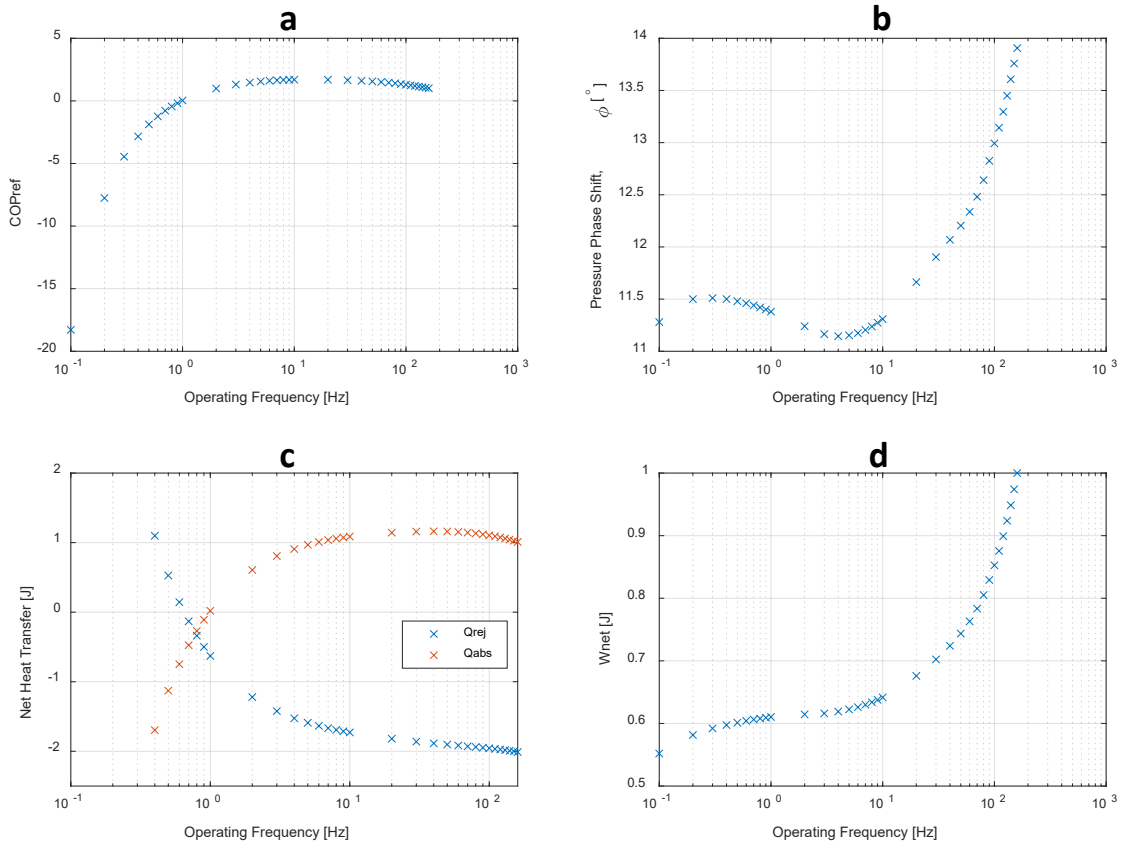

Figure 5-10: a) COP, b) pressure phase shift, c) net heat transfer, and d) net P-V work against operating frequency for the alpha Stirling Sage model

Figure 5-10a shows that the COP of the refrigerator becomes positive at an operating frequency of 1 Hz. This is also reflected by the heat in the rejector and the absorber crossing the x-axis at the same frequency. The reason this occurs is that the temperatures of the hot and cold space are set in Sage, as well as the piston motion and operating frequency. Using these parameters as inputs, Sage calculates the directions and magnitudes of the heat transfer. At frequencies lower than 1 Hz, the refrigerator is

not working as a refrigerator – the work input by the piston is not enough to create a heat lift. Heat is being conducted from the hot space to the cold space, which is shown by the heat being absorbed by the rejector and rejected by the absorber. The small amount of work input is simply rejected into the cold space by the absorber as well.

The more relevant region of interest is at frequencies higher than 1 Hz. This is where the refrigerator begins working, and the trends of heat and work transfer, pressure, volume, and temperature can be analysed in terms of a refrigeration system.

Pressure Amplitude and Phase

It was found that the pressure phase shift and amplitude did not change so much across the entire system as much as it varied with frequency, so mean values of the overall pressure amplitude and the pressure phase shift are shown in Figure 5-11a and 10b, respectively. Figures showing how the pressure phase shift and amplitude changes across all spaces can be found in Appendix I. Both pressure amplitude and phase shift increase with operating frequency – this is different to the phase shift for the single space model, as the pressure phase shift (and net P-V work) has a peak. However, the correlation between pressure phase shift and net P-V work are still the same – in this case, they consistently increase with frequency, shown in Figure 5-12.

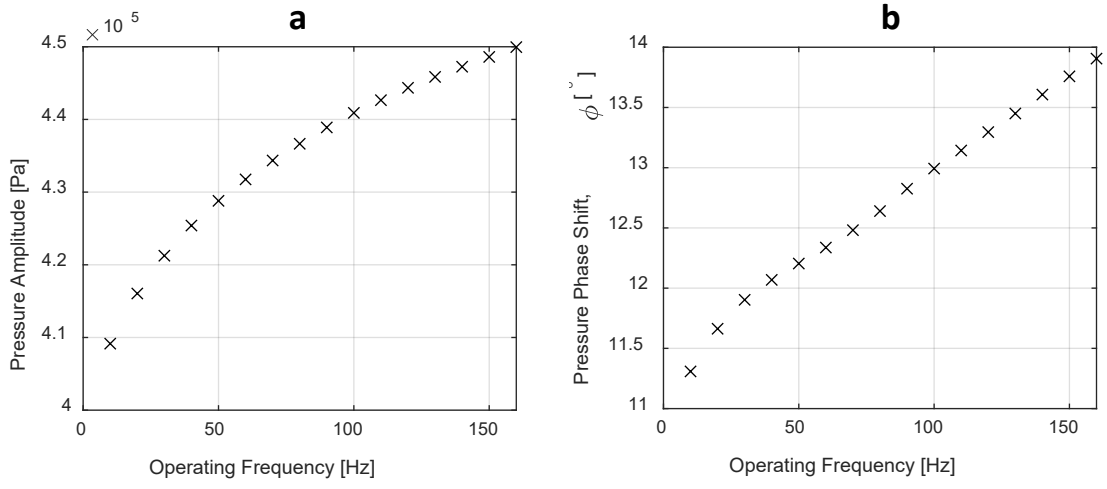

Figure 5-11: a) Pressure amplitude and b) phase shift vs operating frequency for the alpha Stirling Sage model

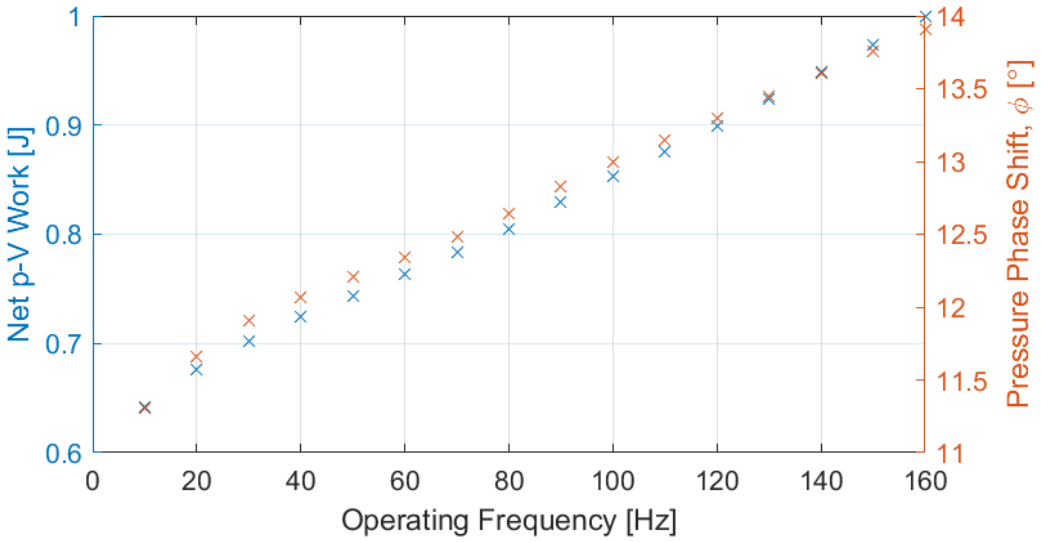

Figure 5-12: Net P-V work and pressure phase shift vs operating frequency for the alpha Stirling Sage model

Net P-V Work Relationship for Stirling Refrigerators

Figure 5-13 shows the net P-V work predicted by Sage and by the P-V work/phase shift equation vs operating frequency on the left axis, with the Sage pressure phase shift on the right. Figure 5-13a shows the results for the alpha Stirling Sage model, while Figure 45-13b is for the single cylinder Sage mode. They show that the phase shift equation derived in Section 4.1 is applicable for both single space systems and refrigeration systems.

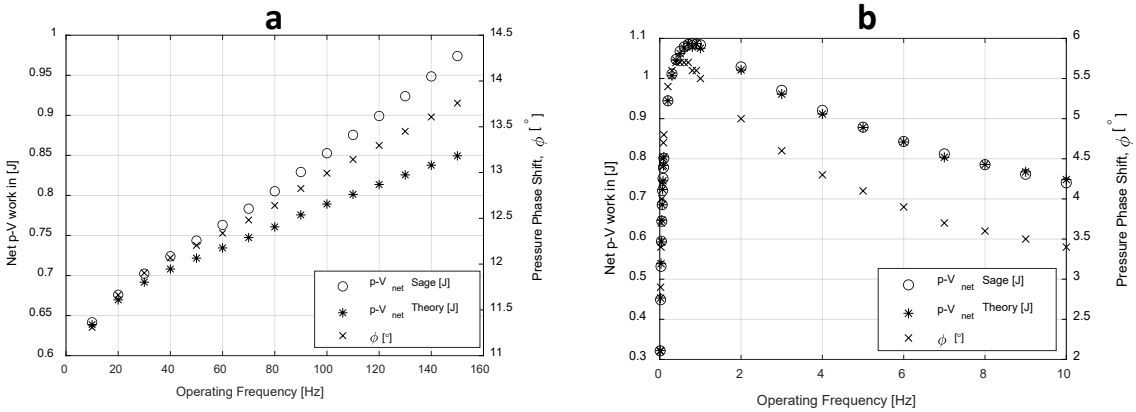

Figure 5-13: Pressure phase shift and net P-V work predicted by Sage and theory (Equation 31) vs operating frequency for a) alpha Stirling Sage model, and b) single cylinder Sage model

Both net P-V work and phase shift correlate extremely well at lower frequencies, but then begin to diverge as the operating frequency increases. This can be attributed to other losses within the system as the operating frequency increases, such as pressure and heat transfer losses across components and fluid friction, resulting in a lower pressure amplitude. The pressure loss across each component can be seen in Figure 5-14.

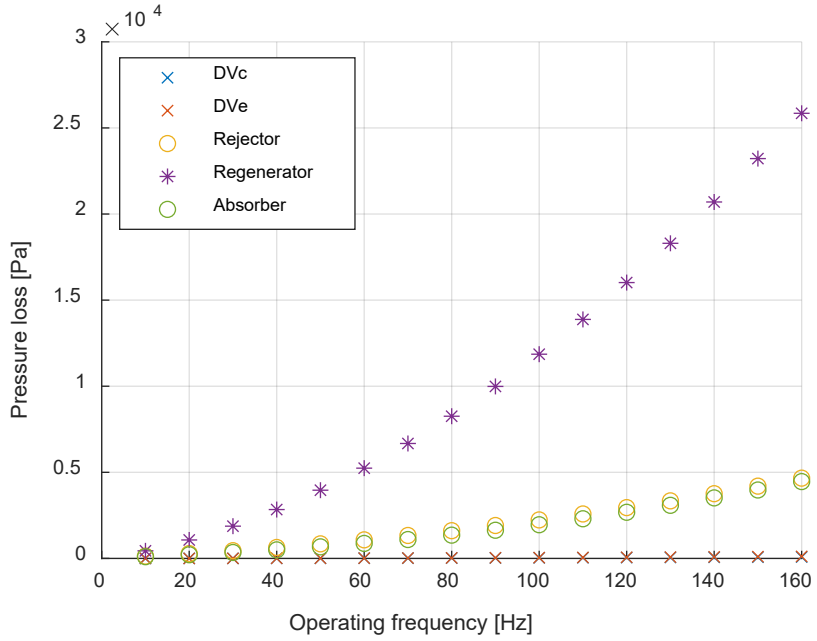

Figure 5-14: Pressure loss across each component of the alpha Stirling model

Additionally, due to the increased operating frequency and pressure losses, the total heat transfer (sum of heat transfer across all components) increasingly becomes less like a simple single harmonic wave and progresses closer to a double or higher harmonic, as can be seen in Figure 5-15. As the P-V equation was derived for a single harmonic, it is therefore only accurate until the system becomes more complex. For 0.1 Hz, the R^2 value of a single harmonic sine fit is 0.98. The RMS error when using a single harmonic fit to the heat transfer wave at 160 Hz is 1.4 times that of a single harmonic fit to 0.1 Hz. To get a similar R^2 value for 160 Hz, a double harmonic sine fit must be used. The curve fit results to a single and double harmonic sine wave for low and high frequencies can be found in Appendix J.

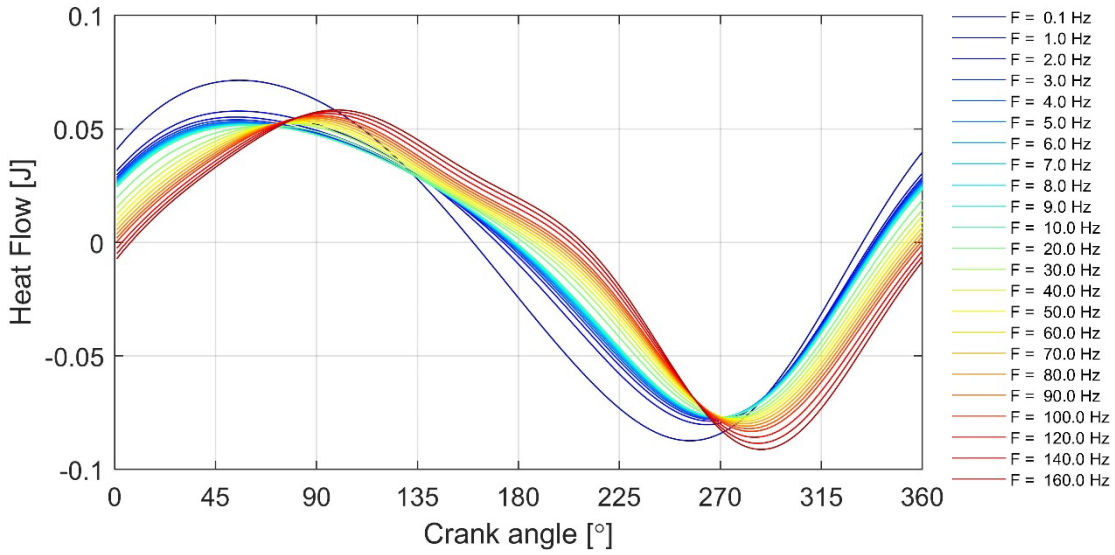

Figure 5-15: Overall heat flow vs crank angle for the alpha Stirling Sage model

5.6 The Peclet Number in Stirling Refrigerators

As Kornhauser found that the non-dimensional loss for a single cylinder system peaked at a Peclet number of approximately 10, better design practices might be established by understanding the Peclet numbers around which Stirling refrigerators typically operate. However, Stirling machines consist of more complex geometry than a simple piston-cylinder experiment. The question arises of how to quantify the Peclet number of a Stirling machine – would it be an overall value, or would each component have a different Peclet number?

Given that the temperature, pressure, and other properties within Stirling machines vary throughout each component, the first approach taken was to quantify the Peclet number within each space. As the Peclet number is based on the hydraulic diameter in the form of the ratio of volume to wetted surface area, each component in a Stirling machine has a different Peclet number. The problem with this approach is that the non-dimensional loss cannot be calculated in constant-volume spaces as the equation (see Equation 18) requires a variation of volume in the form of adiabatic compression and expansion to give a non-zero result. However, the Peclet number may still be quantified and, assuming the critical Peclet number of 10 is still valid, it can be used to identify the high loss spaces and which spaces are closer to isothermal or adiabatic.

As an example, the Peclet numbers were calculated for the alpha Stirling Sage model. This model also uses helium as the operating gas, has a mean pressure of 2 MPa, and has a COP of 1.67 when running with the temperature limits of T_{cold} = 243 K and T_{hot} = 303 K. The volume, wetted area, and respective Peclet numbers for each component are listed in Table 5-3. The operating frequency was set to 60 Hz, which is approximately the frequency for which the largest cooling effect is achieved.

Table 5-3: Volume, wetted area, hydraulic diameter, and Peclet numbers in the alpha-type refrigerator for an operating frequency of 60 Hz using helium

Component	Volume [m³]	Wetted Area [m²]	Hydraulic Diameter [m]	Local Peclet Number Pe_ω
Compression	3.196 x 10^{-6}	0.001253	0.0102	25.36
Expansion	3.196 x 10^{-6}	0.001253	0.0102	44.42
Rejector	1.55 x 10^{-6}	0.01095	0.000566	0.0802
Absorber	1.388 x 10^{-6}	0.009807	0.000566	0.1264
Regenerator	4.156 x 10^{-6}	0.07125	0.0002333	0.0167

The local Peclet numbers in Table 5-3 all fall either well below or well above Pe_ω= 10, with the highest local Peclet numbers being those within the expansion and compression spaces of 44.42 and 25.35, respectively. The local Peclet numbers within all the heat exchangers are very low, all being well under 1. With the ability to quantify local Peclet numbers, the question that arose was: if one was able to change the local Peclet number, would this minimise hysteresis loss and increase the overall COP?

The Peclet number in each space was calculated over the range of operating frequencies, from 1 to 100 Hz. The net heat transfer in each space as well as the overall COP is plotted vs the local Peclet number in Figure 5-16. The COP also does not appear to have a correlation with heat transfer in any separate space, which means that a combination of other phenomena has a larger effect on the COP than the Peclet number or heat transfer within separate components.

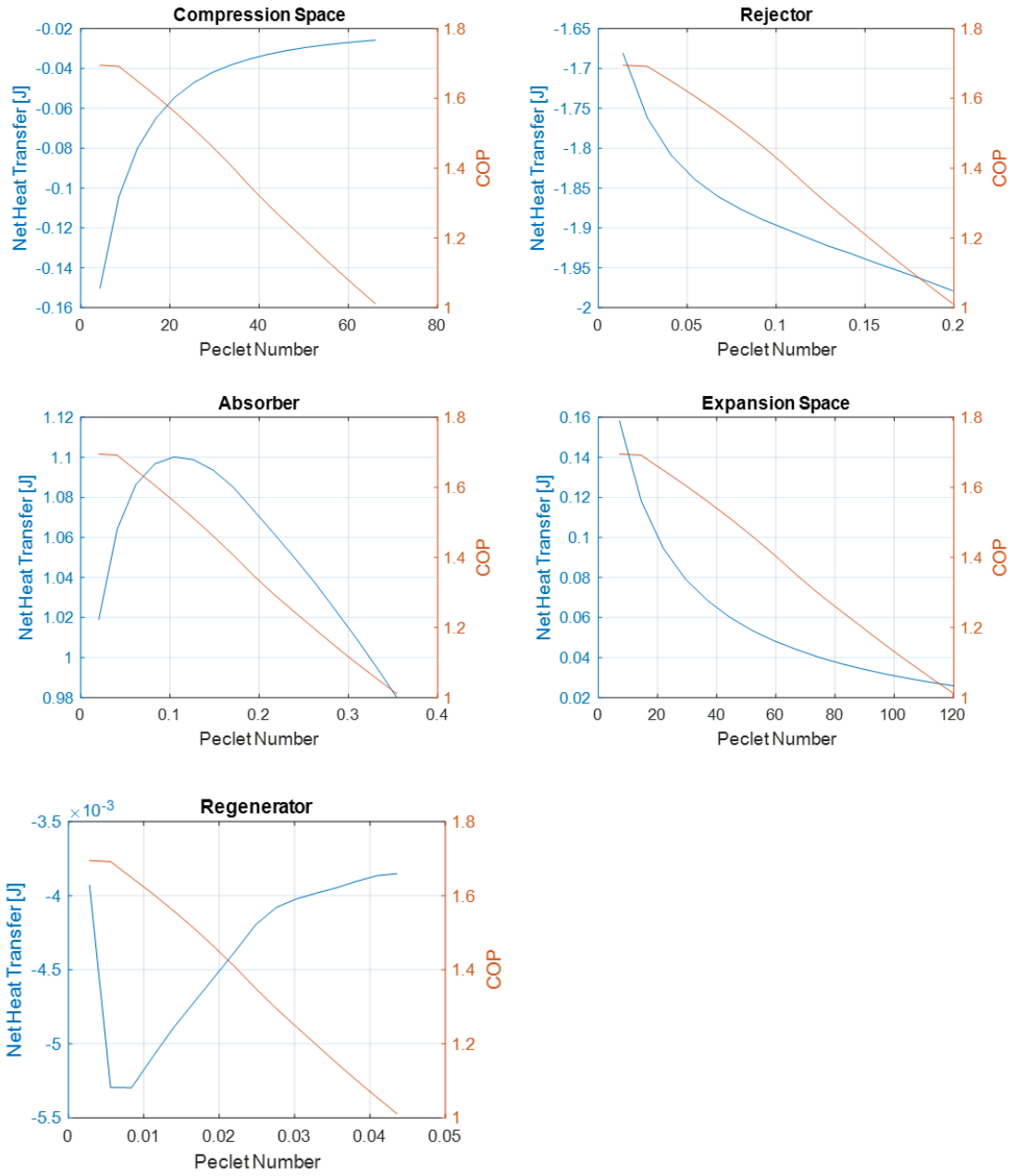

Figure 5-16: Local net heat transfer and overall COP vs Peclet number in the alpha Sage model

The overall Peclet number of the system was also calculated by using the overall hydraulic diameter and a mass-weighted thermal diffusivity to account for the variation in thermal diffusivity and amount of gas in each space. The net P-V work input to the system and COP is plotted against the overall Peclet number in Figure 5-17.

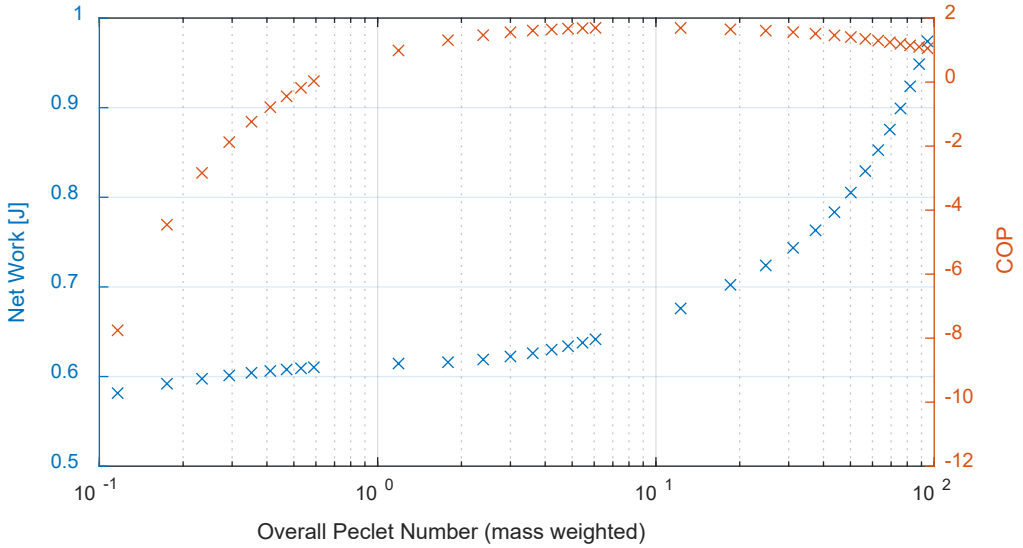

Figure 5-17: Net P-V work input and COP vs mass weighted overall Peclet number in the alpha Sage model

There does not appear to be a relationship between the net P-V work and COP when compared to the mass weighted overall Peclet number. This, along with the previous insights regarding net heat transfer and local Peclet numbers, shows that while spaces can be identified which operate in the isothermal or adiabatic regions with the Peclet number, the Peclet number alone is not a sufficient quantity to use as a design tool to minimise hysteresis loss to increase the COP of a Stirling refrigerator.

5.7 The Effect of a Regenerator

The application of an “isothermaliser” in the form of a high surface area and high heat capacity matrix is suggested within the literature (Breckenridge et al., 1971; Scheck, 1988). For Stirling applications, the regenerator is a component that fits these criteria. It is possible that because the regenerator has an isothermalising effect within Stirling machines, it reduces the effects of hysteresis loss. This section analyses and discusses the effect of regenerator material within the Sage models of a piston-cylinder device and the alpha Stirling refrigerator.

Cylinder with Regenerator Test Rig

A modification was made to the existing single space piston-seal test rig to investigate how the regenerator affects the pressure phase shift and the net P-V work. This consisted of fitting coiled woven screen regenerator material into the bottom of the cylinder. Figure 5-18 shows the regenerator matrix material and the coiled regenerator material for use within the test rig.

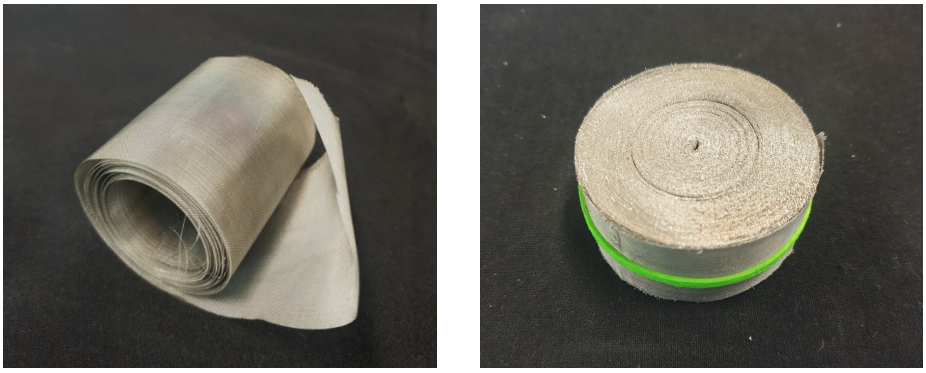

Figure 5-18: a) Regenerator material, and b) regenerator used in the experiment

The schematic for the regenerator test rig and its corresponding Sage model is shown in Figure 5-19. The average gas volume was kept as close as possible to the first single-cylinder experiment, which meant that the zero position of the piston needed to be shifted to make up for the volume occupied by the solid regenerator material.

The Sage model for the regenerator test rig consisted of two main spaces – the cylinder space and a canister space filled with regenerator material. The cylinder wall was modelled as a 'thick surface', and the wall was held constant at a temperature T_w = 300 K to simulate room temperature surroundings, using a line heat source.

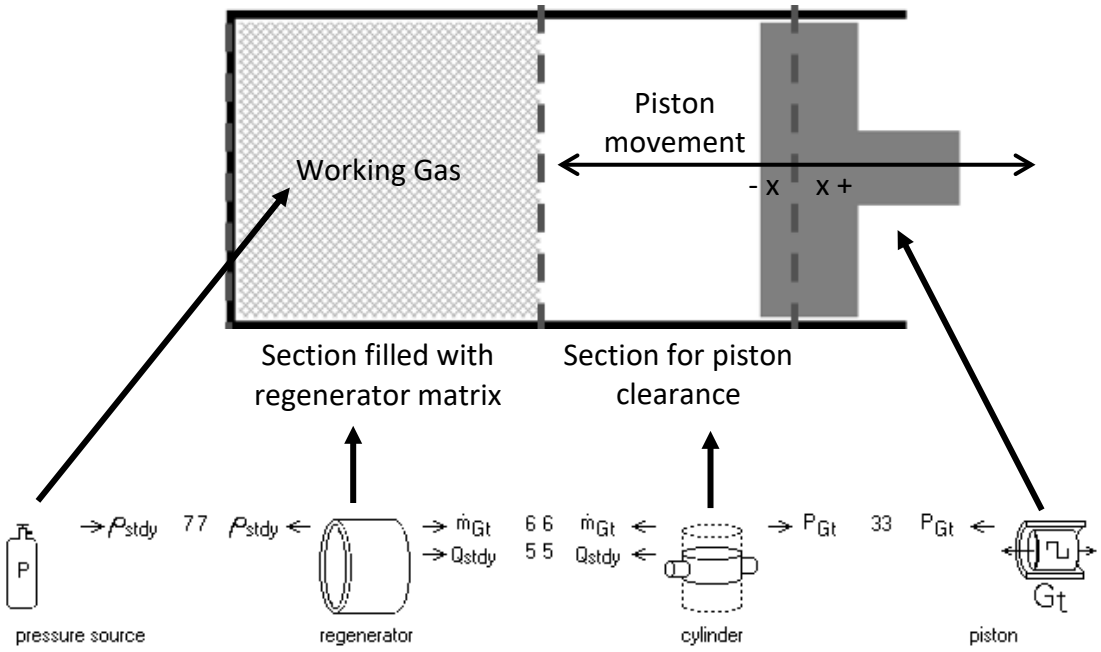

Figure 5-19: Sage model for the piston-cylinder regenerator set up and the corresponding experimental schematic

The regenerator test rig specifications are outlined in Table 5-4**.** In the experiment, the average volumes for the test rig with and without the regenerator material are slightly different – the void space of the regenerator was estimated using the mass and total volume of the regenerator, and then added to the approximate volume in the cylinder with the piston offset so that the compression ratio was kept constant. The Sage model was modelled to have the same constant dimensions. However, it was found that the test rig zero position shifted by approximately ± 3 mm each frequency reading, so the

average volume was modified each time that Sage was run to match the achieved average volume of the test rig.

The regenerator was modelled as a woven screen matrix with a wire diameter of 0.1 mm. The regenerator porosity was also approximated using the weight of the wrapped regenerator matrix, the density of steel, and the total volume of the regenerator assuming it was a solid cylinder. The porosity also could have been determined using submersion, but the matrix was too fine to allow proper drying afterwards, so the approximation was used.

The magnitude and phase data for gas pressure, volume, and temperature were recorded with the working gas as air, and the model was then validated against the regenerator test rig operated at different frequency runs from 1 to 10 Hz.

Table 5-4: Piston-cylinder regenerator test rig model dimensions

Parameter	Value	Unit
Diameter	0.05	m
Stroke	0.01	m
Stroke Volume	1.9634×10^{-5}	m^3
Volume Ratio (Compression Ratio)	1.5178	
Average Volume	3.980×10^{-5}	m^3
Piston Face Area	7.854×10^{-3}	m^2
Regenerator Length	0.0236	m
Regenerator Porosity	0.626	
Offset	7×10^{-3}	m

The tests for the single cylinder test rig with regenerator material followed the same procedure as the original test rig, in Section 3.2. The data collection and processing were carried out in the same manner. The normalised pressure for the test with regenerator material and its representative Sage model are shown with the experimental and Sage results for the cylinder alone in Figure 5-20, which shows very good agreement between the sets of data. The normalised Sage pressure amplitude is consistently higher than the normalised experimental pressures. The full table of errors for each frequency are shown in Appendix E.

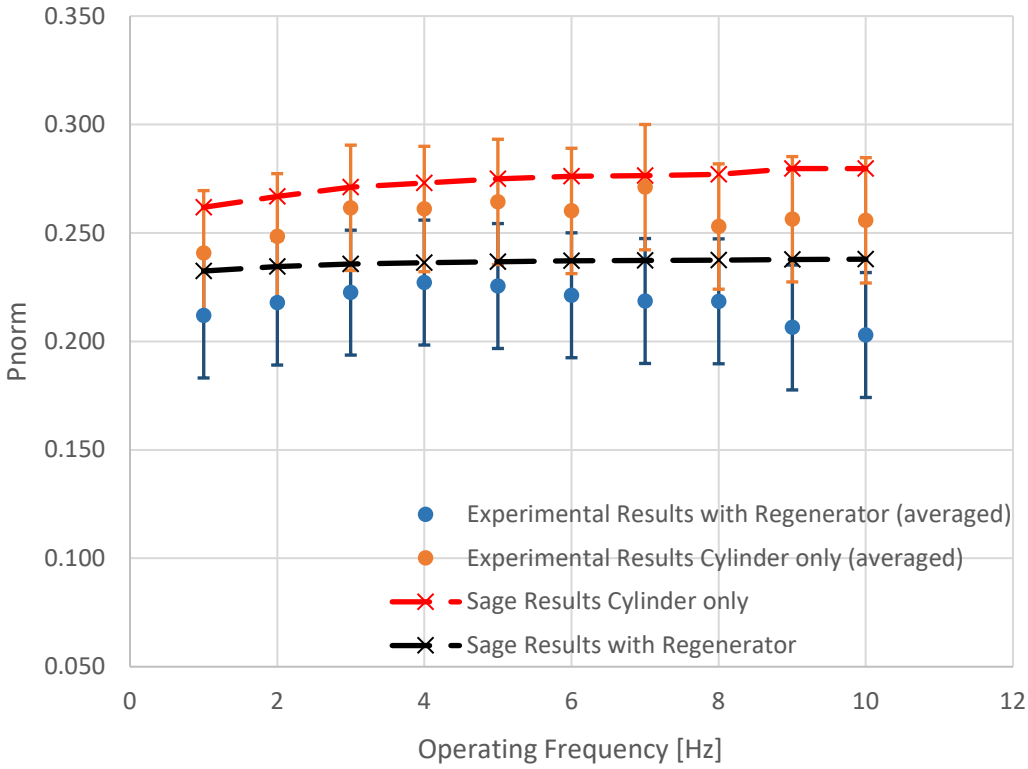

Figure 5-20: Normalised pressure amplitude for experimental cylinder results compared to Sage models with and without regenerator

The regenerator experimental pressure results deviate more from the Sage results at higher frequencies, decreasing as the operating frequency increases. However, the agreements between Sage and both sets of experimental results are enough to confidently use the Sage-predicted quantities such as temperature, heat transfer, and pressure for further analysis into the effect of a regenerator on the pressure phase shift and the net P-V work.

Single Cylinder Sage Regenerator Parameter Study

To understand the effects of the regenerator on net and cyclic heat and P-V work transfer, two scenarios were considered. The first was the single cylinder Sage model, with no regenerator material within. The second was the single cylinder Sage model with regenerator material. This was modified so that the total mean and swept volumes were the same as the first, to keep the volume ratios consistent, which should lead to the same pressure sweep due to the volumetric change. The amount of void volume in the regenerator was half the total mean volume, and the other half was left empty, as shown in Figure 5-21. Equation 45 shows how the length of each cylinder component was adjusted to include only the regenerator void volume. Table 5-5 details the dimensions of the two models. The models were run from 0.01 to 10 Hz, with air as the working gas.

$$L = \frac{4V_{mean}}{\pi D^2} \qquad \text{Equation 45}$$

Table 5-5: Parameters of Sage models comparing cylinder only and a cylinder packed with regenerator material

Parameter	Value	Unit
Diameter, D	0.0508	m
Stroke, S	0.0762	m
Volume Ratio	2	
Average Volume (both)	2.317×10^{-4}	m^3
Porosity, p (regenerator)	0.7	
Average Wetted Surface Area (cylinder only)	2.23×10^{-2}	m^2
Average Wetted Surface Area (with regenerator)	2	m^2

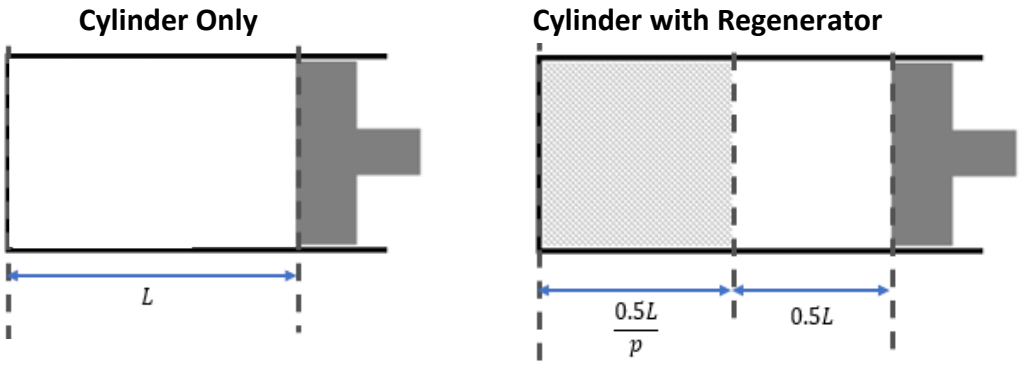

Figure 5-21: Cylinder only and cylinder with regenerator diagrams

The following figures show the results comparing the models with a cylinder only and with a regenerator. Figure 5-22 shows the pressure phase shift and net P-V work vs operating frequency for both models. The cylinder only model has a consistently higher phase shift, which corresponds to a higher net P-V work input. Introducing the regenerator for the same volumetric variation reduces both quantities.

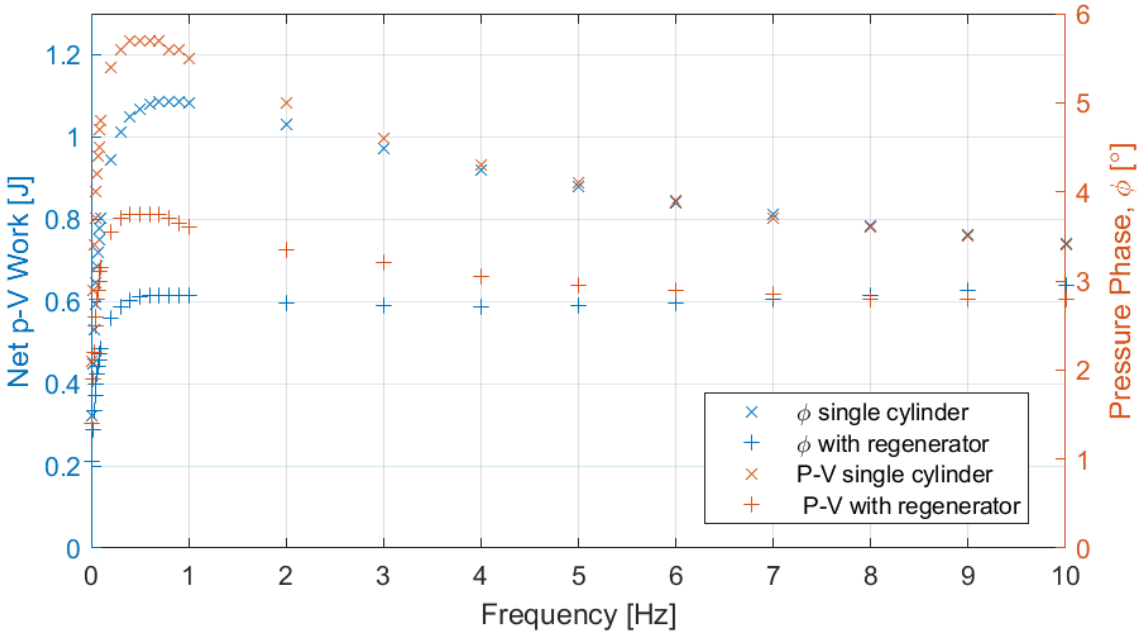

Figure 5-22: Pressure phase shift and net P-V work vs operating frequency for both single cylinder and cylinder with a regenerator

The phase shift between the cyclic P-V work and heat transfer also changes when a regenerator is added. Figure 5-23 shows the phase lag of heat transfer for the cylinder only model and with a regenerator over operating frequency. The overall trend is the same for both – at low frequencies, there is near-isothermal heat transfer, so the phase lag of heat transfer is small. As the operating frequency increases, so does the phase lag. However, the regenerator model phase lag increases at a lower rate than that of the cylinder only. The increased area of the regenerator also has the effect of making the cyclic heat transfer more complete, and therefore more isothermal, which results in the lower phase shift.

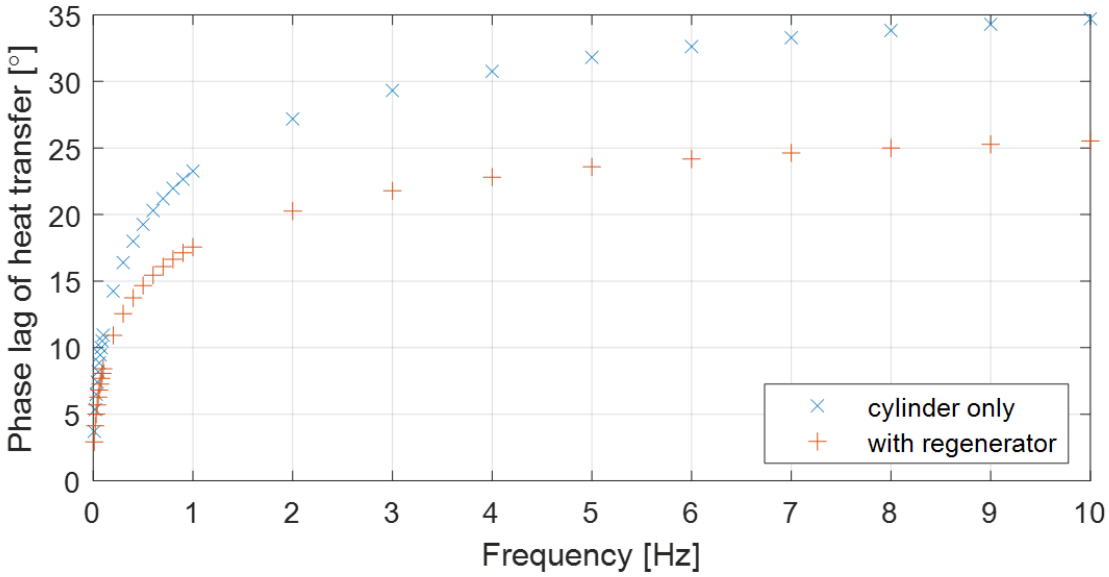

Figure 5-23: Phase lag of heat transfer vs operating frequency for Sage models with cylinder only and with a regenerator

Figure 5-24 shows the cyclic heat transfer and P-V work for both single cylinder Sage models, with and without regenerator material at an operating frequency of 1 Hz, with air as the working fluid. This corresponds to the approximate region of maximum phase shift and P-V work in Figure 5-22. The pressure phase shift without regenerator material is 5.5° and decreases to 3.7° when regenerator material is added. While the P-V amplitude is very similar for both cases, the heat transfer wave follows the P-V work more closely for the regenerator results than without. The amplitude of heat transfer is higher for the case with the regenerator. The higher amplitude of heat transfer, and the decreased net P-V work and pressure phase shift for the case with the regenerator are all indications of more isothermal operation.

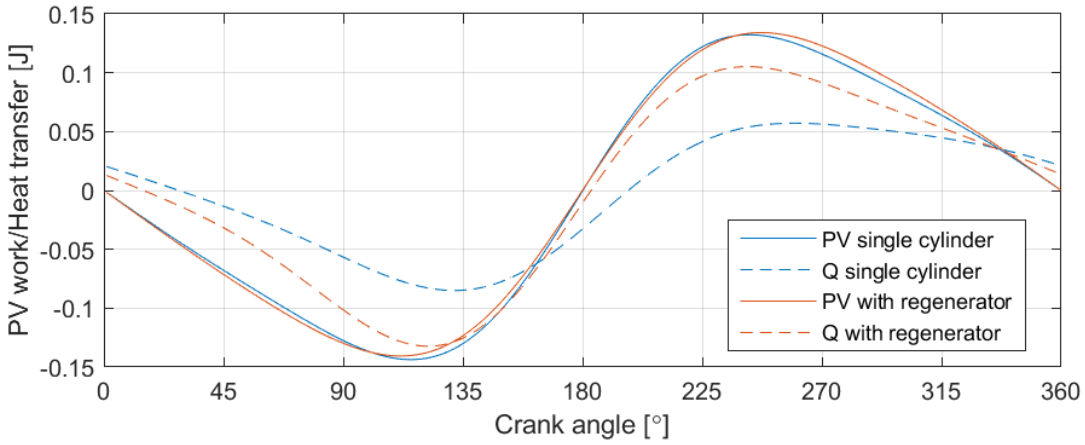

Figure 5-24: Cyclic P-V work and heat transfer for Sage models with cylinder only and with a regenerator

Alpha Stirling Regenerator Parameter Study

The alpha Stirling Sage model from Sections 5.1-5.3 was used again to investigate the effect of a regenerator within a Stirling refrigerator. The heat transfer multiplier, 'Hmult', is a dimensionless multiplier for the heat transfer coefficient between the gas and its adjacent wall within Sage (Gedeon, 2016). The default setting is Hmult = 1.

The reason for changing the heat transfer multiplier within the regenerator is that the heat transfer coefficient can be changed without changing the physical configuration such as areas, channel dimensions, and ratios of swept volumes. While keeping all other parameters the same, the heat transfer multiplier could be varied to understand how the regenerator performance affects the pressure phase shift, net heat and work transfer, and so on. The following results apply for the alpha Stirling model at 60 Hz, which is the same frequency the Peclet number was quantified at in Section 5.6.

Figure 5-25 shows the net heat transfer and the heat transfer amplitude within the regenerator for the range of heat transfer multipliers. An increase in the heat transfer multiplier decreases the net heat transfer but increases the heat transfer amplitude. The net heat transfer in a regenerator is a loss due to it being the difference in the heat absorbed by the regenerator as the gas travels from the hot to the cold space, and the heat the regenerator rejects as the gas returns. The heat transfer amplitude is a measure of the magnitude of heat absorbed and rejected by the regenerator over one cycle. A

decrease in net heat transfer and increase in heat transfer amplitude shows that the heat transfer becomes more isothermal as the heat transfer multiplier increases.

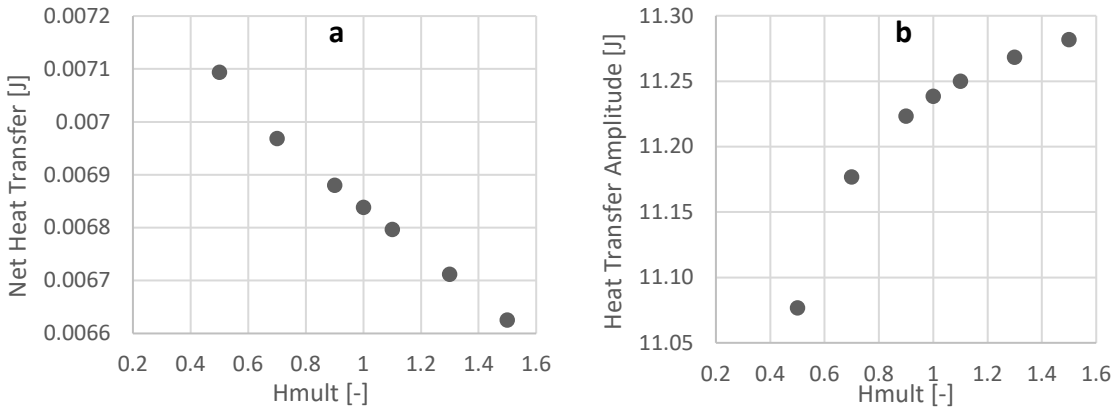

Figure 5-25: a) Net heat transfer and b) Heat transfer amplitude vs H multiplier, 'Hmult', of the regenerator in the alpha Stirling Sage model for 60 Hz

Figure 5-26 shows an inverse relationship between the heat transfer multiplier and the required P-V work input and pressure phase shift. This shows that the isothermalisation of the heat transfer in the regenerator has a beneficial effect on the system, reducing the required input P-V work for a given frequency. This isothermalisation of the cyclic heat transfer in the regenerator and the subsequent reduction on required work input increases the refrigerator COP, as Figure 5-27 shows in a plot of the refrigerator COP against the heat transfer multiplier.

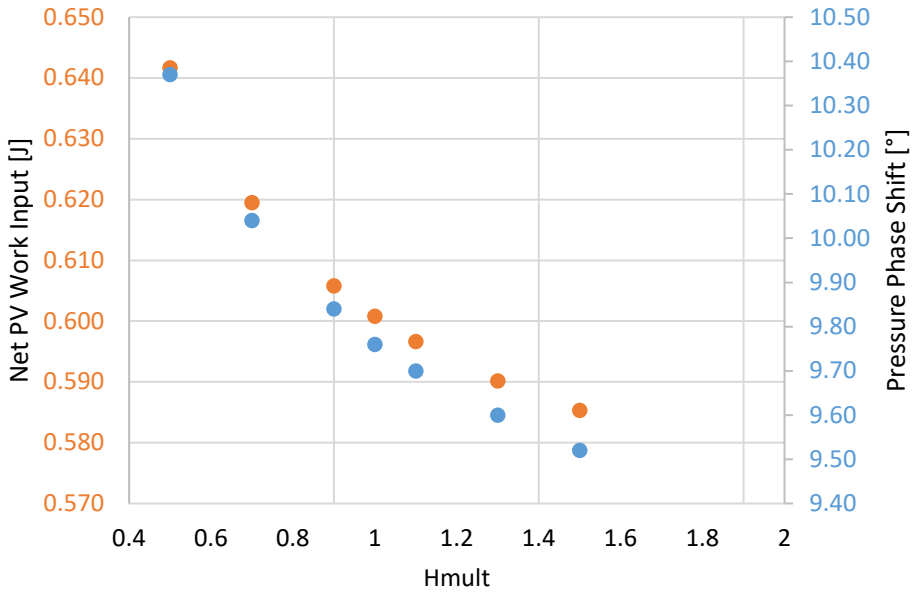

Figure 5-26: Net P-V work and pressure phase shift vs H multiplier, 'Hmult', of the regenerator in the alpha Stirling Sage model for 60 Hz

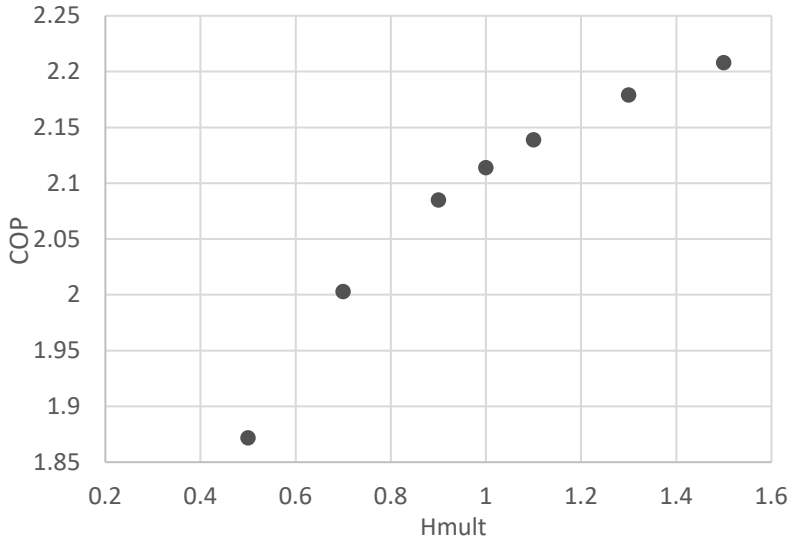

Figure 5-27: COP vs H multiplier of the regenerator in the alpha Stirling Sage model for 60 Hz

5.8 Quantifying Hysteresis Loss

Figure 5-28 shows a schematic of net heat transfer over one cycle for the single cylinder regenerator model obtained in Sage. This schematic allows a more complete understanding of the magnitudes and directions of heat flows within the system. It separates the system into its three levels: the gas level, the fin/matrix level, and the wall level. To be consistent with the first law, the net heat transfer in between each level must equal the net P-V work in. Likewise, the sum of heat flow in and out of each individual block must be zero.

It can be seen from Figure 5-28 that the piston inputs P-V work into the cylinder and adjacent regenerator gas. The heat then transfers through the matrix, the wall, and then to the 'temperature source', which is the Sage terminology for a heat source or sink at a set temperature; in this case, an ambient temperature of 27 °C. The cylinder wall conducts a small amount of heat back into the cylinder gas, but overall, there is a net P-V work input that is equal to the sum of the heat transferred from the walls into the surroundings.

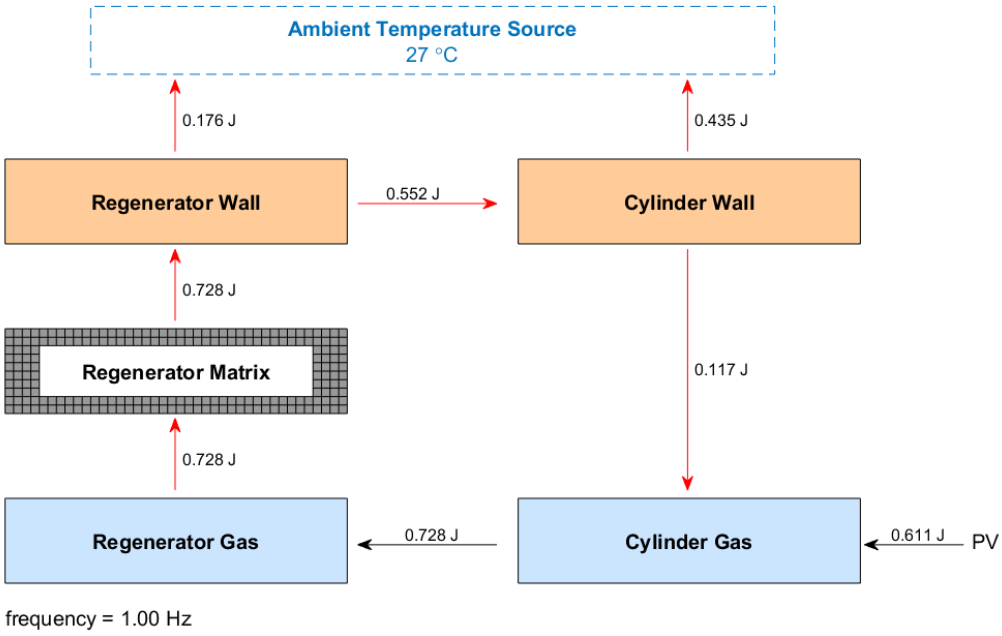

Figure 5-28: Schematic of net heat flows within the single-cylinder regenerator model

Figure 5-31 shows a schematic of net heat transfer over one cycle for the alpha Stirling Sage model. As expected, the compression space has an overall work input while the expansion space has work output, as seen from the blue arrows. The work is transferred through the walls or through the gas in the form of heat. Heat is transferred through both the gas and walls in from the hot side (compression space) to the cold side (expansion space). The refrigeration effect comes from the heat transfer between the walls, fins, and gas.

Looking at each system and considering the first law for closed cycles reveals that no matter how many spaces there are, the net P-V work into the system will still equal the net heat out. In the case of the single cylinder experiment in Figure 5-28 and Figure 5-29, the net heat out is simply the sum of heat lost and recovered during one cycle between the gas and the wall. In the case of a refrigeration system such as in Figure 5-30, the net heat out is the sum of the heat rejected into the hot space, and the heat absorbed from the cold space. No matter where the heat flows go within the system, the pressure phase is simply affected by the net heat flow between the system and the environment.

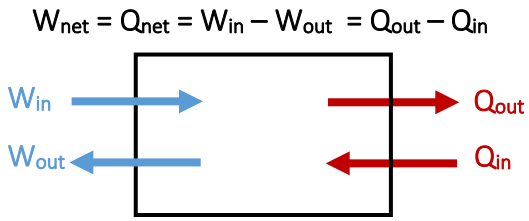

Figure 5-29: Net P-V work and net heat transfer for the single cylinder experiment

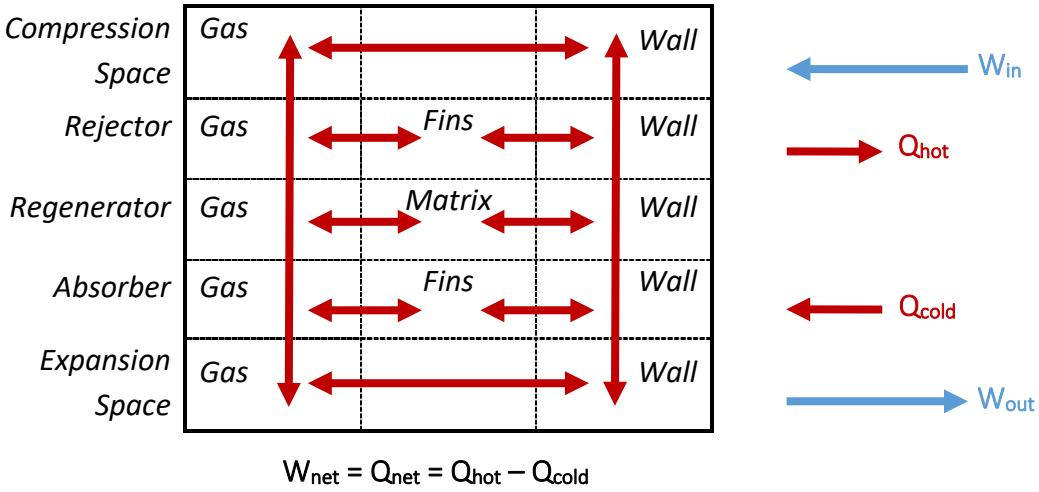

Figure 5-30: Net P-V work and net heat transfer for the Alpha Stirling refrigerator

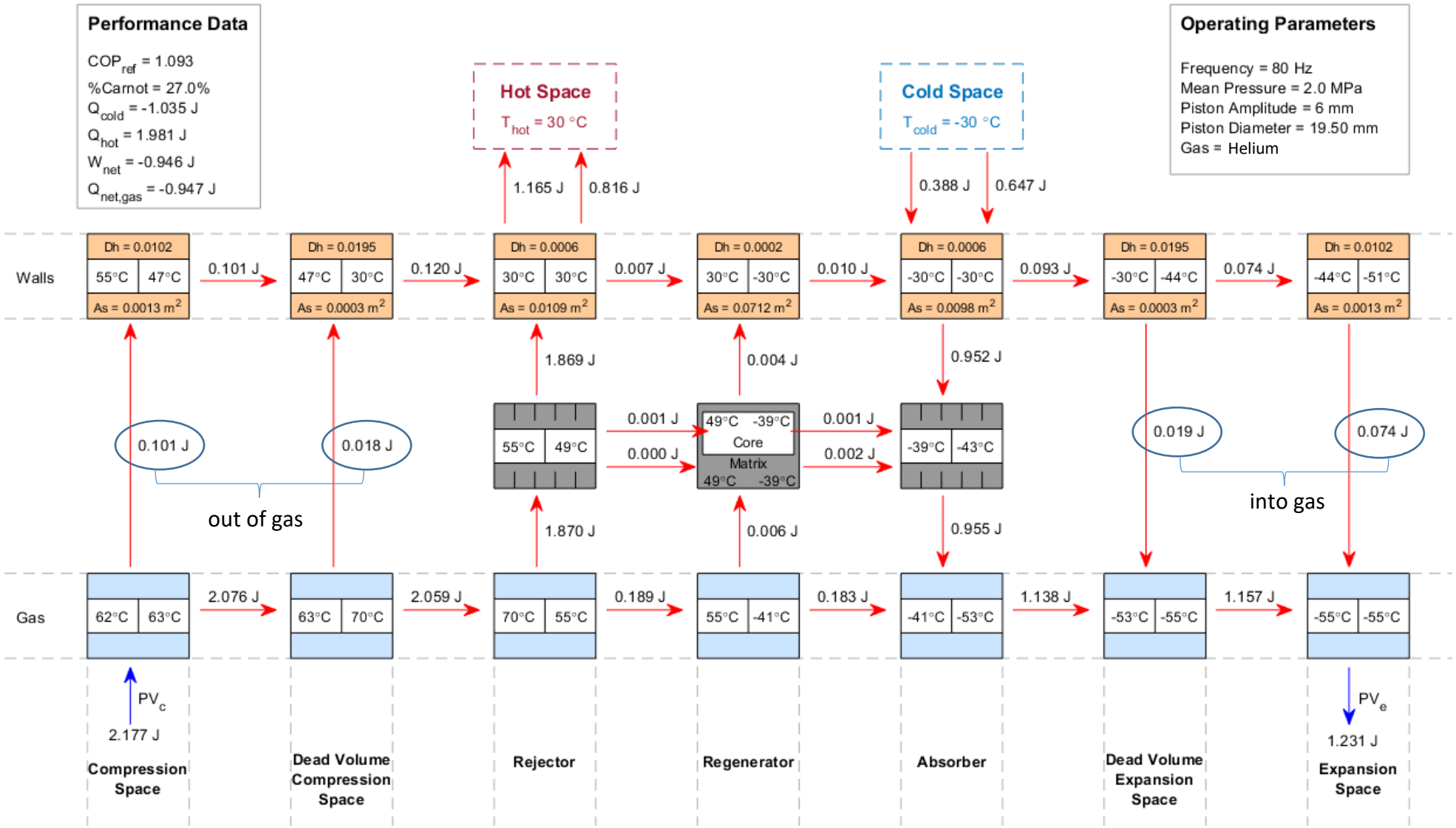

Figure 5-31: Schematic of net heat flow within the alpha Stirling refrigerator Sage model

The effect of an 'isothermal' or 'adiabatic' gas was explored, by attempting to create an idealised working gas within Sage by setting the conductivity of the gas to either be extremely high or extremely low. The reason for this was to try to see the effect of the regenerator if the heat transfer was 'ideal'. However, this resulted in inconsequential findings due to the cold and hot temperatures being fixed inputs in Sage, which always lead to heat conduction from the hot to the cold space, either through the wall or through the gas.

As in a real refrigerator, identifying and quantifying 'hysteresis loss' in this alpha Stirling Sage model is challenging. It cannot be assumed that the net heat transfer out of the gas is hysteresis loss, because the net heat transfer out of the gas is equal to the net P-V work input. It is possible to accidentally account for a heat flow twice as two different losses, therefore over-quantifying the loss. For example, if the compression space and its dead volume has a net heat transfer into the walls from the gas, how much of that heat is being rejected into the hot space, and how much of that is being conducted through the walls as axial heat conduction loss to the cold space?

In an attempt to quantify hysteresis loss from the data given in Sage, it can be theorised that hysteresis loss can be attributed to the spaces in which heat transfer is not beneficial, such as the regenerator as discussed in Section 5.7, the compression and expansion spaces, and their respective dead volumes. If this is the case, the hysteresis loss would be the sum of the net heat out (compression and its dead volume, and the regenerator) minus the net heat into the gas (expansion and its dead volume). In the case of Figure 5-31, the hysteresis loss could be quantified as follows:

$$Q_{hysteresis} = 0.101 + 0.018 + 0.006 - 0.019 - 0.074 = 0.032\,J$$

This means that out of the total 1.981 J of heat rejected into the hot space, 0.032 J of this is due to hysteresis, which is less than 2%. The hysteresis loss quantified in this way is plotted versus operating frequency in Figure 5-32. At some frequencies (10 and 20 Hz), the hysteresis loss is not a loss at all – there is a net heat flow *into* the gas. Interestingly, these correspond to the points of maximum COP, as seen in Figure 5-33. While the Sage data does not show much in terms of net heat transfer changing in each space for that range, the rejector heat transfer amplitude peaks between 10 and 20 Hz,

which could influence the COP. Further study into this net heat gain by the gas should be carried out. The schematic of heat flows for 1 to 100 Hz, and the heat transfer amplitudes and net values for each space can be found in Appendix K.

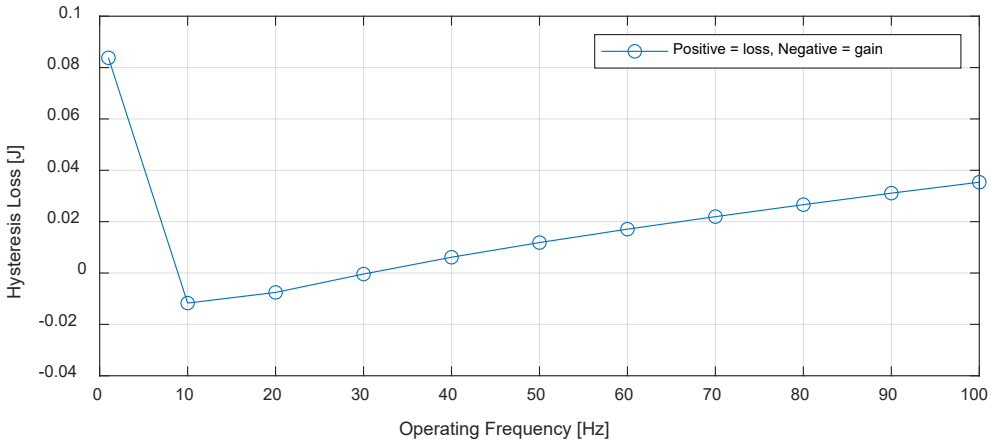

Figure 5-32: Hysteresis loss vs operating frequency

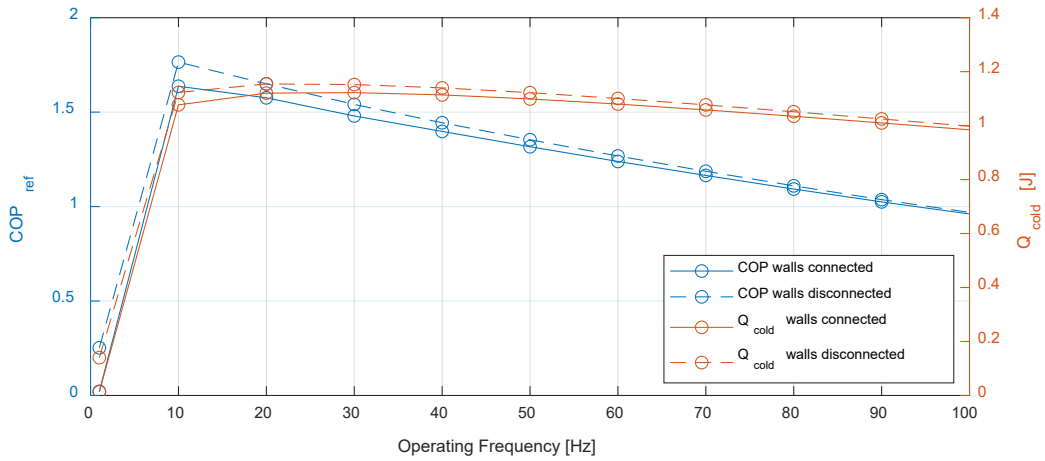

Figure 5-33: COPref and Qcold for alpha Stirling Sage model, with and without hysteresis loss

Figure 5-33 also shows that, if there is no heat flow between the gas and the walls of the compression/expansion spaces and the dead volumes, both COP and heat absorbed from the cold space increase. This was done by removing the heat flow connections between the walls and the working gas within those spaces. It can be noted that as the operating frequency increases, the hysteresis loss decreases to negligible values due to the system behaving more adiabatically. At 10 Hz, where the COP is largest, there is only a 7.3% increase if the heat flow connections are removed.

5.9 Summary

Chapter 5 found, through Sage modelling of a Stirling refrigerator, that the relationship between the pressure phase shift and net P-V work is the same as that of a single space model, and is therefore not indicative of hysteresis loss alone, which reinforces the findings of the transient heat conduction model in that the pressure phase shift is an inherent first-law phenomenon.

In this chapter, the Peclet number was calculated for each space using their respective hydraulic diameters and evaluated in terms of its suitability in predicting hysteresis loss. In addition, hysteresis loss was theorised to be the net heat transfer from spaces which do not require net heat transfer, such as dead volume and the expansion and compression spaces. It was found that if hysteresis loss is quantified in this way, it only contributes to a small difference in COP when an alpha Stirling refrigerator is simulated running within the near-ambient temperature limits.

The reason for hysteresis loss being negligible in Stirling refrigerators was hypothesised in Section 5.7 to be due to the isothermalising presence of the regenerator, which has a large surface area and high heat capacity. The single cylinder experiment was modified to include a coiled regenerator matrix, and a Sage model created to replicate this experiment. With the Sage model of the regenerator matrix validated, it was found that the presence of the regenerator both decreases the net heat transfer and increases the heat transfer amplitude when compared to that of a cylinder with the same volume ratio but with no regenerator. The isothermalisation of the heat transfer due to the regenerator decreased the net P-V work required and increased the refrigerator COP. This shows that the regenerator reduces the effect of hysteresis loss in Stirling refrigerators.

Chapter 6: Conclusion

Stirling refrigerators are machines which operate on cyclic compression and expansion of gas, which causes oscillations of pressure and temperature. The variation of the temperature difference between the working gas and its adjacent walls results in a heat transfer loss from the gas to the wall, which causes an increased net P-V input requirement to the system. This phenomenon of net heat transfer and resulting required net P-V work and pressure phase shift is generally understood as hysteresis loss.

The objective of this study was to carry out a thorough investigation into understanding hysteresis loss and how it may manifest in Stirling refrigerators. These include the ideas developed on how the pressure-volume relationship and hysteresis loss were linked, and the importance of the pressure phase shift. This study showed that the relationship between the pressure phase shift and the net P-V work is the same viewed from a single space or multiple space perspective. Equation 37, derived in Section 4.1 works for both situations.

An experimental validation of a Twinbird 40 W cooler, a beta-type Stirling refrigerator was presented. The Sage model of an alpha Stirling refrigerator was used to explore hysteresis loss within the multiple spaces of a Stirling refrigerator, and to quantify and investigate the relevance of the Peclet number when applied to more complex spaces. The last Sage model was another single cylinder test rig, but with regenerator material to understand the effect of a regenerator on the refrigeration system in terms of heat transfer and work characteristics, and the pressure phase shift.

In addition, the Peclet number as a sufficient parameter for hysteresis loss prediction was investigated, as well as the magnitude of hysteresis loss itself, for a Stirling refrigerator. The regenerator and how it reduces heat transfer and therefore hysteresis loss within Stirling refrigerators was also explored. The key findings of this study are outlined in the following sections.

6.1 Foundations of Hysteresis Loss

Investigating the interactions between different quantities in a single cylinder helped to build a foundation of knowledge to further understand the mechanisms behind hysteresis loss. It was found that the magnitudes of the heat transfer, P-V work, and pressure were more important than considering the non-dimensional loss, which obscures many factors such as the effects of the properties of the working gas. Investigating the single cylinder Sage model results and a transient heat transfer MATLAB step model led to the following key findings:

Key Finding 1: The Effect of Working Gas

For a given operating frequency higher than where the maximum loss occurs, the hysteresis loss can be, for example, as much as five times higher for helium than for air (see Figure 3-13, 10 Hz). In relation to the design and understanding of Stirling refrigerators, it is suggested not to select the working gas based on minimising the thermal diffusivity to mitigate hysteresis loss, as spaces in which heat transfer is required will also suffer from this choice.

Key Finding 2: The Time-Dependence of Heat Transfer

It was found from the step model that even though compression and expansion can be modelled as a polytropic process, there will not be a pressure phase shift and any net heat out (and therefore net P-V work required) unless the heat transfer lags the input P-V work. The heat transfer only had this lag when using the transient heat transfer equation, showing that as heat transfer realistically depends on the time available for it to occur, the phase lag of heat transfer and therefore pressure phase shift and net heat loss are due to this time-dependence.

Key Finding 3: Mechanisms of the Pressure Phase Shift

An explanation for the hysteresis is given from cyclic heat transfer. It was shown that the heat transfer peaks just before the end of the expansion and compression processes, causing the pressure to reach a minimum or maximum, respectively, just before the volume does. This is the pressure phase shift.

From these relationships, it could be argued that the focus should not be on defining it simply as a loss, but rather as the mechanism which links net heat transfer and net P-V work. This leads to the following conclusions, as the pressure phase shift and the way it manifests in Stirling refrigerators was investigated.

6.2 The Pressure Phase Shift

The pressure phase shift was investigated from multiple different approaches to better understand its relationship with the net P-V work. Both sinusoidal and discrete piston motion were analysed. Simple, closed form solutions were first investigated for sinusoidal motion, and following this, the Schmidt equations were extended to derive a relationship for the pressure phase shift. A discussion on discrete piston motion and an apparent phase shift when any net P-V work is present was presented. The key findings in relation to the pressure phase shift and its relationship with net P-V work are as follows:

Key Finding 4: Net P-V Work Equation

A simple, closed-form equation was developed (Equation 37) to describe the relationship for the net p-V work for given pressure and volume amplitudes with a specified pressure phase shift, applied to sinusoidal motion. This equation worked for both single cylinder and Stirling refrigerator models.

Key Finding 5: Modified Schmidt Equations

The Schmidt cycle calculations were extended for the derivation of the ideal pressure phase shift. The modified Schmidt equations show that a Stirling refrigerator executed with sinusoidal piston motion must have a pressure phase shift even in the ideal operation. Without this pressure phase shift, there would be no net P-V work and therefore no refrigeration effect. This is shown when the pressure phase is set to 0, the resulting equation leads to the temperature ratio, $\tau = 1$. This means that there must be a non-zero pressure phase shift for any refrigeration effect to occur.

Even though a refrigerator may be working perfectly at a Carnot COP with no losses, there is still a net heat transfer between the gas and its surroundings required to create the refrigeration effect, and therefore a net P-V work input. It then follows that, even

during completely ideal operation, there will always be a pressure phase shift due to heat transfer between the gas and the walls and heat exchangers. This shows that anything affecting the net P-V work affects the pressure phase shift, not just what is viewed as 'hysteresis loss'. This pressure phase shift requirement for net P-V work applies to both sinusoidal and discrete piston motion, as discussed in Chapter 4.

Key Finding 6: Pressure Phase Shift in Discrete Stirling Cycle

It was shown that the standard textbook Stirling cycle with discrete piston motion can be realised in practice and that even this idealised cycle has an inherent pressure phase shift. For discrete piston motion, the pressure phase shift manifests in the isochoric processes, which create the asymmetry between the compression and expansion. All of them show that the pressure phase shift is the key component required for a heat lift (e.g., opening up the area on the P-V diagram), so there is no net heat transfer and therefore no net P-V work without a pressure phase shift, regardless of piston motion.

Key Finding 7: Pressure Amplitude and Phase Shift for Stirling Refrigerators

Both pressure amplitude and phase shift increase with operating frequency in a Stirling refrigerator. This is different to the phase shift for the single space model, as the pressure phase shift (and net P-V work) has a peak.

6.3 Hysteresis as a Loss or Inherent Phenomenon

The hysteresis effect of heat transfer in devices in which the working gas is cyclically compressed and expanded has been previously understood as three separate phenomena, as outlined by Kornhauser and Smith (1993):

1. a variation in pressure (or force experienced by the piston) with frequency,
2. a phase shift in pressure (or force) relative to the volumetric change (or piston displacement), and
3. "hysteresis loss", or dissipation of net P-V work input.

This study sought to extend the knowledge further and understand the links between these three phenomena. Analysing the relevant quantities within the Sage model of an alpha Stirling refrigerator gave rise to the following key findings:

Key Finding 8: Net Heat Transfer and Pressure Phase Shift

The fact that the pressure phase is affected by the heat transfer between the gas and walls and always represents the net P-V work changed the perspective from which the pressure phase shift is viewed. Initially, it has been viewed as an effect of hysteresis loss alone, assuming that hysteresis loss is a cyclic loss of heat from a cylinder. While this is true for a single cylinder experiment in which no refrigeration effect takes place, this is not the case for a refrigerator.

Hysteresis loss is suggested to cause a pressure phase shift, which is correct. However, previous literature has seemingly failed to realise that net heat transfer will always affect the pressure phase shift in this way. This is important because for the assumption that pressure phase shift is due to a "hysteresis loss" alone, it would result in the understanding that, if this hysteresis loss is eliminated, a Stirling refrigerator can run without a pressure phase shift. This is not the case, due to the necessary net heat transfer between the gas and the refrigerator components for refrigeration to take place. The pressure phase shift is an overall phenomenon related to the net P-V work and heat transfer.

Key Finding 9: The Peclet Number in Stirling Refrigerators

The Peclet number was calculated locally in each space or as an overall number, in the alpha Stirling refrigerator Sage model. It was found that while spaces can be identified in a Stirling refrigerator which operate in the isothermal or adiabatic regions with the Peclet number, the Peclet number alone is not a sufficient quantity to use as a design tool to minimise hysteresis loss to increase the COP of a Stirling refrigerator.

Key Finding 10: Hysteresis as a Net Heat Gain instead of a Loss

Hysteresis loss was theorised to be the sum of the net heat transfer between the wall and the gas in all spaces of a Stirling refrigerator. For the alpha Stirling Sage model, when quantified in this way, at some frequencies (10 and 20 Hz), the hysteresis loss is not a loss at all – there is a net heat flow into the gas. Interestingly, these correspond to the points of maximum COP, as seen in *Figure* 5-33.

Key Finding 11: Discussion on Defining Hysteresis Loss in a Multiple-Space System

While hysteresis loss adds to net P-V work, not all net P-V work is due to hysteresis loss. The net heat transfer and therefore net P-V work in a Stirling refrigerator consists of the net P-V work required for the heat lift, plus heat transfer lost through hysteresis and other losses. As the pressure phase shift is simply a relationship between the net heat transfer and P-V work, one cannot quantify hysteresis loss with the pressure phase shift in a machine which moves heat from one space to another.

The definition of hysteresis as a loss becomes even further complicated in the context of a refrigerator, due to some spaces requiring net heat transfer for a functioning refrigerator, such as the absorber and rejector. Hysteresis loss was therefore considered as the net heat transfer in components in which net heat transfer does not contribute to the refrigeration effect, such as the expansion and compression spaces, and the dead volumes. It was found that there was only a small magnitude of unwanted heat transfer, the highest being -0.0838 J. At 10 Hz, where the COP is largest, there is only a 7.3% increase if the heat flow connections are removed. This is due to the presence of the regenerator.

6.4 The Regenerator

Investigating the interactions between different quantities in a multiple space Stirling refrigerator model and a cylinder with regenerator model and comparing these results with the single cylinder model without a regenerator in Sage allowed further understanding into the importance of the regenerator in terms of mitigating hysteresis loss. The key findings of this part of the study are as follows:

Key Finding 12: The Importance of the Regenerator

The regenerator mitigates the effect of hysteresis loss by providing a buffer between the hot and cold spaces. This means that local gas temperatures in each space oscillate around their respective hot and cold mean temperatures, which limits the hysteresis effect as it decreases the overall temperature differences between the gas and the wall. Without the regenerator, the temperature difference within a Stirling refrigerator could not occur.

Key Finding 13: Heat Transfer Amplitude and Phase in the Regenerator

These observations show that the regenerator works best with a large heat transfer ***amplitude*** between the working gas and the regenerator matrix, and a small ***net*** heat transfer into the regenerator matrix. The net heat transfer within the regenerator can be considered as a loss, while a large heat transfer amplitude is beneficial within the regenerator as it absorbs the fraction of the p-V work that would otherwise increase the internal energy of the gas. It was shown that the regenerator's effects on the heat transfer have a beneficial effect on a Stirling refrigerator, reducing the required input P-V work for a given frequency, leading to an increase in COP.

Key Finding 14: The Regenerator as an 'Isothermaliser'

The last finding re-affirms previous literature such as Scheck (1988), who found that the regenerator mainly decreases the effects of hysteresis loss by 'isothermalising' the overall heat transfer by increasing the overall heat transfer area and reducing the hydraulic diameter. This was confirmed both experimentally and in Sage. As the area increases, the cyclic heat transfer wave becomes closer in form to the P-V wave by increasing the heat transfer amplitude and decreasing the lag between the heat transfer and the P-V work. This was shown in the Sage model results with and without regenerator material, which also shows that using a regenerator for all cases decreases net heat transfer in spaces where heat transfer is unwanted. As a result, the overall pressure phase and net P-V work is decreased. The large loss of performance in Stirling refrigerators is therefore not a consequence of hysteresis loss, and the search for the lost 30% continues.

Bibliography

Alsouda, F., Bennett, N. S., Saha, S. C., Salehi, F., & Islam, M. S. (2023). Vapor Compression Cycle: A State-of-the-Art Review on Cycle Improvements, Water and Other Natural Refrigerants. *Clean Technologies, 5*(2), 584-608.

Annand, W. J. D. (1963). Heat Transfer in the Cylinders of Reciprocating Internal Combustion Engines. *Proceedings of the Institution of Mechanical Engineers, 177*(36), 973-996.

Annand, W. J. D., & Pinfold, D. (1980). *Heat transfer in the cylinder of a motored reciprocating engine. SAE Paper No. 800457*.

ASHRAE. (2001). Designation and Safety Classification of Refrigerants *Safety Standard for Refrigeration Systems*. Georgia, USA: ASHRAE Technology Council.

Bailey, P., Dadd, M., Stone, R., Reed, J. S., & Davis, T. M. (2007). Gas Spring Losses in Linear Clearance-Seal Compressors.

Berchowitz, D. (1979). Analysis of heat transfer in gas springs - personal communication with Scheck, C. G. (1988).

Breckenridge, R. W., Heuchling, T. P., & Moore, R. W. (1971). *Rotary-Reciprocating Refrigeration System Studies, Part 1, Analysis*.

Carnot, N. L. S. (1890). *Reflections on the Motive Power of Heat, Second English Edition*. New York, USA: John Wiley & Sons.

Çengel, Y. A. (2006). *Heat and Mass Transfer: A Practical Approach* (Third Edition (SI Units) ed.). New York, NY 10020: McGraw-Hill.

Chafe, J. N. (1988). *A Study of Gas Spring Heat Transfer in Reciprocating Cryogenic Machinery*. Massachusetts Institute of Technology, Massachusetts, USA.

Chen, N. C. J., & Griffin, F. P. (1983). *A review of Stirling engine mathematical models*. USA: Union Carbide Corporation for the United States Department of Energy.

Chen, P., Zhong, G., Niu, Y., & Liu, Y. (2022). Performance optimization of a free piston stirling engine using multi-section regenerators based on the response surface methodology. *Energy, 261*, 125221. https://doi.org/https://doi.org/10.1016/j.energy.2022.125221

Chirkov, A. A., & Stefanovski, B. S. (1958). O dominiruyushchem sposobye pyeryedachi tepla v tsilindrach dvigatyelyei vnutryennyevo sgoraniya. *Trudy Rostovskova Instituta Injyenyerov Fyelyeznodorovnova Transporta, 21*.

Concept Consulting Group. (2010). *Cost: benefit analysis for increasing the direct use of gas in New Zealand*. Wellington, New Zealand.

Cooke-Yarborough, E. H., & Ryden, D. J. (1985). *Mechanical Power Losses Caused by Imperfect Heat Transfer in a Nearly-Isothermal Stirling Engine*. presented at

the meeting of the 20th Intersociety Energy Conversion Engineering Conference,

Duncan, J., Hamm, A., & Wilkinson, D. (2007). *Understanding the contribution of direct use of gas to New Zealand's future energy efficiency objectives*. Christchurch, New Zealand: A report produced for the Gas Association of New Zealand by the New Zealand Centre for Advanced Engineering (CAENZ).

Eichelberg, G. (1922). *Temperaturverlauf und Wärmespannungen in Verbrennungsmotoren*. ETH Zurich.

Elser, K. (1954). *Der instationäre Wärmeübergang in Dieselmotoren: theoretische und experimentelle Untersuchungen*: Leemann.

Finkelstein, T., & Polanski, C. (1959). *Development and testing of a Stirling-cycle machine with characteristics suitable for domestic refrigeration*. USA.

Foster-Miller Associates, I. (1980). *Design and development of Stirling engines for stationary power generation applications in the 500 to 3000 horsepower range*. United States. https://doi.org/https://doi.org/10.2172/5138610

French, L., Isaacs, N., & Cimilleri, M. (2008). *Residential heat pumps in New Zealand*. presented at the meeting of the 29th AIVC Conference, Kyoto, Japan. Retrieved from https://www.branz.co.nz/cms_show_download.php?id=89c15f9a2e2bcf992a4fa57c9e56dde138707f8d

Garvin, J. (1926). Refrigeration. *Encyclopedia Britannica: Dictionary of Arts, Sciences, Literature General Information; the Three New Supplementary Volumes Constituting with the Volumes of the Latest Standard Edition* (13th ed.). London: The Encyclopaedia Britannica Co., Ltd.

Gedeon, D. (1976). *Hysteresis Losses in a Gas-Filled Vessel*. Athens, Ohio.

Gedeon, D. (1995). Sage: Object-Oriented Software for Cryocooler Design. In R. J. R. G (Chair), *Plenum Press.* Symposium conducted at the meeting of the Cryocoolers 8, Boston, MA.

Gedeon, D. (2016). Sage User's Guide. Athens, USA: Gedeon Associates.

Gedeon, D. (n.d.). *What is Sage?* Retrieved from http://www.sageofathens.com/

Geng, S. M. (2016). *Stirling Research Lab*. Retrieved from https://tec.grc.nasa.gov/rps/stirling-research-lab/

Getie, M., Lanzetta, F., Bégot, S., Admassu, B. T., & Djetel-Gothe, S. (2021a). A non-ideal second order thermal model with effects of losses for simulating beta-type Stirling refrigerating machine. *International Journal of Refrigeration, 130*, 413-423. https://doi.org/https://doi.org/10.1016/j.ijrefrig.2021.05.018

Getie, M., Lanzetta, F., Bégot, S., & Admasu, B. (2021b). Investigation of thermal and fluidic losses and their effect on the performances of a Stirling refrigerator. *2*. https://doi.org/10.21494/ISTE.OP.2021.0719

Goetz, P. W., ed. (1986) *The New Encyclopaedia Britannica* (15 ed., Vol. 26). Chicago: Encyclopaedia Britannica Inc.

Graze, H. R., & Forrest, J. A. (1974). *New design Charts for Air Chambers*. presented at the meeting of the Fifth Australasian Conference on Hydraulic and Fluid Mechanics,

Hargreaves, C. M. (1991). *The Philips Stirling Engine*. Amsterdam, The Netherlands: Elsevier Science Publishers.

Haywood, D. (2004). *Investigation of Stirling-Type Heat-Pump and Refrigerator Systems Using Air as the Refrigerant*. University of Canterbury, Christchurch.

He, X. N., Gong, M. Q., Zhang, H., Dai, W., Shen, J., & Wu, J. F. (2013). Design and performance of a room-temperature hybrid magnetic refrigerator combined with Stirling gas refrigeration effect. *International Journal of Refrigeration, 36*, 1465-1471.

Islam, M. A., Mitra, S., Thu, K., & Saha, B. B. (2021). Study on thermodynamic and environmental effects of vapor compression refrigeration system employing first to next-generation popular refrigerants. *International Journal of Refrigeration, 131*, 568-580. https://doi.org/https://doi.org/10.1016/j.ijrefrig.2021.08.014

Jeong, E. S., & Smith Jr, J. L. (1992). Analytic model of heat transfer with oscillating pressure. *ASME Heat Transfer, 204*, 97-104.

Kagawa, N. (2000). Stirling Refrigerator. *Transactions of the Japan Society of Refrigerating and Air Conditioning Engineers, 17*(1), 1-20.

Kornhauser, A. A. (1989). *Gas-Wall Heat Transfer During Compression and Expansion*. Massachusetts Institute of Technology, Massachusetts, USA.

Kornhauser, A. A., & Smith, J. L. (1987). A Comparison of Cylinder Heat Transfer Expressions Based on Prediction of Gas Spring Hysteresis Loss. *Fluid Flow and Heat Transfer in Reciprocating Machinery, ASME*.

Kornhauser, A. A., & Smith, J. L. (1993). The Effects of Heat Transfer on Gas Spring Performance. *Journal of Energy Resources Technology, 115*, 70-75.

Kornhauser, A. A., & Smith, J. L. (1994). Application of a complex Nusselt number to heat transfer during compression and expansion. *Transactions of the ASME, 116*.

Lee, K. P. (1983). A Simplistic Model of Cyclic Heat Transfer Phenomena in Closed Spaces. *Procedings of the 18th IECEC*, 720-723.

Lee, K. P., Smith, J. L., & Faulkner, H. B. (1980). Performance loss due to transient heat transfer in the cylinders of Stirling engines*The American Institute of Aeronautics and Astronautics.* Symposium conducted at the meeting of the 15th Intersociety Energy Conversion Engineering Conference, Seattle, Washington.

Li, R., & Grosu, L. (2017). Parameter effect analysis for a Stirling cryocooler. *International Journal of Refrigeration, 80*, 92-105. https://doi.org/https://doi.org/10.1016/j.ijrefrig.2017.05.006

Makhnatch, P. (2019). *New refrigerants for vapour compression refrigeration and heat pump systems*. KTH Royal Institute of Technology, Sweden.

Martini, W. R. (1983). *Stirling Engine Design Manual* (Second ed.). USA: U.S. Department of Energy

Mathie, R., White, A., J., & Markides, C. N. (2014). Ultrasonic measurements of unsteady heat transfer in a reciprocating gas spring, 10th International Conference on Heat Transfer, Fluid Mechanics and Thermodynamics.

McLinden, M. O., Seeton, C. J., & Pearson, A. (2020). New refrigerants and system configurations for vapor-compression refrigeration. *Science, 370*(6518), 791-796. https://doi.org/doi:10.1126/science.abe3692

Metscher, J. F. (2014). *Free-Piston Stirling Convertor Model Development, Validation, and Analysis for Space Power Systems*. Embry-Riddle Aeronautical University.

Nikanjam, M., & Greif, R. (1978). Heat transfer during piston compression. *Journal of Heat Transfer, 100*, 527-530.

Nusselt, W. (1923). Der Wärmeübergang in der Verbrennungskraftmaschine. *Forschungsarbeiten auf dem Gebiete des Ingenieurwesens*(264).

Oguri, T. (1960). On the coefficient of heat transfer between gases and cylinder walls of the spark-ignition engine. *Bulletin of JSME, 3*(11), 363-369.

Oriti, S., & Blaze, G. (2007). Advanced Stirling Convertor Testing at NASA Glenn Research Center Symposium conducted at the meeting of the 5th International Energy Conversion Engineering Conference and Exhibit (IECEC)

Orlowska, A. H., & Davey, G. (1987). Measurement of losses in a Stirling cycle cooler. *Cryogenics, 27*, 645-651.

Otis, D. R. (1974). New Developments in Predicting and Modifying Performance of Hydraulic Accumulators Symposium conducted at the meeting of the National Conference on Fluid Power

Overbye, V. D., Bennethum, J. E., Uyehara, O., & Myers, P. (1961). Unsteady heat transfer in engines. *SAE Transactions, 69*, 461-494.

Park, J. S., & Chang, H.-M. (1997). A Stirling Cycle Analysis with Gas-Wall Heat Transfer in Compressor and Expander [Park1997]. In R. G. Ross (Ed.), *Cryocoolers 9* (pp. 147-156). Boston, MA: Springer US. Retrieved from https://doi.org/10.1007/978-1-4615-5869-9_18. https://doi.org/10.1007/978-1-4615-5869-9_18

Pflaum, W. (1961). Wärmeübergang bei Dieselmaschinen mit und ohne Aufladung. *MTZ, 22*, 70.

Polman, J. (1981). Heat Transfer in a Piston-Cylinder System. *Int, J-Heat Mass Transfer, 24*, 184-187.

Pourmovahed, A., & Otis, D. R. (1984). Effects of Thermal Damping on the Dynamic Response of a Hydraulic Motor-Accumulator System. *Journal of Dynamic Systems, Measurement, and Control, 106*, 21-26.

Pourmovahed, A., & Otis, D. R. (1990). An Experimental Thermal Time-Constant Correlation for Hydraulic Accumulators. *Journal of Dynamic Systems, Measurement, and Control, 112*, 112-121.

Qiu, S., & Peterson, A. (2003). *Linear Dynamic Modeling and Numerical Simulation of an STC Stirling Convertor*. presented at the meeting of the 1st International Energy Conversion Engineering Conference (IECEC), Retrieved from https://arc.aiaa.org/doi/abs/10.2514/6.2003-5930 https://doi.org/10.2514/6.2003-5930

Ross, R. G. J., & Boyle, R. F. (2006). An Overview of NASA Space Cryocooler Programs - 2006 Symposium conducted at the meeting of the International Cryocooler Conference, Maryland, USA.

Sapin, P., Taleb, A., Barfuß, C., White, J., Fabris, D., & Markides, C. (2016). Thermodynamic losses in a gas spring : comparison of experimental and numerical results.

Scheck, C. G. (1988). *Thermal Hysteresis Loss in Gas Springs*. Ohio University, Ohio, USA.

Schmidt, G. (1871). Theorie der Lehmannschen calorischen maschine. *Zeitschrift des Vereines Deutscher Ingenieure, 15*.

Smith, N. (2017). *Phase Down Plan Announced for HFCs*. Retrieved from https://www.national.org.nz/phase_down_plan_announced_for_hfcs

Stirling, R. (1817). *Improvements for diminishing the consuption of fuel, and in particular an engine capable of being applied to the moving of machinery on a principle entirely new.* England.

Stirling Ultracold. (2018). *Stirling Solutions*. Retrieved July 8 2018, 2018, from www.stirlingultracold.com/stirling-solutions/

Sunpower Inc. (2018). *About Sunpower*. Retrieved from https://sunpowerinc.com/about/

Svoboda, J., Bouchard, G., & Katz, S. (1978). A Thermal Model for Gas-Charged Accumulators Based on the Heat Conduction Distribution. *Fluid Transients and Acoustics in the Power Industry*.

Taleb, A. I., Barfuß, C., Sapin, P., White, A. J., Fabris, D., & Markides, C. N. (2022). Simulation of thermally induced thermodynamic losses in reciprocating compressors and expanders: Influence of real-gas effects. *Applied Thermal Engineering, 217*, 118738. https://doi.org/https://doi.org/10.1016/j.applthermaleng.2022.118738

The Engineer. (1917). The Centenary of the Heat Regenerator and the Stirling Air Engine *The Engineer* (Vol. 165, pp. 516-157).

Tucker, A. S., Gschwendtner, M. A., & Haywood, D. (2010). *Some insights into Stirling machine behaviour*. presented at the meeting of the 16th International Cryocooler Conference, Atlanta, USA.

Urieli, I. (1983). A current review of the Stirling cycle machine analysis methods. *Proceedings of the 18th Intersociety Energy Conversion Engineering Conference, 2*, 702-707.

Urieli, I., & Berchowitz, D. M. (1984). *Stirling Cycle Engine Analysis*. Bristol, England: Adam Hilger Ltd.

Walker, G. (1973). *Stirling Cycle Machines*. Oxford: Clarendon Press.

Walker, G. (1983). *Cryocoolers Part 1: Fundamentals*. New York: Plenum Press.

Walker, G., Reader, G., Fauvel, O. R., & Bingham, E. R. (1993). *Stirling, near-ambient temperature refrigerators: innovative compact designs*. presented at the meeting of the 6th International Stirling Engine Conference, Eindhoven.

Walker, G., Reader, G., Fauvel, O. R., & Bingham, E. R. (1994). *The Stirling Alternative: Power systems, Refrigerants and Heat Pumps*. Yverdon, Switzerland: Gordon & Breach Science Publishers.

Wang, A. C.-M. (1988). *Evaluation of gas spring hysteresis losses in Stirling cryocoolers*. Massachusetts Institute of Technology.

Wang, S., Liu, B., Xiao, G., & Ni, M. (2021). A Potential Method to Predict Performance of Positive Stirling Cycles Based on Reverse Ones. *Energies, 14*(21), 7040.

West, C. D. (1986). *Principles and applications of Stirling engines*: Van Nostrand Reinhold Company.

Willich, C., Markides, C. N., & White, A., J. (2017). An investigation of heat transfer losses in reciprocating devices. *Applied Thermal Engineering, 111*, 903-913.

Willmott, A. J. (2011, 8/2/2011). *Regenerative Heat Exchangers*. Retrieved 4/07/2018, from http://www.thermopedia.com/content/1087/

Woschni, G. (1967). *A Universally Applicable Equation for the Instantaneous Heat Transfer Coefficient in the Internal Combustion Engine*. presented at the meeting of the SAE Paper No 670931,

Wurm, J., Kinast, J. A., Roose, T. R., & Staats, W. R. (1991). *Stirling and Vuilleumier heat-pumps*. New York, USA: McGraw Hill, Inc.

Yataganbaba, A., Kilicarslan, A., & Kurtbaş, İ. (2015). Exergy analysis of R1234yf and R1234ze as R134a replacements in a two evaporator vapour compression refrigeration system. *International Journal of Refrigeration, 60*, 26-37. https://doi.org/https://doi.org/10.1016/j.ijrefrig.2015.08.010

Zener, C. (1948). *Elasticity and Anelasticity of Metals*: University of Chicago Press.

Zhao, W., Li, R., Li, H., Zhang, Y., & Qiu, S. (2021). Numerical analysis of fluid dynamics and thermodynamics in a stirling engine. *Applied Thermal Engineering, 189*, 116727. https://doi.org/https://doi.org/10.1016/j.applthermaleng.2021.116727

Appendices

Appendix A: Performance Expressions for Refrigerators and Heat-Pumps

A widely used measure of how well a heat-pump or refrigerator functions is the Coefficient of Performance (COP). This is usually in the form of the desired output over required input, as shown in Equation 1.

$$COP = \frac{Desired\ output}{Required\ input}$$

Refrigerators and heat-pumps operate on the same working principles, and can be modelled in the exact same way. The only difference between the two are the objectives of each machine: the desired function of a refrigerator is to remove heat from a desired cold temperature space. The function of a heat-pump, on the other hand, is to maintain a heated space at a required hot temperature by moving heat into that space. The thermodynamic cycles are identical, but the performance for a heat-pump or refrigerator is respectively calculated based on the 'heating effect' (the amount of heat per unit time put into the hot space), $\dot{Q}_H$, or the 'cooling effect' (the amount of heat per unit time removed from the cold space), $\dot{Q}_L$. If the required input for the desired output is defined as the net work rate in, $\dot{W}_{in}$, then the COPs for refrigerators, COP_R, and heat-pumps, COP_{HP}, can be defined as the Equations 2 and 3.

$$COP_R = \frac{Cooling\ Effect}{Work\ Input} = \frac{\dot{Q}_L}{\dot{W}_{in}}$$

$$COP_{HP} = \frac{Heating\ Effect}{Work\ Input} = \frac{\dot{Q}_H}{\dot{W}_{in}}$$

The Carnot COP, as calculated in Equations 2 and 3 for reversible refrigerators and heat-pumps, respectively), imposes a theoretical limit to what cooling capacity can be achieved by a refrigerator for a given power input, based on the second law of thermodynamics and the absolute temperatures between which heat is being pumped. T_H and T_C are the hot and cold reservoir temperatures.

$$COP_{R,Carnot} = \frac{T_C}{T_H - T_C}$$

$$COP_{HP,Carnot} = \frac{T_H}{T_H - T_C}$$

The actual COP divided by the Carnot COP gives the Second Law efficiency in Equation 6, which is not an actual efficiency, but provides a good comparison of all refrigerators and heat-pumps in terms of what they can ideally achieve within the same temperature limits.

$$\eta_{2nd\ Law} = \frac{COP_{actual}}{COP_{Carnot}}\%$$

Appendix B: Lee Equations

$$\frac{\partial T}{\partial t} = \frac{\alpha \partial^2 T}{\partial x^2} + \frac{1}{\rho c_p}\frac{\partial p}{\partial t}$$

$$\Delta \dot{W} = f\int_o^t p\frac{dV}{dt}dt = -\frac{\omega}{2}p_1 V_o \frac{\gamma - 1}{\gamma}\frac{P_1}{P_o}\varepsilon\, sin\phi_T$$

Where $V_o = \frac{mRT_o}{Po}$

Appendix C: Cooke-Yarborough and Ryden Equations

$$D_p = \frac{P\left(1 + b^2 - 2bcos(\theta)\right)^{\frac{1}{2}} V_o}{2cV_m}$$

$$\phi = \sin^{-1}\left(\frac{bsin(\theta)}{\left(1 + b^2 - 2bcos(\theta)\right)^{\frac{1}{2}}}\right)$$

$$\dot{E}_{mean} = \frac{\omega {D_p}^2}{2R_o C_p T_o} f(\alpha h)$$

For the near-adiabatic case, $\alpha h > 5$, and for the near-isothermal case, $\alpha h < 1$.

θ = phase difference between the diaphragm (piston) and the displacer
V_m = total volume of working gas of engine when the diaphragm is at mid-stroke
V_h = volume of hot space when the displacer is at mid-stroke
V_e = swept volume of the displacer
V_r = void volume of the regenerator
V_o = swept volume of diaphragm
T_e = wall temperature of expansion space
T_c = wall temperature of compression space
T_r = mass averaged temperature in the regenerator
P = mean pressure of working gas
The constants b and c are non-dimensional expressions:

$$b = \frac{V_e}{V_o}\left(1 - \frac{T_c}{T_e}\right)$$

$$c = 1 - \frac{V_h}{V_m}\left(1 - \frac{T_c}{T_e}\right) - \frac{V_r}{V_m}\left(1 - \frac{T_c}{T_r}\right)$$

Appendix D: Chafe Non-Dimensional Speed Relations

The following is taken from Chafe (1988, pp. 30, 48-50) for their definitions of the linear velocity Peclet number and the dimensionless SPEED parameter:

$$Pe = \frac{U_p D}{\alpha}$$

Where:

$$U_p = piston\ speed$$
$$D = characteristic\ length, i.e. the\ cylinder\ diameter$$
$$\alpha = cycle - averaged\ helium\ thermal\ diffusivity$$

The piston speed, U_p, is an average speed given by:

$$U_p = \frac{2(stroke\ distance)}{(period)}$$

The SPEED parameter, τ, is a nondimensional speed that related heat transfer rate to piston speed:

$$\tau = \omega r M C_v$$

Where:

$$\omega = angular\ velocity$$
$$r = thermal\ resistance$$
$$M = total\ mass\ of\ working\ gas$$
$$C_v = specific\ heat\ capacity\ at\ constant\ volme\ of\ the\ working\ gas$$

Appendix E: Experimental Errors

Table A-1: Errors for cylinder experiment with and without regenerator material

Frequency [Hz]	Cylinder Only Error [normalised]	Cylinder with Regenerator Error [normalised]
1	± 0.0289	± 0.0303
2	± 0.0291	± 0.0300
3	± 0.0285	± 0.0307
4	± 0.0283	± 0.0277
5	± 0.0288	± 0.0281
6	± 0.0293	± 0.0280
7	± 0.0287	± 0.0273
8	± 0.0284	± 0.0289
9	± 0.0289	± 0.0289
10	± 0.0289	± 0.0286

Table A-2: Errors for Alpha refrigerator experiment

T_h = 50 °C	T_c [°C]	Cooling Capacity Q_c [W]	Voltage V [V]	Current I [A]	WV [± V]	WI [± A]	WQ_c [± W]
	-1.2	48.9	27.3	1.79	0.55	0.03	1.38
	-19.2	38.3	24.1	1.59	0.48	0.03	1.08
	-43.5	26.1	19.9	1.31	0.40	0.02	0.73
	-67.8	11.7	13.1	0.89	0.26	0.01	0.32
T_h = 60 °C	T_c [°C]	Cooling Capacity Q_c [W]	Voltage V [V]	Current I [A]	WV [± V]	WI [± A]	WQ_c [± W]
	4.9	50.6	27.8	1.82	0.56	0.03	1.43
	-11.3	37.9	24.0	1.58	1.58	0.03	2.60
	-34.5	24.8	19.5	1.27	0.39	0.02	0.70
	-63.7	12.4	13.8	0.9	0.28	0.01	0.35

The propagation of errors equation used to calculate the error in Q_c (where Q_c = VI):

$$WQ_c = \sqrt{\left(\frac{dQ_c}{dV}WV\right)^2 + \left(\frac{dQ_c}{dI}WI\right)^2}$$

Appendix F: Temperature and Heat Transfer Results vs Frequency

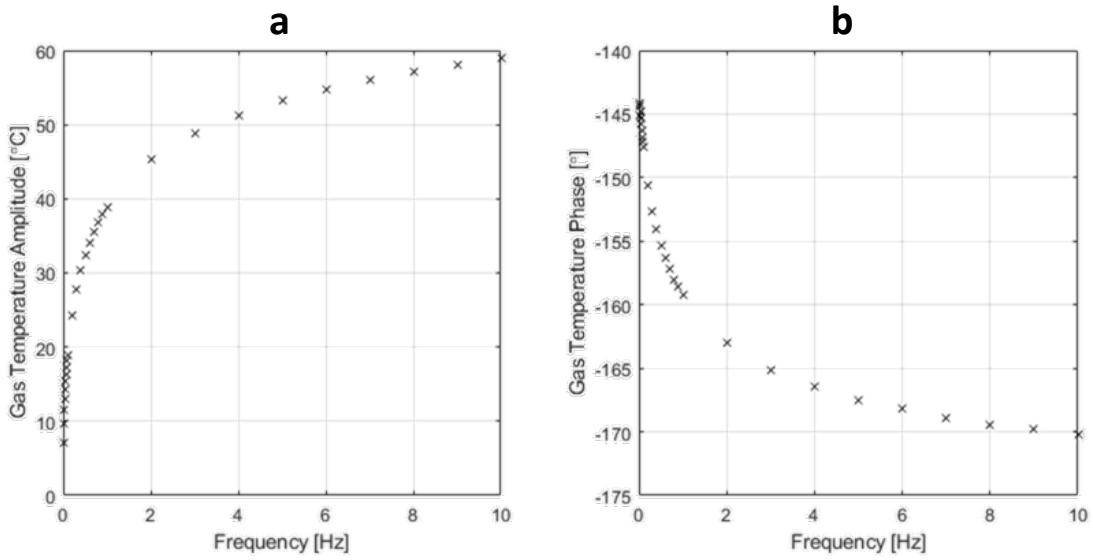

Figure A - 1: Temperature amplitude (a) and phase (b) vs the operating frequency for the single cylinder Sage model

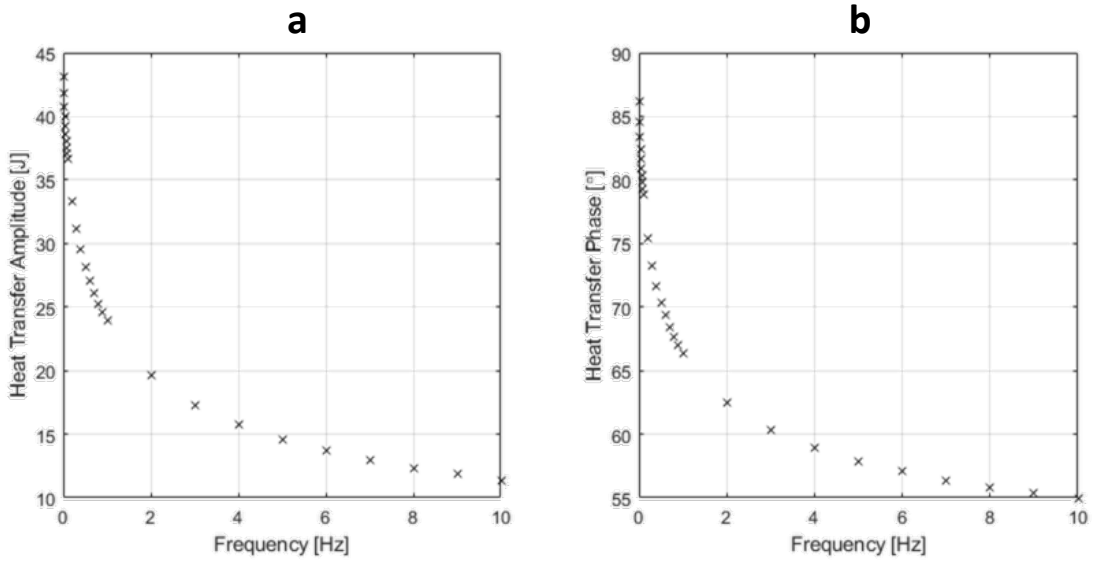

Figure A - 2: Heat transfer amplitude (a) and phase (b) vs the operating frequency for the single cylinder Sage model

Appendix G: Schmidt Equation for when Pressure Phase Shift = 0

$$0 = -\left[tan^{-1}\left(\frac{-\kappa\, sin(\alpha)}{1+\kappa\, cos(\alpha)}\right) + \tan^{-1}\left(\frac{\kappa \sin(\alpha)}{\tau+\kappa\cos(\alpha)}\right)\right]$$

$$tan^{-1}\left(\frac{-\kappa\, sin(\alpha)}{1+\kappa\, cos(\alpha)}\right) = -\tan^{-1}\left(\frac{\kappa \sin(\alpha)}{\tau+\kappa\cos(\alpha)}\right)$$

$$\frac{-1}{1+\kappa\, cos(\alpha)} = \frac{-1}{\tau+\kappa\cos(\alpha)}$$

$$1+\kappa\, cos(\alpha) = \tau+\kappa\cos(\alpha)$$

$$\tau = 1$$

Appendix H: Alpha Stirling Performance on a Linear Scale

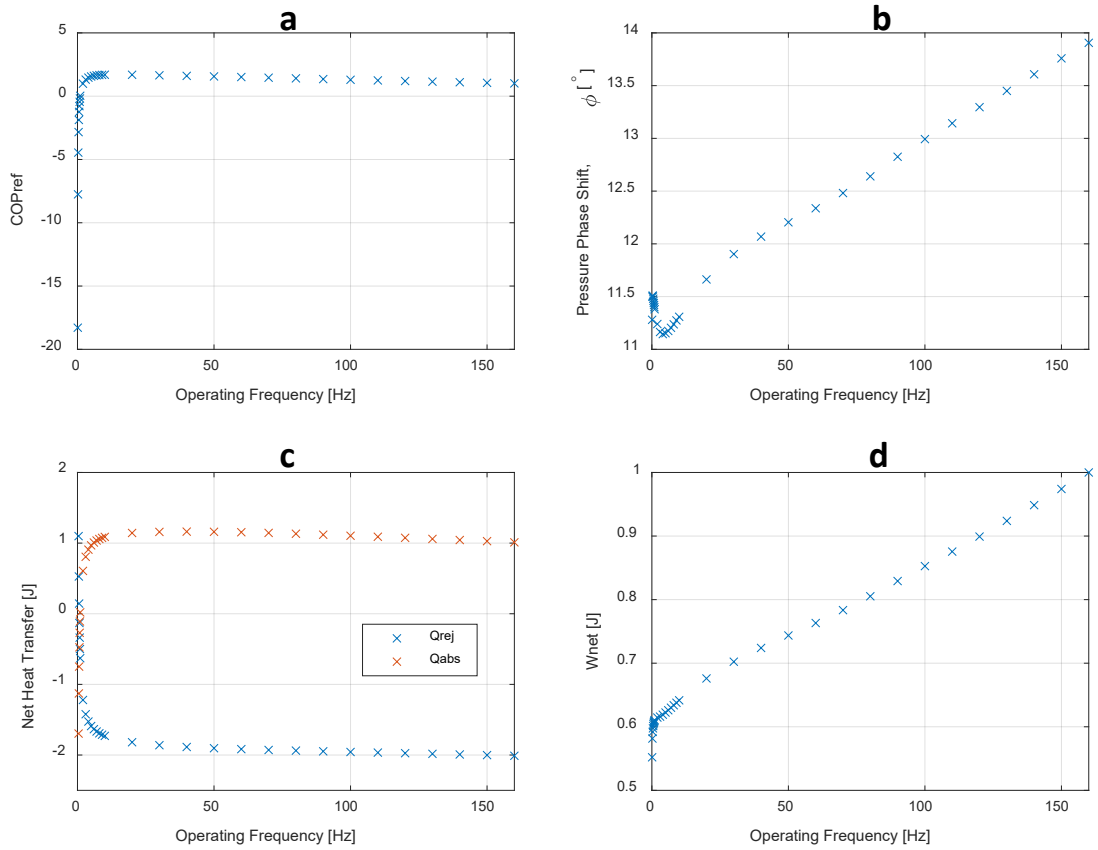

Figure A - 3: a) COP, b) pressure phase shift, c) net heat transfer, and d) net P-V work against operating frequency for the alpha Stirling Sage model

Appendix I: Pressure Variation in Alpha Stirling Sage Model

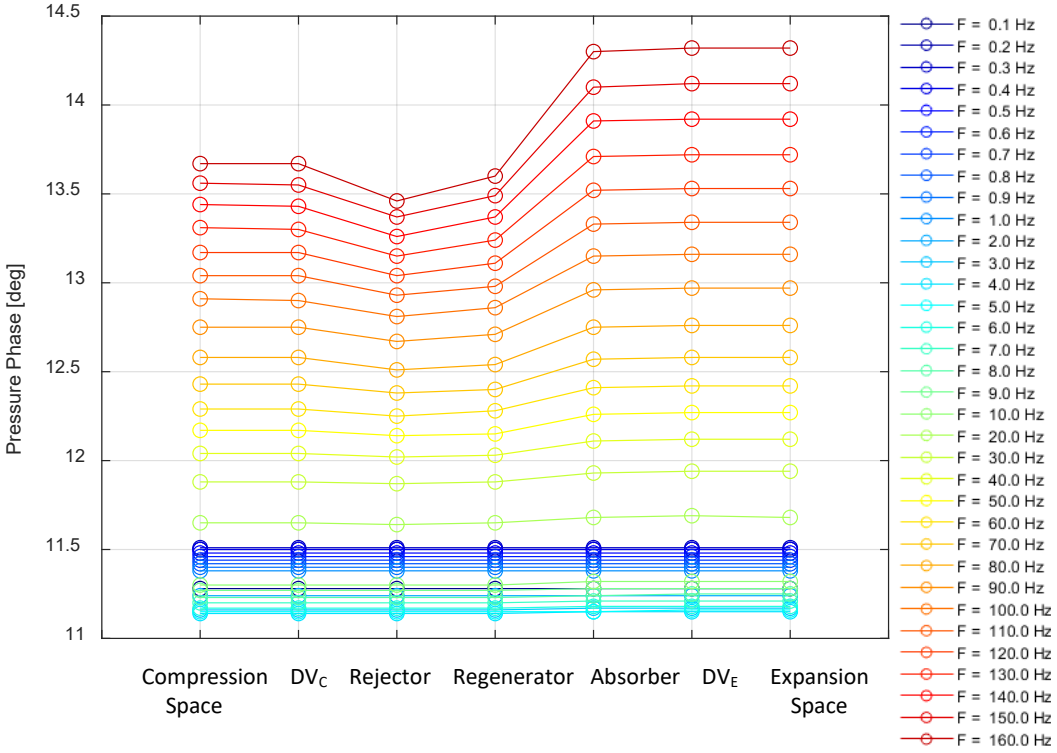

Figure A - 4: Pressure phases in each space of the Alpha Stirling Sage model from 1 to 160 Hz

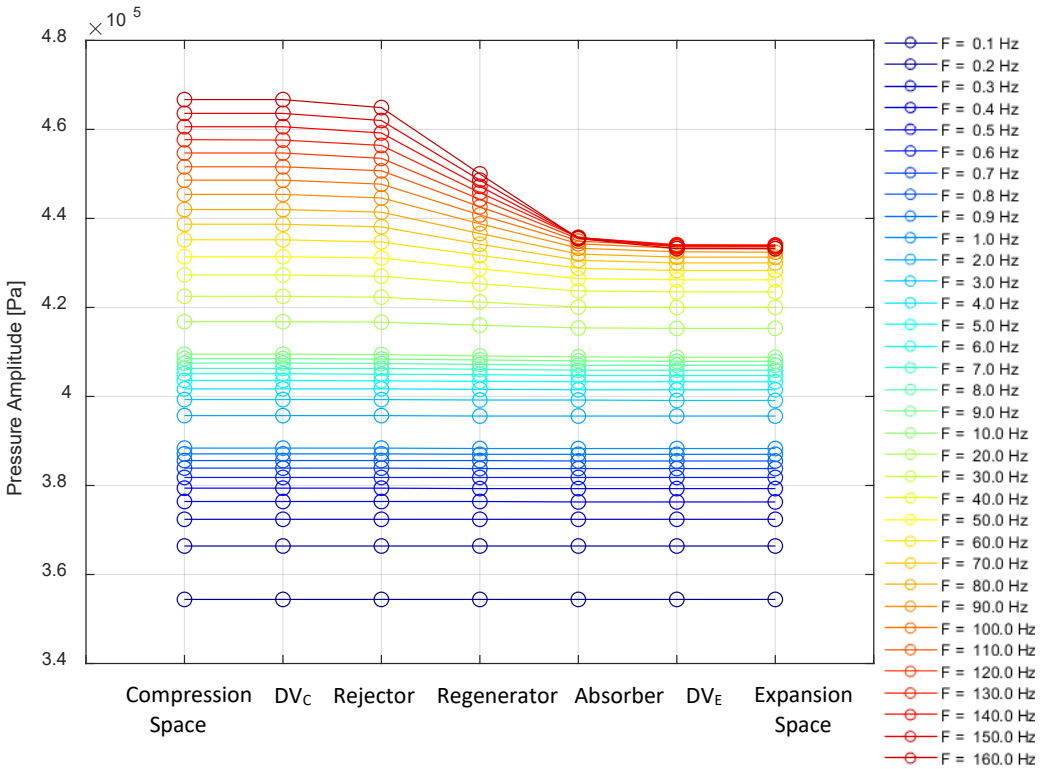

Figure A - 5: Pressure amplitudes in each space of the Alpha Stirling Sage model from 1 to 160 Hz

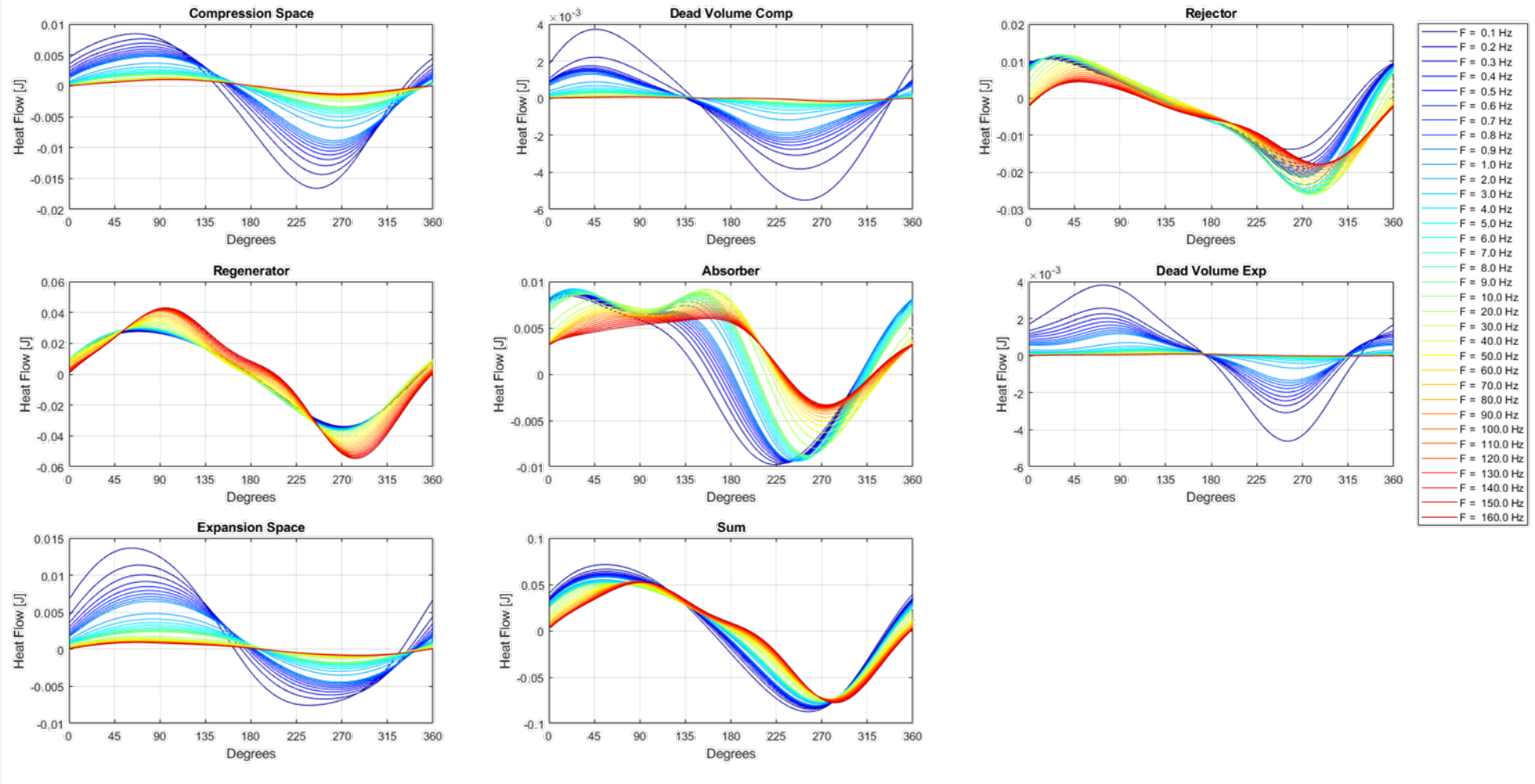

Figure A - 6: Cyclic heat flow in all spaces of the Alpha Stirling Sage model from 0.1 to 160 Hz

Appendix J: R^2 Fit for Heat Transfer

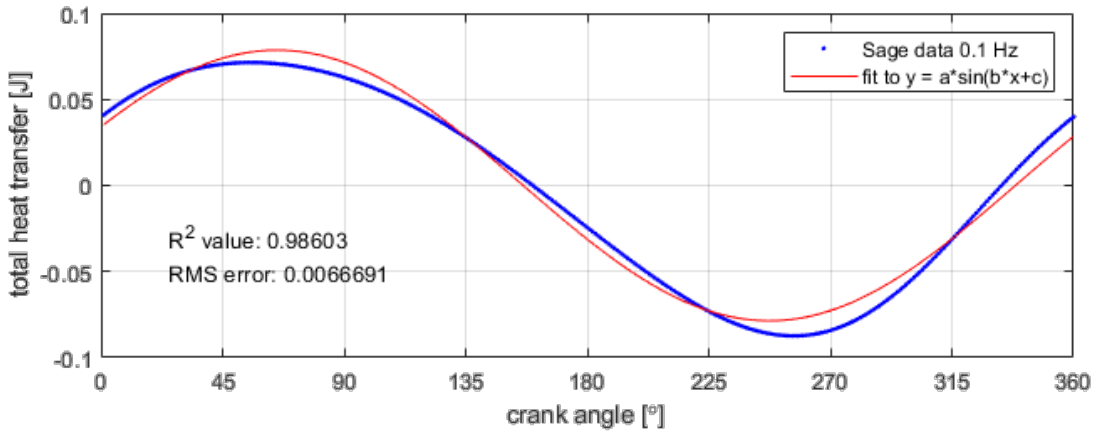

Figure A - 7: Total heat transfer at 0.1 Hz fit to a single harmonic sine wave

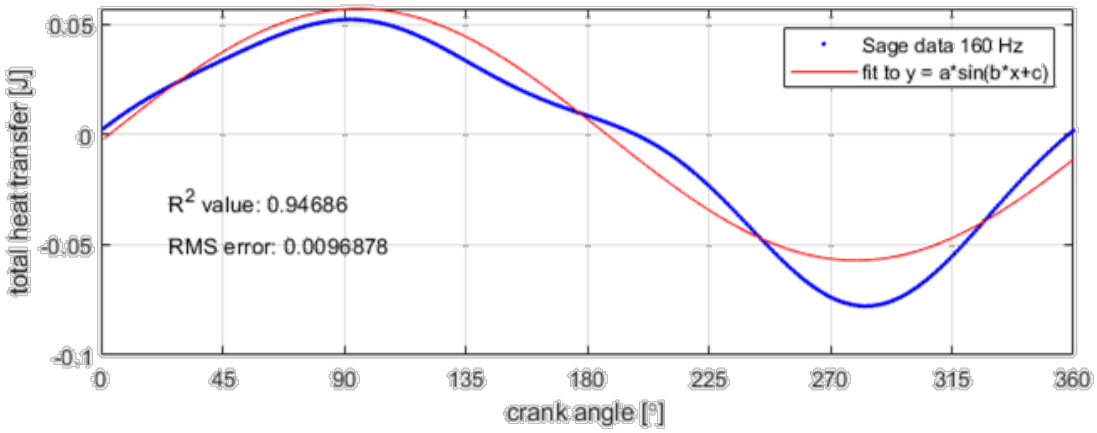

Figure A - 8: Total heat transfer at 160 Hz fit to a single harmonic sine wave

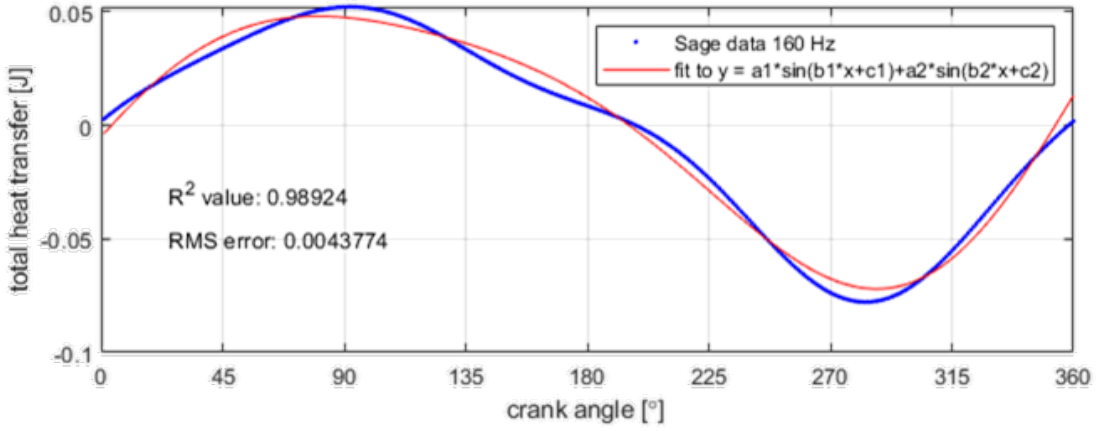

Figure A - 9: Total heat transfer at 160 Hz fit to a double harmonic sine wave

Appendix K: Heat Transfers in Alpha Stirling Model from 1 – 100 Hz

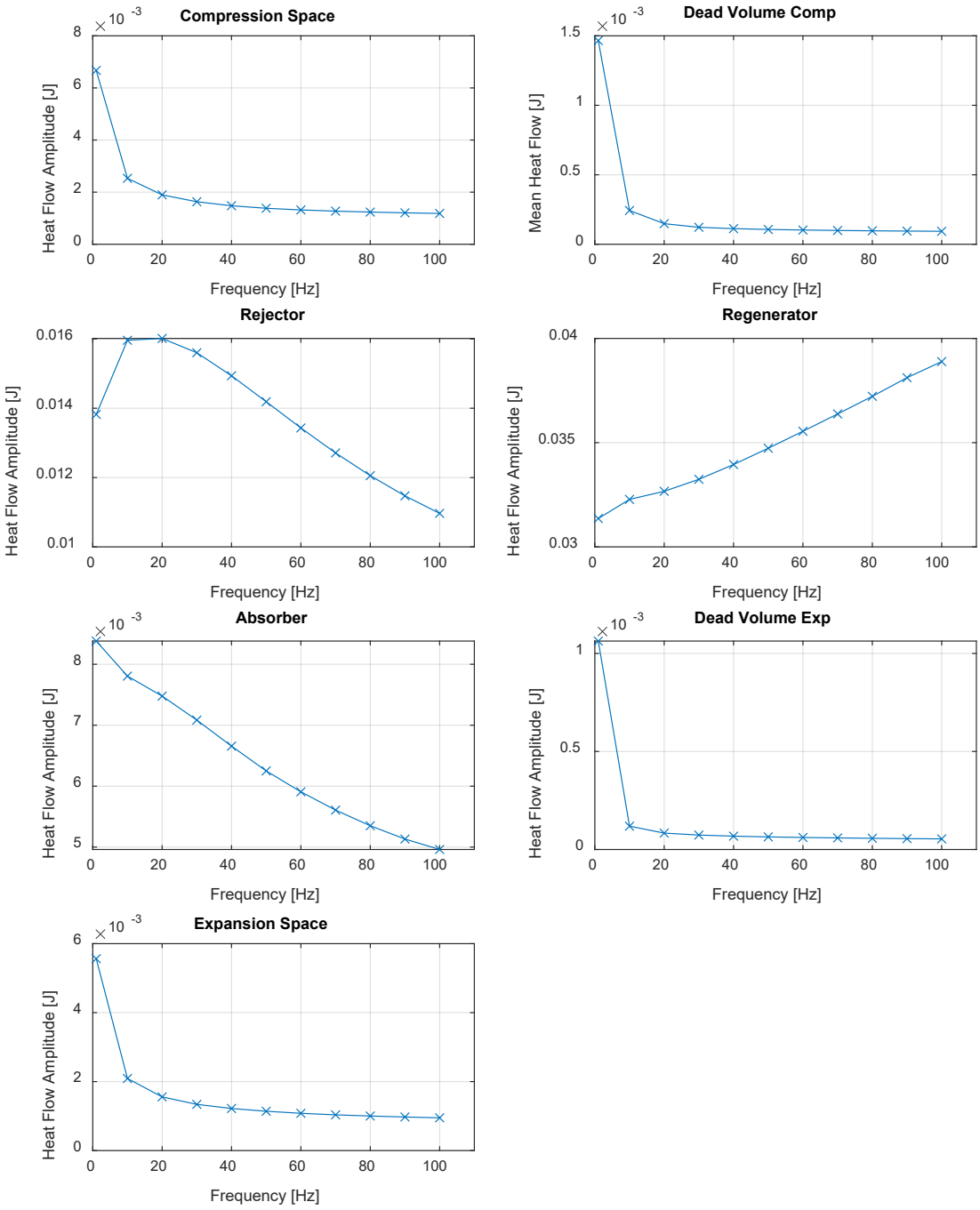

Figure A - 10: Heat flow amplitudes for alpha Stirling Sage model

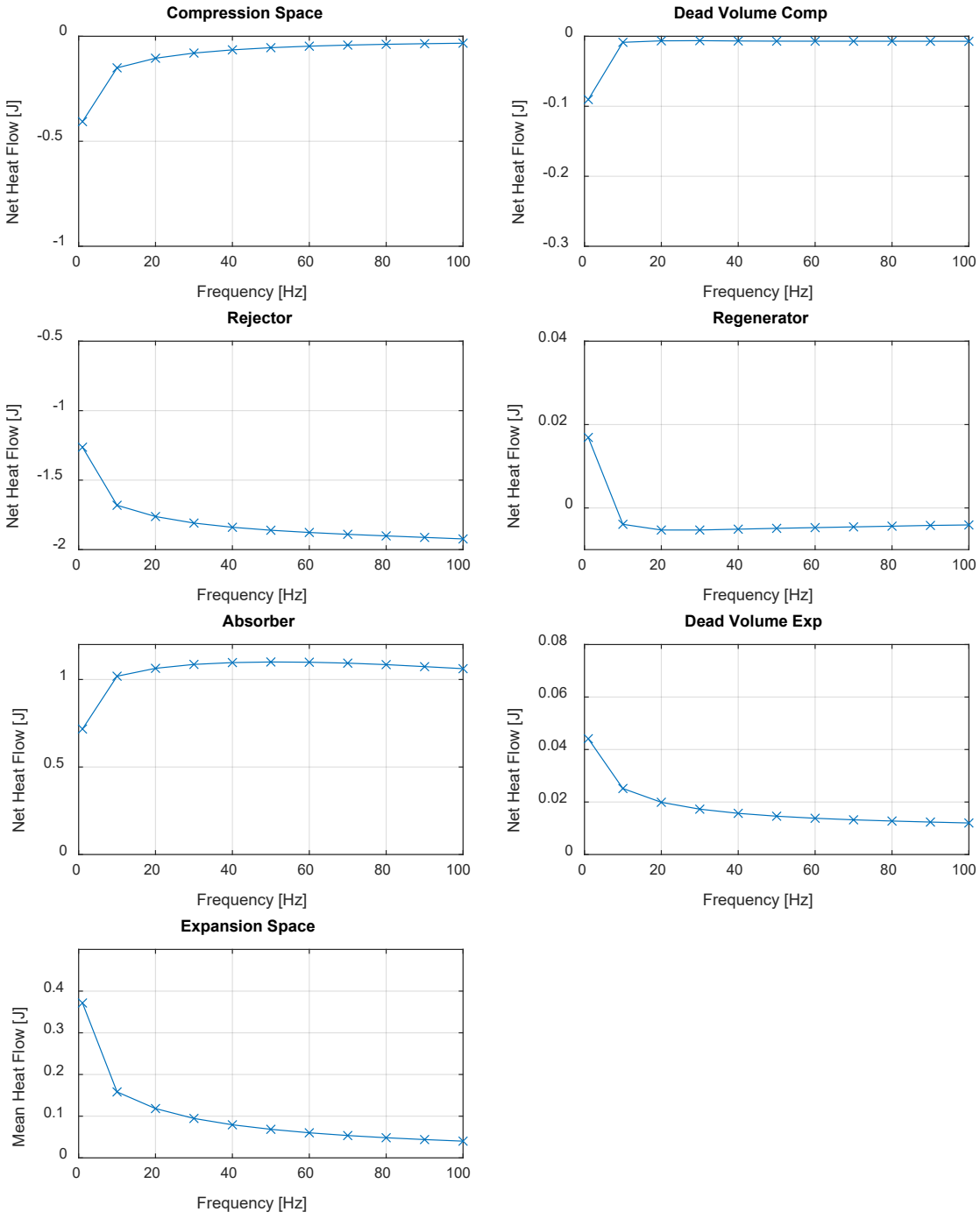

Figure A - 11: Net heat flows for alpha Stirling Sage model

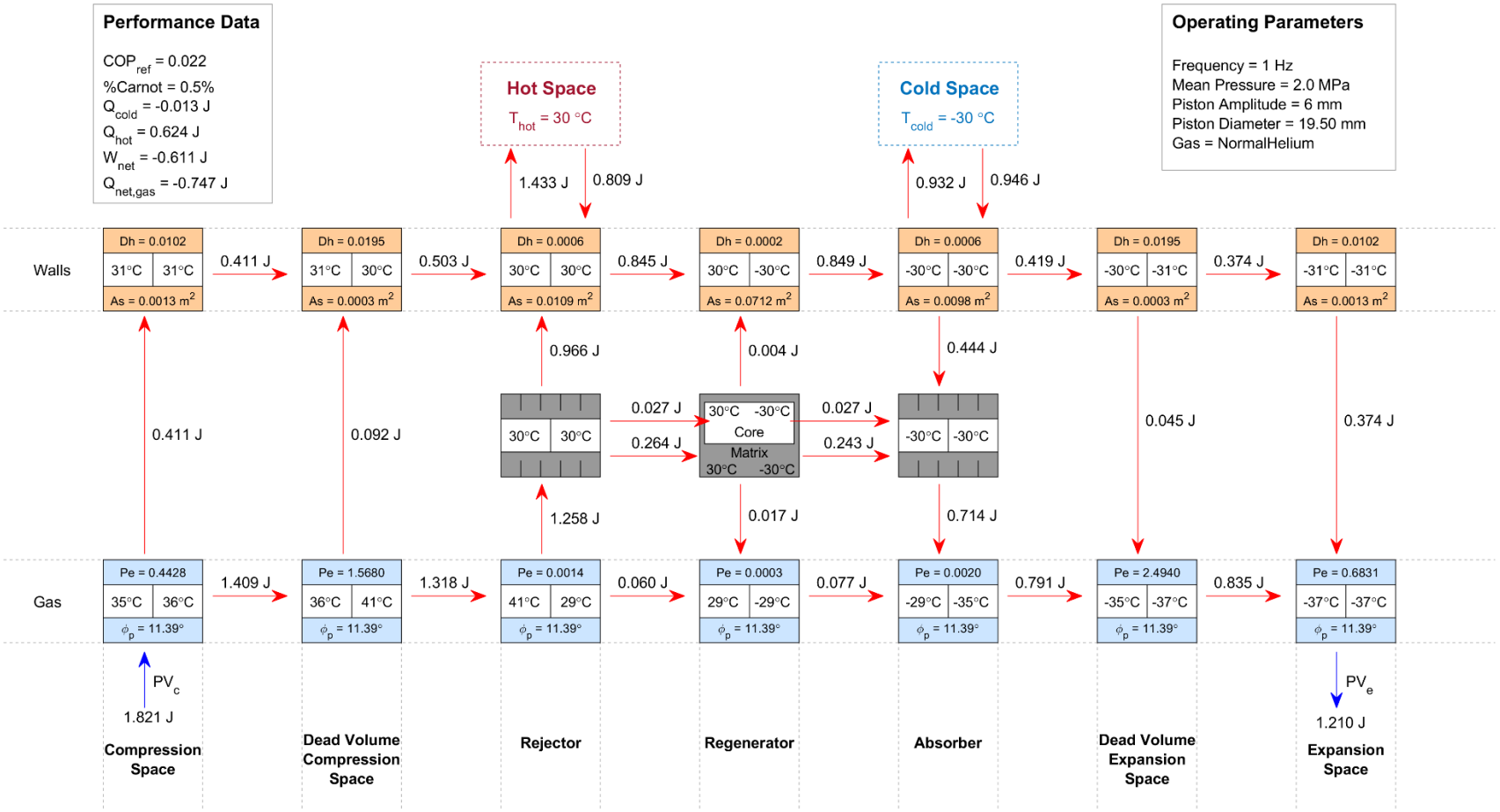

Figure A - 12: Schematic of net heat flow within the alpha Stirling refrigerator Sage model for 1 Hz

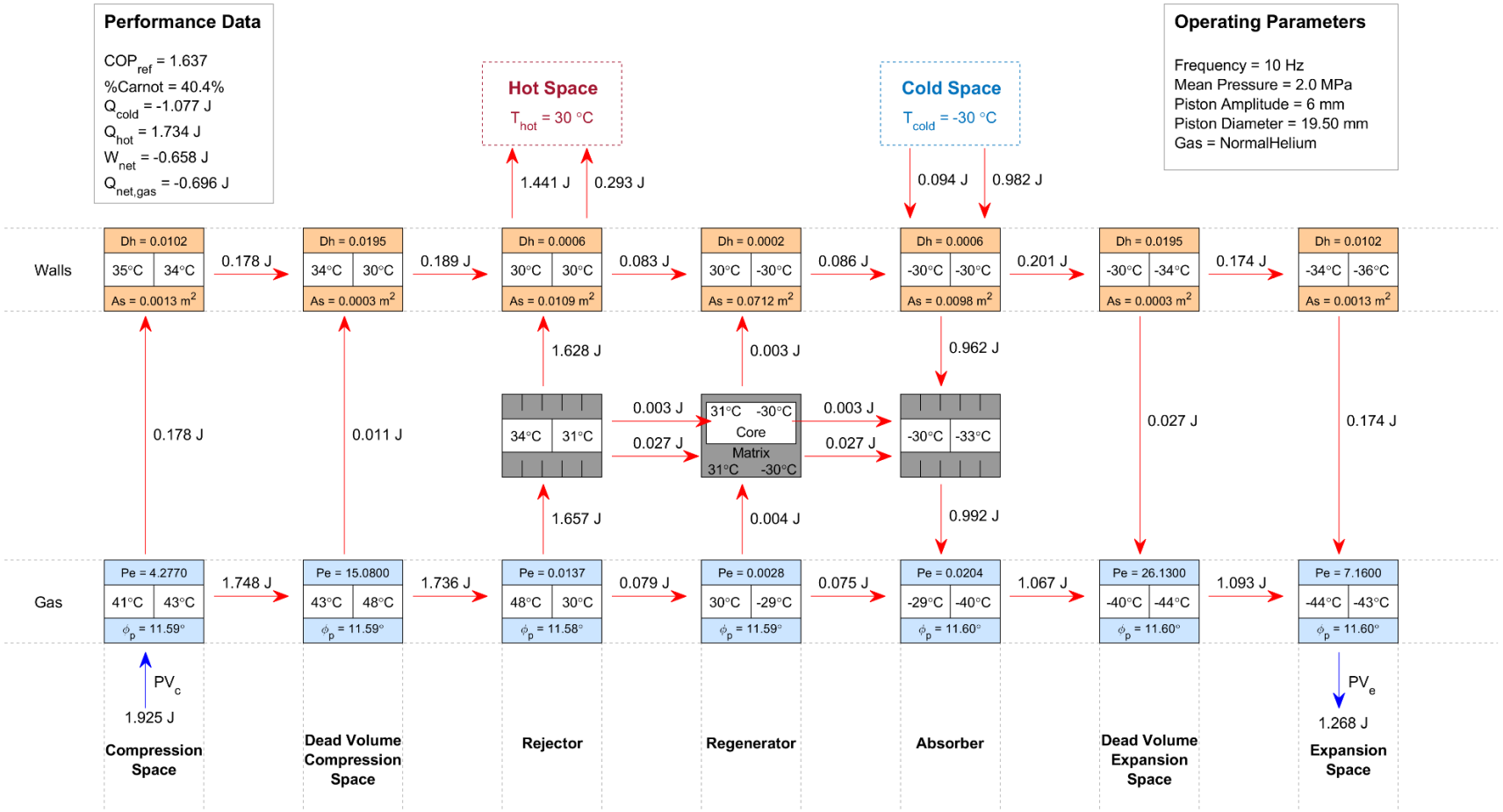

Figure A - 13: Schematic of net heat flow within the alpha Stirling refrigerator Sage model for 10 Hz

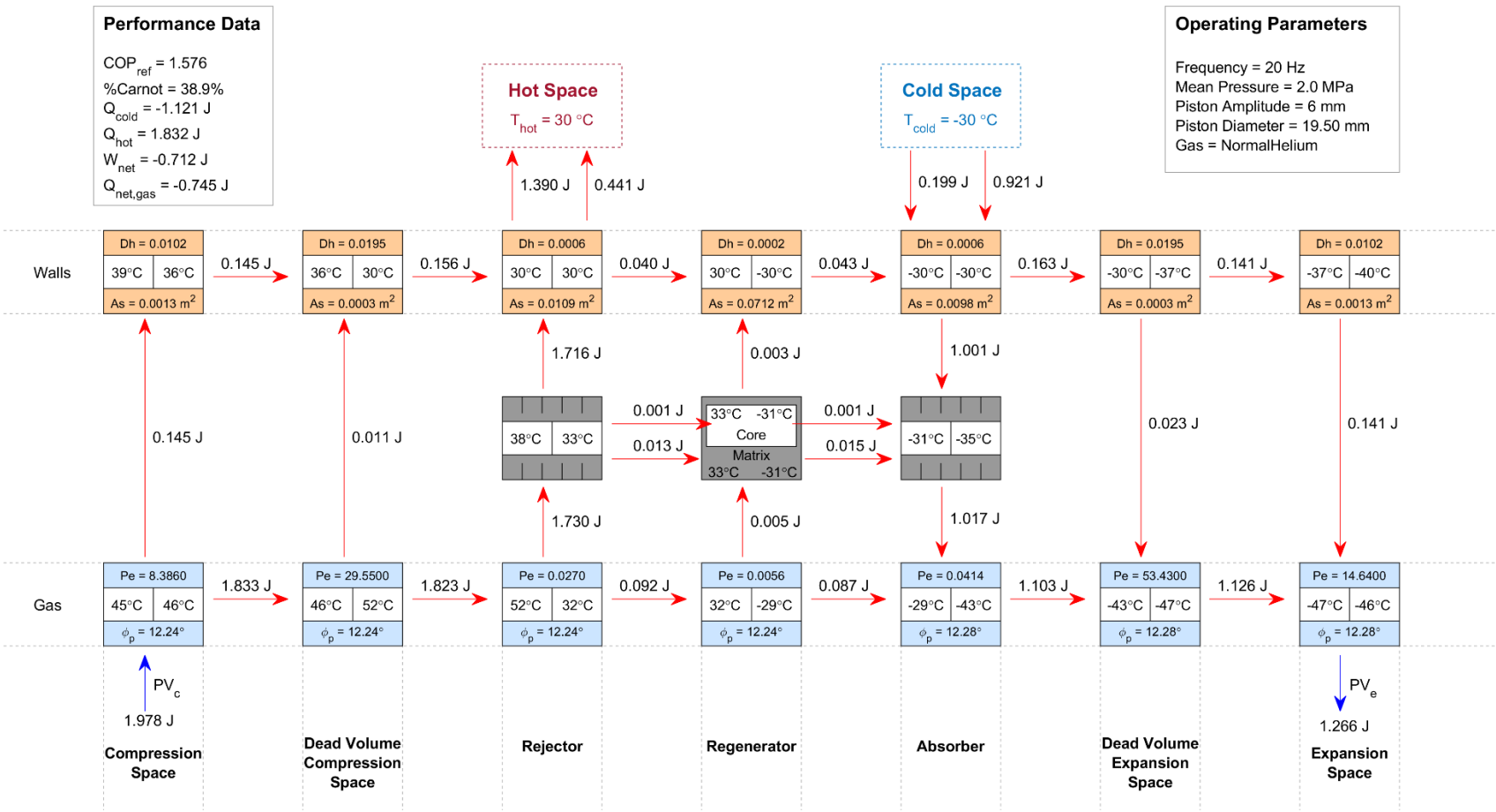

Figure A - 14: Schematic of net heat flow within the alpha Stirling refrigerator Sage model for 20 Hz

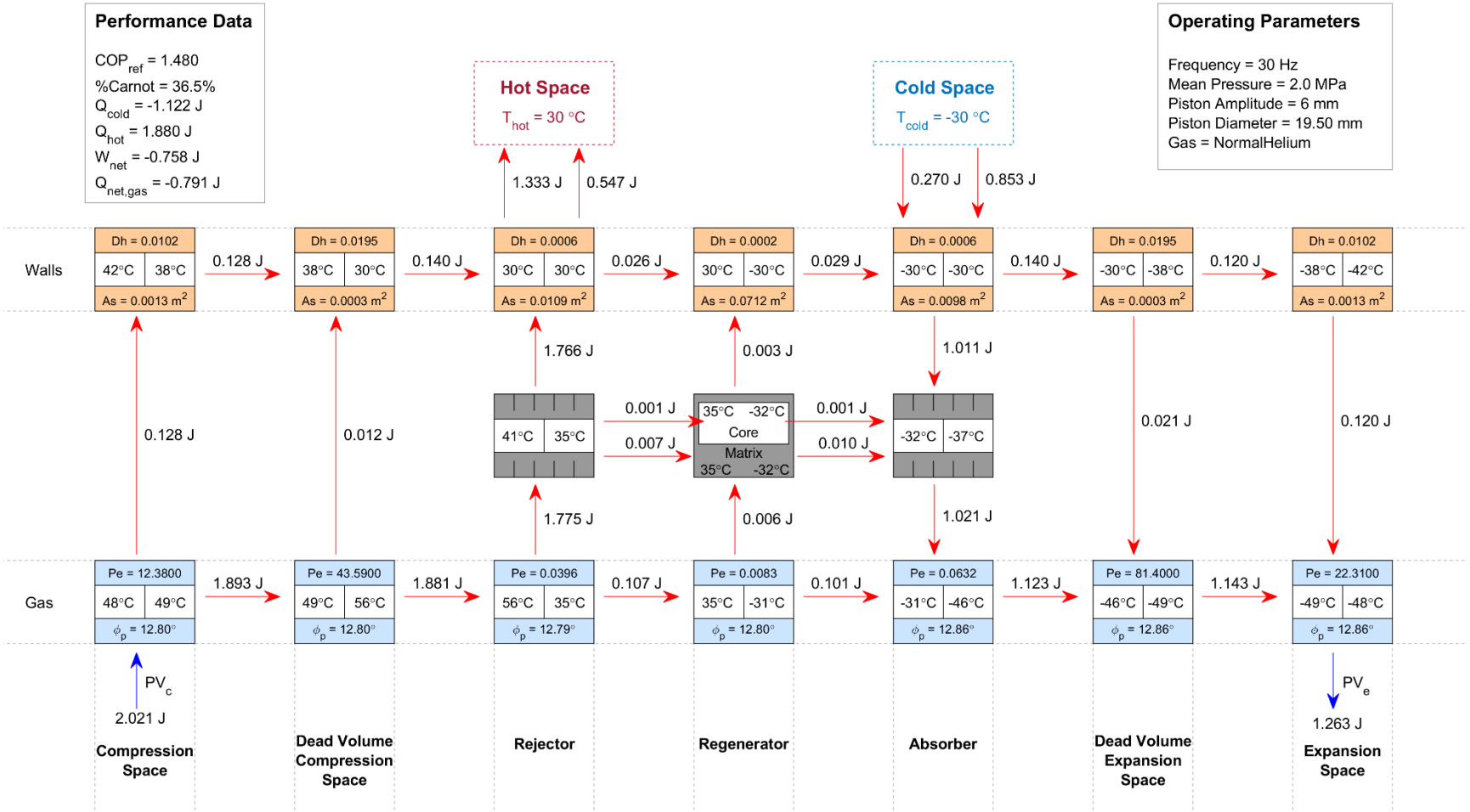

Figure A - 15: Schematic of net heat flow within the alpha Stirling refrigerator Sage model for 30 Hz

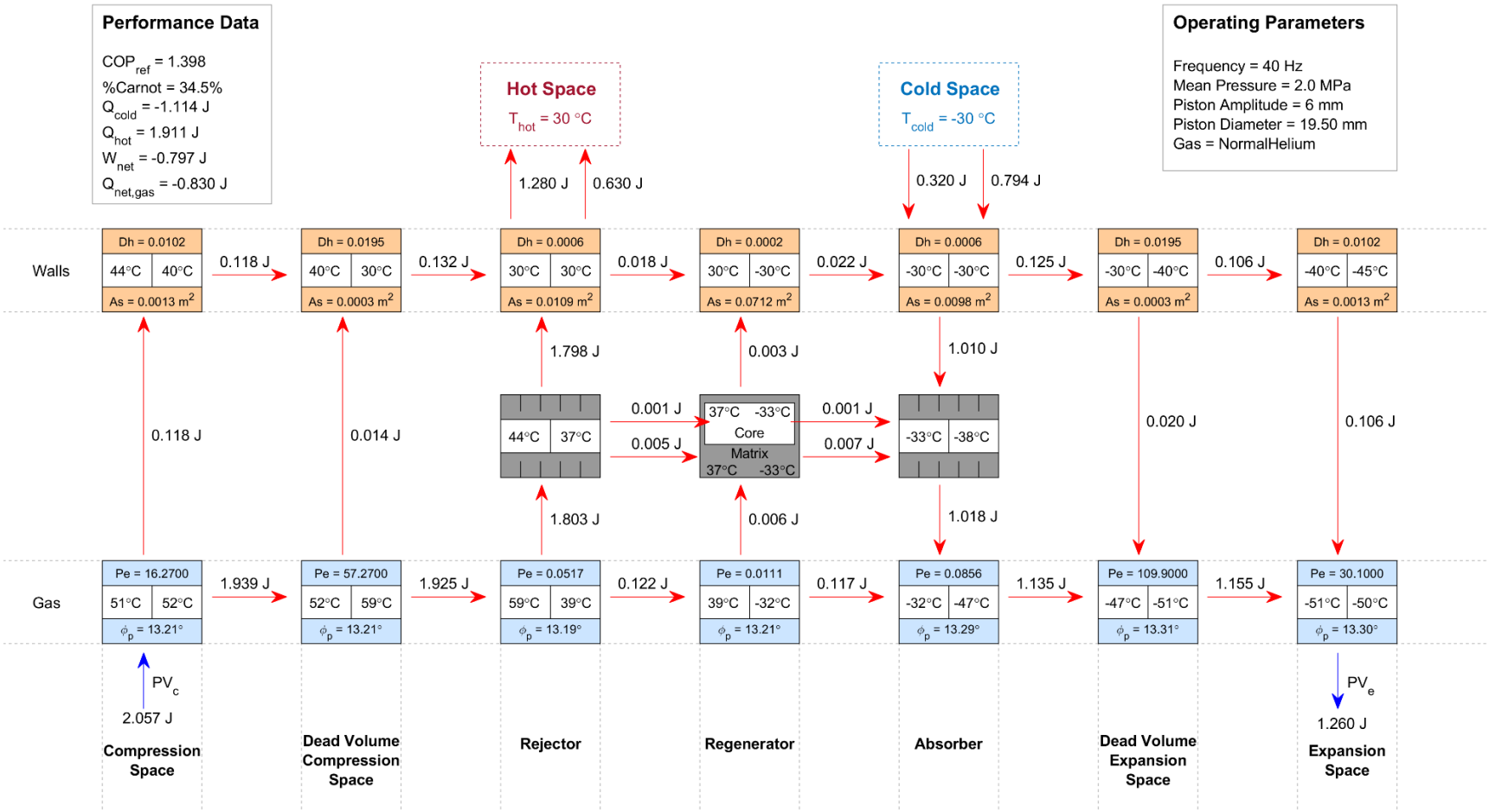

Figure A - 16: Schematic of net heat flow within the alpha Stirling refrigerator Sage model for 40 Hz

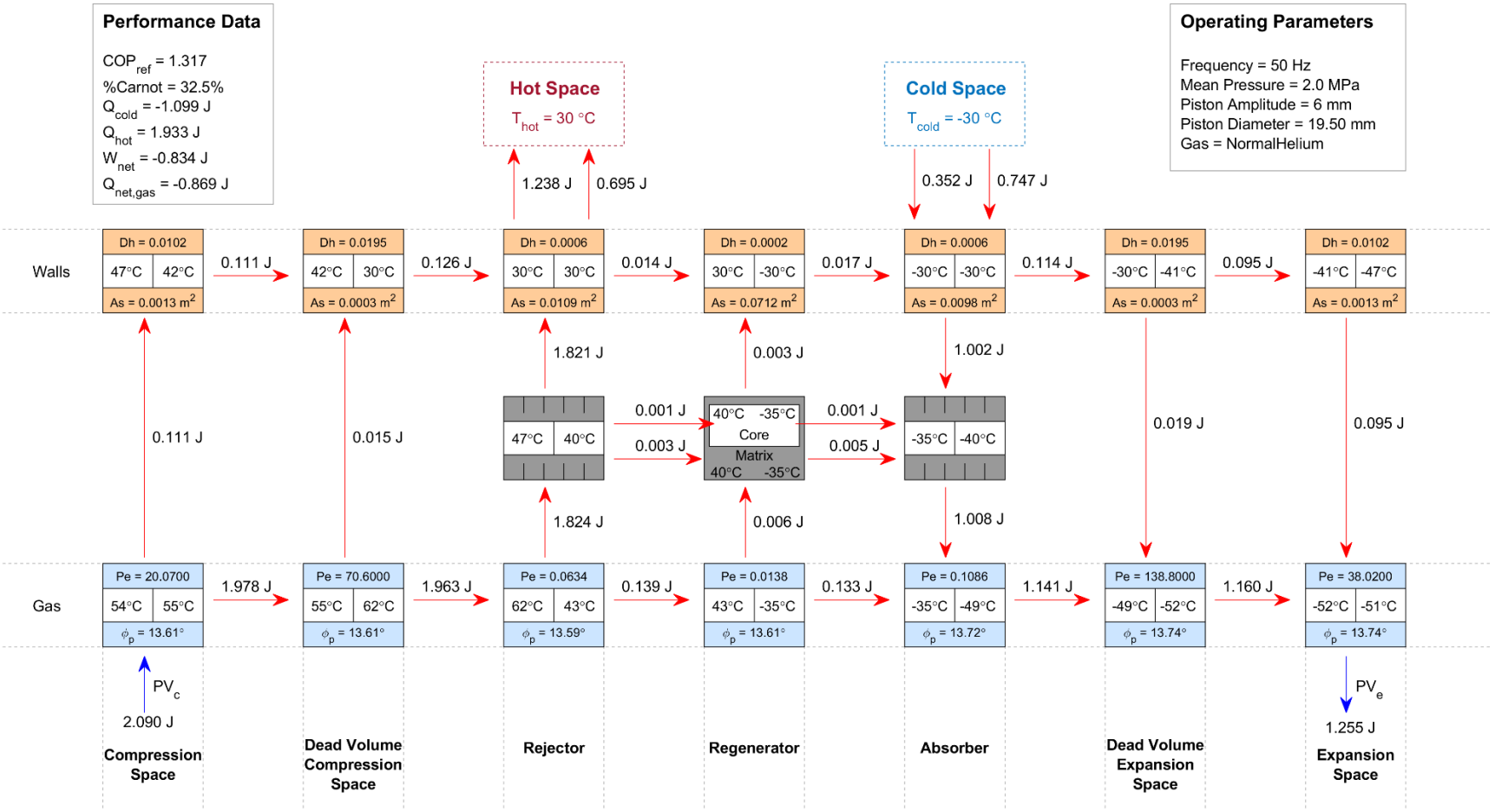

Figure A - 17: Schematic of net heat flow within the alpha Stirling refrigerator Sage model for 50 Hz

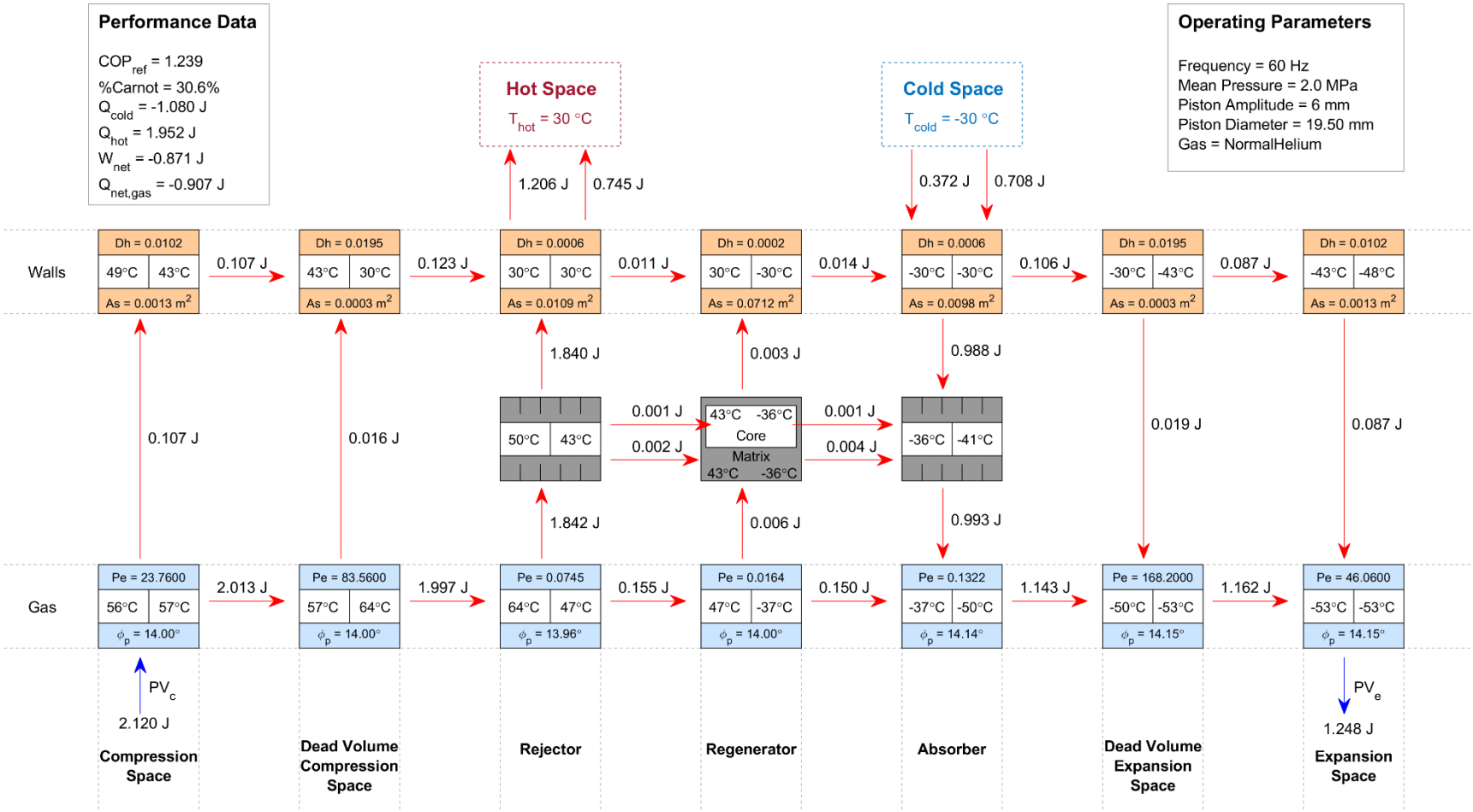

Figure A - 18: Schematic of net heat flow within the alpha Stirling refrigerator Sage model for 60 Hz

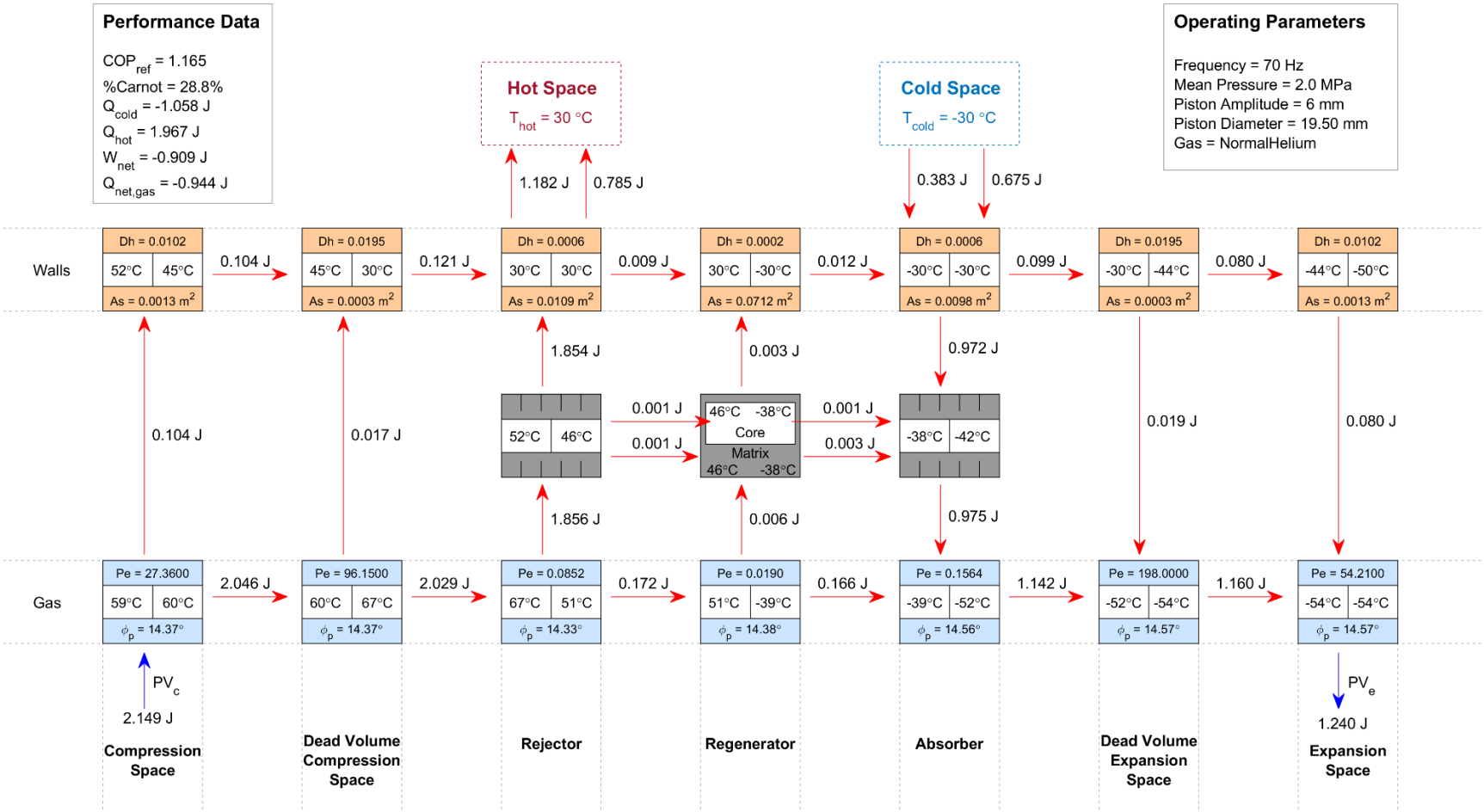

Figure A - 19: Schematic of net heat flow within the alpha Stirling refrigerator Sage model for 70 Hz

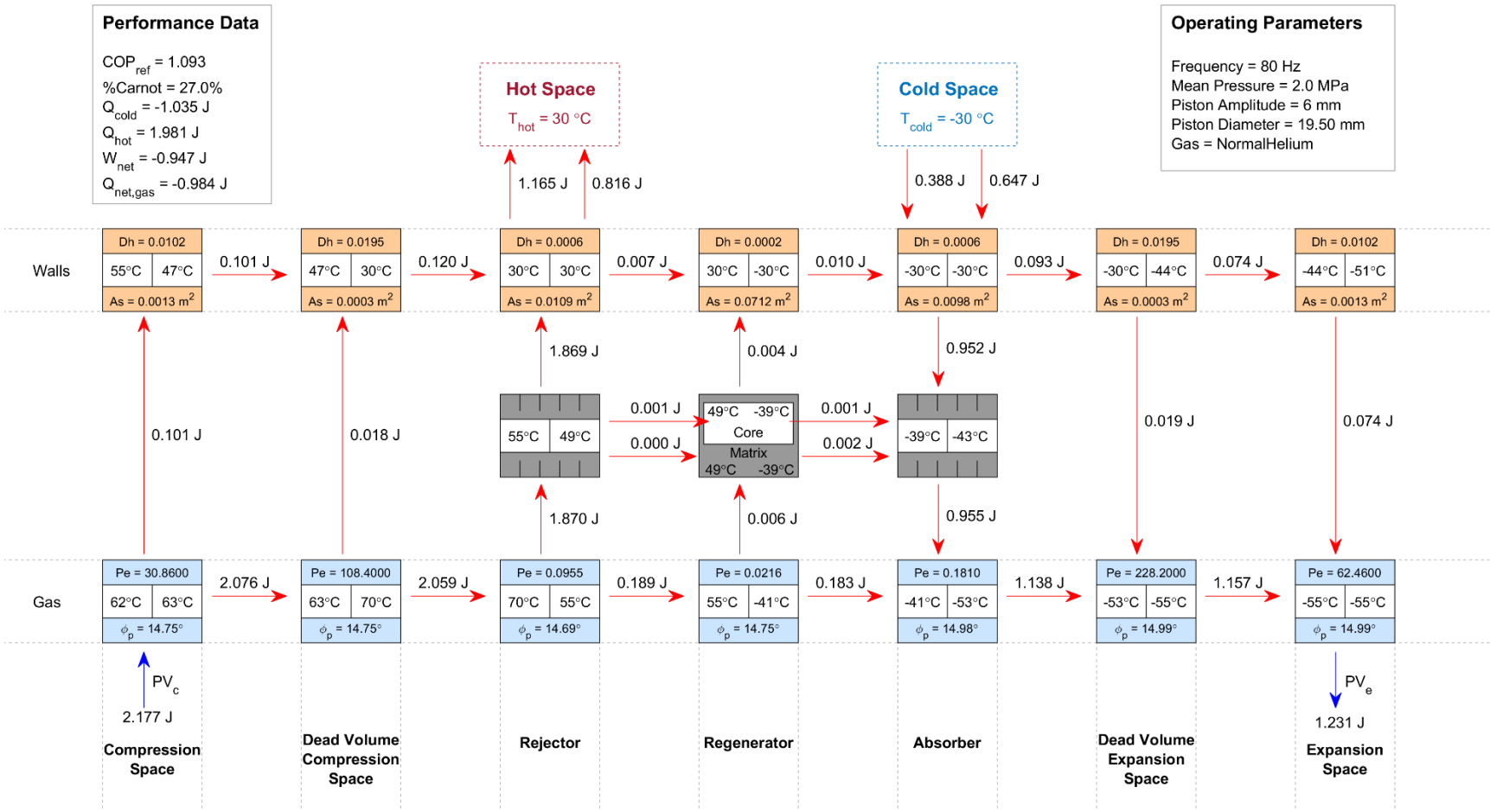

Figure A - 20: Schematic of net heat flow within the alpha Stirling refrigerator Sage model for 80 Hz

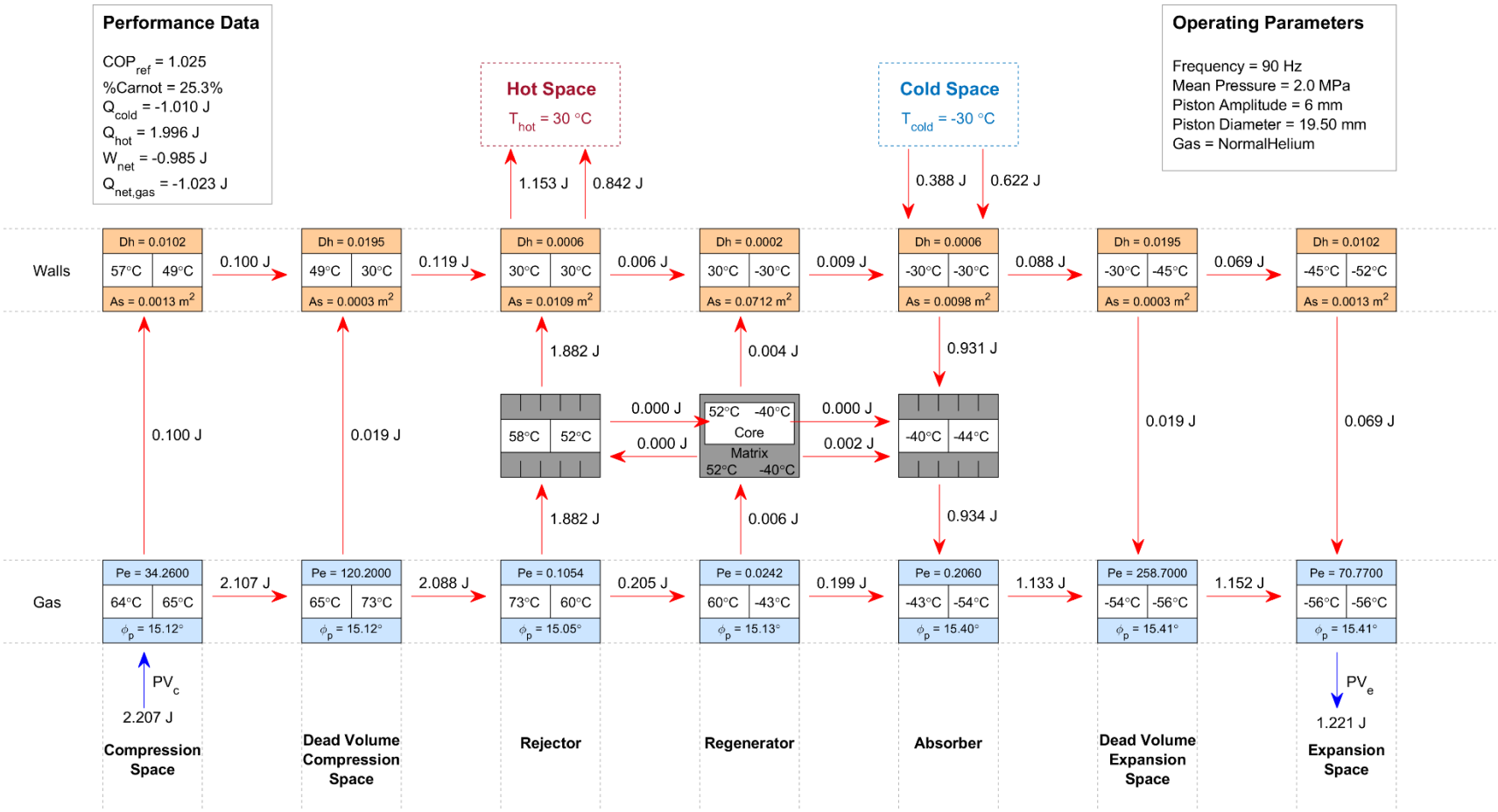

Figure A - 21: Schematic of net heat flow within the alpha Stirling refrigerator Sage model for 90 Hz

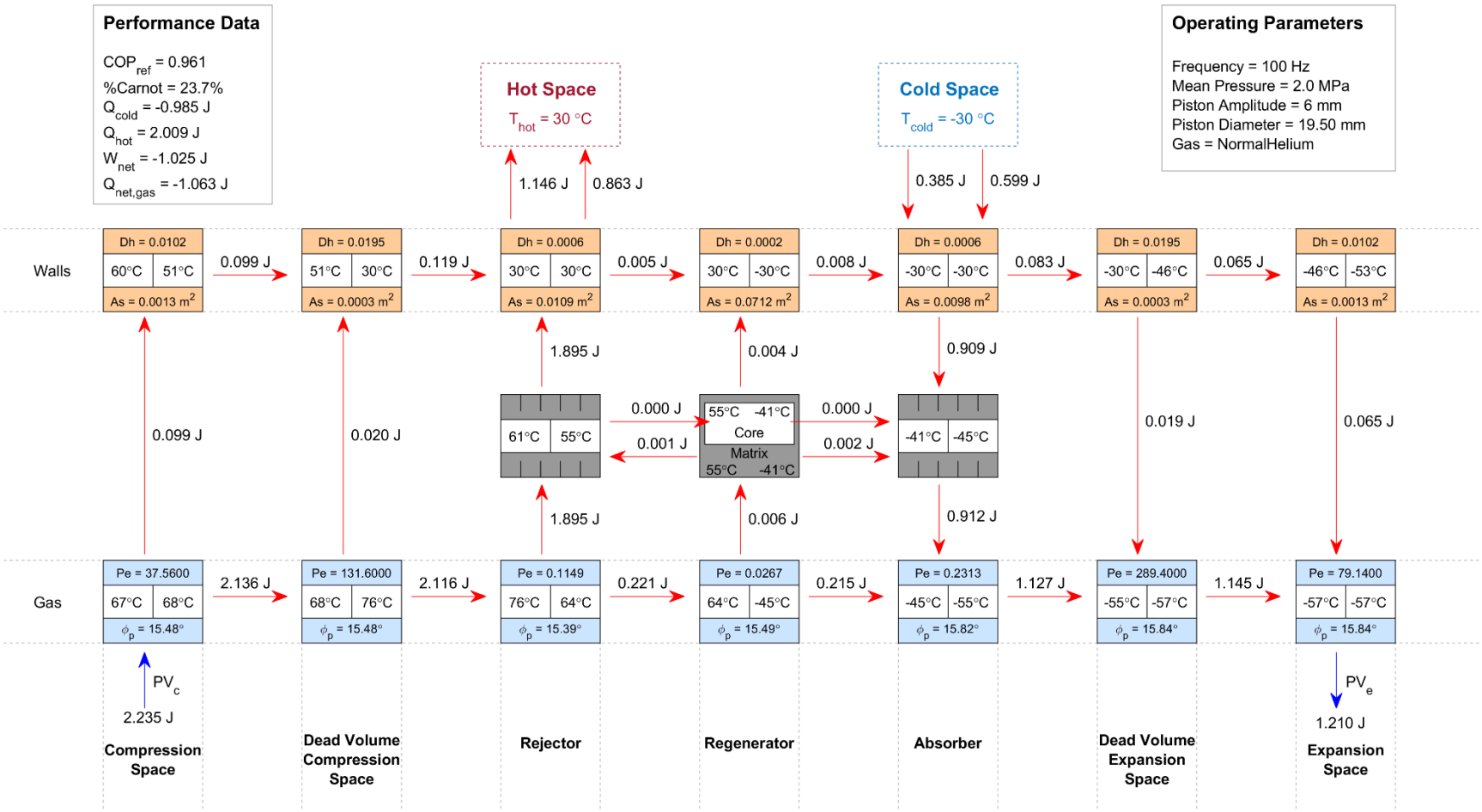

Figure A - 22: Schematic of net heat flow within the alpha Stirling refrigerator Sage model for 100 Hz